

**CYTOSKELETAL PHENOMENA ASSOCIATED WITH NOVEL LATERAL E-CADHERIN JUNCTIONS DURING ORGAN DEGENERATION IN THE RESPIRATORY SYSTEM OF *DROSOPHILA MELANOGASTER***

*By*

**ROJALIN PRADHAN**

**LIFE11201504008**

**National Institute of Science Education and Research**

*A thesis submitted to the  
Board of Studies in Life Sciences  
In partial fulfillment of requirements for the  
Degree of  
DOCTOR OF PHILOSOPHY  
of  
HOMI BHABHA NATIONAL INSTITUTE*



**January, 2024**

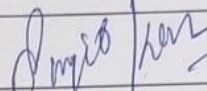
# Homi Bhabha National Institute

## Recommendations of the Viva Voce Committee

As members of the Viva Voce Committee, we certify that we have read the dissertation prepared by Rojalin Pradhan entitled "Cytoskeletal phenomena associated with novel lateral E-Cadherin junctions during organ degeneration in the respiratory system of *Drosophila melanogaster*." and recommend that it may be accepted as fulfilling the thesis requirement for the award of Degree of Doctor of Philosophy.

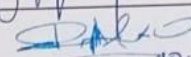
Chairman - Name & Signature with date

Prof. Sanjib Kar

  
10/01/2024

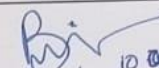
Guide / Convener - Name & Signature with date

Dr. Renjith Mathew

  
10-01-2024

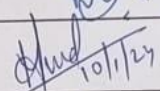
Co-guide - Name & Signature with date (if any)

Dr. Praful Singru

  
10-01-2024

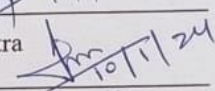
Examiner - Name & Signature with date

Prof. Mohit Prasad

  
10/1/24

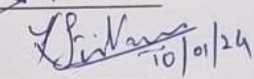
Member 1- Name & Signature with date

Dr. Harapriya Mohapatra

  
10/1/24

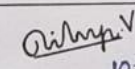
Member 2- Name & Signature with date

Dr. Ramanujam Srinivasan

  
10/01/24

Member 3- Name & Signature with date

Dr. Dileep Vasudevan

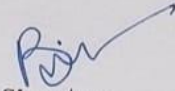
  
10-01-2024

Final approval and acceptance of this thesis is contingent upon the candidate's submission of the final copies of the thesis to HBNI.

I/We hereby certify that I/we have read this thesis prepared under my/our direction and recommend that it may be accepted as fulfilling the thesis requirement.

Date: 10/1/24

Place: NISER

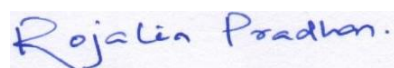
  
Signature  
Co-guide (if any)

  
Signature  
Guide

## STATEMENT BY AUTHOR

This dissertation has been submitted in partial fulfillment of requirements for an advanced degree at Homi Bhabha National Institute (HBNI) and is deposited in the Library to be made available to borrowers under rules of the HBNI.

Brief quotations from this dissertation are allowable without special permission, provided that accurate acknowledgment of source is made. Requests for permission for extended quotation from or reproduction of this manuscript in whole or in part may be granted by the Competent Authority of HBNI when in his or her judgment, the proposed use of the material is in the interests of scholarship. In all other instances, however, permission must be obtained from the author.

A handwritten signature in blue ink that reads "Rojalin Pradhan." The signature is written in a cursive style and is placed on a light blue rectangular background.

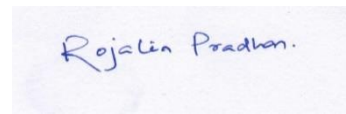
Rojalin Pradhan

## DECLARATION

I, hereby declare that the investigation presented in the thesis has been carried out by me.

The work is original and has not been submitted earlier as a whole or in part for a degree

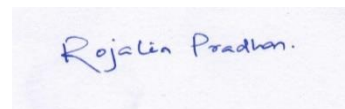
/ diploma at this or any other Institution / University.

A rectangular box containing a handwritten signature in blue ink that reads "Rojalin Pradhan."

Rojalin Pradhan

## CERTIFICATION ON ACADEMIC INTEGRITY

1. I **Rojalin Pradhan**, HBNI Enrolment No. **LIFE11201504008** hereby undertake that, the Thesis titled “Cytoskeletal phenomena associated with novel lateral E-cadherin junctions during organ degeneration in the respiratory system of *Drosophila melanogaster*” is prepared by me and that the document reports the original work carried out by me and is free of plagiarism.
2. I also hereby undertake that this document has been duly checked through a plagiarism detection tool, and the document is found to be plagiarism-free as per guidelines of the institute/ UGC.
3. I am aware and undertake that if plagiarism is detected in my thesis at any stage in future, suitable penalty will be imposed as per the applicable guidelines of the Institute/UGC.



10.01.2024

Signature of the Student

(with date) Endorsed by the PhD Supervisor

I certify that the thesis written by the researcher is plagiarism free as mentioned above by the student.

Signature of the Thesis Supervisor with date. Name: Renjith Mathew

Designation: Reader-F

Department/Centre: School of Biological Sciences

Name of CI/OC: National Institute of Science Education and Research



10.01.2024

## List of Publications arising from the thesis

### Journal

1. Pradhan, R., Kumar, S., Mathew, R. (2023). Lateral adherens junctions mediate a supracellular actomyosin cortex in *Drosophila* trachea. *iScience* (26 (4)).
2. Pradhan, R., Mathew, R. Actin-Microtubule crosstalk via spectraplakins Shortstop facilitates the supracellular arrangement of the actomyosin cortex. (Manuscript under preparation)

### Chapters in books, lecture notes/ Reviews.

1. Pradhan, R., Urbieto-Ortiz, V.A., Kumar, S., Mathew, R., Ríos-Barrera, L.D. Shaping subcellular tubes through vesicle trafficking: Common and distinct pathways, *Seminars in Cell & Developmental Biology*, Volume 133,2023, Pages 74-82, ISSN 1084-9521, <https://doi.org/10.1016/j.semcdb.2022.03.024>.
2. Pradhan, R., Mathew, R. Developmental Staging and imaging of novel Lateral Adherens Junctions in vivo in *Drosophila* respiratory system. (Manuscript under preparation)

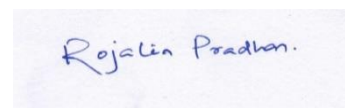
### Conferences

1. Rojalin Pradhan, Renjith Mathew. “Role of ECM Dynamics: from organ sculpting to senile degeneration.” International Cell Biology Conference 2018, (ICCB2018) CCMB Hyderabad
2. Rojalin Pradhan, Renjith Mathew. “Tug of war among epithelial cells: Novel cytoskeletal dynamics in morphogenesis and degeneration.” Asia Pacific *Drosophila* Research Conference 2020 (APDRC5 2020). IISER Pune.

3. Rojalin Pradhan, Renjith Mathew. “Epithelial tissue compression is mediated by a novel lateral noncanonical E-Cadherin associated basal supra cellular actomyosin cortex in *Drosophila* pupal trachea.” 51st NIPS International Symposium Frontiers in epithelial cell biology 2021(online)
4. Rojalin Pradhan, Renjith Mathew. “Lateral non-canonical E-Cadherin associated basal supra cellular actomyosin cortex contributes to global tissue compression in *Drosophila* pupal tracheal epithelium.” InDRC 2021 (online)
5. Rojalin Pradhan, Renjith Mathew. “Lateral non-canonical E-Cadherin organizes a supra cellular actomyosin cortex in *Drosophila* tracheal epithelium”, EMBO Cell polarity and membrane dynamics 2021 (Online)

**Others.**

1. InSDB Imaging Workshop IISER Pune, India (Super resolution Microscopy) Coordinated by IISER Pune and Indian Society of Developmental Biology (2017).
2. Zeiss Workshop on High-end Widefield, Confocal and SR Microscopy (NISER, 2017).
3. B4 Bioimaging Workshop, IISER Pune, India (2019), Coordinated by South Asian Institute, Harvard University and Department of Biotechnology, Govt. of India.



Rojalin Pradhan

**Dedicated to my loving “Maa”**

## ACKNOWLEDGEMENTS

This is a testament to the unwavering help and support of many individuals, and I am deeply grateful for each of their valuable contributions. Allow me to express my sincere appreciation to those who have played a part in organizing this journey.

First of all, my Ph.D. Supervisor Dr. Renjith Mathew, for giving me the opportunity to work in his lab. This would not have been possible without his constant guidance, unwavering support, constructive suggestions, and unending patience. His expertise in *Drosophila* genetics and microscopy has proved invaluable, and I appreciate his continued encouragement beyond his time at Niser. Without his guidance, this work could not have been accomplished. In addition, I am indebted to my Co-Guide, Dr. Praful Singru, for helping me through the most crucial part of my Ph.D. journey. His unwavering motivation helped me overcome periods of procrastination, and his insightful suggestions were invaluable in the writing process.

I express my deep appreciation to my Doctoral Committee members, Dr. Sanjib Kar (Chairman), Dr. Harapriya Mohapatra, Dr. Ramanujam Srinivasan, and Dr. Dileep Vasudevan for their valuable suggestions during our meetings. My Special thanks to Dr. Ramanujam Srinivasan for valuable suggestions during my Ph.D. journey and for giving me opportunities to work in his lab. I would like to thank Dr. Sanjita Banerjee for her timely guidance and suggestions during my experiments, thesis, and manuscript writing, as well as for her moral support. I am also grateful to Professor Richa Rikhy, IISER Pune, for allowing me to learn fly husbandry and genetics in her lab during the starting phase of my Ph.D. I also thank Dr. Swagata Ghatak for her guidance and support.

I am immensely grateful to Mr. Shubham Kumar for his valuable contributions to this project. Working with him during his Master's thesis was a privilege, and his assistance with the image

analysis part was immensely helpful. My gratitude also extends to all the past and present RMRS lab members for fostering a supportive and cheerful environment. I must acknowledge the supportive seniors, Dr. Bimal, Dr. Supriya, Dr. Cyrus, and Dr. Gururaj. To my dear friends Dipika, Saumya, Victor, Ajay, Natasha, Deepshikha, Sakshi, Nibedita, Sonia, Vineet, Tejus, Jyoti, Navita, Madhu, Roman, Shubham, Devanand, Mimansha, I am truly appreciative of your moral and emotional support. Special thanks to Dipika and Saumya for being pillars during the initial lab setup phase. Dipika, your listening ear and cheerful jokes have been a source of solace throughout this journey.

I extend my thanks to the NISER microscopy facility, especially to Dr. Chandramohan, for providing access to the microscopes without time constraints and for his immense help in scope maintenance. My gratitude also goes to Dr. Richa Rikhy, Dr. Krishanu Ray, Dr. Maithreyi Narasimha, Dr. Pralay Majumder, Dr. Romain Levayer, Dr. Basim Hasan, BDSC, VDRC, NCBS, and EMBL for providing fly stocks. I deeply thank NISER for offering state-of-the-art research facilities and fostering a vibrant scientific environment. Additionally, my gratitude extends to DAE for supporting my fellowship.

I am fortunate to have a supportive family, and I sincerely thank them for their unconditional love and support. Special thanks to my brother, Rolin, for being both the best brother and a supportive friend. I also want to thank my mother for standing by me in difficult times. Lastly, I hold my beloved grandfather, 'Dadu,' in my heart, who has always been my inspiration and whom I lost during this Ph.D. journey. To those whose names I have not mentioned, you know who you are, and I am grateful for your contributions to my journey. Thank you all.

I would like to end by quoting Nelson Mandela, which I think is appropriate for completing this journey.

**“IT ALWAYS SEEMS IMPOSSIBLE UNTIL IT IS DONE”**

## CONTENTS

<b>SUMMARY .....</b>	<b>i</b>
<b>SYNOPSIS .....</b>	<b>iv</b>
<b>LIST OF FIGURES .....</b>	<b>x</b>
<b>LIST OF TABLES .....</b>	<b>xiii</b>
<b>LIST OF ABBREVIATIONS .....</b>	<b>xiv</b>
<b>CHAPTER 1: INTRODUCTION.....</b>	<b>1</b>
<b>1.1. General Introduction .....</b>	<b>2</b>
1.1.1 Epithelia .....	4
1.1.2 Hallmarks of Classical epithelium .....	4
1.1.2.1 Apical Domain .....	6
1.1.2.2 The apical-lateral junctions .....	7
1.1.2.3 Tight Junctions .....	8
1.1.2.4 Adherens junctions (AJ).....	9
1.1.2.4.1 Types of AJs.....	11
(a) Zonula adherens .....	11
(b) Lateral Adherens junction .....	11
(c) Spot adherens junction.....	14
(d) Punctate adherens junction .....	15
1.1.2.4.2 Core complexes of Adherens junction .....	16
(a) E-Cadherin .....	16
(b) Catenins .....	17

(c) Rho GTPases at Adherens junction .....	18
1.1.2.3 The basolateral domain .....	20
(a) Septate junction.....	21
1.1.2.4 The basal domain .....	22
1.1.3 Tubular epithelial organs .....	22
1.1.4 <i>Drosophila</i> trachea: a tubular epithelium.....	24
1.1.5 Development of tracheal epithelium .....	25
1.1.6 Epithelial degeneration in the development .....	31
1.1.7 Tracheal degeneration during metamorphosis is an excellent model for studying epithelial degeneration. ....	33
<b>1.1.8 Aims and Objectives of the thesis .....</b>	<b>37</b>
<b>1.1.9 Relevance of the Study .....</b>	<b>38</b>
<b>CHAPTER 2: MATERIALS AND METHODS .....</b>	<b>40</b>
<b>2.1 Materials .....</b>	<b>41</b>
2.1.1 Fly stocks.....	41
2.1.2 Antibodies .....	44
2.1.3 Dyes and stain .....	48
2.1.4 Chemicals and buffers .....	48
2.1.5 Solutions.....	50
<b>2.2 Methods.....</b>	<b>51</b>
2.2.1 General fly husbandry .....	51

2.2.1.1 Preparation of <i>Drosophila</i> media .....	51
2.2.1.2 Preparation of apple juice agar plates .....	52
2.2.2 Fly Genetics and Crosses .....	53
2.2.3 UAS-Gal4 Binary system.....	53
2.2.4 RNAi of genes in the <i>Drosophila</i> trachea by using breathless Gal4.....	55
2.2.5 Synchronized Embryo collection cage setup .....	56
2.2.6 Developmental staging .....	57
2.2.7 Embryo Fixation and Immunostaining.....	58
2.2.8 First instar larval dissection.....	59
2.2.9 Larval and pupal dissection by ventral filleting method .....	59
2.2.10 Immunostaining .....	60
2.2.11 Dissection and immunostaining of other larval tissue .....	60
2.2.12 aECM staining .....	61
2.2.13 Phalloidin staining .....	61
2.2.14 Image Acquisition, Processing, and Quantitation .....	61
2.2.15 Line-plot analysis .....	62
2.2.16 Enrichment analysis of Rho and CDC42 at LAJ.....	62
2.2.17 Directionality analysis.....	62
2.2.18 Length Calculation and posterior tracheal compression analysis .....	63
2.2.19 Inter-taenidial spacing calculation .....	64
2.2.20 Microtubule orientation calculations.....	64

2.2.21 Colocalization of shot and microtubule ..... 64

**CHAPTER 3: LATERAL ADHERENS JUNCTIONS (LAJs) AND ASSOCIATED  
ACTOMYOSIN CORTEX MECHANISMS IN THE TRACHEA OF *DROSOPHILA  
MELANOGASTER*..... 66**

**3.1. Introduction ..... 67**

**3.2. Results ..... 70**

3.2.1 Identification of a novel lateral adherens junction in *Drosophila* larval tracheal dorsal trunk epithelium ..... 70

3.2.2 Characterization of the lateral adherens junction (LAJs) in *Drosophila* larval tracheal dorsal trunk epithelium..... 74

3.2.3 Lateral adherens junctions are present in all larval and pupal stages..... 78

3.2.4 LAJs in other *Drosophila* tissues ..... 79

3.2.5 Distinct actin cortices were associated with both ZA and lateral adherens junctions. 82

3.2.6 Lateral adherens junction mediates a supracellular actin cortex ..... 85

3.2.7 Actin fibers near intersegmental junction ..... 86

3.2.8 Supracellular actin cortex is an actomyosin mesh ..... 86

3.2.9 Rho-GTPases and the Arp- WASP axis are required for generation of the LAJC ..... 88

3.2.10 Supracellular actomyosin cortex redundantly contributes to organ shortening in the posterior trachea ..... 95

3.2.11 Tracheal tube compression induces actin blebs in the posterior pupal DT ..... 98

3.2.12 Differential cytoskeletal arrangement in *Drosophila* pupal tracheal epithelium .... 102

**3.3. Discussions ..... 107**

**CHAPTER 4: SPECTRAPLAKIN SHORTSTOP MEDIATES SUPRACELLULAR  
ACTIN AND MT CROSS-TALK IN POSTERIOR PUPAL TRACHEA. .... 112**

**4.1 Introduction ..... 113**

**4.2 Results ..... 117**

4.2.1 A basal mesh of microtubules form in posterior pupal trachea..... 117

4.2.2 The basal MTs are stable and mostly acetylated..... 122

4.2.3 Actin supracellular cables and MT alignment in posterior pupal DT cells are distinct  
yet concurrent events..... 126

4.2.4 Spectraplakín Shortstop mediates actin-MT cross talk ..... 128

4.2.5 Mnat9a is essential for Shot binding to Actin-Microtubules. .... 134

4.2.6 Microtubules stabilize actin supracellular cortex in *Drosophila* pupal DT. .... 135

**4.3 Discussions ..... 137**

**CHAPTER 5: BASAL EXTRACELLULAR MATRIX REMODELS IN *DROSOPHILA*  
PUPAL TRACHEA ..... 140**

**5.1 Introduction ..... 141**

**5.2 Results ..... 146**

5.2.1 Basal ECM remodeling in *Drosophila* posterior pupal DT ..... 146

5.2.2 Remodeling of basal Extracellular Matrix starts around the cell boundary in ML3. 148

5.2.3 Basal ECM remodeling and supracellular actin bundle formation follow the same

developmental window .....	149
<b>5.3 Discussions .....</b>	<b>153</b>
<b>CHAPTER 6: CONCLUSION.....</b>	<b>155</b>
<b>REFERENCES.....</b>	<b>159</b>

## SUMMARY

Epithelial tissue is the most studied tissue type in metazoans to understand tissue architecture and organogenesis. Epithelial cells exhibit apicobasal polarity and adhere to adjacent cells and the extracellular matrix via adhesion molecules to shape organs, form boundaries, and help in barrier function. Tightly regulated cellular processes mediate the formation and maintenance of polarized epithelium. The epithelial architecture is maintained by global and local force generation and transmission, which are orchestrated by adherens junction proteins and the associated actomyosin cortex during organogenesis. Organ formation has been well studied, although organ degradation is equally important. The degenerating processes involved in altering epithelial topology contribute to organ degradation or, eventually, shortening. All three layers of the epithelium are involved in degenerating processes during organ deformation. We studied degenerating epithelia, focusing on junctional components and associated cytoskeletal proteins, during metamorphosis, using the *Drosophila melanogaster* respiratory system (trachea) as our model.

We identify that the *Drosophila* tracheal epithelium has a non-canonical belt of lateral punctate E-cadherin molecules in addition to the classical zonula adherens (ZA). Lateral punctate E-cadherin molecules are present below the septate junction, close to the basal edge of the broad Dlg domain, throughout the larval and early pupal stages. These lateral adherens junctions (LAJs) encircle the cells in the lateral membrane basal to the ZA and are functional, having all ZA components, that is,  $\alpha$  catenin,  $\beta$ -catenin, and p120 catenin. The LAJs are active receptor complexes. Two distinct actomyosin cortices are associated with the ZA and LAJs. Both cortices show differential actin organization from the larval to pupal phase. The lateral

adherens junction-associated actin cortex (LAJC) transforms into a supracellular actomyosin mesh in late larvae. Starting from the Mid L3(110h) larva, actin bundles start from the LAJs and the cytoplasm. In wandering L3 (115h), a thick lateral pericellular F-actin belt forms at the LAJs, providing a scaffold for incorporating cytoplasmic actin extensions. The actin cables become longer, denser, and continuous, progressively connecting across cell boundaries and thus becoming supra-cellular throughout the 0h and 1h pupa. The F-actin belt disappears in 1h pupa. LAJs are present throughout the process. Actin organizers Rho1 and CDC42 are present at lateral E-cadherin contacts, which regulate the initiation of the basal actin cortex in the third instar larval trachea (L3). Knockdown of Rho1, CDC42, ROK, Sqh, ARP, and WASP in the trachea showed reduced basal F-actin, suggesting that the Rho1-ROK-MRLC and CDC42-ARP-WASP pathways independently regulate basal actin cortex formation.

This supracellular network alternate bands of  $\alpha$ -actinin and phospho-myosin accumulate on the cables, confirming the formation of stress fibers along the AP axis of the dorsal trunk in early pupae. These stress fibers contribute to force generation and transmission, thus facilitating tissue compression by aECM remodeling in the posterior pupal trachea in the early pupa.

Furthermore, we investigated the relationship between the LAJs and microtubules. Microtubules also show a similar pattern of supracellular arrangement in the early pupal stages, which coincides with actin events. The spectraplakin group of proteins crosslinks the microtubules with the actin cortex. We found that shortstop(shot), the only spectraplakin in *Drosophila*, mediates actin microtubule crosstalk during supracellular cable formation. In the early larval stages, shot is enriched in the apical membrane near the taenidial F-actin rings and at the LAJs. Shot enrichment at the LAJs showed an active interaction between actin and

microtubules. Overexpression and loss of function of Shot lead to disruption of both taenial actin and LAJC in the early larval stages. Shot binds to both actin and microtubule in 1h pupa, promoting the supracellular actin arrangement. Knockdown of shot leads to disruption of actin and microtubule arrangement in 1h pupa. However, disruption of microtubule arrangement by knockdown of microtubule plus end binding protein Eb1 and minus-end binding protein Patronin showed less altered supracellular actin cortex. Shot tends to bind to stable acetylated microtubules. Microtubule-associated N-acetyl transferase 9(Mnat9) facilitates N-terminal acetylation of both alpha and beta tubulin. Disruption of microtubule stability by Mnat9 knockdown disrupts shot activity, microtubule arrangement, and actomyosin cortex.

To understand the basal extracellular matrix behavior and its relationship with the actomyosin cortex, we examined the basal ECM (bECM) component collagen (Viking) and found that bECM is severely sheared in pupae, indicating a delamination event in *Drosophila* tracheal DT. We also analyzed integrin, given their role in mechanosensing. In Early L3, integrin distribution is uniform, whereas the onset of pupation shows punctate integrin, which is localized around LAJs. In 6h pupa, integrin becomes highly punctate and irregular. The timeline of bECM remodeling phenotypes coincides with actin-bundling events, thus suggesting a supportive role.

This study is the first to identify and characterize the in vivo existence of LAJs in the *Drosophila* tracheal epithelium. The LAJs contribute to force generation via LAJC, which redundantly supports aECM-mediated tracheal compression in early pupae. We also showed the cytoskeletal arrangement and extracellular matrix behavior during the larval-to-pupal transition, which provides insight into other functional roles of LAJs and the associated LAJC.

## SYNOPSIS

Epithelia is the most studied metazoan tissue type to understand tissue architecture during development and organogenesis. It is composed of cells attached to each other by adhesion molecules. These cells are arranged on the extracellular matrix via focal adhesions or dot junctions. The epithelium protects and shapes organs, acts as a barrier, and sets boundaries. It has three domains: apical, lateral, and basal. Establishing apicobasal polarity and maintaining the above three domains are key cellular processes in development (C. E. Buckley & St Johnston, 2022).

The *Drosophila* respiratory system(trachea) is a network of ramified tubes with varied architecture that helps transport oxygen to different target tissues (Bate & Arias, 1993; G. & A, 1993; Loganathan, Cheng, & Andrew; Wigglesworth). It has been used extensively to understand tubular epithelial architecture, its development, and disassembly (F. Chen & Krasnow, 2014; Fraire-Zamora, Tosi, Solon, & Casanova, 2021). The cells in the tracheal epithelium are attached to each other via homophilic cadherin molecules at the adherens junction. Below the adherens junctions, septate junctions are present in the basolateral region of the lateral membrane. Different polarity proteins are distributed in the three domains of the tracheal cells. Crumbs-Par3-Stardust are present at the apical domain, E-cadherin and Catenins are present at the adherens junctions below the apical domain, and Scrib-Dlg-Lgl are present in the lateral domain (C. E. Buckley & St Johnston, 2022). Adherens junctions are associated with the actomyosin cortex. *Drosophila* trachea is a specialized epithelium with two extracellular matrices. One is the apical ECM, which is secreted by tracheal cells and is composed of polysaccharide chitin and glycoproteins, and the basal extracellular matrix is composed of collagen, perlecan, nidogen, and laminin.

Tracheal development is complex and intriguing. During embryogenesis from ten epithelial placodes, a complete trachea is formed (Hayashi & Kondo, 2018). The largest of these is the dorsal trunk (DT), a multicellular tubular structure. The branches that emerge from DT are unicellular and subcellular. The signalling processes involved in post-embryonic and larval (1st, 2nd and, 3rd instar) branching morphogenesis are the same (Hosono, Matsuda, Adryan, & Samakovlis, 2015). These mechanisms regulate radial and axial length increases and the patterning of the tubular epithelium. During metamorphosis, half of the posterior DT (tr-6-tr8) gets degenerates. The larval trachea is replaced by a temporary pupal trachea, followed by a de novo formed adult trachea in the late pupa. Organ disassembly occurs in late pupae by larval cell apoptosis. Chen et al. showed that, during metamorphosis, the posterior trachea is replaced by progenitor cells that are regulated by an FGF-mediated morphogen gradient secreted by decaying cells (F. Chen & Krasnow, 2014). Zamora et al. showed that tracheal tube shortening occurs through an aECM-mediated remodelling process (Fraire-Zamora et al., 2021). Caspase-3 mediated cell death in the posterior tracheal cells is the final step in organ degradation.

Degenerating larval DT in pupae provides an excellent model for studying programmed epithelial degeneration at the cellular level. A detailed information regarding the subcellular and supracellular changes during epithelial degeneration is missing. We investigated degenerative changes in all three layers of *Drosophila* pupal DT at subcellular level and obtained some exciting results. We examined the junctional, cytoskeletal, and extracellular matrix phenotypes in this study.

There are five chapters in the thesis. Chapter one is the introduction, a brief review of the

available literature that introduces the central idea of the thesis, i.e., cellular mechanisms in epithelial degeneration. The introduction summarises the research on the junctional, cytoskeletal, and extracellular matrix mechanisms involved in *Drosophila melanogaster* development and degeneration. The study focuses on the theme of cellular processes in the metamorphic trachea of *Drosophila melanogaster*. The second chapter describes the reagents, materials, and protocols used for the study. It includes the list of fly lines with genotypes and source information, antibodies and chemicals used, and detailed protocols. The results of the study are described in the remaining 3-5 chapters. Each chapter has distinct objectives. The discoveries provide information about cellular and supracellular mechanisms involving junctional, cytoskeletal, and extracellular matrix alterations that occur in the tracheal epithelium during metamorphosis.

Chapter 3 describes the *in vivo* existence of novel lateral E-Cadherin junctions (LA) similar to the classical adherens junction and its function. In this part of the work, we have identified a non-canonical belt of lateral punctate E-cadherin molecules in addition to the classical zonula adherens (ZA) in the *Drosophila* tracheal epithelium. LA was present in the tracheal epithelium throughout the larval and pupal stages. Adherens junction component E-cadherin had two pools, clearly showing a very tight belt like ZA and another layer of lateral punctate E-cadherin present below the septate junction near the Dlg domain. LA had all the ZA components, i.e., armadillo,  $\alpha$ -catenin, and p120 catenin. Two distinct actomyosin cortices were present in ZA and LA. Actin organizers small GTPases, Rho1, and CDC42 present at the lateral cadherin junctions regulate the initiation of basal actin cortex formation in the third-instar larval trachea (110h AEL). It is known that Catenin and actin organizers are important

players in maintaining the actin cortex (Ratheesh & Yap, 2012). Assembly of the junctional actin cortex is a key function of the E-cadherin cytoplasmic domain (Mason, Tworoger, & Martin, 2013). This junction-associated actomyosin cortex is crucial for force generation during organ formation (Levayer & Lecuit, 2013; Röper, 2013; S. K. Wu & Yap, 2013). We looked at the functional aspect of lateral junction-associated actomyosin cortex (LAJC). The LAJC organization started progressively from the LA and perinuclear space in the MidL3 larva. In WL3 a thick lateral pericellular F-actin belt was formed, which act as a scaffold for the incorporation of cytoplasmic actin extensions. The actin extensions grew longer thicker and denser in late larval and early pupal stages and transformed in to thick supracellular cables in 1h pupa. Actin organizers Rho1 and CDC42 were present at LA, which regulated the initiation of the basal actin cortex. Knockdown of Rho1, CDC42, ROK, Sqh, ARP, and WASP in the trachea showed reduced basal F-actin, suggesting that basal actin cortex formation is independently regulated by the Rho1-ROK-MRLC and CDC42-ARP-WASP pathways. Accumulation of  $\alpha$ -actinin and phospho-myosin on the supracellular bundles indicated the formation of stress fibres. These stress fibres facilitated tracheal tube compression redundantly by aECM remodelling in the posterior pupal trachea in the early pupa.

In chapter 4, we investigated the interaction between microtubules and LAJs. In early pupal stages, microtubules have a supracellular arrangement pattern that is comparable to actin events. Microtubules and the actin cortex are crosslinked by a protein family called spectraplakins. Loss of spectraplakins has been demonstrated to have notable impacts on cell adhesion, cell polarity, microtubule organisation, and cell shape in vivo (Röper, Gregory, & Brown, 2002; Suozzi, Wu, & Fuchs, 2012). *Drosophila* possesses a single spectraplakins that is

encoded by short-stop (shot) (Gregory & Brown, 1998; Röper et al., 2002). Shot binds to microtubule and helps in microtubule actin cross-linking contributing to the cytoskeletal organization (Applewhite et al., 2010; A. J. R. Booth, G. B. Blanchard, R. J. Adams, & K. Röper, 2014).

We discovered that *Drosophila*'s sole spectraplakin, shortstop (also known as shot), promotes actin-microtubule crosstalk while creating supracellular cables. Shot was more abundant in the early larval stages at the LAJs and close to the taenidial F-actin rings in the apical membrane. Actin and microtubules were found to be actively interacting through shot enrichment at the LAJs. In the early larval stages, disruption of taenidial actin and LAJC was caused by overexpression and loss of function of Shot. Shot promotes the supracellular actin arrangement by binding to both actin and microtubules in the 1h pupa. In 1h pupa, shot knockdown disrupted the organization of actin and microtubules. Shot is prone to bind to acetylated microtubules that are stable (Ricolo & Araujo, 2020). N-terminal acetylation of alpha and beta tubulin is made possible by the enzyme microtubule-associated N-acetyl transferase 9 (Mnat9) in *Drosophila*. Shot activity, the architecture of the microtubules, and the actomyosin cortex were all affected when Mnat9 was knocked down in the trachea. To understand the relation between actin cortex and MT arrangement we disrupted MT organisation by Eb1 and Patronin KD. Disruption of the microtubule arrangement revealed less altered supracellular actin cortex. Disruption of actin cortex by ARP and WASP KD in 1h pupa also showed less affected MT mesh in 1h pupa.

Chapter 5 describes further about the ECM changes during tracheal metamorphosis. Collagen (Viking), a component of basal extracellular matrix (bECM), was examined to better understand the behaviour of the basal extracellular matrix and its relationship to the actomyosin

cortex. We discovered that bECM is severely sheared in pupae, indicating a delamination event in *Drosophila* tracheal DT. Given their importance in mechanosensing, we also studied talin and integrin. Integrin is distributed uniformly in Early L3, but it becomes punctate when pupation begins and is concentrated near LAJs. Integrin became very punctate and irregular in 6h pupa. Actin-bundling events and the timeframe of bECM degradation phenotypes coincides, suggesting a supporting function.

In summary, these studies identified the cellular and supracellular phenomena involved in epithelial degeneration using *Drosophila* trachea as a model. These data provide the first evidence of in vivo existence of lateral junction and its function in *Drosophila* trachea and several other cellular events related to the degeneration of tubular epithelium. The processes can provide light on the deteriorating epithelial alterations that take place in conditions that affect tubular organs.

## LIST OF FIGURES

**Figure 1.1:** Complexity of levels of organization in biological systems

**Figure 1.2:** Schematic of structure and function of simple epithelium.

**Figure 1.3:** Schematics illustrating the arrangement of apical junctional complexes in polarized insect and vertebrate epithelia.

**Figure 1.4:** Schematic representing the crystal structure of core adherens junction complex Cadherin-Catenin

**Figure 1.5** Model showing different types of adherens junctions.

**Figure 1.6:** Small GTPases at AJ

**Figure 1.7:** Schematic showing the resemblance of human lungs with *Drosophila* respiratory system.

**Figure 1.7:** *Drosophila* tracheal system in embryo

**Figure 1.8:** Timeline showing programmed cell death events in *Drosophila* development.

**Figure 1.9:** Schematics showing larval trachea and pupal trachea.

**Figure 1.10:** Schematics showing the degenerative pupal trachea.

**Figure 2.1:** UAS-Gal4 binary system

**Figure 2.2:** UAS-IR (Inverted Repeats)

**Figure 2.3:** Knockdown of genes in trachea using breathless Gal4 system

**Figure 2.4:** Timeline showing the developmental staging of the *Drosophila* larva and pupa

**Figure 3-1.** Identification and characterization of lateral adherens junction in *Drosophila* larval trachea

**Figure 3-2:** LAJs are present close to the basal membrane

**Figure 3-3:** LAJs are active cadherin receptor complexes

**Figure 3-4:** LAJs in embryo, larval trachea, body wall, salivary gland, and wing imaginal disc

**Figure 3-5:** The LAJC and the supracellular actin cortex

**Figure 3-6:** Filopodia-like actin extensions at the intersegmental junction

**Figure 3-7:** Rho1 and Cdc42 preferentially localize at LAJ

**Figure 3-8:** LAJ localized Rho-GTPases involved in the formation of the supracellular actin bundles

**Figure 3-9:** The supracellular actomyosin has stress fibers and redundantly contributes to organ shortening

**Figure 3-10:** Actin blebs form in the posterior DT cells during the acute tube compression phase

**Figure 3-11:** Differential actin bundle arrangement in anterior and posterior pupal trachea in 0h APF

**Figure 3-12:** Graphical representation of the supracellular actin cable-mediated tracheal tube compression

**Figure 4-1:** Basal MT mesh forms in *Drosophila* posterior pupal trachea.

**Figure 4-2:** The basal MTs are stable and mostly acetylated MTs.

**Figure 4-3:** The stable basal MTs follow parallel alignment like the supracellular actin cortex, indicating distinct yet concurrent events.

**Figure 4-4:** Spectraplakins Shortstop (shot) crosslinks actin and microtubule and is responsible for this parallel arrangement.

**Figure 4-5:** Spectraplaklin Shortstop (shot) unable to crosslink actin and microtubule in Mnat9 KD.

**Figure 4-6:** MTs stabilize the actin supracellular cortex

**Figure 5-1:** Schematic showing the interaction of Integrin receptor complexes with ECM proteins

**Figure 5-2:** Image showing the basal ECM and apical ECM during larval to pupal transition

**Figure 5-3:** Basal ECM remodels in the posterior pupal dorsal trunk

**Figure 5-4:** Basal ECM remodeling starts around LAJ in ML3

**Figure 5-5:** Basal ECM remodeling coincides with the actin dynamics in the early pupal trachea.

## **LIST OF TABLES**

**Table 2.1.1.1** Gal4 lines

**Table 2.1.1.2** UAS Reporter lines

**Table 2.1.1.3** RNAi lines

**Table 2.1.2.1** Primary antibodies

**Table 2.1.2.2** Secondary antibodies

**Table 2.1.3** Dyes and stains

**Table 2.1.4** Chemicals and buffers

**Table 2.1.5** Solutions

**Table 2.2.1.1** Preparation of *Drosophila* media

**Table 2.2.1.2** Preparation of apple juice agar plates

## LIST OF ABBREVIATIONS

aECM	Apical Extracellular Matrix
AEL	After Egg Lay
AJ	Adherens junction
APF	After Puparium Formation
aPKC	atypical Protein Kinase C
Arp2/3	Actin Related Protein 2/3
Baz	Bazooka
bECM	Basal Extracellular Matrix
bnl	branchless
BSA	Bovine serum Albumin
btl	breathless
Cora	Coracle
DB	Dorsal Branch
Dial	Diaphanous 1
Dlg	Disc large
DT	Dorsal Trunk
E-Cad	E-Cadherin
ECM	Extracellular Matrix
EGFP	Enhanced Green Fluorescent Protein

EL3	Early L3
Fas III	Fasciclin III
GFP	Green Fluorescent protein
L1	First Instar Larava
L2	Second Instar Larva
L3	Third Instar Larva
L3S	Stagnant L3
LAJ	Lateral Adherens Junction
LAJC	Lateral Adherens junction-associated actin cortex
LB	Lateral Branch
lgl	Large giant larva
LSM	Laser Scanning confocal Microscopy
MAGUK	Membrane-associated guanylate kinase
ML3	Mid L3
MLCK	Myosin Light Chain Kinase
MRLC	Myosin Regulatory Light Chain
MT	Microtubules
PA	Puncta Adherentia
PAJ	Punctate Adherens Junction
PAT	Pupal Abdominal Trachea
PBS	Phosphate Buffer Saline
PFA	Paraformaldehyde
PH-PLC	PH domain of PhosphoLipase C- $\delta$

Rho1	Rhomboid 1
ROCK	RHO-associated protein kinase
ROI	Region of Interest
SAJ	Spot Adherens Junction
Scrib	Scribble
SJ	Septate Junction
TC	Terminal Cell
WASP	Wiskott-Aldrich syndrome protein
W13	Wandering L3
ZA	Zonula Adherens
ZO	Zonula Occludens

# **CHAPTER 1**

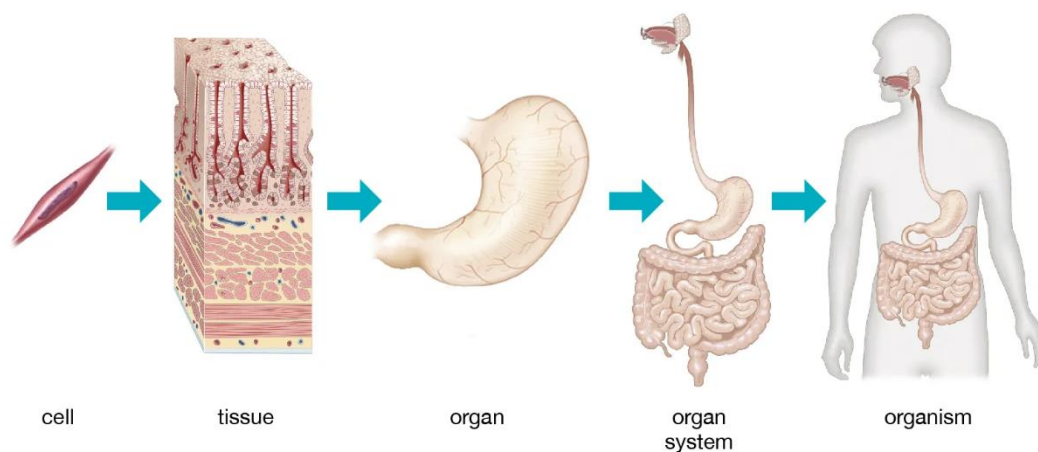
## **INTRODUCTION**

## 1.1 General Introduction

Cells are the fundamental units of life that execute diverse array of biological functions in living organisms. The diversity in their shape, size, and function makes each cell type unique. Cells are broadly categorized into prokaryotic and eukaryotic (Bruce Alberts et al., 2008). Prokaryotic cells, like bacteria, lack a distinct nucleus and other membrane-bound organelles. In contrast, eukaryotic cells, found in plants, animals, and fungi, have distinct nuclei and other membrane bound organelles. Eukaryotic cells are more complex than prokaryotic cells. The complexity extends further as eukaryotic cells organize into tissues to perform common functions. Epithelial, connective, muscular, and nervous tissues are the four broad classifications of tissue types. Epithelial tissues line interior cavities and cover the body's surface. They play a role in processes like secretion, absorption, and defence. Bone, cartilage, and blood vessels all belong to the category of connective tissues, which give the body structure and support. Movement is mediated by muscle tissues, which include skeletal, cardiac, and smooth muscle. Finally, nervous tissues, composed of glial cells and neurons, are involved in transmitting and processing information (B. Alberts, (2015)). To attain the intricate process of organ development, the cells constituting tissues must establish polarity and undergo a multitude of biological processes, such as cell division, cell death, shape alteration, cell migration, and differentiation. This process of complexity thus begins at the cellular level, progresses through the tissue, then organs, and culminates in the organism (T. Lecuit & Le Goff, 2007). **(Figure 1.1)**

Most of the organs in the human body are epithelial in origin. One of the examples is the skin, the largest epithelial organ made up of squamous epithelium and acts as a primary line of defence against the external environment and pathogens. Similarly, the lining of the intestine, respiratory tract, reproductive organs, and the excretory system comprises epithelial cells. It is responsible for essential activities, including the absorption of nutrients, gas

exchange, and waste elimination. Any disruption of these functions can severely impact our physiological and biochemical activities. Therefore, it is imperative to achieve an in-depth understanding of the design and functionality of the organs, and the biology of the underlying epithelia, to diagnose and treat various diseases and ailments effectively (B. Alberts, (2015); Bruce Alberts et al., 2008; Bryant & Mostov, 2008).



© Encyclopædia Britannica, Inc.

### **Figure 1.1: Complexity of levels of organization in biological systems**

Schematic illustrating how complex biological systems are organized. The building block of life is a single cell. Organs are formed by the arrangement of cells into functioning tissues. After that, multiple tissues form an organ system, and finally, an organism is created. (Image adapted from the Encyclopedia Britannica website)

### **1.1.1 Epithelia**

Epithelial tissue is the most ubiquitous tissue type in metazoans. Around 60% of mammalian cell types are epithelial or epithelial-derived, making epithelia the most archetypally polarised tissues in metazoa from an evolutionary perspective (Bruce Alberts et al., 2008). In an epithelium, the cells are attached to each other by cell junctions and arranged on top of a basement membrane. Focal adhesions or dot junctions act as the anchor between cells and the extracellular matrix. During organogenesis, the cells in epithelia are arranged, remodelled, or migrated to mould into stereotype shapes and forms to develop into an organ (Coopman & Djiane, 2016). The epithelial cells are organized into squamous or stratified lattice-like arrangements in the form of sheets to cover the external and internal sides of various organs for separating different environments or protection from the external environment. Epithelia also acts as a barrier to prevent or regulate the exchange of nutrients and macromolecules (Bryant & Mostov, 2008). The epithelium's role in protecting the organism from harmful chemical exposure and external infections is another crucial one. This function of epithelia depends on the proper positioning of the cell adhesion molecules to form impermeable septate junctions in insects and tight junctions in vertebrates. Apicobasal polarity is another crucial aspect of classical epithelium. Polarised secretion of the cargos, ECM proteins, ion channels, and signalling molecules highly depends on this. Thus, it is essential to maintain the integrity of the epithelia. The schematics of the epithelial architecture and functions are showed in **(figure 1.2)**.

### **1.1.2 Hallmarks of classical epithelium**

To understand the complexity of the epithelial organization, the epithelial tissue is broadly categorized into three distinct domains; apical, basal, and lateral domain (C. E. Buckley & St Johnston, 2022). The apical domain faces outside the tissue or organ or inside the lumen; the

lateral domain is attached to the neighbouring cells in an epithelium, and the basal domain connects the cell with the extracellular matrix. Different types of polarity proteins are distributed throughout these domains, demarcating three distinct regions (C. E. Buckley & St Johnston, 2022).

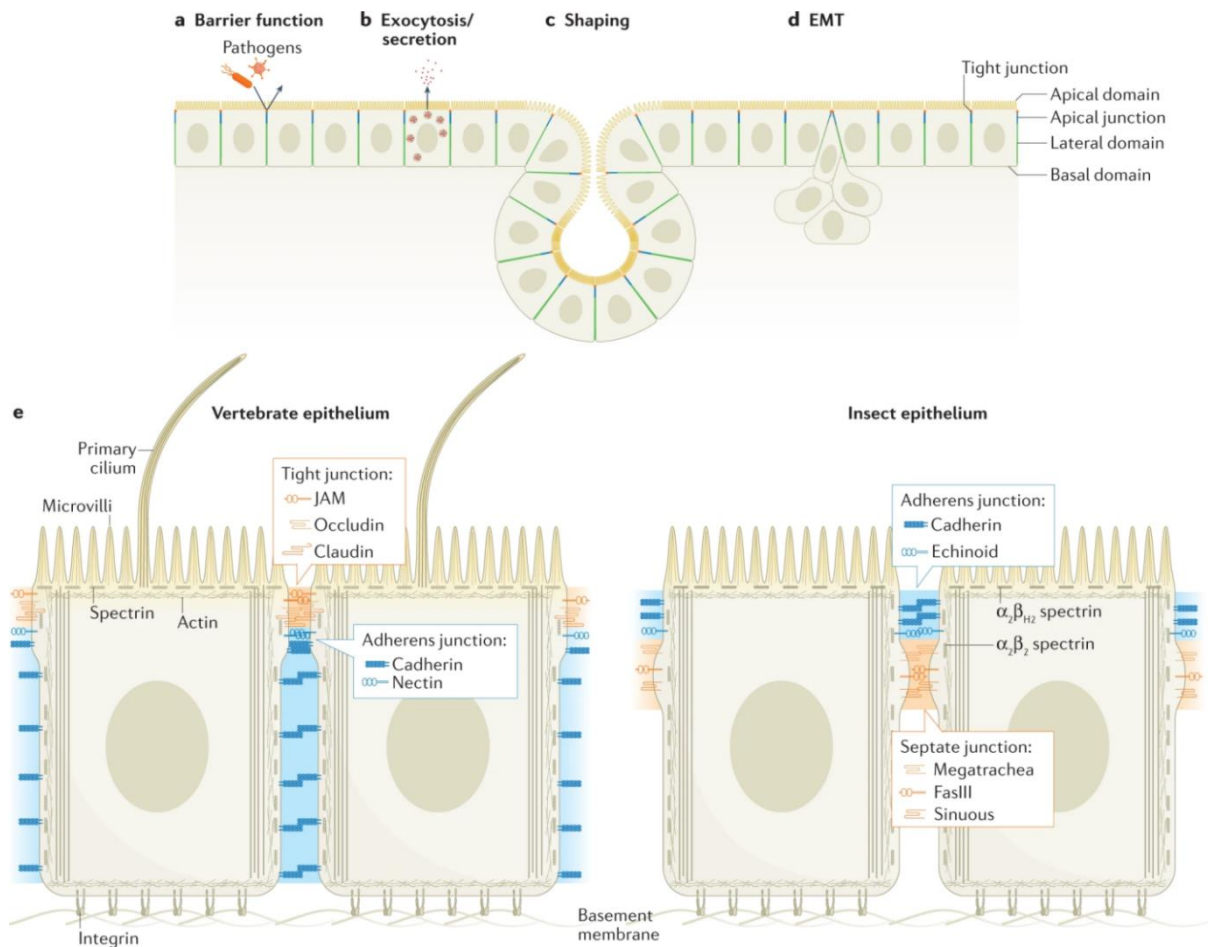


**Figure 1.2: Schematic of structure and function of simple epithelium.**

Diagram showing the structure and function of simple epithelium. (a, b, c, d) The epithelia play an important role in shaping the organs, takes part in secretion, act as a barrier from the external environment and pathogens. The epithelia have three domains, apical domain, apical junctions, lateral domain and basal domain. (e) The apical junctions consist of tight junctions, adherens

junctions etc. Lateral domain has lateral membrane and septate junctions or gap junctions. Basal membrane comprises of basal domain. Integrins and focal adhesion proteins present on the basal membrane interacts with the basement membrane. The image adapted from (C. E. Buckley & St Johnston, 2022)

### **1.1.2.1 Apical Domain**

The apical domain is defined by the distribution of certain proteins throughout the apical membrane. These proteins are called apical polarity proteins. The apical polarity marker proteins are the atypical protein kinase C (aPKC), PAR-6, CDC42, and the Crumbs complex proteins (C. E. Buckley & St Johnston, 2022). The crumbs complex is a conserved set of apical markers thoroughly distributed in the apical membrane consisting of MAGUK (Membrane associate guanylate kinase) family of scaffolding protein Stardust, PATJ, and LIN7 (Assémat, Bazellières, Pallesi-Pocachard, Le Bivic, & Massey-Harroche, 2008; Bulgakova & Knust, 2009). These apical polarity proteins play an essential role in maintaining vital cellular processes. Apical polarity protein aPKC phosphorylates Par-3 and lateral polarity markers Lethal giant larvae (lgl), Par-1, and Yurt to restrict them at the apical domain. Given this function, aPKC is regarded as the primary determinant of apical polarity (Betschinger, Mechtler, & Knoblich, 2003; Plant et al., 2003; T. Yamanaka et al., 2003). PatJ and Lin7 support apical polarity proteins, nevertheless (C. E. Buckley & St Johnston, 2022).

The apical domain is frequently absent in crumbs mutants of the *Drosophila*, but Crumbs overexpression extends the apical domain, thereby garnering Crumbs the appellation "apical determinant" (Campbell, Knust, & Skaer, 2009; Tepass, Theres, & Knust, 1990; Wodarz, Hinz, Engelbert, & Knust, 1995). However, not all cells require it to establish an apical domain. The survival or epithelial polarity of *C. elegans* is unaffected by a triple deletion of all three Crumbs orthologues (Waaijers, Ramalho, Koorman, Kruse, & Boxem, 2015). The fly embryonic

epithelia require Crumbs to maintain the apical-basal polarity. Knock down of Crumbs (CRB2 or CRB3) in the mice, the majority of epithelia are appropriately polarised, but their morphogenesis is impaired (C. E. Buckley & St Johnston, 2022).

### 1.1.2.2 The apical-lateral junctions

Cell-cell adhesion is characteristic of classical epithelium. This adhesion is maintained and coordinated by different types of cellular junctions in the metazoans. The apical junction in vertebrate epithelia is the tight junction, and in insect or fly epithelia, it is the adherens junction.

**(Figure 1.3)** Apart from cell adhesion, these junctions are crucial in defining a boundary between apical and lateral domains and act as a mechanical and biochemical signalling hub in the cell. The localization of Par-3 proteins regulates the position and formation of tight junctions in vertebrates in fly epithelia. The positioning of the adherens junction is determined by Bazooka (Par-3 in fly)(Morais-de-Sá, Mirouse, & St Johnston, 2010).

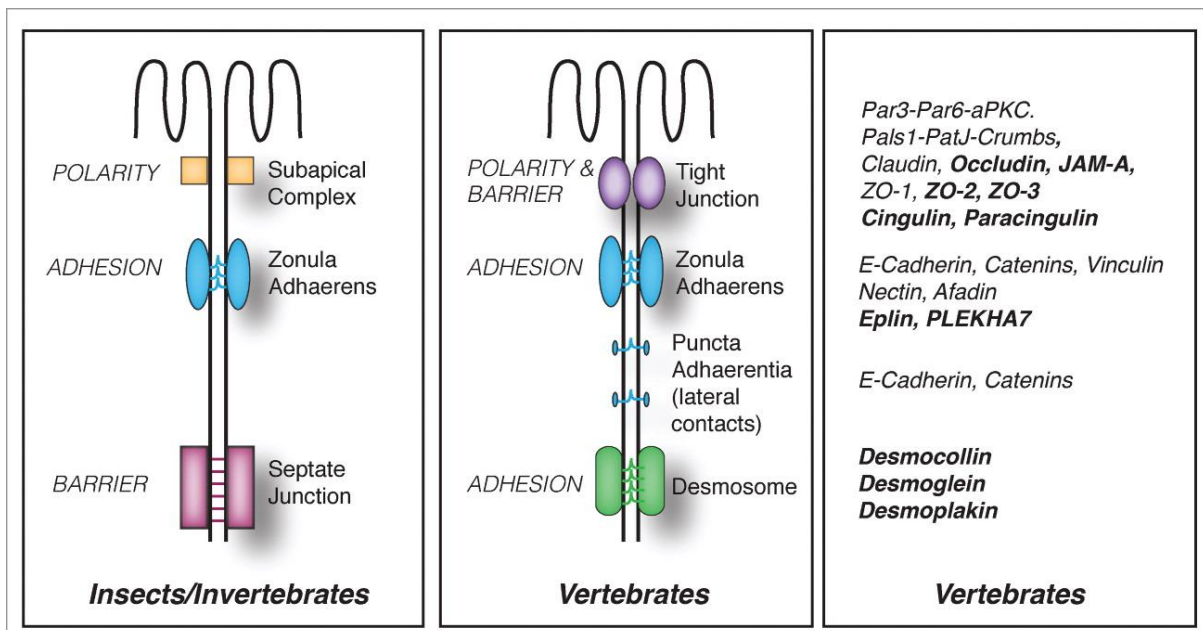


**Figure 1.3: Schematics illustrating the arrangement of apical junctional complexes in polarized insect and vertebrate epithelia.** On the left of each type of junction and the canonical functions are shown. The type of junctions are (sub-apical complex, zonula adhaerens (ZA), septate junction, tight junction, and desmosome). In Vertebrates, E-cadherin-based junctions are found along the lateral contacts of epithelial cells (puncta adherentia). A list of proteins linked to the junctions is displayed on the right. Bold text indicates proteins of vertebrate epithelia. The image is adapted from (Citi, Guerrero, Spadaro, & Shah, 2014)

### 1.1.2.3 Tight Junctions

Tight junctions or Zonula occludens (ZO) are the apical most junction in vertebrates. Apart from Par-3, the core tight junction proteins are nectin family proteins, afadin, and Zonula occludens proteins ZO-1 and ZO-2. Par-3 is required for the formation of tight junctions (Fanning et al., 2007; Ooshio et al., 2007; Umeda et al., 2006). Knockdown of these proteins in mouse mammary gland epithelia lead to disruption of Par-3 localization at tight junctions affecting its function. KD of only ZO-1 and ZO-2 shows that ZO-1 and ZO-2 play a role in Par-3 localization redundantly (Matsuzawa et al., 2021). The MAGUK family proteins help in Claudin assembly and interact with the components of tight junctions. The discovery that ZO proteins and Par-3 generate phase-separated condensates has recently shed new light on this intricate web of interconnections. The PDZ3-SH3-GUK domains of ZO-1 and ZO-2 oligomerize to produce condensates in substantial part (Beutel, Maraspini, Pombo-García, Martin-Lemaitre, & Honigmann, 2019). Other tight junction proteins found in these phase separated condensates include claudins, occludin, cingulin, and afadin. These proteins also connect directly to the actin cytoskeleton (Beutel et al., 2019). The anchoring, positioning and endocytic delivery of JAMs (Junctional Adhesion Molecules) are regulated by Par-3.

Interactions between JAMs with the underlying actin cytoskeleton are under the direction of PAR-3, which also places and stabilizes the apical junction. PAR-3 binds also to the nectins and JAM1-3 in mammals (Ebnet et al., 2003; Takekuni et al., 2003).

The concentration of claudins at tight junctions has a significant impact on the permeability of ions passing through the paracellular route. Claudins are responsible for creating selective openings that act as gates for ions within the paracellular diffusion barrier. Additionally, these junctions contribute to the segregation of the apical and basolateral cell surface domains in polarized epithelial cells, thereby maintaining cell polarity and preventing the intermixing of polarity proteins between these domains. Tight junctions are crucial for the regulation of signaling pathways involved in epithelial cell polarization and the development of distinct apical domains, which is a conserved process across evolution. They serve as bidirectional signaling platforms, receiving signals from the cell interior to regulate cell assembly and transmitting signals to the cell interior to control essential cellular processes such as proliferation, migration, and differentiation (C. E. Buckley & St Johnston, 2022; Rusu & Georgiou, 2020).

#### **1.1.2.4 Adherens junctions (AJ)-**

Adherens Junctions (AJs), a distinguishing characteristic of all epithelial sheets, are apical adhesive structures where the homophilic interactions of single-pass transmembrane E-Cadherin (E-Cad) molecules mediate and strengthen the close membrane apposition between neighbouring epithelial cells. The development of a dense actin filament-based cortical network, and in particular the molecular connections that bind E-Cad clusters to the inner cytoskeleton, stabilizes these structures (Baum & Georgiou, 2011; Coopman & Djiane, 2016; Harris, 2012; Harris & Tepass, 2010; K. Röper, 2015). There are currently four forms of AJ

known: Zonula adherens (ZA), Lateral AJ (LAJ), Punctate AJ (PAJ), and Spot AJ (SAJ)(S. K. Wu & Yap, 2013). Notably, these junction types have primarily been identified based on their morphology and organization pattern. However, their formation, core complexes, biochemical processes, and functions are extensively investigated by many scientists (S. K. Wu & Yap, 2013). The fundamental adhesion unit of AJs is E-Cadherin clusters. In the AJs, E-Cadherin clusters and their higher-order organization depend on the AJ-associated cytoskeleton.

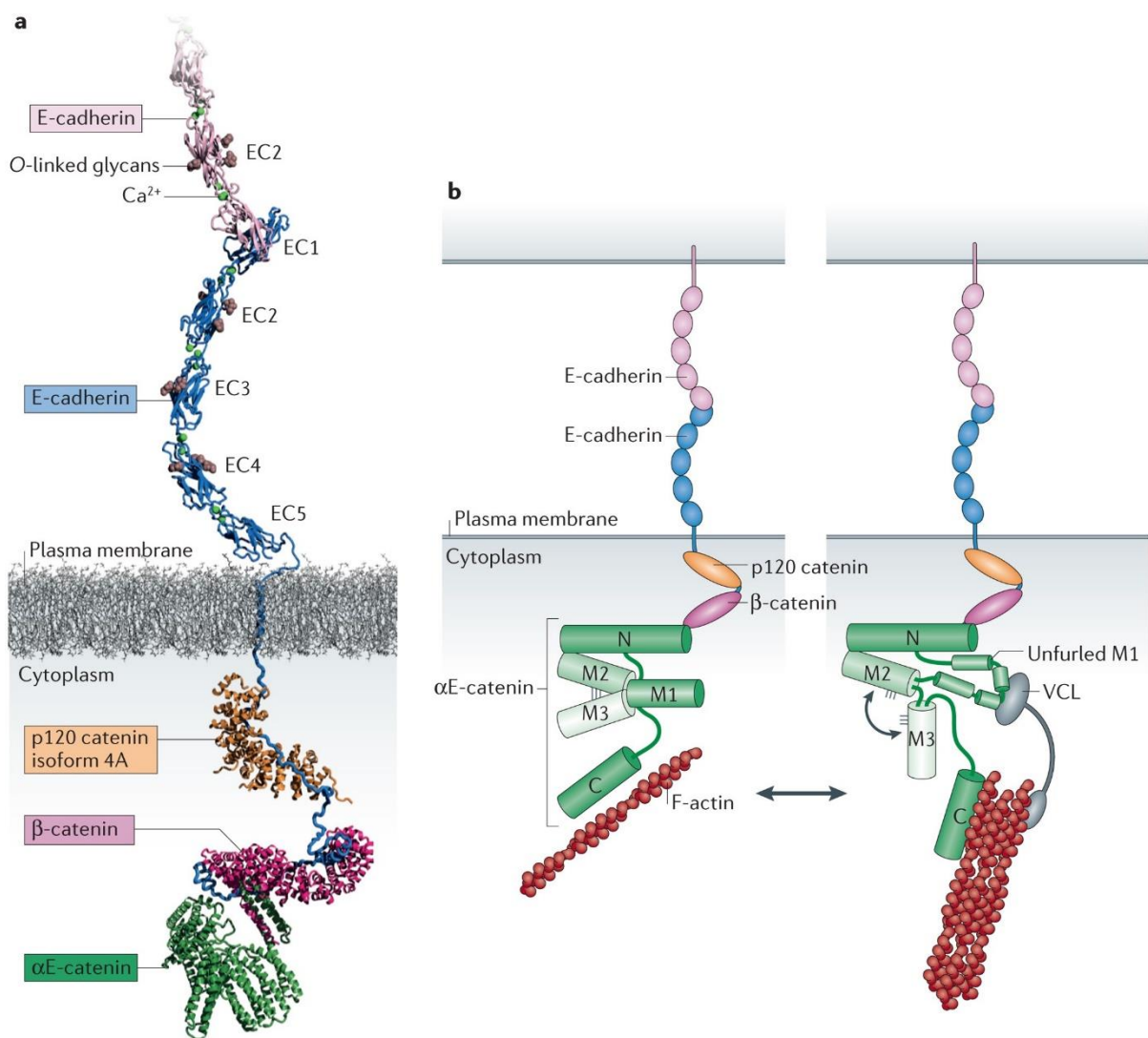


**Figure 1.4: Schematic representing the crystal structure of core adherens junction complex Cadherin-Catenin** (a) A model showing the AJ arrangement based on the crystal structures obtained from PDB. Image showing the five EC domains of E-Cadherin and other cytoplasmic domains interacting with p-120 catenin and β-Catenin. (b) A model showing the

two states of adherens junction. The interaction between Cadherin-catenin complex and F-actin is possible in presence of vinculin (VCL). Image adapted from (M. Takeichi, 2014)

#### **1.1.2.4.1 Types of AJs-**

##### **(a) Zonula adherens**

The Zonula adherens (ZA) is the most common type of adherens junction found in polarised epithelia as a dense, continuous band of E-Cadherin that spans the apical circumference of the cells (Miyaguchi, 2000; S. K. Wu & Yap, 2013). Initially, ZA was discovered as an electron-dense region between cells by Electron microscopy, which later was visualized as a ring-like band at the apical cell membrane by immunofluorescence microscopy (Farquhar & Palade, 1963; Hirokawa & Heuser, 1981; Meng, Mushika, Ichii, & Takeichi, 2008; Miyaguchi, 2000). Localization of ZA varies in vertebrates and insects. In vertebrates, ZA is present basal to the tight junctions, whereas, in insect epithelia i.e., in *Drosophila* epithelia, ZA is located at the starting of the lateral membrane below subapical complexes (Coopman & Djiane, 2016; Meng & Takeichi, 2009).

Junctional F-actin bundles are closely associated with the ZA E-Cadherin belt.. The F-actin bundles interact with the ZA E-Cadherin via the E-cadherin effector alpha-catenin. Catenins are the downstream effector proteins of E-cadherins. The F-actin bundles or ZA actin cortex plays an important role in force generation and transmission by closely acting with E-cadherin. Disruption of F-actin leads to junctional deformities or irregular E-cadherin dispersions(Cavey, Rauzi, Lenne, & Lecuit, 2008).

##### **(b) Lateral Adherens junction**

E-cadherin receptors are also found at other locations of epithelial cell-cell contacts, despite the fact that apical ZAs are conspicuous in basic epithelia, particularly when examined by

immunofluorescence microscopy. ZA is the primary AJ present in the simple epithelium, another prominent AJs found in the vertebrate epithelium (cell culture models) is lateral adherens junctions (LAJ). First, LAJs were discovered in cross-sections of rat colonic crypt tissue, where cadherin-catenin complexes had equally distributed over the lateral membrane of the cells(Larsson, 2006).Experiments using in vitro cell culture demonstrated that both primary and transformed cell lines included LAJs. Below the traditional ZA in cell lines, LAJs were a dispersion of E-cadherin clusters (Y. Kametani & M. Takeichi, 2007). LAJs form after the establishment of ZA in primary keratinocytes and Caco-2 cells (Vaezi, Bauer, Vasioukhin, & Fuchs, 2002). Actin-rich lateral contacts gradually form at the lateral region after initial contact below ZA and they protrude downward in an apical-to-basal direction under the control of rho associated protein kinase (ROCK)-dependent cortical contractility (Zhang et al., 2005). Lateral AJ then appear as the lateral interface expands suggesting that lateral AJ assembly coincides with, and may contribute to, growth in cell height (Vaezi et al., 2002).These lateral E-Cadherin junctions are highly dynamic and they flow from the basal to apical direction (Soonjin Hong, Troyanovsky, & Troyanovsky, 2013; Yoshiko Kametani & Masatoshi Takeichi, 2007; Priya & Yap, 2015; Vaezi et al., 2002).Lateral AJ associated actin cables were joined to trans-interacting E-cadherin molecules, which most likely represented adhesion clusters, and were embellished with non-muscle myosin II. E-cadherin promotes F-actin network assembly at lateral junctions by recruiting Arp2/3, similar to the situation at adherens junctions, as evidenced by the concomitant reduction of both the actin-nucleating Arp2/3 complex that localised at E-cadherin clusters and the accompanying lateral F-actin network upon reduction of E-cadherin expression. Wu et al noticed that N-WASP was being redistributed from apical domains to lateral junctions at the boundary between untransformed and transformed H-RasV12-expressing cells (Priya & Yap, 2015). This redistribution inhibited E-cadherin movements and enhanced lateral junctional tension, whereas tension at apical junctions was decreased, which

is consistent with N-WASP's role in stabilising actin. Additionally, lowering N-WASP expression in transformed cells made it more difficult for cells to extrude by reducing stress at lateral junctions (Yoshiko Kametani & Masatoshi Takeichi, 2007). Kametani et al suggested that cadherin flow might be a cell-cell contact sliding mechanism for cellular motility in cancer metastasis because it was particularly noticeable in altered cells (Yoshiko Kametani & Masatoshi Takeichi, 2007). According to them, cadherin flow was only detected in untransformed MDCK cultures when collective cell migration began during wound healing but not in confluent cultures (Yoshiko Kametani & Masatoshi Takeichi, 2007).

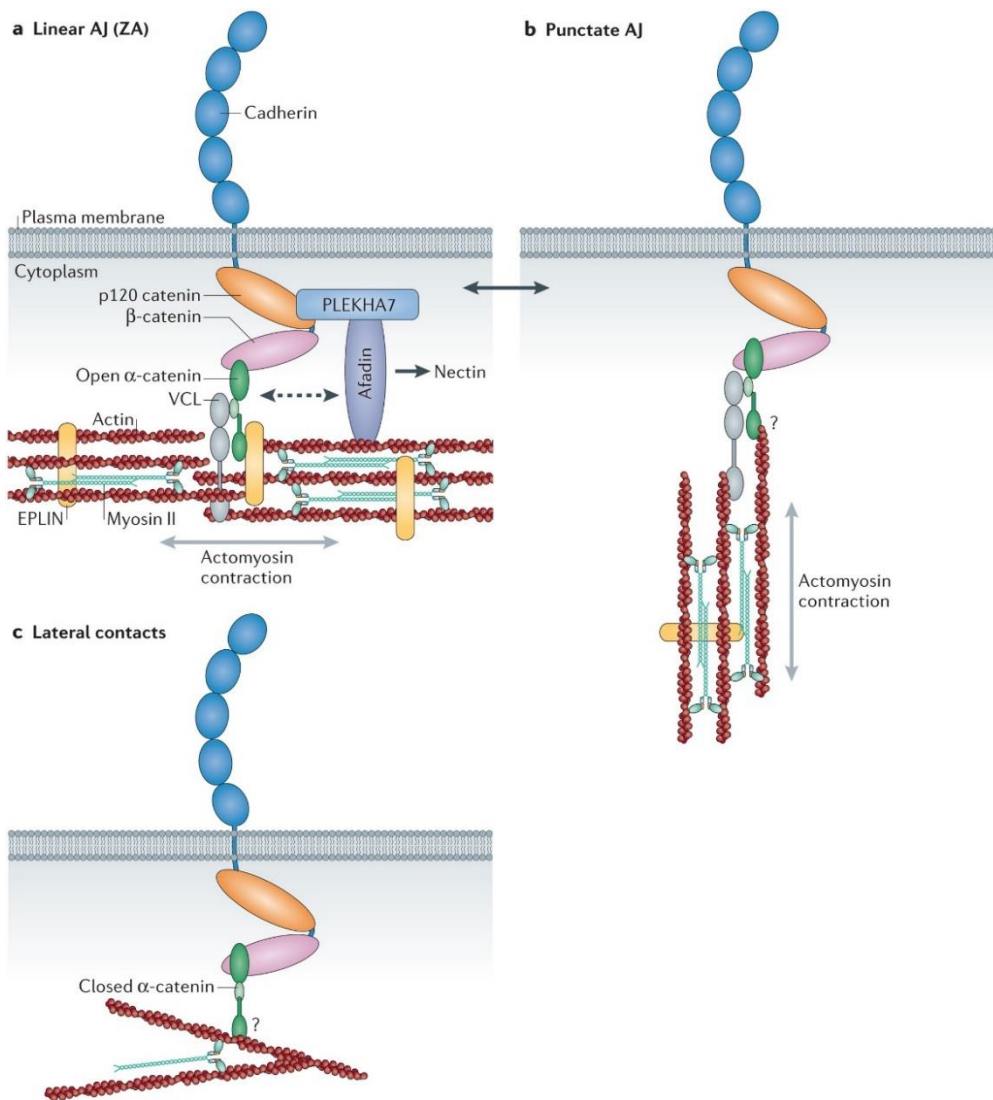


**Figure 1.5 Model showing different types of adherens junctions.** (a) Actin filaments run parallel to cell borders to form linear adherens junctions (AJs), which are also known as the zonula adherens (ZA). The dashed arrow indicates an indirect interaction between  $\alpha$ -catenin and afadin. (b) Punctate adherens junctions appear like puncta and are attached with actomyosin filaments via vinculin and catenins. (c) Lateral contacts or lateral adherens junctions are non-specialised contacts found below the ZA. Image adapted from (M. Takeichi, 2014).

### **(c) Spot adherens junction**

The conspicuous areas of E-cad accumulation close to the apical cell connections were called spot adherens junctions (SAJ). In the early and mid-embryonic stages of *Drosophila melanogaster*, these spot junctions were originally discovered close to the apical membrane (Tepass & Hartenstein, 1994). Subsequent immunofluorescence investigation using DE-Cadherin showed that they were associated with significant DE-cadherin spots found in the apical-most region of cell-cell interactions (Cavey et al., 2008; Tepass, 1996). SAJs are initially transient or present for a brief period of time. In the posterior endoderm and ectoderm, SAJ concentrates at apical cell-cell junctions during and immediately after gastrulation and eventually merge into the continuous ZA (Cavey et al., 2008; Tepass & Hartenstein, 1994). Nevertheless, distinct, high-intensity foci of transgenically expressed DE-cadherin-GFP may still be seen within the ZA even after fusion. Based on FRAP (Fluorescence recovery after photobleaching) data, these are cadherin foci that are stable, as opposed to the cadherin population that is distributed throughout the rest of the ZA, which is characterized by a higher rate of turnover. In contrast to the remainder of the ZA, which was lost, it is remarkable that these SAJs continue to exist at junctions even after Latrunculin A inhibits F-actin polymerization (Cavey et al., 2008).

#### **(d) Punctate adherens junction**

PAJs are described as emerging points of contact where elongated bundles of F-actin, oriented towards the plasma membrane, are linked to concentrated patches of E-cadherin. During the initial stages of cell contact formation, multiple clusters of E-cadherin form along the growing interface and promptly engage with small bundles of actin filaments aligned perpendicular to the plasma membrane (Taguchi, Ishiuchi, & Takeichi, 2011; Yonemura, 2011). As contacts lengthen, more PAJs are formed at the contact's margins, increasing the density of PAJs (Yamada & Nelson, 2007). The ZA is established by the ensuing rise in E-cadherin density at junctions. As a result, the actin cytoskeleton is reorganized, with bundles now oriented parallel to the cell-cell connections. Additionally, the recruitment of the actin-binding protein epithelial protein lost in neoplasia (EPLIN) correlates with the contraction of numerous PAJ at the same time during wound closure which in turn correlates E-Cad with actin (Abe & Takeichi, 2008; Taguchi et al., 2011). At the apical region of cell-cell contacts in a colony of EpH4 cells, the ZA, which is situated inside the colony, is covered with circumferential actin filaments. Through the colocalization of E-cadherin with these actin filaments, the zonula adherents (ZA) are organized. E-cadherin is observed at lateral cell-cell connections (LAJs) below the ZA, where it overlaps with amorphous actin networks, which are typically depicted as tilted intercellular boundaries. Punctate AJs are located near the border of the cell colony. When actin filaments perpendicularly terminate at plasma membranes, they drag E-cadherin puncta (Masatoshi Takeichi, 2014). In A431 cells, the PAJs are micrometre-sized adhesion structures made up of tightly and loosely packed cadherin regions. Additionally, it is shown that non-junctional cadherin is mainly monomeric. A small percentage of the cadherin molecules in PAJs were labelled using two distinct methods, and that allowed scientists to demonstrate that these structures are continually and entirely rebuilt in a sub-minute period. According to a dynamic model of AJs proposed by both structural biology studies and live imaging findings, AJ

plasticity is based on controllable actin filament-driven instability of the intra-junctional cadherin adhesive clusters (I. Indra et al., 2018). The two different sections that make up PAJ-associated actin bundles are the bundle stalk (AJ-BS) and the tip (AJ-BT), which is situated in between the stalk and cadherin clusters. The actin-bundling protein calponin is absent from the tip, and it has a substantially higher rate of F-actin turnover, two features that set it apart from the stalk. Although the F-actin in the stalk moves centripetally, it is static in the tip. The cadherin cluster stability, which is controlled by F-actin, is necessary for the F-actin turnover in both the tip and stalk. The "dynasensing" mechanism, which is proposed by (Indrajyoti Indra, Troyanovsky, Shapiro, Honig, & Troyanovsky, 2020) referred to as the intimate bidirectional link between the stability of cadherin and related F-actin, demonstrates how PAJs and maybe other AJs enable cells to detect and coordinate the dynamics of the actin cytoskeleton in neighbouring cells.

#### **1.1.2.4.2 Core complexes of Adherens junction-**

##### **(a) E-Cadherin**

The Ca<sup>2+</sup>-dependent cell-cell adhesion protein E-Cad is a large single-pass transmembrane glycoprotein that has undergone evolutionary conservation. E-cadherin or epithelial cadherin, along with neural cadherin (N-Cad), placental cadherin (P-Cad), and vascular endothelial cadherin (VE-Cad), is one of the prominent classical Cadherins present in metazoan (Gumbiner, 2005). It is also known as CDH1 in humans and Shotgun in *Drosophila*. The molecular family of E-, N-, VE-, and other cadherins have five extracellular cadherin domains (ECs), transmembrane, and cytoplasmic domains. Extracellular cadherin (EC) domains engage in homophilic trans interactions with the E-cad molecules of neighboring cells. The Cadherin intracellular domain facilitates interactions with a variety of effectors on the cytoplasmic site that regulates E-Cadherin functionality (Katja

Röper, 2015) (**Figure 1.4**). The cytoplasmic domain of the E-Cad molecule is highly conserved, which allows regulated binding of  $\alpha$ -,  $\beta$ - and p120-catenins and carry out various cellular processes (Baum & Georgiou, 2011; Harris, 2012). In particular, they enable E-Cad's association with the ZA actin-myosin cortex, its transport and recycling, and its interactions with the various apicobasal and planar polarity machinery at work in epithelial cells. These downstream E-Cad binding proteins also interact with actin regulators to mediate and regulate the activity of actin remodelling and E-Cad.

## **(b) Catenins**

The two important cytoplasmic adapter proteins of E-Cadherin are the  $\beta$ -catenin ( $\beta$ -Cat) and p120 catenin. Through its interaction with beta catenin, alpha-Cat plays a major role in mediating the link to the actin cytoskeleton. These proteins are highly conserved and contain repeats of the armadillo domain (Coopman & Djiane, 2016). The connection of E-Cad molecules with the actin/myosin network has been attributed to a complex that includes actin, alpha-Cat, beta-Cat, and E-Cadherin (**Figure 1.4**). In fact, both in human cell culture experiments and in *Drosophila*, the assembly of E-Cad/alpha-Cat fusions can directly link alpha-Cat and E-Cad, thereby rescuing the majority of E-Cad loss-of-function defects, including remodelling (Desai et al., 2013). Alpha-cat also plays a vital role in force transduction to the ZA E-Cadherin. Under mechanical stress, E-Cad/alpha catenin binds directly to F-actin (C. D. Buckley et al., 2014). Alpha catenin can bind to many actin binding proteins and actin regulators such as formins, alpha actinin. Vinculin, afadin, ZO-1 and ELPIN (Abe & Takeichi, 2008; Bershadsky, 2004; Yonemura, 2011).

The crucial function of p120-Ctn in the control of AJs has been underlined by numerous investigations in mammalian systems. It has been demonstrated that p120-Ctn interacts with a number of microtubule regulators, including CLASP2 and kinesin, as well as actin regulators, including the small GTPase Rho regulator p190RhoGAP, to mediate local Rho/Rac activity (X.

Chen, Kojima, Borisy, & Green, 2003; Noren, Liu, Burrridge, & Kreft, 2000; Shahbazi et al., 2013; Wildenberg et al., 2006). It also controls the endocytosis and turnover of E-Cad(X. Chen et al., 2003). In addition, p120-Ctn transiently interacts with a number of its upstream and downstream effectors, including ROCK1, to dynamically regulate Rho-GTPase activity (Smith, Dohn, Brown, & Reynolds, 2012). These findings further indicate that p120-Ctn modulates the stability of E-Cadherin in epithelial cells, which helps to maintain cell-cell adhesion. Interestingly, *Drosophila* does not require p120-Ctn function, implying p120 role is minor or supportive function (Myster, Cavallo, Anderson, Fox, & Peifer, 2003). In *Drosophila*, p120 catenin facilitates E-Cad-Par3 endocytosis and recycling (Bulgakova & Brown, 2016).

E-Cad and catenins are the crucial components of AJ that interact with the Rho family of GTPases, which modulates other downstream effectors and thereby regulates the dynamics of F-actin dynamics. These are important processes in the regulation of cell adhesion, force production, and AJ remodelling.

### **(c) Rho GTPases at Adherens junction**

Small GTPases, notably the RHO GTPases RHO, RAC, and CDC42, and their effectors, play significant roles in a number of mechanisms that control the polymerization and stability of actin filaments at AJs (M. Takeichi, 2014). The WAVE2 (also known as WASF2)-actin-related protein 2/3 (ARP2/3) complex, a RAC effector, appears to be essential for junctional actin nucleation (Tang & Briher, 2012; Verma et al., 2012). A CDC42 effector known as neural Wiskott-Aldrich syndrome protein (NWASP) is crucial for maintaining actin networks at AJs (Kovacs et al., 2011; Otani , Ichii , Aono , & Takeichi 2006). As described below, formins, another actin regulator class that works after small GTPases, also encourage junctional actin polymerization. These mechanisms organize actin filaments which are connected to non-muscle myosin IIA, myosin IIB, and/or myosin IIC at the ZA and other junctions (Ivanov et

al., 2007). The small GTPases RHO and repressor/activator protein 1 (RAP1; also known as TERF2IP) homologue, which are members of the RHO and RAS GTPase families, respectively, are particularly significant in controlling the circumferential actomyosin belt at adherens junction (M. Takeichi, 2014).

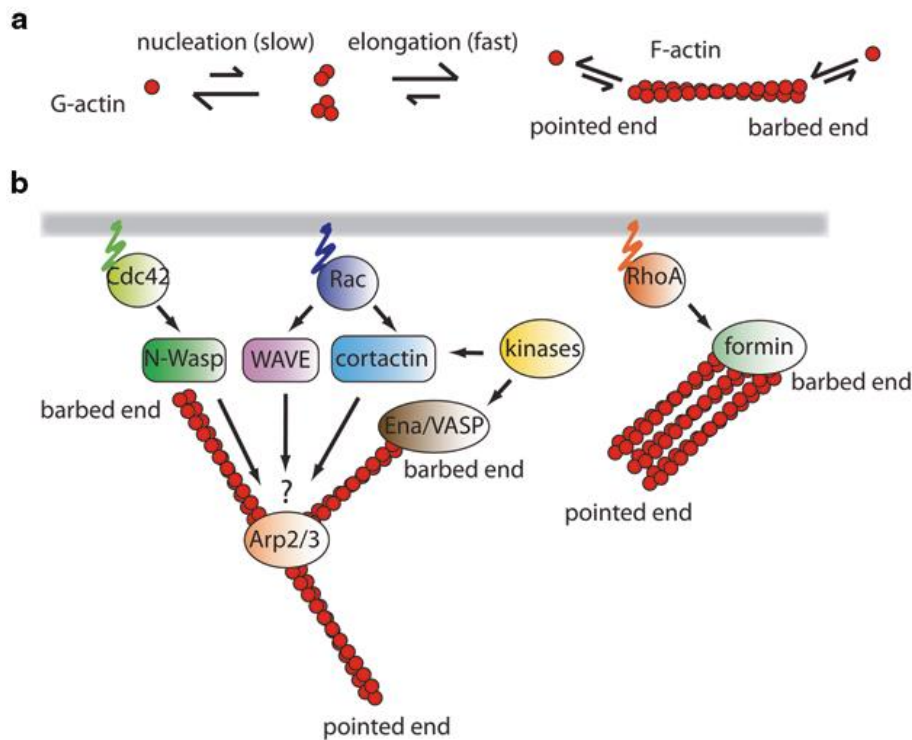


**Figure 1.6: Small GTPases at AJ** (a) G-actin and F-actin are in a state of dynamic equilibrium where the slow nucleation process controls the rate of actin polymerization. The G-actin polymerizes to form F-actin. (b) Important actin regulators are regulated Rho, Rac, CDC42 take part in actin bundling. They regulate formins to initiate and extend filament length, Arp2/3 initiate the branching, and Ena/VASP regulate and helps the filament growth. The figure is adapted from (Han & Yap, 2012)

RHO inhibition causes the ZA to be disrupted, according to early investigations (Citi, Spadaro, Schneider, Stutz, & Pulimeno, 2011). Diaphanous homologue 1 (DIA1; also known as DIAPH1 in *D. melanogaster*) and RHO-associated protein kinase (ROCK; also known as RHO kinase

or Rok in *D. melanogaster*) are two of the effectors that RHO positively regulates at the ZA (Goode & Eck, 2007). Under the direction of small RHO GTPases, the formin family protein DIA1 stimulates actin polymerization. The ZA is disrupted when DIA1 is depleted, whereas actin buildup at junctions is increased when DIA1 is overexpressed (Homem & Peifer, 2008; Sahai & Marshall, 2002). Formin 1 is yet another formin that is crucial for AJ maintenance (Kobielak, Pasolli, & Fuchs, 2004). RHO thus appears to maintain actin polymerization via formins at the ZA to support ZA stability. The actomyosin contraction is brought on by the Ser/Thr kinase ROCK, another RHO target, which phosphorylates the MLC and MLC phosphatase (Riento & Ridley, 2003). ROCK can only be detected at a moderate level along the ZA in epithelial cell lines. Junctional ROCK levels have been suppressed by an atypical protein kinase C (aPKC)-dependent mechanism (Ishiuchi & Takeichi, 2011). Linear connections are messed up when ROCK is constitutively activated, though. The actomyosin filaments that are perpendicularly linked to AJs are thought to contract as a result of enhanced ROCK activity, allowing them to pull the junctions in radial directions as seen in peripheral AJs, which is how this phenomenon was explained. As a result, when ROCK is hyperactive, it can act as an inhibitor of ZA formation. The two RHO effectors DIA1 and ROCK operate in balance for maintenance of ZA in epithelial cells (Warner & Longmore, 2009).

### **1.1.2.3 The basolateral domain**

The key polarity factors that make up the basolateral domain are the Scribble (scrib), Discs large (dlg), and Large giant larva (lgl) collectively known as the Scribble complex. They define the basolateral domain in fly and vertebrate epithelia. However, several other paralogues of Scribble (Scribble, Erbin, Lano (LRRC1) and Densin), Lgl (LLGL1 and LLGL2) and Discs large (DLGL1-5) are found in mammals (C. E. Buckley & St Johnston, 2022). Single protein knockdowns or knockouts of these proteins result in unexpected phenotypes and have

negligible influence on polarity speculating their redundant role in apicobasal polarity. But, triple knockouts of the genes Scribble, Erbin, and Lano completely alter the polarity of colon carcinoma cells, but single knockouts frequently have no impact on apical-basal polarity (Choi, Troyanovsky, Indra, Mitchell, & Troyanovsky, 2019). Due of Lgl's ability to inhibit aPKC, the scrib complex prevents apical proteins from entering the basolateral region (Bonello & Peifer, 2019b; Riga, Castiglioni, & Boxem, 2020; Stephens et al., 2018). In *Drosophila*, the Scribble complex controls the transport of Crumbs and other cargo from early endosomes to the Golgi apparatus via the retromer pathway (de Vreede et al., 2014). The Scribble proteins operate via a common pathway to govern AJ formation, limit apical determinants to the apical domain, and regulate cell growth in *Drosophila* (Bonello & Peifer, 2019a; Tomoyuki Yamanaka & Ohno, 2008). They are mutually dependent on their localization. It has been identified to have a very early role in organizing AJs in the developing *Drosophila* embryo, upstream of other polarity regulators including Baz/par3 (Bonello & Peifer, 2019a). Another group of basolateral polarity markers [Yurt, Coracle (Cora), Neurexin IV, and Na<sup>+</sup>K<sup>+</sup>-ATPase] counteracts apical polarity regulators to maintain basolateral polarity during mid-embryogenesis in *Drosophila* (Laprise et al., 2009; Tepass, 2012). Another important feature of the basolateral domain is septate junction.

### **(a) Septate junction**

Septate junctions (SJ) emerge later in development as the epithelium matures and are not seen in all epithelia. The initial distribution of septate junction proteins in the lateral membrane is uniform; nevertheless, these proteins organize into a continuous band eventually right below the adherens junction and create stationary complexes (Oshima & Fehon, 2011). The Scribble complex also plays distinct functions that govern establishment of the lateral domain in flies and vertebrates. Dlg and Scribble are essential for the formation of the septate junctions in flies,

which act as barriers to the paracellular diffusion in a manner akin to tight junctions (Bilder, Schober, & Perrimon, 2003; Tanentzapf & Tepass, 2003). The failed localization and continued immobility of the septate junction proteins in *dlg* and *scrib* mutants indicate that these proteins are crucial for positioning the junctions to establish a continuous barrier. However, they are dispensable for junction assembly.

#### **1.1.2.4 The basal domain**

The basal domain comprises of the basal plasma membrane of the cells that is attached to the basement membrane via focal adhesions or dot junctions. These basal membranes are interacting with the basement membrane proteins i.e., Collagen, Laminin, Perlecan and Nidogens via integrins (Barrera-Velázquez & Ríos-Barrera, 2021). Integrins serve as transmembrane intermediaries that mediate interactions between the extracellular matrix and the cytoskeleton (Bruce Alberts et al., 2008). The majority of integrins are joined to networks of F-actin bundles. Talin and the integrin-linked kinase (ILK), interact with the actin cytoskeleton and the microtubules, respectively. The alteration in the integrin-mediated cell-ECM interaction leads to many morphogenetic defects of the epithelia and altered bECM composition (Barrera-Velázquez & Ríos-Barrera, 2021).

#### **1.1.3 Tubular epithelial organs**

Epithelial tubes are the structural and functional units of tubular epithelial organs. Tubular epithelial organs are specialized organs primarily consisting of hollow tubes lined by a single layer of epithelial cells, and they can be found in many organisms, including humans. These organs, including the respiratory system (trachea and bronchi), digestive system (salivary glands, intestines), urinary system (renal tubules, lining of urethra), and reproductive system (fallopian tubes), play crucial roles in processes like transportation, secretion, absorption, and

excretion. The efficient transportation of gases, liquids, nutrients, and waste items is made possible by their tubular form. The interchange of molecules and ions between the interior of the organ and its surrounding tissues is regulated by the epithelial lining, which serves as a selective barrier. Significant scientific interest exists in figuring out how these organs arise, work, and are maintained. Several molecular mechanisms and signalling pathways crucially involved in the generation and patterning of tubular structures throughout embryonic development have been revealed in the past (Lubarsky & Krasnow, 2003). Congenital malformations and illnesses affecting tubular organs can have underlying dysregulation of these systems. For instance, research on renal tubule formation has shed light on the molecular causes of diseases like polycystic kidney disease (PKD) (Dow & Romero, 2010). The pathology of respiratory disorders, including COPD and pulmonary fibrosis, have been better understood by studying the development of the respiratory system (Scholl, Ndoja, & Jiang, 2021). *Drosophila melanogaster* has been used as a model organism extensively to investigate the fundamental biology of epithelial tubular systems.

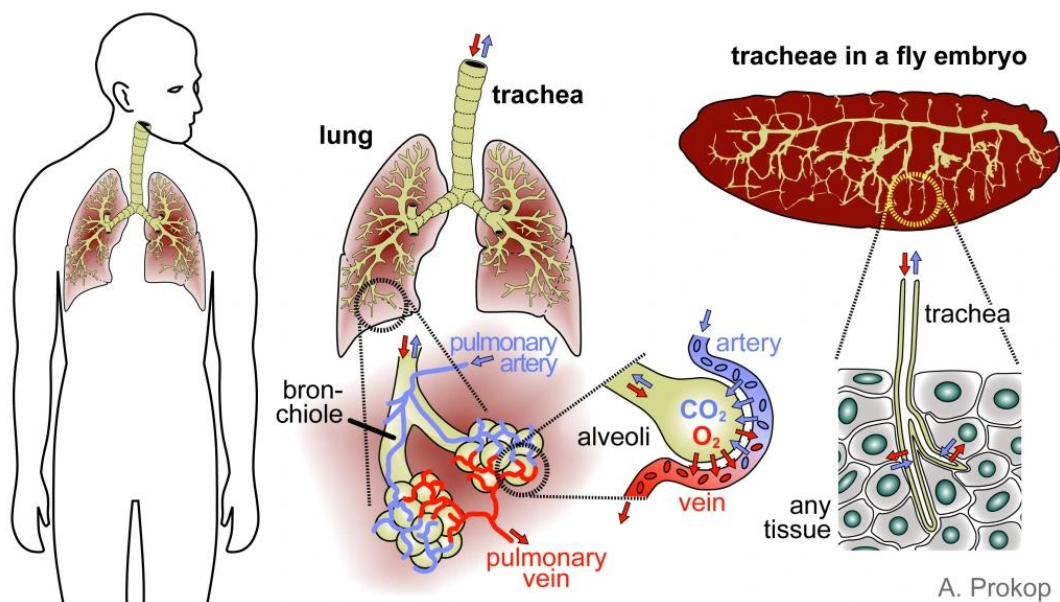


**Figure 1.7: Schematic showing the resemblance of human lungs with *Drosophila* respiratory system.** Both the systems are made up of tubes made up of epithelium. Image by A. Prokop and adapted from [droso4schools.wordpress.com](http://droso4schools.wordpress.com).

#### **1.1.4 *Drosophila* trachea: a tubular epithelium**

The development of tubular tissue architecture and organogenesis to create functional tubular organs is an integral part of all metazoan development. In most multi-cellular organisms, major cellular processes like the generation, secretion, storage, and transport of physiological fluid and gas depend on tubular organs. The emergence of tubular tissue topologies and their significance in respiration is an essential physiological phenomenon of all metazoans (Loganathan, Cheng, & Andrew, 2016). Holometabolous insects have a network of epithelial tubules that serve as their respiratory organs, called trachea, to deliver oxygen to the target tissue. The tracheal system, made up of a network of ramified tubules stretching throughout the body cavity, allows air to pass through openings in the body wall known as spiracles and transports it to the destination cells via highly branched tracheal termini. Waste gas (carbon dioxide) diffuses from the terminal to the spiracles across the broad surface area of the tracheole lumen. In contrast, oxygen diffuses in the opposite direction (Wigglesworth). The *Drosophila* trachea, is a widely used developmental model to comprehend the cellular and physiological mechanisms that underlie the formation and function of tubular organs (Markus Affolter & Caussinus, 2008; G. & A, 1993; M, 1980; R. Pradhan, Urbietta-Ortiz, Kumar, Mathew, & Ríos-Barrera, 2022; Samakovlis, Hacohen, et al., 1996).

The development of the trachea in *Drosophila* has been utilised to study the genetic, molecular, and cellular mechanisms driving tubulogenesis in the embryonic and larval stages. The trachea is comprised of an interconnected web of different-sized tubules and sacs of epithelial origin with diverse cellular-scale architectures. The three-dimensional tissue space

of the entire body is permeated by the tracheal tubules, which are largely responsible for gas exchange and transport. Cuticle secretion in the tubules and oxygen storage in the air sacs, respectively, are instances of its secretory and storage roles. Consequently, the cellular processes and physiological functions of the *Drosophila* trachea are relatable to a substantial number of physiological roles carried out by equivalent but more intricate tubular organs in higher metazoans including humans (Hayashi & Kondo, 2018).

### **1.1.5 Development of tracheal epithelium**

Tracheal formation starts in stage 10 of embryogenesis, approximately 5 hours after the egg laying. The process starts with the specification of 10 pairs of epithelial placodes which are located in the lateral part of the second thoracic (T2) to eighth abdominal (A8) segments of the embryo (**Figure 1.7**). These placodes invaginate into the body cavity while retaining epithelial integrity and go through regulated branching and fusion processes that create a network of tubular epithelium (Campos-Ortega José A., 1997). However, early studies concentrated on determining the factors that determine the fate of tracheal cells and tracheal tissue-specific attributes. Those are tracheless, breathless and branchless. Breathless (Btl), which encodes the FGF receptor, is one of many tracheal genes regulated by the transcription factor Trachealess (Trh), which is expressed in all tracheal cells from the beginning of tracheal placode specification through adulthood (Chung, Chavez, & Andrew, 2011; T. Ohshiro & Saigo, 1997). Tracheal placode invagination is a multi-mechanistic process. The apical surface of the epithelium is shifted basally to generate the tracheal pit via the constriction of apical cell surfaces in the middorsal placode. This process progresses through EGF receptor (EGFR) signalling, which is governed by Rho GTPase signalling and controlled by the EGF ligand activator molecule Rhomboid (Rho) and the intracellular signal transducers ERK and MEK

(Brodu & Casanova, 2006; Llimargas, 1999). The invasion of the tracheal placode cells into the body triggers the final embryonic mitosis (cycle 16).

Most tracheal cells in the larval stage grow by endo cycling. The process of primary branching commences as the tracheal primordia begin to express the FGF receptor tyrosine kinase, i.e., Btl, which is activated by Branchless (Bnl), one of the three FGF ligands in *Drosophila* (Glazer & Shilo, 1991; Klämbt, Glazer, & Shilo, 1992; Shishido, Higashijima, Emori, & Saigo, 1993). Each branch moves in the direction of a certain target tissue; for instance, the dorsal branch migrates in the direction of the dorsal epidermis, the visceral branch proceeds in the direction of the intestine, and the ganglionic branch moves in the direction of the ventral nerve cord. Bnl, which is expressed in a number of nontracheal tissues, directs branch migration. Bnl-Btl signalling promotes the development and expansion of terminal cells, seamless tracheal tubes that extend their cytoplasmic branches into target regions to facilitate respiration during stages 15 and beyond (Du et al., 2017; Tomokazu Ohshiro, Emori, & Saigo, 2002; Sutherland, Samakovlis, & Krasnow, 1996). After being activated by Bnl, Btl forms a complex with the FGFR adaptor protein Dof and activates ERK MAP kinase via the RAS signaling pathway which plays a significant role in the primary branching morphogenesis (Imam, Sutherland, Huang, & Krasnow, 1999; Michelson, Gisselbrecht, Buff, & Skeath, 1998; Vincent, Wilson, Coelho, Affolter, & Leptin, 1998).

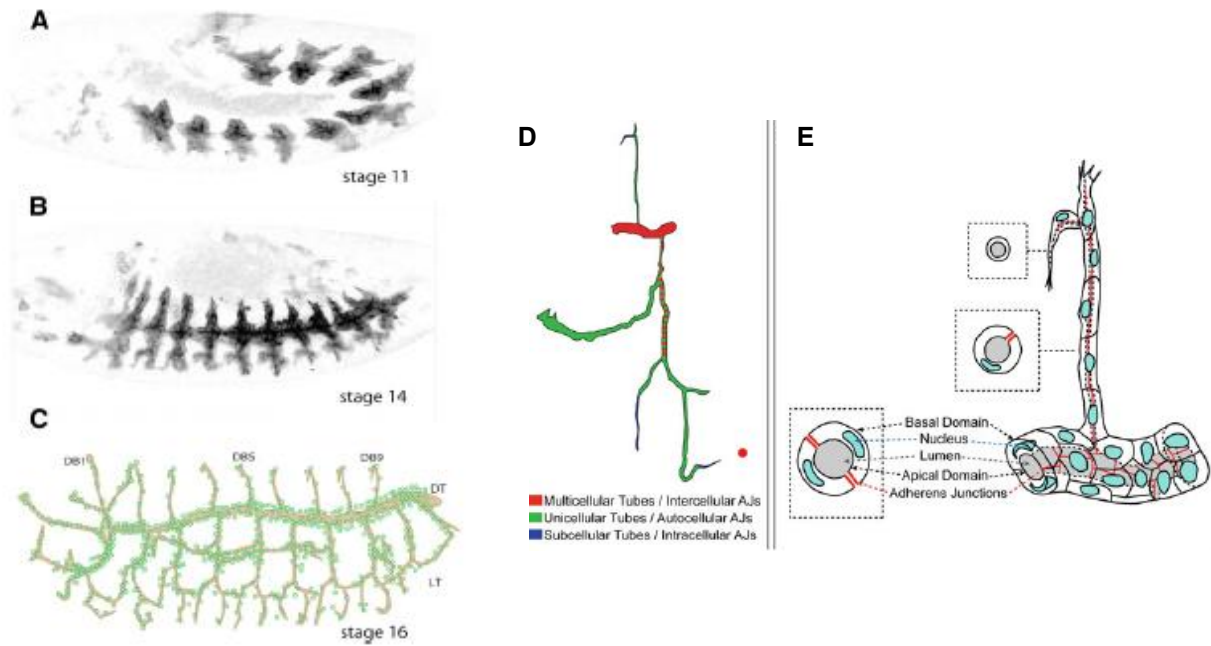


**Figure 1.7: *Drosophila* tracheal system in embryo** (A) ten epithelial placodes in Stage 11 (B) Stage 14 of tracheal development showing dorsal trunk branch fusion and (C) developed embryonic trachea of stage 16 embryo, green dots represent the nuclei. Images adapted from (Hayashi & Kondo, 2018) (D) Types of tracheal tubes embryo (E) Cellular arrangement in tracheal DT. Images adapted from (Loganathan et al., 2016)

The branches formed during primary branching are distinct in their pattern and cellular composition. The transcription factors Knirps/Knirps-like (Kni/Knrl) and Spält(Sal), which are expressed in a complementary pattern, are responsible for the most significant aspects of tube structure, cell composition, and target organ specificity: Sal is expressed in the dorsal region and results in the development of the dorsal trunk and branch, whereas Kni/Knrl is expressed in the ventral region and results in the development of the lateral trunk and the ganglionic and visceral branches. The dorsal trunk (DT) is distinctive in that cells with multicellular junctions cover the lumen surface, resulting in a multicellular tubule with a comparatively broad diameter. Other branches, such as the dorsal branch (DB) and lateral branch (LB), are composed of single cells with auto-cellular junctions and have small-diameter unicellular

tubules (Hayashi & Kondo, 2018; Ribeiro, Neumann, & Affolter, 2004). In the dorsal branch, auto-cellular junctions are created by cell intercalation, which is aided by increased E-cadherin turnover (Shindo et al., 2008) and hindered in the dorsal trunk by increased endosomal recycling (Shaye, Casanova, & Llimargas, 2008), which is induced by Sal (Ribeiro et al., 2004).

When secondary branching occurs, tracheal branch termini become more complex by the emergence of the terminal branch. This single-cell extension has an intracellular lumen that repeatedly extends and branches while repeatedly extends and branches while also growing the lumen that encompasses the target organ. The terminal cell growth is regulated by tissue-specific oxygen demand, which is controlled by Sima, a HIF-alpha homolog (Centanin et al., 2008). In contrast to other cell types, terminal cells create lumens by the inward expansion of the apical plasma membrane at the intersection of the terminal branch and stalk cells (Sara Sigurbjörnsdóttir, Renjith Mathew, & Maria Leptin, 2014). Lumen expansion happens in the direction of terminal branch outgrowth, most likely via adhering to microtubule tracts (Gervais & Casanova, 2010). *Ikk* mutants (Oshima et al., 2006), *btsz* mutants (JayaNandanan, Mathew, & Leptin, 2014), and *Slik* mutants (JayaNandanan et al., 2014) are examples of mutants with defective actin filament organization, where lumen growth does not follow the direction of cell growth. As they develop, larvae need an ongoing supply of apical membranes, and the lengthening of the terminal branch lumen is facilitated by dynein-dependent transport and constrained by endocytosis (Schottenfeld-Roames, Rosa, & Ghabrial, 2014). Subcellular tubulogenesis in the embryonic trachea uses apical-to-basal transcytosis to transport plasma membrane to the proper domains of the emerging tube branch, as demonstrated by Mathew et al. (Mathew, Rios-Barrera, Machado, Schwab, & Leptin, 2020).

Each primary branch's tip has a single ERK-active cell that directs the development of tubules and branch migration. These cells are known as tracheal tip cells. In contrast to anterior open, an ETS-domain transcriptional repressor which inhibits the fate of the tip cell in stalk

cells by opposing ERK and Wingless signalling, activated Notch restricts Bnl/FGF activity to the Delta-high tip cell and suppresses ERK signalling (Caviglia & Luschnig, 2013; Chihara & Hayashi, 2000; Llimargas, 2000). Tip cells stick to the target tissues and move in the direction of the sources of dynamically shifting Bnl expression. Wingless signalling causes the tip cells to start expressing the genes *escargot* (*esg*) and *dysfusion* (*dysf*), which specifies a fusion cell fate. The expression of the transcription factor SRF, which is encoded by *blistered*, starts to increase in the nearby terminal cells at the same time that ERK expression decreases in the tip cells (M. Affolter et al., 1994; Guillemin et al., 1996). Branch fusion (anastomosis) is accomplished at the dorsal midline by de novo lumen generation and interaction between fusion cells. Fusion cells from both directions establish contact with one another and adhere together by assembling E-cadherin at the interface of contact. Only fusion cells from opposing sides may form an E-cadherin adhesion. After a solid attachment has been made, the paired fusion cells exploit Golgi-mediated secretion to regulate new lumen formation at the contact interface (Gervais, Lebreton, & Casanova, 2012; Kato et al., 2016; Samakovlis, Manning, et al., 1996; Tanaka-Matakatsu, Uemura, Oda, Takeichi, & Hayashi, 1996).

Tracheal tube geometry is maintained by various factors. Those factors were unraveled by morphometric analysis and mutant analysis. The proteins that are responsible for tube size can be categorized into three major groups: mutants affecting tube diameter, tube length, and both diameter and length. The main regulators are aECM and its regulators, apicobasal polarity proteins, planar polarity proteins, and proteins associated with apical membrane biosynthesis and transport (Hayashi & Kondo, 2018).

Tube maturation and air filling of the trachea happens after the tube attains growth in size and length. Before air filling, the tracheal DT is filled with liquid. The tracheal cells start secreting Chitin like a cylindrical tube which later gets the shape of a circumferential ridge on the apical membrane called as taenidial ring. The formation of cortical F-actin rings, which are

perpendicular to the DT long axis precedes the event of taenidial ring formation. The cortical F-actin rings act as a template for the taenidia and cuticle secretion in DT (Matusek et al., 2006; Öztürk-Çolak, Moussian, & Araújo, 2016; Öztürk-Çolak, Moussian, Araújo, & Casanova, 2016). In order to remove a significant portion of the luminal macromolecules within the lumen, tracheal cells break down and absorb the aECM components (Behr, Wingen, Wolf, Schuh, & Hoch, 2007; Tsarouhas et al., 2007). The liquid is cleared by rapid endocytosis of these aECM components by the tracheal cells. In the end, a portion of the cuticle surface releases a gas that is independent of its surroundings outside, which swiftly spreads throughout the entire tracheal lumen to fill the tube with gas. It requires the apical membrane protein Uif, even if the process of gas formation is still a mystery. It is believed that the development of a hydrophobic wax layer on the cuticle is a necessary condition for gas generation since fatty acyl-CoA reductase is identified as a crucial component (Jaspers et al., 2014). In the past, cavitation-bubble creation on a hydrophobic surface has been proposed as a mechanism for the synthesis of bubbles from gas saturated in the luminal liquid by the surface (WIGGLESWORTH, 1953). After air filling, the tracheal development in the embryo is complete. The developed trachea includes epithelial tubes of varied architecture.

The largest multicellular tube, the dorsal trunk, extends from the anterior spiracles to the posterior spiracles at the posterior end. In *Drosophila*, there are two parallel dorsal trunks. Ten metameres that are connected by intersegmental junctions make up each DT. Each metamere is a representation of an early DT metamere established during embryonic development. The dorsal trunk metameres can be distinguished as anterior and posterior tracheal metameres. Thoracic1(tr1)–thoracic5 (tr5) stands for the anterior trachea, and tr6–tr10 for the posterior trachea. The largest tube diameter is found at the posterior end of the dorsal trunk, where it connects to the posterior spiracle that opens to take in air as the larva hatches. Although the dorsal trunk is multicellular, it gradually narrows towards the anterior because

Hox genes operate differently in each metamere (Matsuda, Hosono, Saigo, & Samakovlis, 2015). The other tracheal branches, such as the dorsal branch and lateral branch, are unicellular in nature, and tracheal terminal cells are seamless tubes.

As development proceeds, the embryo enters the larval stages and, subsequently, pupal stages. There are three larval stages: first instar, second instar, and third instar. The Pupal stage is an intermediate stage between the larva and the adult *Drosophila*. Most tracheal cells cease division and continue endo cycling when larvae hatch so that ploidy and cell size will increase. The larvae keep feeding, and the tracheal tubules also increase in length and width to keep up with the larvae's growth. There are three molting events that happen during each larval instar. During second and third instar molting, the tracheal cells remodel their apical membrane and cortical F-actin along with apical extracellular matrix, i.e., taenidial folds, by secreting new cuticles (Hosono et al., 2015). These massive cuticular changes are modulated by apically secreted matrix metalloproteinase 1 (MMP1). During this time taenidial fold increases up to twice its size, matching the growth of the larvae (Glasheen, Robbins, Piette, Beitel, & Page-McCaw, 2010). The spiracular branch that connects the tracheal tubule to the epidermal region at the site of the initial tracheal pit created at the beginning of tracheal development is populated by tracheal histoblasts (also known as tracheoblasts), which are descended from cut-positive cells. Tracheal histoblasts or progenitor cells are also present at tr-2, and air sac primordium is present at tr-4 and tr-5 branch points. During metamorphosis, these special cells, which multiplied greatly in the third instar, replace larval tracheal cells and create tracheal branches in adult *Drosophila*.

### **1.1.6 Epithelial degeneration in the development**

Epithelia grow, multiply, differentiate, and evolve into working organs during organogenesis. Although disassembly is an equally significant and a crucial component of development, it has

received relatively less attention. A fundamental step for achieving or maintaining a homeostatic condition is the disassembly of pre-existing organs and the development of new organs. Examples include the elimination of apoptotic cells during the development of digits in vertebrates (Milligan et al., 1995), the involution of the mammary gland after breastfeeding in adult females (Watson & Kreuzaler, 2011), and the regression of the Mullerian or Wolffian ducts during the development of the gonad in the fetus, among others (Hannema & Hughes, 2007; Mullen & Behringer, 2014). It is yet unknown what signalling cascades lead to organ degeneration or disintegration of a functional organ. To attain the right number of neurons during *Drosophila* neuron development, apoptotic neuroblasts are removed from the nervous system (Yalonetskaya, Mondragon, Elguero, & McCall, 2018). Apoptotic elimination of cells occurs during tracheal development. In holometabolous insects, the transition from the larval to the adult stage takes place via an intermediate pupal stage. Half of the larval tissues deteriorate during metamorphosis, and these are eventually replaced by transient pupal structures, which are subsequently replaced by adult organs (G. & A, 1993). During the metamorphosis process in *Drosophila*, the salivary glands and midgut are removed (**Figure 1.8**) (Yalonetskaya et al., 2018), and the trachea is partially removed (F. Chen & Krasnow, 2014; Fraire-Zamora et al., 2021). Organ degradation, in our opinion, cannot be a one-step process. It is more likely to be a regulated process where tissue degeneration and, eventually, organ disassembly are brought about by underlying organised architectural alterations in epithelial components. Hence, organ degeneration events are preceded by epithelial degeneration at the cellular level.

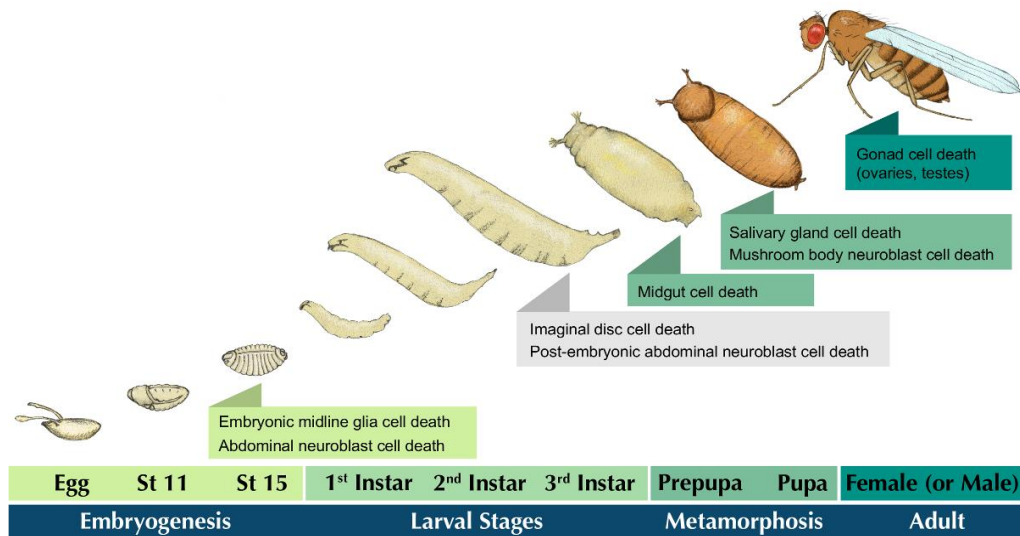


**Figure 1.8: Time line showing programmed cell death events in *Drosophila* development.**

In embryogenesis to the metamorphosis and in adult organs like gonads degenerative events happen. Programmed cell death events are an integral part of development. During metamorphosis midgut cell death and salivary gland cell death happens. Image adapted from (Yalonetskaya et al., 2018)

### **1.1.7 Tracheal degeneration during metamorphosis is an excellent model for studying epithelial degeneration.**

The majority of larval tissues, including the tracheal epithelium, histolyze and are replaced by adult tissues during metamorphosis. These tissues arise from clusters of primordial imaginal cells or tracheal histoblasts (tracheoblasts) present at tr2, tr4, and tr5 junctions as clusters of air sac primordium cells. This causes the tracheal system to undergo a number of crucial physiological and structural alterations because it must continue to meet the respiratory needs of tissues that persist from larva to adulthood as well as those that degenerate during this time. The spiracular branch is populated by tracheal histoblasts, which are derived from cut-positive cells (Pitsouli & Perrimon, 2010, 2013). These distinct cells, which multiply extensively in the

third instar, replace the larval tracheal cells to generate adult-specific tracheal branches during metamorphosis. After mitosis in embryonic cycle 16, the dorsal branch stalk cells in the second to fifth tracheal metameres (Tr2-Tr5) and the Tr2 of dorsal trunk cells are quiescent before restarting the cell cycle and proliferating to become adult tracheal cells in late L3. While other tracheal cells start their endocycle, these precursor cells can continue to divide. By blocking the endocycle-promoting gene *fzr*, the nuclear proteins Htx and Exd, along with their binding partner Ubx, these cells are thought to maintain cell cycle arrest and multipotency in these cells (Sato, Kitada, & Tabata, 2008). The air sac primordia (ASP) become apparent in the third instar larvae, which are joined to the basal side of the presumptive notum of the wing imaginal disc. These ASPs are the precursor structures that form air sacs in the adult fly. The primordial tracheoblasts express *btl*, whereas the wing imaginal disc expresses *bnl*, and the activation of FGF signalling encourages this migration towards the posterior (Sato & Kornberg, 2002). This invasive process necessitates significant remodelling of basement membranes at the wing imaginal disc (Guha, Lin, & Kornberg, 2009).

During metamorphosis while some larval branches undergo extensive remodelling and pruning events, whereas some major tracheal tubes degenerate, and an interim set of pupal branches forms to supply oxygen to the growing adult structures. These pupal structures are replaced later by the adult branches (M, 1980; Robertson, 1936; WHITTEN, 1957).

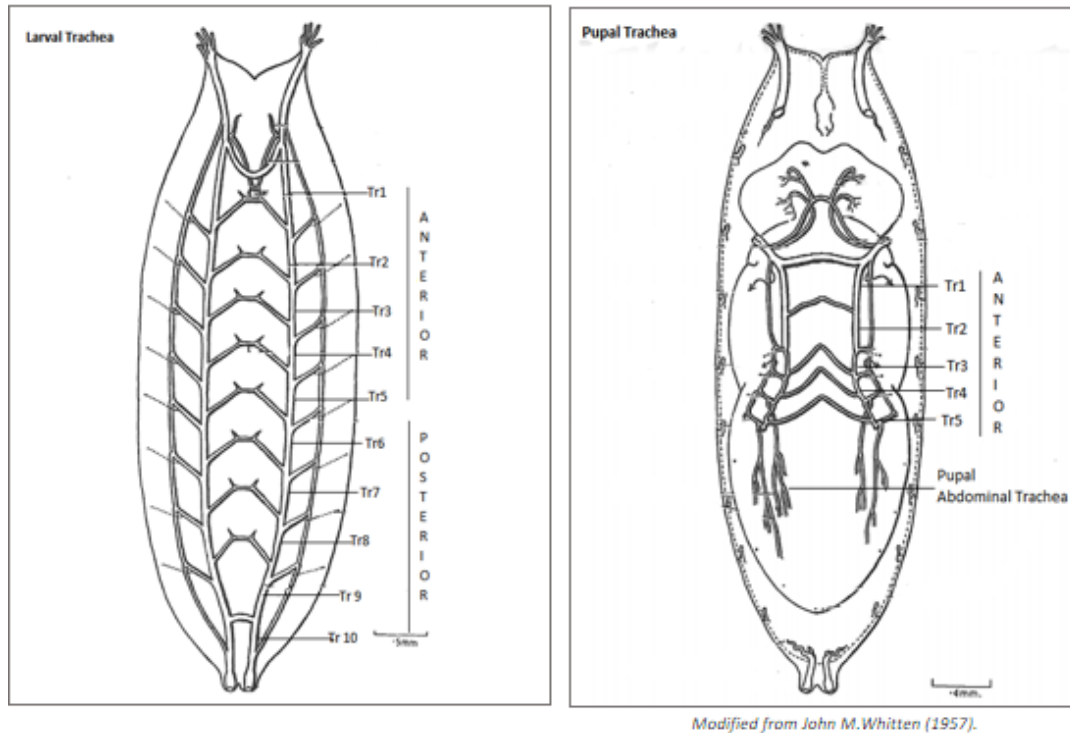


**Figure 1.9: Schematics showing larval trachea and pupal trachea.**

The larval trachea showing ten metameres tr1-tr10, whereas pupal trachea showing anterior trachea tr1-tr5, posterior trachea in pupa is replaced by pupal abdominal trachea. Image adapted from (WHITTEN, 1957).

During larval to pupal transition, the posterior metameres (tr6-tr10) undergo a dramatic remodelling event and are replaced by interim pupal abdominal trachea (PAT) after 12h of puparium formation. These PATs are very fine tracheoles that arise at the base of tr5, which supply oxygen to the de novo-formed adult trachea (**Figure 1.9**). The guidance of PAT formation is intriguing. the adult progenitor cells escape the branch points of tr4 and tr5 metameres and migrate towards the posterior tracheal cells during pupation. The pathfinding take-over happens on a template provided by the previous larval tracheal system(F. Chen & Krasnow, 2014).

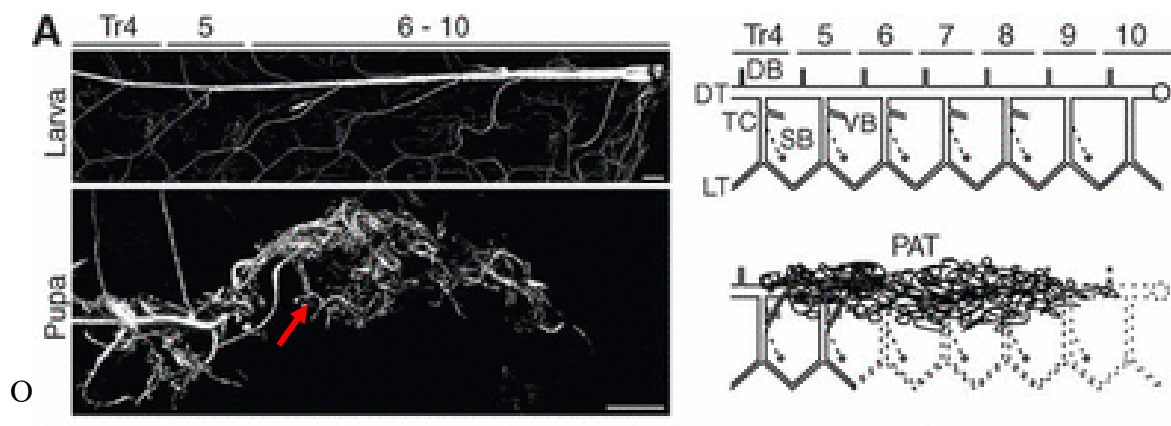


**Figure 1.10: Schematics showing the degenerative pupal trachea.** The posterior larval trachea degenerated in the pupa (tr6- tr10) and replaced by pupal abdominal trachea shown in red arrow. Image adapted from (F. Chen & Krasnow, 2014).

Organ disassembly occurs in late pupae in which the existing larval cells undergoes apoptosis or programmed cell death. Chen et al. showed that, during metamorphosis, the posterior trachea is replaced by progenitor cells that are regulated by an FGF-mediated morphogen gradient secreted by decaying cells (**Figure 1.10**) (F. Chen & Krasnow, 2014). Recently, Zamora et al. showed that *Drosophila* larval trachea exhibits sequential organ disassembly in a highly stringent hormone-driven process during pupation (Fraire-Zamora et al., 2021). It happens in two stages: first, remodelling of the apical extracellular matrix (aECM), which is mediated by matrix metalloproteases which causes a progressive shortening of the entire trachea. During the first phase, nuclear-to-cytoplasmic relocation of the Hippo effector Yorkie (Yki) is observed in the tracheal cells. Second, the posterior half of the trachea perish from apoptosis due to a decrease in the transcription of the Yki target Diap1 in the posterior metameres. These events lead to the activation of caspases. However, the anterior trachea is retained in the pupa. In metamorphosis, the posterior trachea is selectively eliminated

by an Ecdysone-driven ECM remodelling process, which further regulates apoptotic cell elimination and tube shortening through the transcriptional activity of Yki, ultimately leading to tracheal degradation (Fraire-Zamora et al., 2021).

### **1.1.8 Aims and objectives of the thesis**

As discussed earlier the tissue degeneration events orchestrated in *Drosophila* tracheal metamorphosis is crucial to understand the programme driving these changes. Surprisingly very little is known that how these degenerative changes contribute to the tube disassembly. What are the degenerative changes happening in all three layers of epithelium in metamorphosis? How individual cells contributing the degenerative processes? How the epithelial architecture changes due to these event? What is the physiological significance of these processes? Investigating the intricate genetic mechanisms underlying this programmed tissue degeneration could enhance our understanding of developmental degenerative processes not only in *Drosophila* respiratory epithelia but also in other organisms. The main premise of my research is that **organised and sequential epithelial degenerative changes are orchestrated during the metamorphosis of the *Drosophila* trachea affecting all three layers of the epithelium and eventually culminating in tube disassembly.**

In order to examine this hypothesis, the following objectives are designed:

- 1. Identification of adherens junction phenotypes and behaviour adherens junction associated proteins in *Drosophila* tracheal epithelium during metamorphosis.**
- 2. Assessment of the cytoskeletal phenotypes in *Drosophila* tracheal cells during larval to pupal transition**
- 3. Elucidate the basal ECM mechanisms in *Drosophila* pupal tracheal epithelium**

### 1.1.9 Relevance of the Study

Tracheal disassembly during metamorphosis is not a well-researched phenomenon, and has been predominantly explored within the context of apoptosis or programmed cell death. However, one intriguing aspect that continues to pique scientific curiosity is the selective elimination of the posterior trachea. This raises the question of the specific program in place that promotes tissue degeneration in this region. Despite extensive investigations, the underlying mechanisms leading to organ disassembly remain largely unknown. Previous studies on tracheal disassembly have primarily focused on the signalling level, leaving a huge knowledge gap regarding the cell and tissue scale architectural patterns and events that precede this process. It would be highly pertinent not merely to fly biology, but to understanding degeneration in general, to unravel whether there is a programmed epithelial degeneration and how the tissue architecture is altered during this intricate process. One significant limitation in the current body of research is the lack of high-resolution information at both the cellular and subcellular scales. Obtaining detailed insights into the cellular changes occurring during tracheal disassembly would provide valuable clues about the mechanisms driving this phenomenon. By delving deeper into the microscopic alterations within the tissue, we can shed light on the molecular signals and cellular interactions involved in orchestrating the breakdown of the tracheal structure.

In conclusion, while extensive research has been conducted on tracheal disassembly during metamorphosis, several key questions remain unanswered. Exploring the existence of programmed epithelial degeneration and unravelling the cellular and subcellular events underlying this process would significantly advance our understanding of organ disassembly and tissue remodelling. In this study, we focus on the degenerative changes occurring at the subcellular and supracellular levels in all three layers of the *Drosophila* pupal trachea (DT).

Our findings have yielded some exciting results, particularly in relation to the examination of junctional, cytoskeletal, and extracellular matrix phenotypes.

**CHAPTER 2**

**MATERIALS AND METHODS**

## 2.1 Materials

### 2.1.1 Fly stocks

All the fly strains used in these experiments are enlisted in Table-1 and described briefly.

**Table 2.1.1.1** Gal4 lines

<b>Gal4</b>	<b>Chromosome</b>	<b>Specific for</b>	<b>Stock information</b>
Btl-Gal4	II	Respiratory system or trachea-specific expression	Kyoto <i>Drosophila</i> Resource Centre #109128
Btl-Gal4	II	Respiratory system or trachea-specific expression	Markus Affolter laboratory, University of Basel, Switzerland (3rd chromosome)

**Table 2.1.1.2** UAS Reporter lines

<b>Reporter transgenic lines</b>	<b>Chromosome</b>	<b>Specific for</b>	<b>Stock information</b>
UAS-Ut-ABD-GFP	II	Utrophin actin-binding domain tagged with GFP, Labels F-actin	(JayaNandanan et al., 2014)
UAS-PLC $\delta$ -PH-GFP	II	Pleckstrin homology domain of PLC $\delta$ tagged with GFP, Labels plasma membrane	(JayaNandanan et al., 2014)

UAS-PLCd-PH-Cherry	III	Pleckstrin homology domain of PLC $\delta$ tagged with mCherry, Labels plasma membrane.	(Mathew et al., 2020)
Crb: GFP	II	Endogenously expressing Crumbs tagged with GFP	(Huang, Zhou, Dong, Watson, & Hong, 2009)
shg::GFP	II	Endogenously expressing Shotgun tagged with GFP.	(Huang et al., 2009)
shg::mCherry	II	Endogenously expressing Shotgun tagged with mCherry	(Huang et al., 2009)
Ubi:: Cadherin GFP	II	Ubiquitously expressing Shotgun tagged with GFP	M. Narashimha Lab, TIFR Mumbai
Sqh AX3; Sqh-Utr::GFP; Sqh-mCherry	II, III	Utrophin GFP expresses from the sqh promoter labels F-actin, mCherry tagged with Spagetti squash which is Myosin Regulatory Light chain	Leptin lab, EMBL Heidelberg
UAS-Lifeact ruby	II	mCherry tagged with lifeact under UAS binds to F-actin	BDSC 35545
Bazooka::GFP	II	Protein trap line having p element insertion of GFP in an intronic region of Bazooka (Par-3) gene.	BDSC 51572
Viking-GFP	II	Protein trap line having p element insertion of GFP in an intronic	(Buszczak et al., 2007)

		region of Viking (Collagen IV) gene.	
UAS-Shot-L(A)-GFP	X	Expresses the L(A) isoform of shot tagged with GFP under UAS control (Loss of function)	BDSC 29044
UAS-Shot-L(C)-GFP	III	Expresses the L(C) isoform of shot tagged with GFP under UAS control (Overexpression)	BDSC 29043

**Table 2.1.1.3 RNAi lines**

<b>RNAi</b>	<b>Chromosome</b>	<b>Specific for</b>	<b>Stock information</b>
UAS-Cdc 42 RNAi	II	Small GTPase CDC 42 down regulation	BDSC 29006
UAS-Arp14d RNAi	III	Actin branching protein Arp2/3 down regulation	BDSC 27705
UAS-Wasp RNAi	II	Acton nucleating protein wasp down regulation	BDSC 25955
UAS-Rho RNAi	II	Small GTPase Rho1 down regulation	BDSC 28690
UAS-Sqh RNAi	III	Myosin regulatory light chain down regulation	BDSC 33892
UAS-Sqh RNAi	II	Myosin regulatory light chain down regulation	BDSC 38222

UAS-ROK RNAi	III	Rho associated Kinase down regulation	VDRC KK-104675
UAS-Mnat9 RNAi	III	Microtubule N-terminal acetylation 9 down regulation	VDRC 104497
UAS-Shot RNAi	II	down regulation of shortstop a microtubule-actin crosslinker	BDSC 64041
UAS-Eb1 RNAi	III	down regulation of end binding protein 1 (binds to plus end of microtubule)	VDRC 24451
UAS- Patronin RNAi	III	down regulation of Patronin (binds to minus end of microtubule)	VDRC 27654

### 2.1.2 Antibodies

All the primary and secondary antibodies used in these experiments are enlisted in a table and described briefly.

**Table 2.1.2.1** Primary antibodies

<b>Name of the primary antibody</b>	<b>Name of the antigen</b>	<b>Host species</b>	<b>Dilution used in the study</b>	<b>Source</b>
E7	Beta-tubulin	mouse	1:200	DSHB
anti-shot	Shortstop	mouse	1:100	DSHB
DE-cad	DE-Cadherin	Rat	1:100	DSHB
anti-Dlg	Disc Large	mouse	1:250	DSHB
anti-Rho1	Rho1	mouse	1:250	DSHB
CF.6G11	Integrin $\beta$ PS	mouse	1:200	DSHB
anti-GFP	GFP	mouse	1:100	DSHB
Sn7c	Singed	mouse	1:100	DSHB
40-1A	LacZ	mouse	1:250	DSHB

DDA2.7	EcR Common	mouse	1:100	DSHB
anti-Enabled	Ena	mouse	1:10	DSHB
anti-tubulin	alpha tubulin	rabbit	1:250	Abcam ab18251
anti-tubulin	Alpha tubulin	rabbit	1:500	Sigma /NA
Anti tyrosinated tubulin	Tyrosinated tubulin	rat	1:500	Sigma Aldrich MAB1864
Anti acetylated tubulin	Acetylated tubulin	rabbit	1:1000	Sigma Aldrich SAB5600134

**Table 2.1.2.2** Secondary antibodies

<b>Secondary antibody</b>	<b>Host species</b>	<b>Raised in</b>	<b>Dilution</b>	<b>Source</b>
Alexa Fluor- 488	mouse	Goat	1:500	Invitrogen AB_2534069

Alexa Fluor- 488	rabbit	Goat	1:1000	Invitrogen
Alexa Fluor- 568	mouse	Goat	1:300	Invitrogen A11004
Alexa Fluor- 568	rabbit	Goat	1:500	Invitrogen / NA
Alexa Fluor- 647	mouse	Goat	1:500	Invitrogen A12135
Alexa Fluor- 647	rabbit	Goat	1:500	Invitrogen A21244
Alexa Fluor- 680	mouse	Goat	1:500	Invitrogen/ NA
Alexa Fluor- 680	rabbit	Goat	1:500	Invitrogen/ NA

### 2.1.3 Dyes and stain

All the dyes and stains used in these experiments are enlisted in a table and described briefly.

**Table 2.1.3** Dyes and stains

<b>Name</b>	<b>Used for</b>	<b>Dilution</b>	<b>Source</b>
DAPI	Nucleus	1:1000	Sigma-Aldrich D9542
Fluostain	Chitin	1:500	Sigma-Aldrich
CBP	Chitin	1:50	NEB
Phalloidin-FITC	F-Actin	1:1000	Sigma-Aldrich/NA
Phalloidin-Alexafluor647	F-Actin	1:1000	Invitrogen A22287

### 2.1.4 Chemicals and buffers

All the chemicals and buffers used in this study were listed in the table below.

**Table 2.1.4** Chemicals and buffers

<b>Name of the Reagents</b>	<b>Source</b>
Triton X100	MP Biomedicals
Tween-20	MP Biomedicals
BSA Fraction V	Sigma-Aldrich
Formaldehyde	MP Biomedicals
Hepten	MP Biomedicals
Para-formaldehyde	Sigma-Aldrich
MeOH	Sigma-Aldrich
EtOH	Merck
Glacial Acetic Acid	MP Biomedicals
Glycerol	Sigma-Aldrich

DABCO	Sigma-Aldrich
Halocarbon Oil	Sigma-Aldrich
Vectashield	Vector labs
10X PBS	Himedia
Acetone	MP Biomedicals

### 2.1.5 Solutions

The solutions used for this study is listed below.

<b>Solution</b>	<b>Content</b>
PBT	1X PBS 0.2% Triton 100
4% PFA	1X PBS

	4% Para formaldehyde
PBT+BSA Solution	1X PBS 2% BSA 0.2% Triton 100
DABCO mounting media	2.5mg/ml DABCO 90% Glycerol 10% 1XPBS

## 2.2 Methods

### 2.2.1 General fly husbandry

The general fly husbandry includes the culture of *Drosophila melanogaster* in the standard laboratory condition using a corn meal agar-based media and setting up genetic crosses of the flies for overexpression, knock down, or genetic manipulation of the desired gene, setting up embryo collection cages in apple juice agar plates.

#### 2.2.1.1 Preparation of *Drosophila* media

Reagent	Final concentration	Amount
Bacto agar	9g/L	7.2g

Yeast Extract	15g/L	12g
Sucrose	40g/L	32g
Glucose	20g/L	16g
Corn flour	80g/L	64g
Methyl 4-hydroxybenzoate	1.25g/L	1.2g
Propionic Acid	4ml/L	3.2ml
Orthophosphoric Acid	0.6ml/L	0.48ml
ddH <sub>2</sub> O	n/a	800ml
Ethanol	n/a	5ml
<b>Total</b>	<b>n/a</b>	<b>800 mL</b>

Solution 1 was prepared by adding D-Glucose, Sucrose, agar, yeast extract, and 800ml of warm water in a beaker. It was heated for 3-5 mins with continuous stirring. Solution 2 is a slurry made up of corn flour and water. Corn flour slurry was prepared with 100ml of water in a beaker and slowly poured into solution 1. While pouring the slurry, it was mixed thoroughly to avoid clumps. The prepared food was cooked for 5 minutes in a microwave and poured into a glass bottle which was autoclaved for 15 minutes. When the temperature of the media was around 65°C, Propionic acid, Ortho-phosphoric acid, and TEGO (dissolved in 5ml Ethanol) were added and mixed thoroughly. The media was poured into vials and bottles depending on the requirement.

### 2.2.1.2 Preparation of apple juice agar plates (Adapted from CSHL("Apple juice-agar plates," 2009))

Reagent	Final concentration	Amount
---------	---------------------	--------

Bacto agar	24g/L	12g
Sucrose	20g/L	10g
Grape Juice	n/a	200ml
Methyl 4-hydroxybenzoate	1.2g/L	0.6g
ddH <sub>2</sub> O	n/a	300ml
<b>Total</b>	<b>n/a</b>	<b>500 mL</b>

Solution 1 was prepared by adding 700ml of H<sub>2</sub>O in agar and autoclaving for 40 minutes. Methylparaben was added to ethanol in a 15ml falcon tube and mixed thoroughly. Solution 2 was prepared by adding Methyl paraben solution into 300ml of apple juice. Solutions 1 and 2 were mixed in a beaker and poured into Petri plates quickly to avoid solidifying the solution in the beaker.

### 2.2.2 Fly Genetics and Crosses

All the genetic crosses used in this study were set up in standard corn meal agar media at 25°C. All the RNAi experiments were performed by using *btl-Ut-ABD-GFP/CyO*; *UAS-Dicer/TM6Tb* fly line in 25°C.

### 2.2.3 UAS-Gal4 Binary system

In order to accomplish tissue-specific expression or downregulation of targeted genes in the trachea, we have used a yeast UAS-Gal4 binary system. Gal4 is a yeast transcriptional factor that controls the galactose operon and prefers the UAS above other DNA sequences (Duffy, 2002). The UAS-Gal4 system is a widely used binary system for spatial expression in

*Drosophila melanogaster* (Brand & Perrimon, 1993). Tissue-specific expression happens, when flies having the upstream activator sequence regulating either an shRNA or overexpression construct or any fluorescent reporter line, are crossed with Gal4 containing transgenic lines. When Gal4 binds to UAS, it activates any genes or RNAi that are nearby the UAS site. For trachea-specific RNAi or overexpression lines under the UAS site, we have used a breathless Gal4 line (Btl-Gal4), in which the Gal4 gene is expressed under the trachea-specific promoter breathless, i.e., FGF receptor.

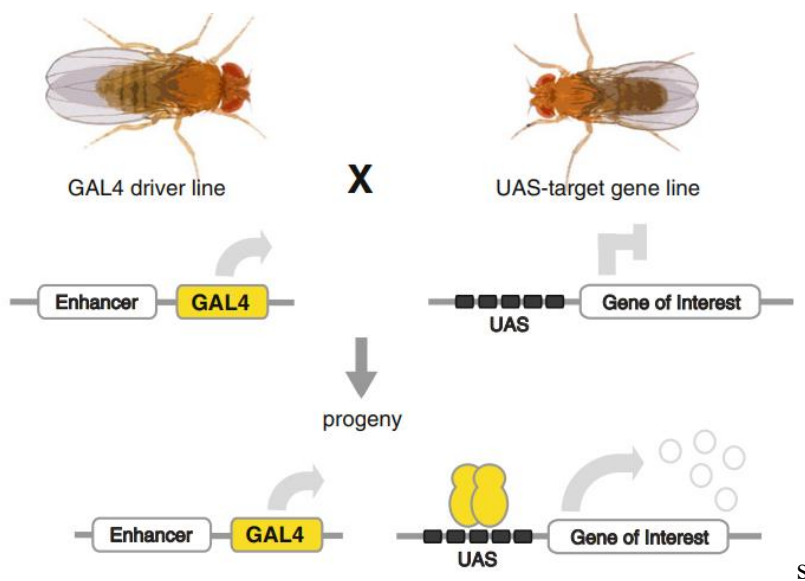


**Figure 2.1: UAS-Gal4 binary system**

The ectopic gene activation or repression system has two components. Gal4- a yeast transcriptional factor and UAS or upstream activator sequence adapted from yeast. The Gal4 element can be expressed spatially using a tissue-specific enhancer. The targeted gene is under the UAS element. Genetic cross showing the Gal4 containing female is mated with UAS-target gene containing male fly. The progeny has both the Gal4 and UAS elements, hence tissue-specific Gal4 expression and Gal4 will bind to the UAS element of the target gene. (Image adapted from (Caygill & Brand, 2016)).

## 2.2.4 RNAi of genes in the *Drosophila* trachea by using breathless Gal4

For knocking down desired genes in the trachea, a breathless gal4 driver line was used. A recombinant line was created by crossing breathless Gal4 with the UAS actin-binding domain of Utrophin tagged with GFP. The recombinant line Btl-Ut-ABD-GFP was again crossed with a UAS-Dicer fly line to create a stable, balanced line Btl-Ut-ABD-GFP/CyO; UAS-Dicer/TM6Tb. Dicer and the F-actin marker Ut-ABD-GFP are expressed in the trachea. Virgins from this line were crossed with desired UAS-RNAi lines having inverted repeat sequences or short hairpin loop RNA of the desired gene. IRs/Sh RNAs were produced in the trachea. The IR repeats bound to the mRNA of the desired gene, and Dicer ensured the binding and cleaving of the double-stranded mRNA led to the depletion of the mRNA. Thus, regulating the gene expression at the mRNA level.

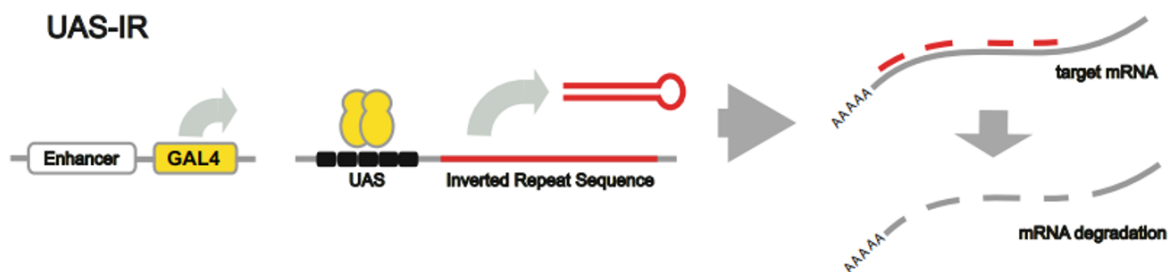


**Figure 2.2: UAS-IR (Inverted Repeats)**

Inverted repeats of the target gene are under the UAS element. Gal4 is expressed under a tissue-specific promoter, leading to the expression of IR in the target tissue. The expressed IRs bind to the mRNA and block the gene expression at the mRNA level. (Image adapted from (Caygill & Brand, 2016))

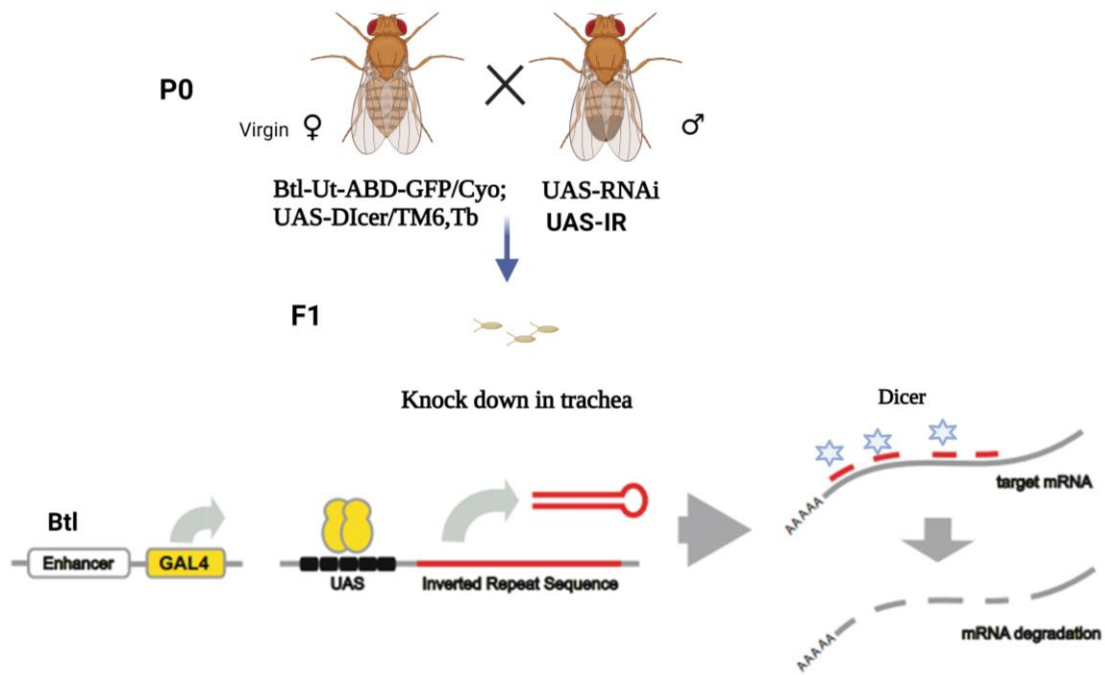


**Figure 2.3: Knockdown of genes in trachea using breathless Gal4 system**

Inverted repeats of the target gene are under the UAS element. Gal4 is expressed under a trachea-specific promoter, i.e., breathless (*Btl*), leading to the expression of IR/ shRNA in the trachea. The driver line used here is line *Btl-Ut-ABD-GFP/Cyo; UAS-Dicer/TM6Tb*. Dicer is over-expressed using the *Btl-Gal4* driver. Dicer binds to double-stranded RNA and cleaves it, blocking the gene expression. (Image modified from (Caygill & Brand, 2016))

### 2.2.5 Synchronized Embryo collection cage setup

For setting up the embryo collection cage, fresh apple juice agar plates were prepared. A small amount of yeast paste was applied to the plate, and a good number of flies were added to the cage. The ratio of male and female flies was kept at 2:1. The embryo cage was kept in a 25°C incubator. The apple juice agar plates were changed every 4h interval. The flipping time was considered as 0h after the egg lay (AEL). Embryos were collected from the changed plate with

the help of a wet paintbrush. The embryos were kept in a food vial for developmental staging. These embryos can be used for embryo staining or live imaging after a few hours of development by keeping the changed plate directly in a closed box in the 25°C incubator.

### **2.2.6 Developmental staging**

For staging of the larvae and pupa, both egg laytime and morphological phenotypes were used. Staging can be divided into three broad periods, i.e., Embryo-MidL3 (ML3) stage, ML3 to late ML3 stage, and pupal stages. Crosses set up for staged collection were flipped every 4 hours intervals. The flipping time was considered as 0h after egg lay. The flipping time was noted. For staging the embryo to the midL3 (ML3) stage, mostly AEL timing was used for developmental staging. The first larval instar begins around 24-27h AEL. The second and third molt happens approximately at 49h AEL and 72h AEL respectively, which is the beginning of the early second and third instar larva (Ashburner, Golic, & Hawley; Hosono et al., 2015). The early L3(EL3) larvae (approximately 90h AEL) are thin and buried in the food. This is the voracious feeding stage. MidL3 larvae are approximately 110h AEL are fat and remain mostly on the surface layer of the food and still feeding. The late third instar larvae are categorized into two groups. Wandering third instar larva (WL3), Stagnant third instar larva (L3S). Staging of late third instar larva is very difficult. The wandering L3 stage is reversible, and the duration variable (Bainbridge & Bownes, 1981; M, 1980). Morphological characteristics were used to stage the WL3 and L3S larvae. WL3 are the fat larvae that climb the vial wall post-feeding and crawl around in preparation for pupation. Once the WL3 larva stopped moving, a circle was drawn around it. If the larva remains in the circle and maintains stagnancy for 30 minutes, then it is considered as L3S stage. L3S larvae stop moving and evert their anterior spiracles. They become shorter in length, but they can move if disturbed. The L3S larva becomes prepupa within 30-45 minutes. The prepupa can be easily recognized by its transparent white colour

and withdrawn first three anterior segments. In Prepupa, the pupariation begins, and it is much shorter in length. It sticks to the wall as cuticle secretion starts, and it stops moving altogether. The prepupa stage is considered as 0h APF (after puparium formation), and further pupal stages are timed. The prepupa was marked on the vial surface, and the time was recorded. From the pupation time, 1h APF, or 2h APF time, was calculated.

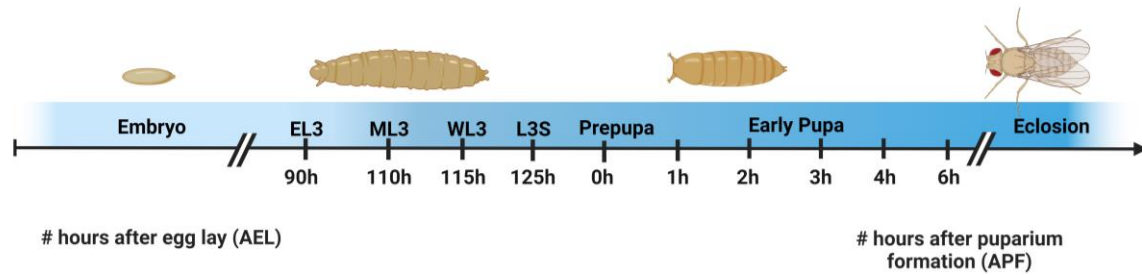


**Figure 2.4: Timeline showing the developmental staging of the *Drosophila* larva and pupa**

### 2.2.7 Embryo Fixation and Immunostaining

For immunostaining, embryos were collected and dechorionated with Sodium Hypochlorite 4% (v/v) for 5 minutes. Dechorionated embryos were collected using a paintbrush and put into 1.5 ml Eppendorf tubes with Heptane and 37% Formaldehyde (1:1). Formaldehyde was used for fixation. Embryos were vortexed for 15s in fixing solution and kept for 5 minutes in RT. The bottom phase formaldehyde was removed, and methanol was added for devitalization. The embryos were vortexed for the 30s, and the interphase was removed. The fixed embryos were rehydrated with 70%, 50%, and 30% Methanol in PBS for 10 minutes. After that, the samples were washed twice in PBT for 10 minutes and blocked for one hour in the block buffer. The samples were incubated in primary antibodies overnight at 4°C. The antibody solution was removed, and the samples were washed three times in PBT for 10 minutes. Required Alexa fluor conjugated secondary antibodies, stains, and probes were added to the block buffer, and

samples were incubated at room temperature for two hours in the dark. The embryos were washed three times in PBT for 10 minutes and mounted in Vectashield™ (Vectorlabs).

### **2.2.8 First instar larval dissection**

L1 larvae were smaller in size and very thin. The L1 larvae were dissected or torn in 1X PBS carefully without damaging the trachea with the help of fine needles and forceps. Fat Bodies and gut were carefully removed and fixed using 4% Paraformaldehyde (Sigma) for 20 minutes. The larval carcass was transferred carefully on a glass slide. All the washings were done carefully on the slide.

### **2.2.9 Larval and pupal dissection by ventral filleting method**

The ventral filleting method is widely used by developmental biologists to dissect the trachea (Feng Chen; Levi, Ghabrial, & Krasnow, 2006; Weaver & Krasnow, 2008). We have used the ventral filleting method to dissect the trachea of L2, L3, and early pupa. The dissection was performed under a stereo microscope on a silicone elastomer plate. Vannas scissors, Dumont 5 Forceps, and a good number of insect pins were required for this microsurgery. On the dissection plate, the developmentally staged larva or pupa was aligned ventral up position and pinned at both ends using fine insect pins. 1X PBS was added to the plate. The ventral body wall was lifted near one end and cut along the midline by a pair of Vannas scissors. The edge of the body wall was stretched using forceps and pinned at all four ends to the plate. The larval or pupal carcass was fixed by 4% Paraformaldehyde. The internal organs were carefully removed without damaging the tracheal dorsal trunk. The fillets were fixed for 20 minutes at room temperature. PFA solution was removed from the dissection plate, and the fillets were thoroughly washed with 1X PBS. The pins were carefully removed, and the fillets were transferred to a 24-well plate containing PBS.

### **2.2.10 Immunostaining**

The dissected larval and pupal fillets were washed with 0.2% PBT (1XPBS+ 0.2% Triton X100) three times for 10 minutes each. The last PBT was discarded, and the fillets were incubated in a block buffer (2% BSA+ 0.2% PBT) for 1 h at room temperature. All the steps were performed on a platform rocker with gentle shaking. The samples were incubated in primary antibody overnight on a rocker at 4°C. The fillets were washed four times in 0.1% PBT and incubated in fluorophore-conjugated secondary antibody for 2h at room temperature. Then washed three times for 10 mins each and mounted in Vectashield or DABCO. The ventral side of the fillets was arranged towards the coverslip side. The anterior, and posterior arrangement of all the fillets was kept similar. The slides were sealed with transparent nail polish to avoid leakage.

### **2.2.11 Dissection and immunostaining of other larval tissue**

Dissection of the *Drosophila* larva was performed by ventrally opening the larva by cutting across the midline, starting from the anterior to the posterior end. The larvae were dissected in 1X PBS for a brief period, fixed using 4% Paraformaldehyde (Sigma) for 20 minutes at room temperature. The larval tissues were removed carefully. Fat bodies and wing imaginal discs were carefully taken out and collected separately in Eppendorf tubes. The anterior larval mouth part and the intact salivary gland were removed. The fillets were cleaned from unnecessary tissue and used for body wall staining. The collected larval tissues were washed three times with 0.2% PBT for ten minutes each and then incubated in a block buffer (2%BSA+0.2%PBST) for 1h in RT, followed by incubation with primary antibody solution overnight in 4°C. The staining step was done on a platform rocker. The tissues were washed four times in 0.2% PBT and incubated in fluorophore-conjugated secondary antibody and phalloidin for 2h at room

temperature. Then washed three times for 10 mins each in 0.2% PBT and mounted in Vectashield or DABCO mounting media.

### **2.2.12 aECM staining**

Calcofluor white (1mg/ml, Sigma) in 1:500 and chitin-binding probe 647 (1:50) were used for aECM staining with the secondary antibody step during immunostaining for 2h in the block buffer. aECM stains can also be used with the PBT step for 2h at RT after primary antibody staining.

### **2.2.13 Phalloidin staining**

For phalloidin staining, Phalloidin 647 was diluted in block buffer in 1:500 concentration or added directly with the secondary antibody step during immunostaining for 2h at RT.

### **2.2.14 Image Acquisition, Processing, and Quantitation**

Fluorescent images were acquired by an inverted Leica SP8 laser-scanning confocal microscope using a 63x oil immersion objective (1.45 NA) with 1024×512pixel format and 0.3 μm spacing in the z-axis. The images were taken along the half diameter of tr7 or tr8 of the dorsal trunk. The scan speed was 400Hz, and the line averaging 4 during image acquisition. To calculate the posterior tracheal DT for length measurements, confocal images were acquired in the Leica SP8 Laser scanning confocal microscope using a 20x oil objective with a 1024×1024-pixel image format, 3 μm spacing z stack using Leica Las X software. The images acquired were processed using Leica LASX software and Fiji (ImageJ)

### **2.2.15 Line-plot analysis**

To visualize the enhancement of CDC42 and Rho signals at LAJ over ZA, line plots were used. Background subtraction of Sum intensity projections of 15-30  $\mu\text{m}$  stack was done first from the selected images. Identical straight lines were drawn, intersecting ZA and LAJ at corresponding adjacent locations and perpendicular to the junctions on sum intensity projection images. Line profiles were generated in Fiji, by using its line profile tool, and the peak intensity value for each junction in the DE-Cad channel was identified. A line of 0.9 mm on either side of the peak point, covering 5 intensity measurement points separated by 0.18 mm each, was used for quantification. The intensity values along this 1.8mm line in the DE-Cad channel and the corresponding GTPase channel were collected, and mean values were used to generate the line profiles at ZA and LAJ.

### **2.2.16 Enrichment analysis of Rho and CDC42 at LAJ**

Images from the DE-Cad channels were utilized to define the LAJ and ZA regions in order to quantify the enrichment of Cdc2 and Rho GTPase signals at LAJ in comparison to ZA. The sum intensity projections of 15–30  $\mu\text{m}$  stacks were used, and identical area ROIs were determined for the LAJ and ZA. Following background subtraction, fluorescence enrichment was calculated by integrating the Cdc42 and Rho channel pixel intensity values for ZA and LAJ.

### **2.2.17 Directionality analysis**

Maximum intensity projections of 15–30  $\mu\text{m}$  stacks of the Ut-ABD-GFP channel of 1hAPF images were used to determine the orientation of actin cables. First, the horizontal axes of the acquired images were aligned with the cylindrical axes of the DTs. After converting the images to 8-bit format, regions of interest (ROIs) were identified. The background noise was reduced

during pre-processing, and the image contrast was increased to the optimum for fibre detection and segmentation. Bright pixels were eliminated from the duplicate ROIs using the "Remove Outliers" function, and the pixel-removed images were subtracted from the unprocessed original images. The resulting images were then despeckled and smoothed after receiving additional processing using the logarithmic function. Using the "local gradient orientation" technique of the "Directionality" plugin was used to determine the optimal orientation of the structures evident in the input image. By visual inspection, the regions that have been identified were confirmed. Last but not least, the anisotropy of cable directionality in various images was measured using the standard deviation associated with the mean direction with respect to the horizontal axis. For Dicer control and KD conditions, an average of standard deviations of actin cable orientation for different images were calculated.

### **2.2.18 Length calculation and posterior tracheal compression analysis**

The maximum intensity projections of the 20x images of posterior tracheal metameres (tr6-tr8) were used for the length calculation for control and knockdown lines of WL3, 2h, and 6h. The length of the metameres (tr6- tr8) was measured using Fiji by drawing a line from one end of the inter-segmental junction (ISJ) to the other end of ISJ. To determine the posterior tracheal length, the length of tr6-tr8 was added. The ratio of the posterior tracheal length of the control versus RNAis were calculated, and the percentage of tube shortening was calculated by multiplying the ratio by 100. The data sets were plotted using GraphPad PRISM, and significance was calculated using Two-way ANOVA.

### **2.2.19 Inter-taenial spacing calculation**

Calculation of inter-taenial distance was adapted from (Fraire-Zamora et al., 2021). For this objective, bright field images of posterior DT metameres (Tr8) were examined. Dark and light bands, respectively, denoted the chitinous ridges and the gaps between them. Using the appropriate z-slices, lines orthogonal to the bands were drawn with identical lengths. For three different regions of a single metamere, line-plot profiles were created. For better representation, metameres from various DTs were included under each data class. To plot pixel intensity versus distance and determine the separation between two successive intensity peaks, a Python program was written. The estimated differences of peak distances and related standard deviations were averaged to determine inter-taenial distances. Using GraphPad PRISM, the data sets were plotted, and significance was calculated using Two-way ANOVA.

### **2.2.20 Microtubule orientation calculations**

Microtubule orientation was calculated by an ImageJ plugin 'OrientationJ' developed by EPFL (<http://bigwww.epfl.ch/demo/orientationj/>). We analysed an average of 10-15 images from tr-8 metamere of 1h pupa of Dicer control and RNAi. The images were aligned properly along the long axis of the tube. The images were pre-processed by background subtraction and thresholding before doing the orientation analysis. The data obtained were plotted as a rose plot using Matlab (Matis, Russler-Germain, Hu, Tomlin, & Axelrod, 2014; Rezakhaniha et al., 2012).

### **2.2.21 Colocalization of shot and microtubule**

Colocalization shot and microtubule and shot and F-actin was performed separately by using a Fiji plug in Colocalization Finder plug in. Identical region of interest was selected in both the

channels for colocalization analysis. Background subtraction and thresholding was done. To perform the analysis colocalization threshold parameters were set before doing the analysis. A scatter plot was generated for both the set of colocalization analysis showing the overlapping regions.

**CHAPTER 3**

**LATERAL ADHERENS JUNCTIONS (LAJs) AND**  
**ASSOCIATED ACTOMYOSIN CORTEX MECHANISMS IN**  
**THE TRACHEA OF *DROSOPHILA MELANOGASTER*.**

### 3.1. Introduction-

Epithelia is one of the most common tissue types of metazoans, and plays an important role in shaping the organs and forming the boundaries (Bryant & Mostov, 2008). The cells in an epithelium attach to each other and form sheets or tubes, which act as barriers and help in compartmentalization. The epithelial cells have three domains, apical domain, lateral domain, and basal domain. In general, the apical domain comprises the apical area of the cell facing outside the tissue, the lateral domain has junctions that attach to the nearby cells, and the basal domain adheres to the extracellular matrix (C. E. Buckley & St Johnston, 2022). The adherens junctions (AJs), septate junctions, gap junctions, and dot junctions or focal adhesions are the main types of junctions found in the epithelium. The most apical junctions in the vertebrate epithelium are known as tight junctions. Adherens junctions can be found underneath tight junctions at the apico-lateral membrane. In contrast, the epithelium in *Drosophila* lacks tight junctions. The apex apical junction in *Drosophila* is the adherens junction, below which the septate junction is present. Septate junctions are absent in vertebrate epithelium. . However, in *Drosophila*, adherens junctions (AJs) are classically positioned at the apical part of the lateral membranes and mediate the linking of apposing cells through homophilic interactions between extra-cellular domains of the E-cadherin(E-Cad) proteins.

E-Cadherins exhibit a belt-like organization of AJ around the cell periphery, called Zonula Adherens (ZA) (M. Takeichi, 2014). Apicobasal polarity pathways are important in regulating the positioning of the AJs (Tepass, 2012). E-Cad or epithelial cadherin is the classical cadherin molecule which is primarily a glycoprotein. E-cad has four major domains, five extracellular cadherin domains 1 to 5 (EC1–5), the transmembrane region, and the cytoplasmic tail. The cytoplasmic domain interacts with the effector proteins, which primarily include the juxtamembrane domain (JMD) and the catenin-binding domain (CBD) (Ishiyama & Ikura, 2012). The extracellular domain or EC domain interacts with other

extracellular EC domains to form trans homodimers during cell adhesion (S. K. Wu & Yap, 2013). The cytoplasmic domain interacts with other E-Cad adapter proteins to carry out intracellular activities and downstream signalling pathways.  $\alpha$ ,  $\beta$ , and p120 catenins are the core members of E-Cadherin adapter proteins (Coopman & Djiane, 2016). Many other proteins also interact directly and indirectly with the cytoplasmic domains of E-cad molecules (Niessen, Leckband, & Yap, 2011). These adapter proteins allow the cytoplasmic domain to interact with actin organizers and the F-actin (Ratheesh & Yap, 2012). An essential function of the cytoplasmic interactions of E-cad is in the assembly of the junctional actomyosin cortex (Mason et al., 2013). The actomyosin cortex plays an important role in tissue and organ morphogenesis, and dynamics by modulating force generation and transmission in a sheet of epithelium via cell junctions (Levayer & Lecuit, 2012; Röper, 2013; S. K. Wu & Yap, 2013). Such mechanisms depend on the generation of tension through interactions between the actomyosin cortex and cellular adhesions at junctions. Due to its involvement in junction formation and cortex establishment, E-cad is crucial to the functioning of this network (Mason et al., 2013; S. K. Wu & Yap, 2013).

The *Drosophila* respiratory system, trachea, is a highly ramified network of epithelial tubes that transport gas to the target cells (G. & A, 1993; Loganathan et al.). The tracheal cells have all hallmarks of classical epithelia, including apicobasal polarity, junctions, and adhesions. Therefore, the organ has been used as a model to study epithelial biology, as well as tube morphogenesis (Markus Affolter & Caussinus, 2008; Hayashi & Kondo, 2018). Regulatory events at AJ play crucial roles in morphogenetic changes in trachea, as in other epithelial tissues (Thomas Lecuit, 2005). In the trachea, E-cad trafficking is essential for cell intercalation during the embryonic development of the tracheal DT (Shaye et al., 2008). Axial elongation of the developing DT depends on AJ remodelling via Src42A-mediated recycling of E-cad (Förster & Luschnig, 2012; Shindo et al., 2008). The formation of additional tracheal branches

requires junctional remodeling as well (Cheshire, Kerman, Zipfel, Spector, & Andrew, 2008; Kerman, Cheshire, Myat, & Andrew, 2008).

E-cad clusters complexed with catenins that are linked to the actin cytoskeleton have also been seen as a distribution on the lateral membrane of epithelial cells basal to the ZA, even though the majority of these functions are examined in the context of AJ (Otani et al., 2006). The functional role of these lateral cadherins and whether these are bona fide AJs have remained puzzling (M. Takeichi, 2014). The flow of cadherin molecules along the lateral membrane has been suggested to enable a function in permitting relative motion between two apposing membranes in transformed cells and during dynamic morphogenetic events (Yoshiko Kametani & Masatoshi Takeichi, 2007). Several cell culture experiments have shown that at least some of the E-cad molecules distributed on the lateral membrane below the AJ are junctions composed of trans-interactions that move apically (S. Hong, Troyanovsky, & Troyanovsky, 2010; Yoshiko Kametani & Masatoshi Takeichi, 2007). Cis and trans cadherin interactions and direct interaction with actin cytoskeleton are crucial for the stability and directionality of movement of lateral clusters of E-cad (Soonjin Hong et al., 2013). The Yap group's experiments have led to the theory that the lateral E-cad clusters are LAJ linked to an actomyosin cytoskeletal cortex. Intriguingly, the contractility of this cortex is different from the ZA cortex, and the heterogeneous contractility patterns across the various cadherin junction types are crucial for the integrity of Caco-2 cell monolayers with implications for the extrusion of cells from epithelial sheets on malignant transformation (Selwin K. Wu, Budnar, Yap, & Gomez, 2014; Selwin K. Wu, Gomez, et al., 2014). While a similar lateral cadherin distribution has been shown in mouse small intestinal cells (Larsson, 2006) a clear demonstration of LAJs in vivo and the functional significance of associated proteins, have been missing in the literature.

Here, we demonstrate distinct LAJs in the cells of the *Drosophila* trachea and characterize it in the larval and early pupal DT. Our research reveals a distinct band of *Drosophila* E-Cad (DE-Cad) based junctions that runs basally and adjacent to the ZA of the DT cells. The LAJ-associated actomyosin cortex is more dynamic than the ZA cortex and mediates a supracellular cortex of actomyosin cables that develops in the late larva and extends to the early pupa. The development of the supracellular cortex depends on LAJ-localizing Rho-GTPases. In the early pupal stages, activated myosin and actinin accumulate in the bundles of the actomyosin cortex, akin to stress fibers. These stress fiber-like bundles redundantly contribute to the shortening of the DT in the early hours of pupation. It has been recently reported that dorsal trunk shortening on pupariation is mediated by an apical ECM mechanism independent of actomyosin (Fraire-Zamora et al., 2021), in congruence the DT shortening achieves completion when the actomyosin bundles are disrupted. However, our data shows that the actomyosin system provides an initial accelerating impetus that facilitates the early phase of the DT compression. This report is the first clear demonstration of the presence of distinct LAJs with downstream adapters and cytoskeletal operators in vivo. We also establish a functional role for LAJ in generating a specialized dynamic actomyosin cortex.

## **3.2. Results**

### **3.2.1 Identification of a novel lateral adherens junction in *Drosophila* larval tracheal dorsal trunk epithelium**

When investigating the mid-L3 (ML3) larval DT, we discovered that in addition to the prominent and distinct ZA accumulation of DE-Cad along the cell boundaries of DT, another distinct accumulation of the protein was observed on the lateral membrane, slightly basal to the ZA (**Figure 3-1Ai**). In contrast to ZA, the DE-Cad enrichment was more diffuse and punctate at the latter location. DE-Cad has been described in numerous contexts as constituting

a lateral junctional complex basal to the ZA (M. Takeichi, 2014; Selwin K. Wu, Gomez, et al., 2014).

Similar to those instances, the lateral E-cad pattern's visibility and pattern of the distribution in the DT cells also varied, probably owing to the lateral membrane's varying tilt. Interestingly, the lateral DE-Cad that we saw formed a more compact belt-like pattern closely following the ZA, in contrast to other findings of LAJs where E-Cad was observed to be widely dispersed in a membrane region basal to ZA. The two DE-Cad tracks' morphologies, however, were notably different, with the lateral enrichment appearing straighter than the wavier pattern at ZA. This would imply variations in the geometry of the cell's perimeter and probably in the forces applied to these two distinct orthogonal, adjacent planes of the lateral membrane. PtdIns(4,5)P<sub>2</sub> (PIP<sub>2</sub>) sensor PLC-PH-Cherry is a known marker widely used to label plasma membrane. This has been used to demarcate the partition to the junctional and apical plasma membrane area of cells in the DT cells (JayaNandanan et al., 2014; Mathew et al., 2020). In the DT cells, it showed a domain of enrichment extending from ZA to the lateral E-Cad belt (**Figure 3-1Aii**). The borders of this domain, which correspond to the two DE-Cad belts, seemed to have more PIP<sub>2</sub> enrichment, which was frequently more prominent towards the lateral border. We investigated the YZ orthogonal view of the tube to define the relative topology of the two types of junctions in the epithelial layer (**Figure 3-1Aiii**). ZA and the lateral E-Cad belt were separated in the XY plane of the epithelial cell rather than the thickness of the z plane, i.e., the thickness of the tube wall. This proved that the DT epithelium is highly flattened, with minimal membrane present at a plane perpendicular to the apical and basal domains in the conventional orientation of the lateral membrane. This was reinforced by the fact that we always found the DT wall very flat, only 2-3 microns thick within the resolution limit of Laser scanning confocal microscopy.

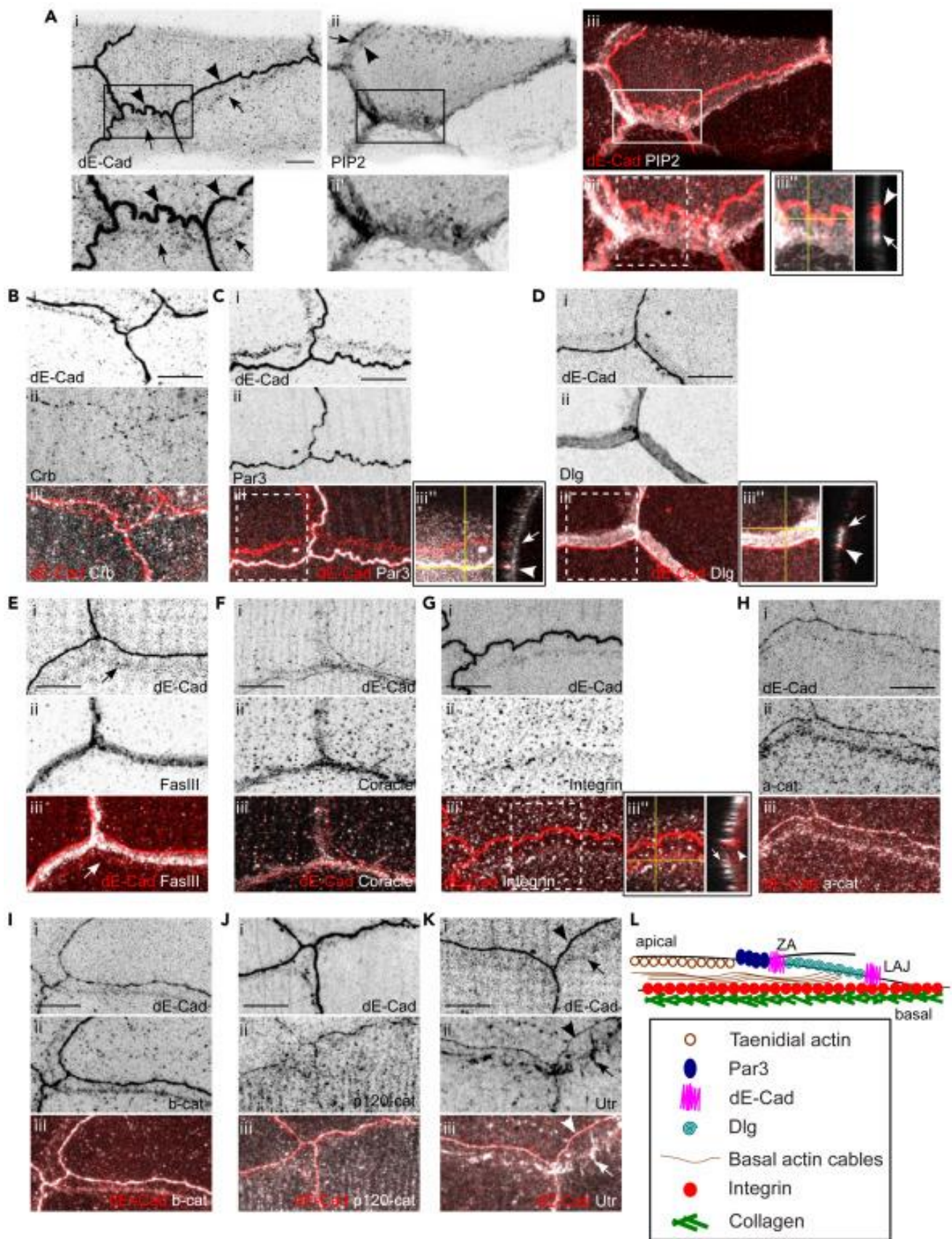


**Figure 3-1. Identification and characterization of lateral adherens junction in *Drosophila* larval trachea**

(A) Images of posterior metameres, tr7/tr8 of the dissected DT of *btl > PLC $\delta$ -PH-Cherry* (PIP2), immune-stained for DE-Cad. Anterior is to the left, and posterior is to the right. 1Ai shows the two belts of DE-Cad along the boundary of the DT cells. The bright and sharp junction indicated by the arrowhead is ZA, and the arrow indicates the additional punctate lateral accumulation of DE-Cad. (Aii) PIP2 enrichment at the junctional region. (Aiii) Merge of the two channels. Aiii'' shows the Y-Z orthogonal view from the ROI indicated by the box in Aiii'. Arrowheads indicate the location of ZA, and arrows indicate the location of the lateral DE-Cad accumulation. Larvae in which endogenous Crb is tagged with GFP.

(B) and Par3 protein trap (C) were immune-stained for DE-Cad. Crb and Par-3 localize close to ZA with no enrichment visible near lateral DE-Cad. Larvae in which endogenous DE-Cad is tagged with mCherry were immune-stained for Dlg

(D). Dlg extends from ZA until the lateral DE-Cad accumulation. Ciii'' and 1Diii'' show the Y-Z orthogonal view from the ROI indicated in Ciii' and Diii', respectively Arrowheads indicate the location of ZA and arrows indicate the location of the lateral DE-Cad accumulation.

(E and F) Larvae in which endogenous DE-Cad is tagged with mCherry were immune-stained for SJ markers FasIII and Coracle. The arrow in E indicates the location of lateral DE-Cad accumulation.

(1G) Larvae in which endogenous DE-Cad is tagged with mCherry were immune-stained for Integrin  $\beta$  subunit. Giii'' shows the Y-Z orthogonal view from the ROI indicated by the box in 1Giii'. Arrowheads indicate the location of ZA and arrows indicate the location of the lateral DE-Cad accumulation.

(H and I)  $\alpha$  and  $\beta$  catenins are associated with both the ZA and the lateral DE-Cad. Larvae of Ubi-E-Cadherin:GFP or with endogenous DE-Cad tagged with GFP were immune-stained for  $\alpha$  and  $\beta$  catenin, respectively.

(J) p120 catenin localization is more prominent at ZA than at the lateral DE-Cad. Endogenous DE-Cad:GFP larvae immune-stained for p120 catenin.

(K) Distinct actin cortices are associated with ZA (arrowhead), and the lateral E-Cad (arrow). *btl* > Ut-ABD-GFP larva immune-stained for DE-Cad.

(L) A diagrammatic representation of our view of the organization of the highly flattened epithelial cells of DT. Unless otherwise mentioned all images are maximum intensity Z-projections of 15–30  $\mu\text{m}$  stacks, imaged at a Z-resolution of 0.3  $\mu\text{m}$ . Scale bars indicate 10  $\mu\text{m}$ .

### **3.2.2 Characterization of the lateral adherens junction (LAJs) in *Drosophila* larval tracheal dorsal trunk epithelium**

We next looked at representative proteins from the apicobasal polarity complexes that function close to the junctional region to understand whether the formation of the lateral DE-Cad belt was associated with alterations in any of these patterns. Crumbs (Crb) (**Figure 3-1B**) and Par3-Bazooka (**Figure 3-1C**), two key protein members of the apical polarity complexes, localized as expected. Both proteins showed a tight enrichment nearly inseparable from the ZA in our images, as expected for the highly squamous cells of the DT epithelium. These proteins were never visualized at LAJ, even on considerably hiking the signal in the images.

For basolateral polarity markers, we examined Disc-large (Dlg) which was present spread out in a domain immediately basal to ZA (**Figure 3-1D**). The Dlg domain was fairly broad, extending from ZA to the lateral DE-Cad belt. The basal border of the Dlg domain was closely followed by the lateral DE-Cad enrichment in all the cases. It is known that Dlg, along with its partners Scrib and Lgl, are associated with the septate junctions in *Drosophila* (Woods

& Bryant, 1991). Fasciclin III (FasIII), another septate junction associated protein (Beitel & Krasnow, 2000) occupied a more limited region than the dig domain (**Figure 3-1E**). FasIII accumulation extended from ZA and stopped just above the lateral DE-Cad. FasIII has been shown in embryonic DT to demarcate the apical third of the lateral membrane (Norum et al., 2010). Coracle, another component of the septate junctions was also enriched in a similar domain (**Figure 3-1F**). The DT epithelium in the ML3 larva is thus organized according to the conventional organization of AJs and apical and basolateral polarity complexes. However, the bottom edge of the SJ/basolateral polarity complexes defines the zone where these cells establish an additional belt of DE-Cad on the lateral membrane. It can also be seen from **Figure 3-1D–H** that we were able to visualize the lateral E-Cad accumulation by other means such as a fly line where the endogenous DE-Cad is tagged by a fluorescent reporter.

The position of the lateral E-Cad was further characterized by observing at the orthogonal view of the DT cells with apicobasal polarity markers. The Y-Z orthogonal views of DT stained for Par3-Bazooka and Dlg (**Figure 3-1Ciii” and 1Diii,” respectively**) provided further evidence for the highly flattened nature of the DT epithelium. While Par3-Bazooka overlapped with the ZA E-Cad (**arrowhead**), the Dlg signal occupied the space between the two E-Cad belts along the XY plane of the tube wall. The lateral E-Cad signal (**arrow**) overlapped with the basal edge of the Dlg signal. Dlg is a core member of the basolateral polarity complexes and septate junction. This shows that the lateral membrane of these cells is highly flattened along the plane of the tube wall and only minimal membrane associated with the junctions remains in the classical lateral membrane orientation. However, this does not appear to be a regular patterned flattening, as the apparent separation between the two E-Cad populations and the direction of tilt are highly variable. We measured separations ranging from 2.5 to 6.5  $\mu\text{m}$  (mean 4.5  $\mu\text{m}$ ) between the E-Cad belts (**Figure-3-2D**) from a random set of

projected images where the separation between junctions was clear. The values are presented as an acceptable approximation of the real spacing given the flat epithelium, with a caveat that these separations were measured in the XY plane of projected images. We are currently unable to establish if this is due to variable relative positioning of the junctions or uneven folding or flattening of the intervening membrane. To fully understand this fascinating organisation, electron microscopy studies of the junction-associated membrane domains would be necessary. However, the radically altered form of the membrane at the apical junction may be an indication that the cell or the apical membrane face requirements to adapt shape or membrane area. We further investigated the relation between AJs and basal membrane protein, integrin, and basal ECM component Collagen (**Figure 3-1G and Figure 3-2-C**). We did immunostaining for Integrin  $\beta$  subunit which showed signal coating in the basal domain of the cells. As the cells were highly flattened, both the E-Cad junctions were nearly in apposition with the integrin layer. For basal ECM visualization, a protein trap for Viking (*Drosophila* collagen IV) was used. The basal ECM marker Collagen also showed a similar pattern like integrin (**Figure 3-2-C**).

We believe that the novel E-Cad junctions we have discovered are on the flattened lateral membrane, despite the fact that it is tempting to speculate if they are novel basal E-Cad junctions given that the junctions overlap the border of the basolateral polarity complex. However, in order to resolve this issue unambiguously, electron microscopy would be needed. E-cad based LAJ in epithelial cells have been reported before (M. Takeichi, 2014; Selwin K. Wu, Budnar, et al., 2014; Selwin K. Wu, Gomez, et al., 2014). The LAJ in such cases were shown to be functional AJs that associate with the downstream signalling partners and organize cortical actin on the plasma membrane. In order to examine whether we have identified a similar *in vivo* LAJ complex in the DT, we stained the ML3 larvae for  $\alpha$  and  $\beta$  Catenins. The catenins are E-Cad adapter proteins essential for interacting with E-Cad intra cellular domain

with cytoskeleton. Both the catenins showed clear enrichment at the ZA and the lateral E-cad belt (**Figure 3-1H and 3-1I**). The enrichment was higher at ZA than at the lateral belt, akin to the distribution of DE-Cad. We also examined p120-catenin; a protein that regulates the E-cad based adhesive complex (**Figure 3-1J**). p120-catenin demonstrated clear enrichment at the ZA and some enrichments were also seen at the LA, although less prominent than other catenins. E-cad protein functions as adhesion receptors that facilitate cell-cell communication through trans-interactions. These processes depend on interactions between E-cad and the cytoskeleton, in which catenins serve as an essential mediating factor (M. Takeichi, 2014). Having seen that catenins localize at the lateral DE-Cad belt, we next examined the behavior of the actin cytoskeleton of these cells. Actin, as seen by tracheal specific expression of the actin-binding domain of Utrophin fused to GFP (Ut-ABD-GFP), formed distinct cortices at the ZA and the lateral DE-Cad belt (**Figure 3-1K**). The ZA cortex appeared as a clear and sharp signal overlapping the ZA. At the lateral junction, the Ut-ABD-GFP signal was much more heterogeneous with fibrous extensions, breaks, and regions of signal enrichment. These patterns broadly overlapped the LA DE-Cad belt, rarely forming a sharp cortex corresponding to the belt as at ZA. The cells also displayed patches of organized actin labeled by the reporter at various locations in the cell, especially in the vicinity of the nucleus (**Figure 3-2E**).

Given all these features, we summarized that the lateral DE-Cad enrichment that we have visualized constitutes LAJ (LAJs) that run parallel and just basal to ZA, and is associated with classical intra-cellular functional partners of AJs. We proposed a model which is diagrammatized in (**Figure-3-1 L**).

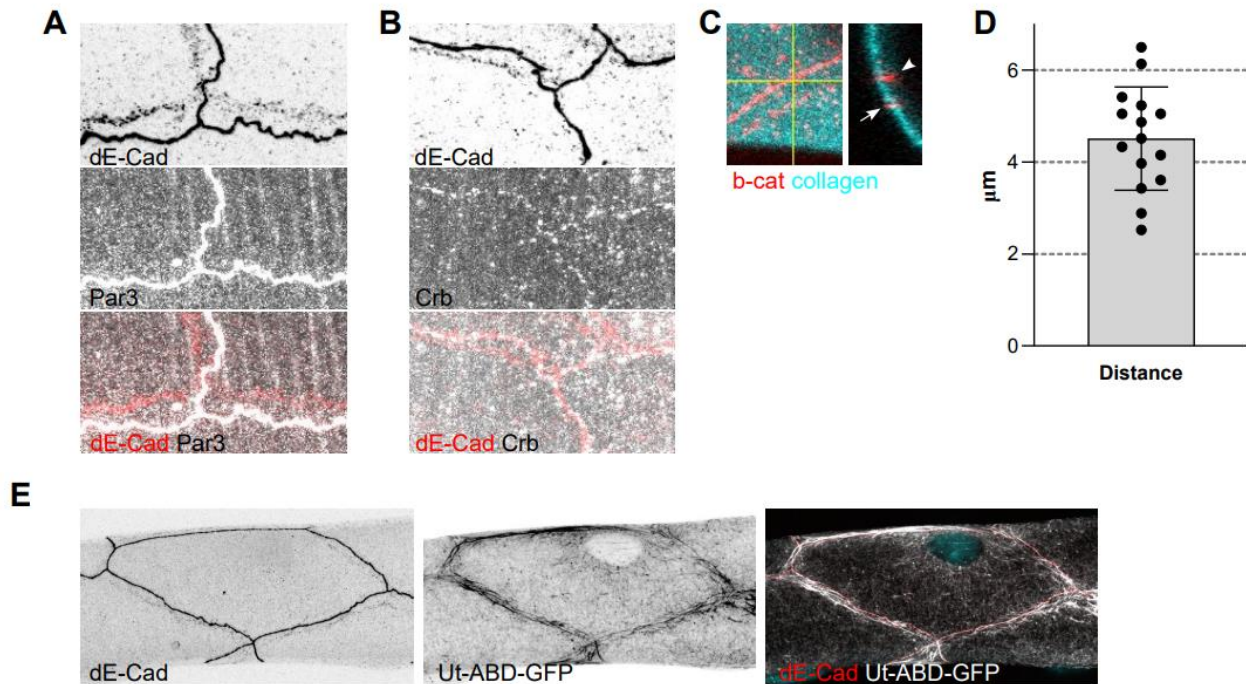


**Figure 3-2 LAJs are present close to the basal membrane**

(A, B) Hiked signal of Crumbs and Par-3 in DT cells shows no localization at LAJ (C)

Larvae in which Viking-GFP protein trap was immune-stained for E-Cad, the image showed in ortho view in YZ plane. (D) The separation between ZA and LAJ (Analysis done by Shubham Kumar) (E) Larval DT cell showing actin organization around the nucleus, actin is labeled by Ut-ABD-GFP, Immunostained for DE-Cad and DAPI. Scale bar 10  $\mu\text{m}$ .

### 3.2.3 Lateral adherens junctions are present in all larval and pupal stages

We next decided to extend the examination of DT LAJs toward embryonic and pupal stages. The experiments analyzed tracheal segments posterior to Tr7 because those permit easy examinations extending into the early hours of pupariation since the migrating cells of the developing pupal abdominal trachea would not cover these segments during this period (F. Chen & Krasnow, 2014; Weaver & Krasnow, 2008). We found no clear lateral DE-Cad

patterns in the DT cells of stage 16 embryonic trachea (**Figures 3-3-Ai**) (**Figure 3-4-D**), although given the smaller cells of embryonic DT higher resolution imaging would help to conclude this. In the L1 and especially L2 DT, LAJ like patterns were occasionally seen, but these results have not been sufficiently consistent, and hence we have not followed these stages further (**Figure 3-4A**). LAJ was clearly identifiable in early L3 (EL3), midL3 (ML3), wandering L3 (WL3), stagnant L3, 0h pupa (0hAPF), and 1 h after puparium formation (1hAPF) (**Figure 3-3-Aii-vii**). At 0hAPF, the DE-Cad staining was consistently weak all over the DT, and the LAJ was difficult to discern.  $\alpha$  (**Figure 3-3B**) and  $\beta$  (**Figure 3-3C**) catenins also showed LAJ signal in all the stages where LAJ DE-Cad was identifiable. Indeed,  $\beta$  catenin signal was often more distinct than DE-Cad, and we used either DE-Cad or  $\beta$  catenin to identify LAJ in further experiments. We also investigated many of the other branch types of the trachea for the presence of LAJ. LAJ was seen in the lateral and dorsal branches, although less markedly than in DT (**Figure 3-4B**). We were not able to identify LAJ like patterns in the junctions of the terminal cells with the preceding cells.

### **3.2.4 LAJs in other *Drosophila* tissues**

We wanted to know if LAJs were present only in trachea or any other organs. Hence, we looked for the presence of LAJs in other larval tissues including body wall epithelium, salivary gland, and imaginal wing discs (**Figure 3-4C**). LAJ belt similar to trachea could not be identified in any of these. DE-Cad signal was visible sharply only at ZA in the body wall and imaginal disc epithelial cells. Interestingly, in the salivary gland another tubular epithelial organ DE-Cad puncta were visible on the apical luminal surface, and on the lateral wall of the salivary gland cells diffuse signal was visualized. However, a discrete organised lateral belt of LAJs was never seen. Collectively, these data show that LAJ is a feature of the larval DT cells and possibly the majority of larval tracheal tubes with extra-cellular lumens.

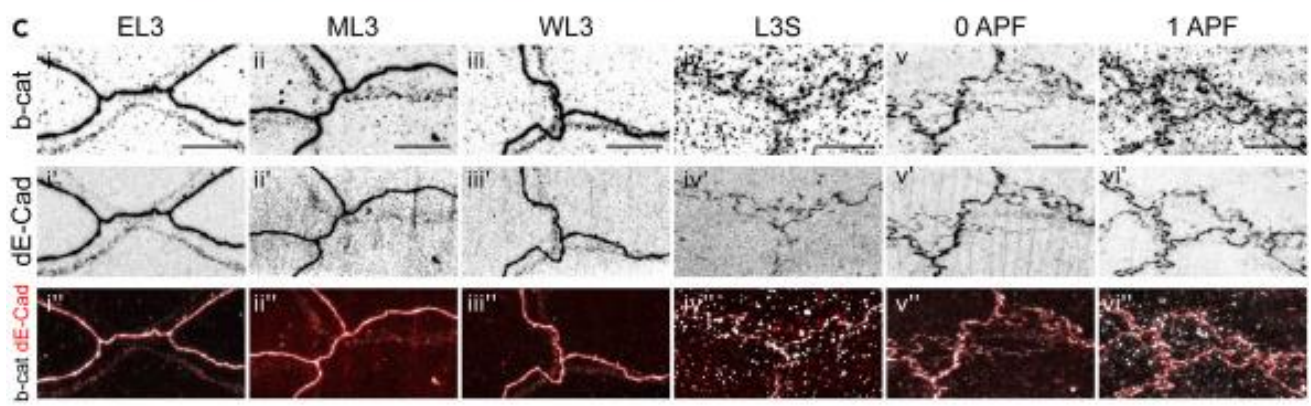
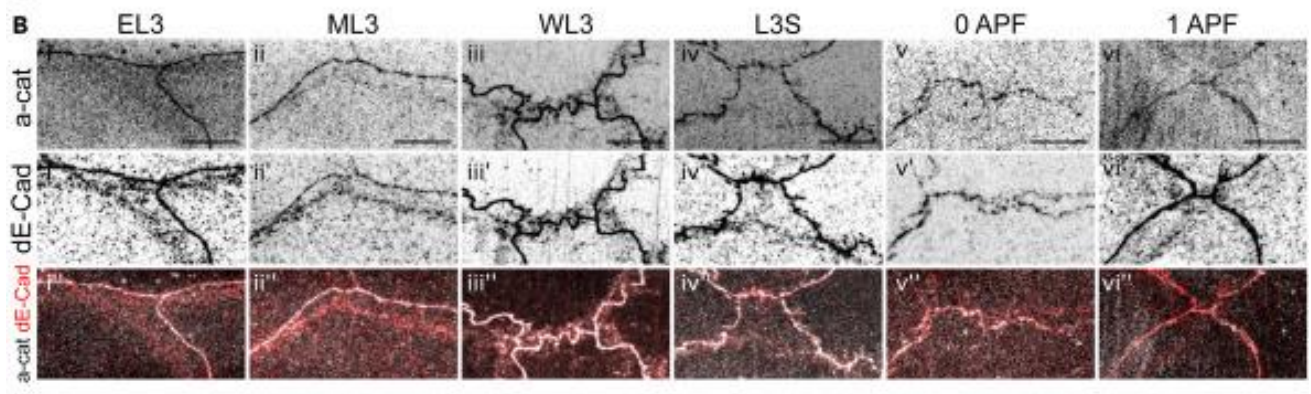
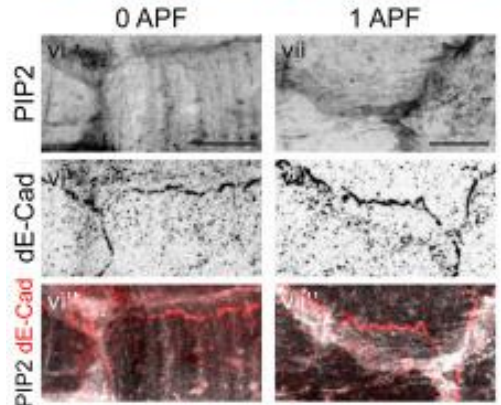
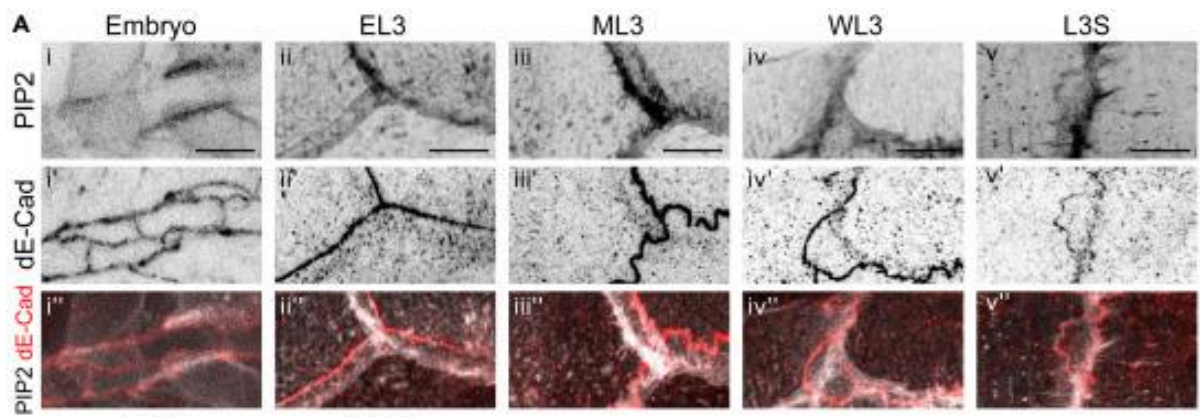


**Figure 3-3. LAJs are active cadherin receptor complexes**

(A) Images from the posterior metameres, tr7/tr8 of the DT of *btl > PIP2-mCherry* larvae immune-stained for E-Cadherin. The Anterior is to the left, and the posterior is to the right. Scale bar is 10  $\mu$ m (A) LAJ is absent in stage 16 embryonic trachea (3-3Ai), whereas LAJ is clearly seen in EL3, ML3, WL3, L3S, 0hAPF, and 1hAPF DT cells (3-3Aii-vii).

(B and C)  $\alpha$  (B) and  $\beta$  (C) Catenins localize at ZA and LAJ in EL3, ML3, WL3, L3S, 0hAPF, and 1hAPF (i-vi). Larvae of *Ubi-E-Cadherin: GFP* or endogenous DE-Cad tagged with GFP were immune-stained for  $\alpha$  and  $\beta$  catenin, respectively. Unless otherwise mentioned, all images are maximum intensity Z-projections of 15–30  $\mu$ m stacks, imaged at a Z-resolution of 0.3  $\mu$ m. Scale bars indicate 10  $\mu$ m.

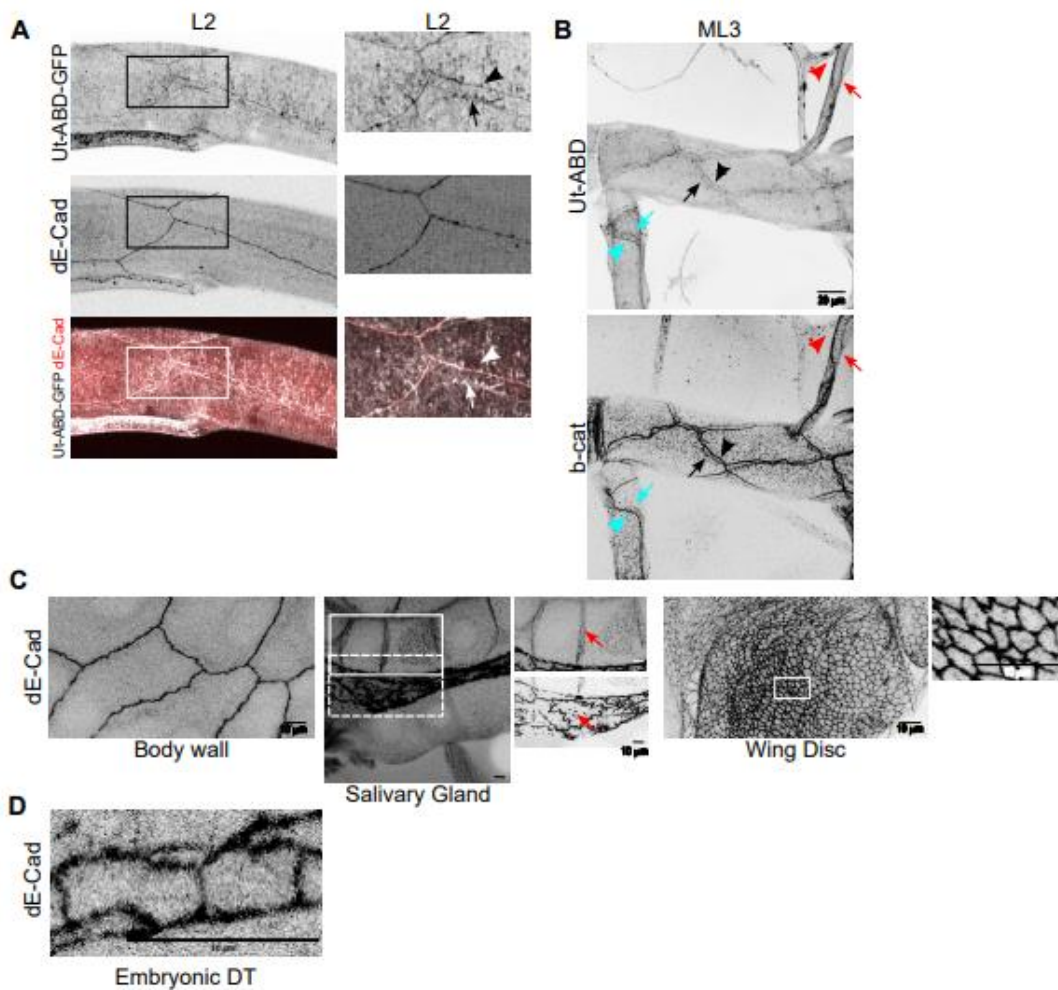


**Figure 3-4. LAJs in embryo, larval trachea, body wall, salivary gland, and wing imaginal disc**

(A) Images from the posterior metameres, tr7/tr8 of the DT of *btl > Ut-ABD-GFP* larvae immune-stained for E-Cadherin. The Anterior is to the left, and the posterior is to the right. Scale bar is 10  $\mu\text{m}$  (B) LAJ is present in DT (Black arrow), dorsal branch (red arrow), and lateral branch (cyan arrow). (C) DE-Cad stained in body wall, salivary gland, and wing imaginal diac. Dispersed lateral distribution of DE-Cad is shown in salivary gland and wing disc. (Inset-zoomed images) (D) DE-Cad in embryo shows that LAJs are absent in the embryos.

**3.2.5 Distinct actin cortices were associated with both ZA and lateral adherens junctions**

The junctional cortex associated with LAJ (LAJC) was more fibrous and heterogeneous in appearance than the one associated with the ZA (ZAJC) at ML3 (**Figure 3-1Jii**). We examined more stages to understand whether this suggested greater actin dynamicity at the LAJC. Distinct cortices associated with the two kinds of junctions were clearly visible from the EL3 stage (**Figure 3-5A**). The LAJC at EL3 while appearing sharper and thinner than at ML3 (**Figure3-1J and 3-5Aii**), still looked heterogeneous with fibrous extensions associated (**Figure 3-5-Ai**). In the YZ orthogonal view (**Figure 3-5-Aii''**) the fibrous actin could be seen to occupy the region between the ZA and LAJ. These actin extensions emanating from LAJC appeared much more prominent and elongated at the WL3 stage (**Figure 3-5Aiii**). The extensions increased in both frequency and length, and a large proportion of these extensions appeared directly connected to the cortex. In addition, the actin structures visible in the rest of the cells also showed increased organization into fibers. A bias for these fibers to be aligned parallel to the anteroposterior axis was apparent by WL3. The LAJC itself thickened by the WL3 stage to form a pericellular bundle. However, the ZAJC showed little change and could be seen as a relatively thin, sharp cortex in regions where ZA and LAJ had sufficient separation.

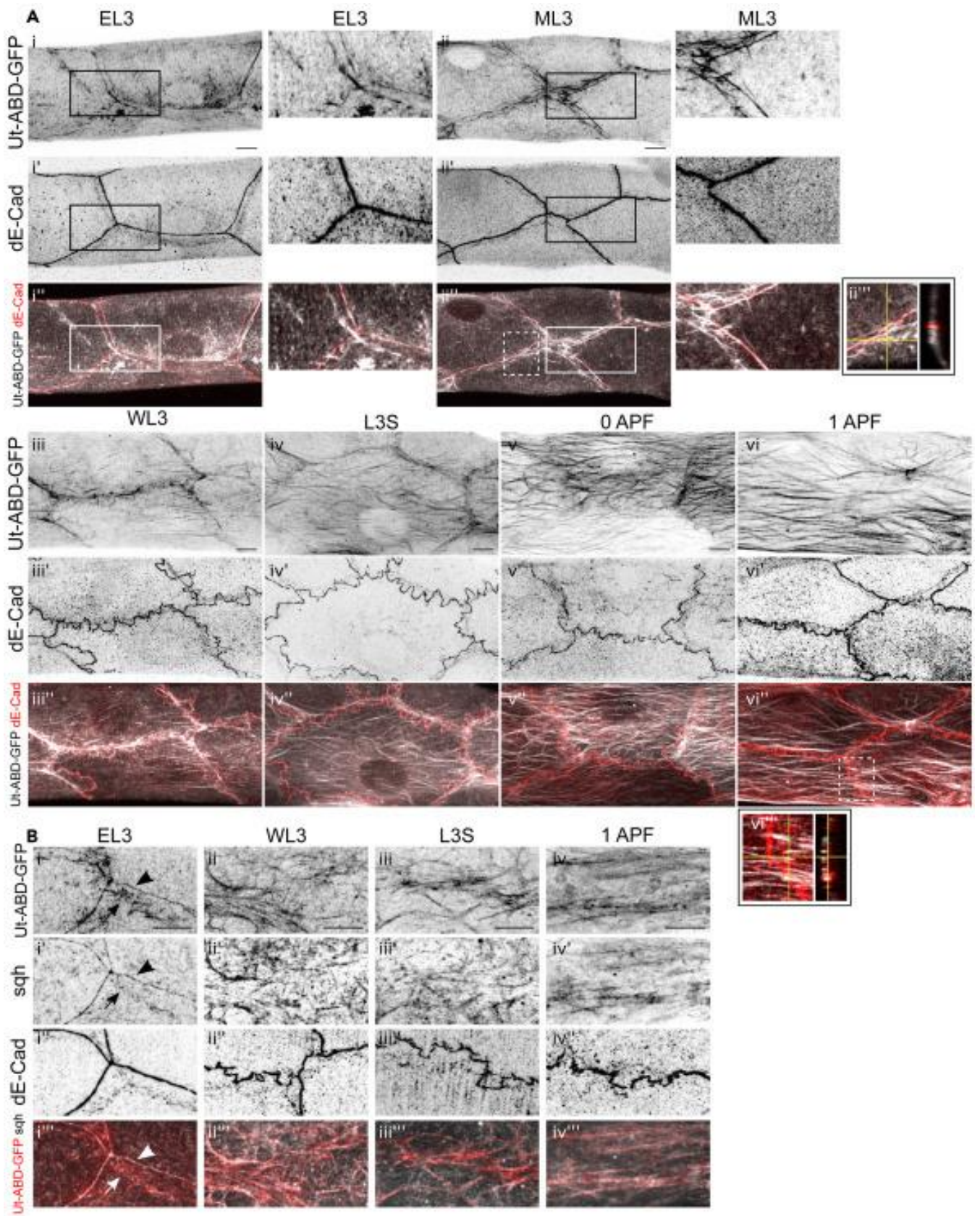


### **Figure 3-5. The LAJC and the supracellular actin cortex**

(A) The posterior larval DT metameres, tr7/tr8 of *btl > Ut-ABD-GFP* immune-stained for DE-Cad. The *Ut-ABD-GFP* channel shows actin (i-vi) and (i'-vi') shows DE-Cad. Two distinct cortices associated with ZA and LAJ are clearly visible at EL3 (Ai) and ML3 (Aii). The junctions turn less identifiable, and the progressive development of the long actin bundles is visible from WL3 to 1APF

(iii to vi). The zoomed area corresponding to the ROI indicated by solid lined box is shown adjacent to figures i to ii''. 3-5Aii''' and 3-5Avi''' show the Y-Z orthogonal view from the ROIs indicated by dashed lines in 3-5Aii'' and 3-5Avi'', respectively. Anterior is to the left, and posterior is to the right. Scale bar 10  $\mu\text{m}$ .

(B) The actin bundles are associated with *sqh*. *sqh AX3; sqh:Utrophin:GFP; sqh:mCherry* larvae were immune-stained for DE-Cad. Distinct myosin localization at LAJ and ZA can be seen (3-5Bi).

3-5Bi''' to iv''' show the merge of *Ut-ABD-GFP* and *sqh* channels. As the actin cables form, *sqh* decorates most of the cables. Arrowheads indicate ZAJC, and arrows indicate LAJC. Unless otherwise mentioned, all images are maximum intensity Z-projections of 15–30  $\mu\text{m}$  stacks, imaged at a Z-resolution of 0.3  $\mu\text{m}$ . Scale bars indicate 10  $\mu\text{m}$ .

### **3.2.6 Lateral adherens junction mediates a supracellular actin cortex**

The next stage we examined, L3S was characterized by a further increase in the length of the fibers, and the appearance of connections between fibers emanating from different locations of the cell covering most of the cell with actin cables (**Figure 3-5Aiv**). At regions where the separation between ZAJC and LAJC was distinct the extensions were often attached to the

latter. The LAJC still had the appearance of a thick actin bundle, but it had diminished in intensity and appeared more interrupted along the perimeter of the cells. The ZAJC was indiscernible amid the signal from the actin structures, except at a few locations where it still appeared as the sharp actin cortex. There were sites along the cell boundaries where both cortices appeared absent, and the long actin bundles appeared to cross the boundary region. 0hAPF and 1hAPF DTs showed further progression of these phenotypes (**Figure 3-5A, v and vi**). The actin bundles became denser, longer, and more continuous, covering the whole cell and connecting across cell boundaries. In 1hAPF samples, cell boundaries in the Ut-ABD-GFP channel were nearly indiscernible (**Figure 3-5Avi**), although clearly visible by DE-Cad and catenin staining (**Figure 3-5Avi'**). By this stage, actin took the appearance of a supracellular structure made up of long bundles. This structure was organized with most of the bundles running parallel to the anteroposterior axis of the DT. The YZ orthogonal view showed that the actin bundles were located very close to the basal membrane of the cells (**Figures 3Avi''**). The data described above indicated that the actin cytoskeleton of DT cells undergoes a dramatic remodeling process during the late larval phase to generate a supracellular actin cortex close to the basal membrane of the cells. The LAJC is associated with a large portion of actin bundles populating the cell. The pericellular LAJ-C actin bundle demarcates the cells in the earlier stages but appears to deplete later as bundles across cells form the supracellular structure at the onset of pupariation.

### **3.2.7 Actin fibers near intersegmental junction**

The actin fibers emanated from the LAJs and around the nucleus in the DT cells. We further examined how the fibers were behaving across the segments. We looked at the intersegmental cells for more details. We found that the actin fibers were interacting with the other cells across the segments through filopodia like cellular protrusions, presumably encased in plasma

membrane (**Figure 3-6i**). Filopodia are actin rich, highly dynamic membrane protrusions involved in various cellular mechanisms like cell-cell interaction, cell migration, wound healing, epithelial sheet fusion, cell adhesion etc (Faix & Rottner, 2006; Gallop, 2020; Martín-Blanco & Knust, 2001; Mattila & Lappalainen, 2008). The number of filopodial protrusions are more in WL3 and L3S (**Figure 3-6ii, iii**). The filopodia like structures are probably interacting with the cells across the inter segmental boundary and plays an important role in supracellular cable formation. It would be interesting to further study more about these dynamic structures and their significance in establishing the supra-cellular cables.

### **3.2.8 Supracellular actin cortex is an actomyosin mesh**

Higher-order actin structures in cells are usually actomyosin meshes. We examined the status of nonmuscle myosin in these cells using a reporter for spaghetti squash (sqh) (the regulatory light chain of the nonmuscle type 2 myosin) (**Figure 3-5Bi-iv**). At the EL3 stage, myosin enrichment could be seen at both ZA and LAJ cortices, although, in contrast to the actin pattern, the myosin enrichment was much weaker at LAJ than at ZA (**Figure 3-5Bi**). Enrichment of sqh on actin was visible by WL3 in a pattern reminiscent of that of Ut-ABD-GFP (**Figure 3-5Bii**). As the DT cells generated actin cables by L3S and 1hAPF stages, myosin progressively accumulated on the cables, clearly demonstrating that the supracellular structure observed is an actomyosin cortex (**Figure 3-5Biii and iv**).

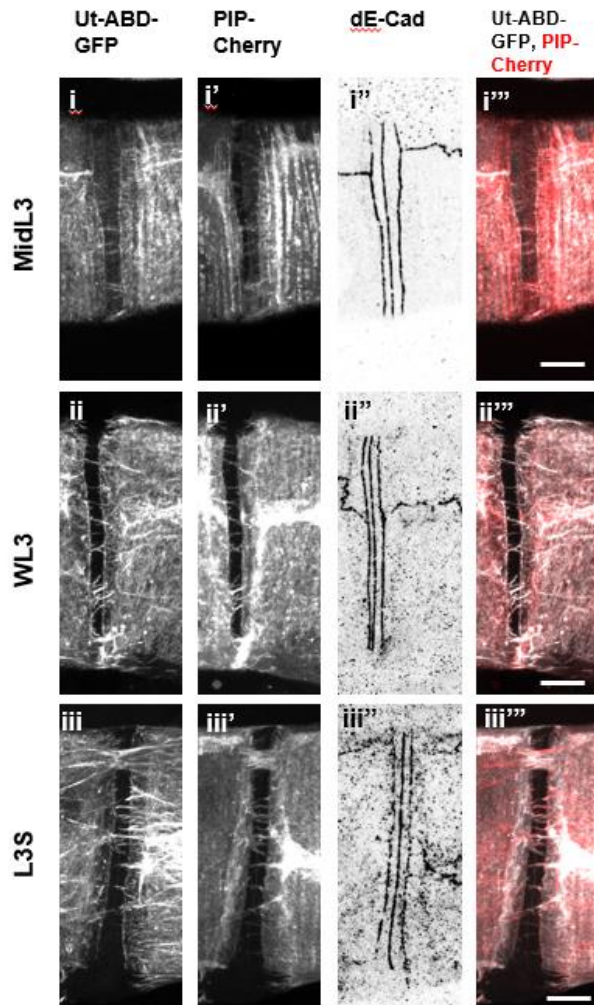


**Figure 3-6. Filopodia-like actin extensions at the intersegmental junction**

(A) The inter-segmental junction of posterior larval DT, ISJ between tr7-tr8 of *btl > Ut-ABD-GFP*; *btl > PIP2-mCherry* immune-stained for DE-Cad. The *Ut-ABD-GFP* channel shows actin (i-iii), (i'-iii') shows membrane, and (i''-iii'') shows DE-Cad. Filopodia-like actin extensions are clearly visible at ML3 (i) and WL3 (ii), and L3S (iii) at ISJ. These extensions are membrane extensions that protrude from the adjacent cells at ML3 (i') and WL3 (ii') and L3S (iii'). In L3S (iii), these filopodia-like extensions are more visible. Scale bars indicate 10  $\mu$ m.

### **3.2.9 Rho-GTPases and the Arp- WASP axis are required for generation of the LAJC**

Rho-GTPases are a very diversified group of GTPases of varied cellular functions. Rho1 and CDC42 are two prominent members of the family. Rho-GTPases play important roles in regulating actin dynamics at the junction, including actin nucleation, as well as initiation of filopodia and actin bundling.

We examined the localization of Rho-GTPases, Rho1, and Cdc42 in the DT epithelium by immune-staining animals with UAS-Lifeact-Ruby (Lifeact) driven by *btl*-GAL4 and endogenous DE-Cad tagged with GFP. At the EL3 stage, no distinct pattern of localization was visible for either of the proteins (**Figures 3-7Ai and 3-7Bi**). At the ML3 stage, both Rho1 and Cdc42 showed clear junctional localization, and it could be seen that both the proteins were associated with LAJ and not ZA at regions with sufficient separation between the two kinds of AJs (**Figures 3-7Aii and 3-7Bii**). To quantitatively identify the preferential localization of both GTPases at LA at ML3, identical lines (1.8  $\mu\text{m}$  long) were drawn centered across corresponding LAJ and ZA peaks. The mean intensity profiles along the lines were plotted for both the GTPases and E-cadherin channels (**Figures 3-7C and 3-7D**;  $n = 16$  ROIs). We also measured intensities of GTPase staining in identical ROIs at a number of LAJs and ZAs at EL3 and ML3. The mean intensity of both GTPases increased at LAJ at ML3 stage. Enhanced enrichment of the GTPases at LAJ over ZA was not discernible at EL3 but was significant at ML3 (**Figures 3-7E and 3-7F**). It was notable that these GTPase enrichments broadly overlapped the LAJC as seen in the Lifeact channel. At WL3 and 1hAPF, although the GTPase staining tended to be progressively more diffused, the LAJ localization was still discernible (**Figures 3-7Aiii & iv and 3-7Biii and iv**). Accumulation of the GTPases at LAJ from the ML3 stage coincided with

the phase of increasing length and density of the actin filaments, suggesting a role in the LAJC actin activities and potentially in the supracellular cortex formation.

In order to test this, we knocked down Rho1 and Cdc42 and downstream effectors that mediate actin organization including Arp, WASP, Rho-dependent kinase (ROK), and sqh. The knockdowns (KDs) were carried out with flies expressing *Ut-ABD-GFP* and *Dicer2* in the trachea, driven by *btl-GAL4* and trachea were examined at WL3 and 1hAPF stages (**Figure 3-8A**). At WL3, AJs were relatively unaffected in the KDs, and the actin cortices were affected to varying degrees. LAJC appeared to be more affected as it was either not visible (**Figure 3-8Ai' and iv'**), or when identified, appeared as a thin cortex lacking the features characteristic of this stage (**Figure 3-8Aii', iii',iv', v' and vi'**). In Rho1-KD WL3, the cortices were unidentifiable in thick projections (**Figure 3-8Ai'**), but the ZAJC was discernible on a thin projection of Z-planes of the junctional region. At the 1APF stage, the junctions were affected to varying degrees, appearing most fragmented in WASP and sqh KDs. However, all the KDs had a range of defects in the actin cables at 1APF. While cables were not detectable in Cdc42 and Arp KDs (**Figure 3-8Aii''' and iii'''**) thin and sparse cables were observed in Rho1, Rok, and Wasp KDs (**Figure 3-8Ai''', iv''', and v'''**). The images presented are representative of the predominant phenotypes observed, and the distribution of variations in phenotypes in the animals examined for different KDs is shown in (**Figure 3-8B**). Though a large number of cables were seen in sqh-KD DT (**Figure 3-8Avi'''**), the cables were very thin and disorganized compared to the Dicer control (**Figure 3-8Avii'''**). Indeed, most of the sqh-KD cells had cables forming a loose pericellular organization at 1APF lacked the appearance of supracellular bundles crossing boundaries, and a significant proportion of the cables orientated perpendicular to the DT long axis (**Figures 3-8Avi'''**). In case of KDs there were phenotype variations observed in Rok-KD and sqh-KD. The diversity in the phenotypes limited the quantification of the cables to ascertaining their thickness and dispersal wherever possible.

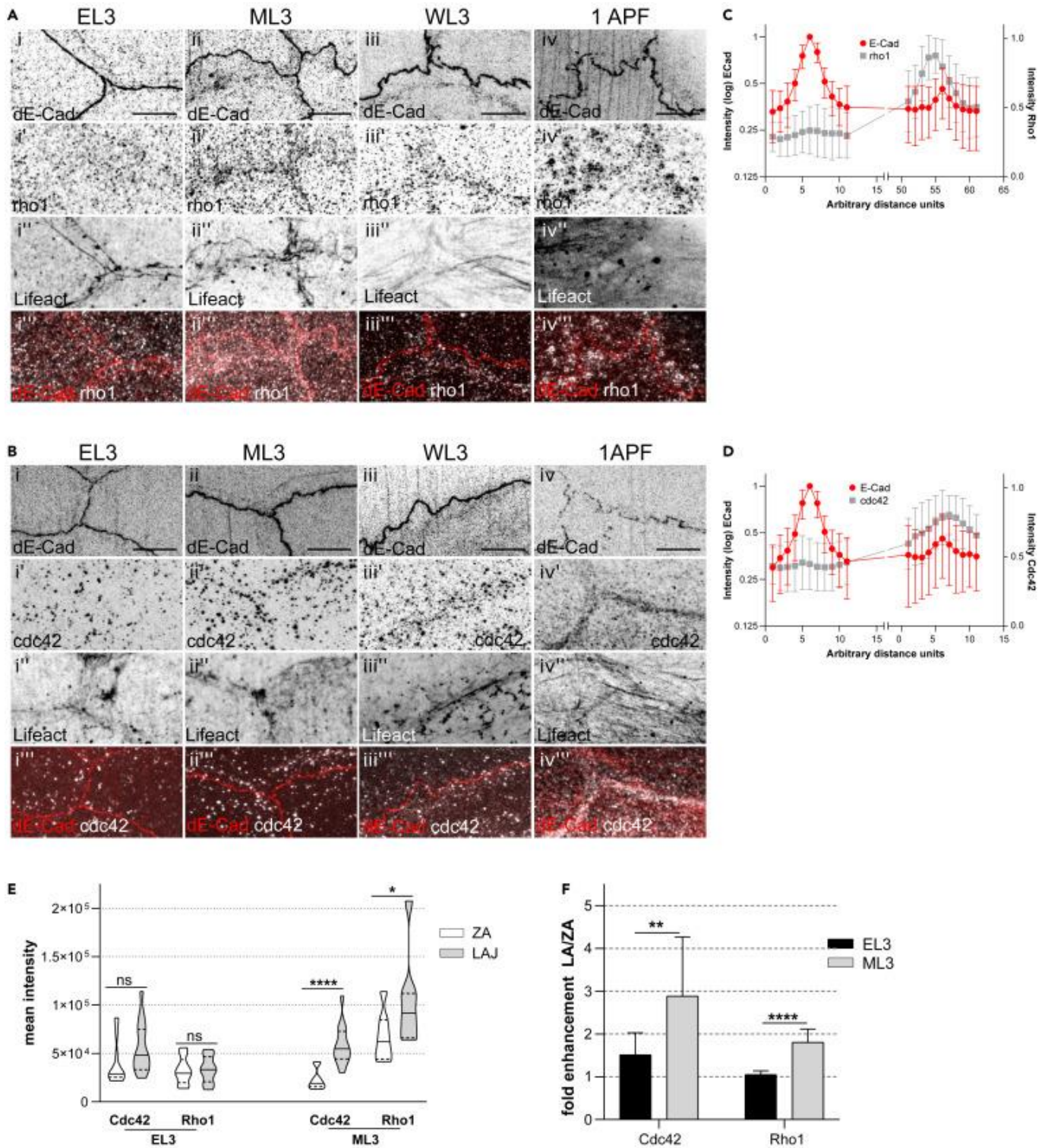


**Figure 3-7. Rho1 and Cdc42 preferentially localize at LAJ**

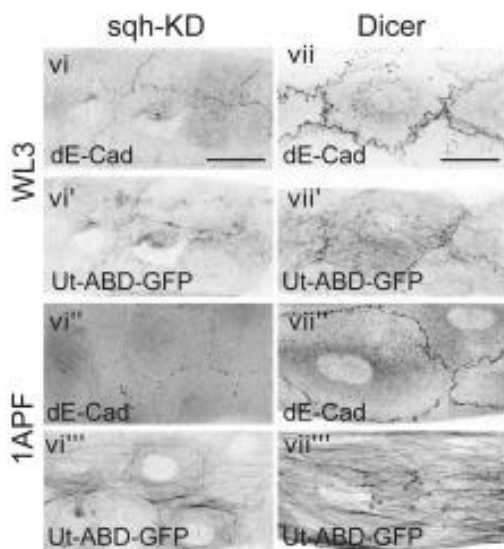
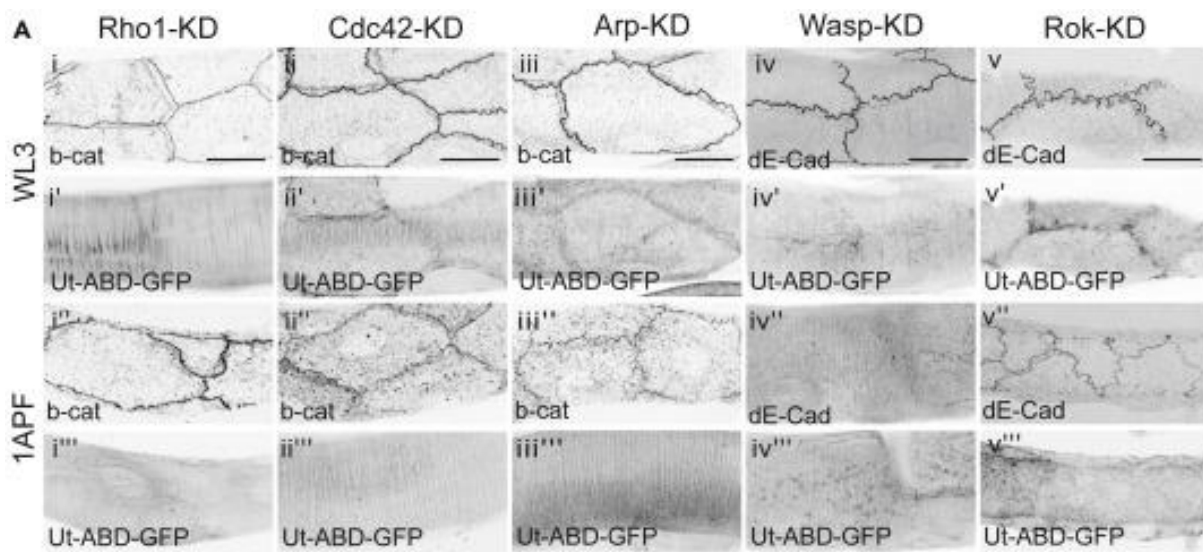
(A and B) Larvae of various stages as indicated carrying *btl>Lifeact-Ruby* (3-7A and B, i''-iv'') and endogenous DE-Cad:GFP (A and B, i-iiv) immune-stained for Rho1(Ai'-iv') or Cdc42

(Bi'-iv'). Merges of DE-Cad and Rho1 channels (Ai''-iv''), and DE-Cad and Cdc42 (Bi''-iv'') are also shown. Rho1 and Cdc42 show no clear junctional pattern at EL3 and association with LAJ is seen from ML3 onwards. The anterior is to the left, and the posterior is to the right. Unless otherwise mentioned, all images are maximum intensity Z-projections of 15–30  $\mu\text{m}$  stacks, imaged at a Z-resolution of 0.3  $\mu\text{m}$ . Scale bars indicate 10  $\mu\text{m}$ .

(C and D) Mean fluorescence intensity values along identical lines drawn across ZA (corresponds to the higher DE-Cad peak in the plot) and LAJ, for DE-Cad, and Rho1 or Cdc42, respectively. The midpoint of all lines corresponds to the peak intensity in the DE-Cad channel, and the separation between points is 0.18 microns. The separation between the ZA and LAJ peaks shown is arbitrary. Note that DE-Cad intensity is presented in log scale and Rho-GTPase intensities in linear scale. N = 16 ROIs from 10 animals for both graphs. The data points are the means and the error bars indicate standard deviation.

(E) Mean intensity of GTPase signal at ROIs drawn over ZA and LAJ at stages EL3 and ML3. N = 16 ROIs from 10 animals. The integrated intensity of each ROIs was averaged over area, and the median of all such average values of each condition and the quartiles are indicated by the solid and dotted lines, respectively in the violin plots (\*,  $p < 0.5$ ; \*\*\*\*,  $p < 0.0001$ ; n.s, not significant). (F) Enhanced enrichment of GTPase signal at LAJ over ZA at EL3 and ML3. The ratio of the mean intensity of the GTPase at LAJ to that at ZA is plotted in the graph. Mean values are derived from the same calculations used in 4E, and error bars indicate standard deviation (\*\*,  $p < 0.01$ ). (E&F was done by Shubham Kumar.)

While Cdc42 and Arp had no discernible cables at 1 APF, the cables of other KDs were significantly thinner than the control (**Figure 3-8C**). We next attempted to quantify cable alignment with respect to the tube axis. This was successful only in the control and sqh-KD as the cables of other KDs were too thin, and the interfering signal from the taenidial actin rendered it impossible to achieve adequate segmentation of the cables. sqh-KD showed significantly more dispersal of angles between cables than the control (**Figure 3-8D**). It needs to be mentioned that we often found the taenidial signal to be much more prominent in the KD that lacked significant actin cables, even when the Z stacks projected were similar to the control. Whether this is merely because the prominent Ut-ABD-GFP signal from the actin bundles is absent or because there is also increased availability of the reporter protein to bind the taenidial actin in the absence of cables cannot be ascertained at this point. Nevertheless, these observations collectively suggest that junction associated Rho-GTPases and actin organizers downstream to them play a role in organizing the LAJC and the supracellular actin cortex. However, these experiments do not exclude the possibility that the phenotypes observed might also have contributions from functional deficiency of Rho-GTPases or their downstream roles elsewhere in the cell, independent of junctions.



**B**

Phenotypes KD (n)	Actin Bundles				
	None	Sparse Thin	Thin	Thick Irregular	Thick Aligned
Rho1 (10)	2	8	0	0	0
cdc42 (11)	11	0	0	0	0
Arp (8)	8	0	0	0	0
Wasp (4)	1	3	0	0	0
Rok (7)	2	3	0	2	0
Sqh (8)		0	8	0	0
Dicer (6)	0	0	0	0	6

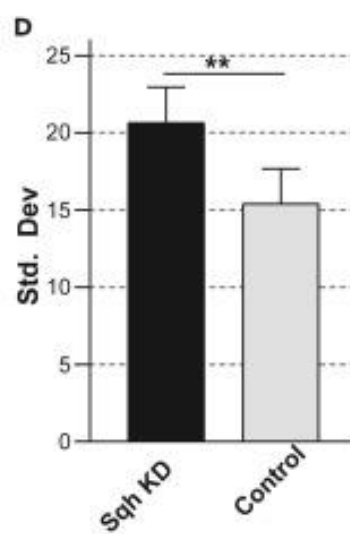
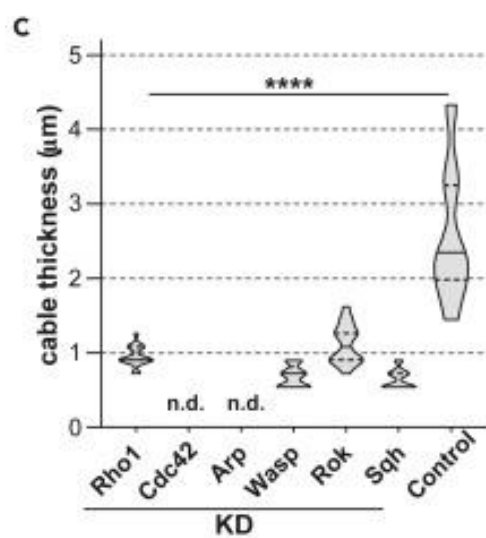


**Figure 3-8. LAJ localized Rho-GTPases involved in the formation of the supracellular actin bundles**

(A) *btl-gal4 > Ut-ABD-GFP; UAS-Dicer* flies were crossed to UAS-RNAi lines of *Rho1* (i-i'''), *Cdc42* (ii-ii'''), *Arp* (iii-iii'''), *Wasp* (iv-iv'''), *Rok* (v-v''') and *sqh* (vi-vi'''). 3-8Avii shows the images from control *btl-gal4 > Ut-ABD-GFP; UAS-Dicer* animals. 3-8Ai' to vii' (WL3) and 3-8Ai''' to vii''' (1APF) shows actin as indicated by the Ut-ABD-GFP channel. The junctions are labeled by  $\beta$ -catenin immune-staining in i to iii (WL3) and i'' to iii'' (1APF) or by DE-Cad immune-staining in iv to vi (WL3) and iv'' to vi'' (1APF). Unless otherwise mentioned all images are maximum intensity Z-projections of 15–30  $\mu$ m stacks, imaged at a Z-resolution of 0.3  $\mu$ m. Scale bars indicate 10  $\mu$ m.

(B) The table shows the distribution of the various bundle phenotypes observed in the KDs analyzed at 1APF stage.

(C) Mean thickness of the actin cables measured in various KDs and control at 1APF stage. No cables could be detected by our segmentation protocol in *Cdc42* and *Arp*-KD conditions. N = 9 ROIs from animals for *WASP* and 15 ROIs for the rest, and the number of animals corresponds to the N shown for different KDs in 5B. (\*\*\*\*,  $p < 0.0001$ ; n.d = not determined). The solid lines represent the median value, and the dotted lines represent the quartiles.

(D) Measurement of polarization of the actin cable alignment along the DT long axis. Standard deviation of the angles of distribution of cables with respect to the axis was calculated for 6 ROIs for *sqh*-KD and 5 ROIs for the control. Mean and SD for each condition is plotted in the graph (\*\*,  $p < 0.01$ ). (B,C&D was done by Shubham Kumar.)

### **3.2.10 Supracellular actomyosin cortex redundantly contributes to organ shortening in the posterior trachea**

The orientation of the supracellular actomyosin cortex along the AP axis strongly suggested its involvement in forces generated along the same axis. A recent article about disassembly of DT during pupariation identified an initial contractile phase that shortens the organ without affecting cell numbers (Fraire-Zamora et al., 2021). This organ shortening was shown to be independent of actomyosin, and was driven by remodeling of the apical extra-cellular matrix. While this shortening phase in DT extended until about 9hAPF, most of the reduction in length was achieved by 3hAPF. We noticed that the supracellular actomyosin mesh appears disorganized by 4hAPF and nearly completely disassembles by 6hAPF (**Figure 3-9Av**), suggesting any functional role to be likely affected in the early hours of pupariation. Enrichment with 95phosphor-myosin and actinin is a characteristic of contractile stress fibers. The DT actin cables show enrichment of both the above proteins starting mildly at 1hAPF, reaching a peak at 2hAPF and nearly disappearing by 4hAPF (**Figure 3-9A**). Such patterns were not visible at the earlier stages (EL3, WL3 or ML3). To test whether this reflects contractile functions in the early hours of pupariation, the compression of posterior DT (Tr6 to Tr8) was assessed between WL3 and 2hAPF, or 6hAPF (**Figure 3-9B**).

From the WL3 to 2hAPF stage, the control DT shortened by  $36.1 \pm 6.7\%$ . By 6hAPF, the control shortened further to  $41.4 \pm 5.4\%$  with respect to WL3 values. Rho1-KD and sqh-KD DTs shortened by significantly lesser values at 2hAPF ( $25.0 \pm 10.9\%$  and  $27.9 \pm 5.2\%$ , respectively). However, at 6hAPF both these KDs achieved compression values comparable to the control ( $35.1 \pm 4.3\%$  and  $40.6 \pm 3.5\%$ , respectively). These data corroborated the previous finding that the role of actomyosin was redundant in DT compression on puparium formation and mechanisms based on apical ECM remodeling achieve complete compression of the organ

by 6hAPF. However, the supracellular actomyosin mesh contributes to providing an initial acceleration step to the shortening process allowing it to reach peak compression by 2hAPF.

It is interesting to note that both sqh-KD and Rho1-KD produce comparable delayed shortening of the DT, but while Rho1-KD does not properly organize actin cables in sqh-KD some cables are detectable. The cables formed in sqh-KD have altered properties and disturbed polarity (**Figures 3-8A-vi''**). Myosin motors and associated proteins including various crosslinkers have been shown to affect bundling and polarity of actin superstructures in various systems (Chandrasekaran, Upadhyaya, & Papoian, 2019; Liu et al., 2021; Medeiros, Burnette, & Forscher, 2006). Indeed, in many instances the structure and function of the actin cables formed has been shown to depend on the relative myosin concentration (Saczko-Brack et al., 2016; Wollrab et al., 2018). A more detailed analysis of the structure and binding partners of the cables formed in the sqh-KD could be an interesting direction to shed light on the functional characteristics of the actomyosin mesh identified in this work.

The aECM remodeling and shortening of DT are reflected in the reduction of the separation between taenidial chitinous ridges (Fraire-Zamora et al., 2021). Accordingly, control DT showed a progressive reduction of intertaenidial distance accompanying organ shortening. In the Rho1-KD DTs that showed deficient shortening at 2hAPF, the intertaenidial distance also remained elevated compared to the controls (Figure 3-8C). Nevertheless, by 6hAPF in concurrence with the shortening, the intertaenidial distances were also reduced to control levels in the Rho1-KD. This demonstrates that while actomyosin facilitates the initial stage of shortening it is largely redundant with respect to the aECM driven mechanisms, and the latter achieves organ remodeling given sufficient time.

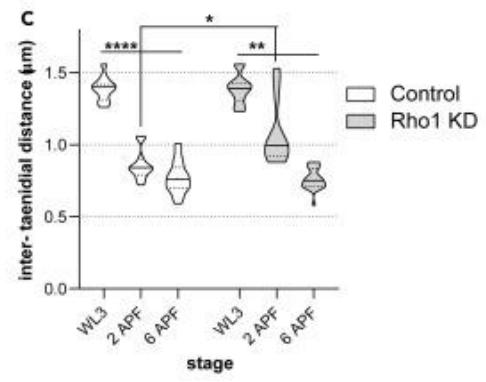
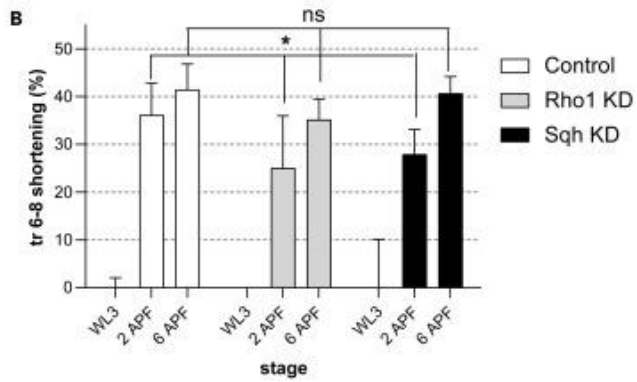
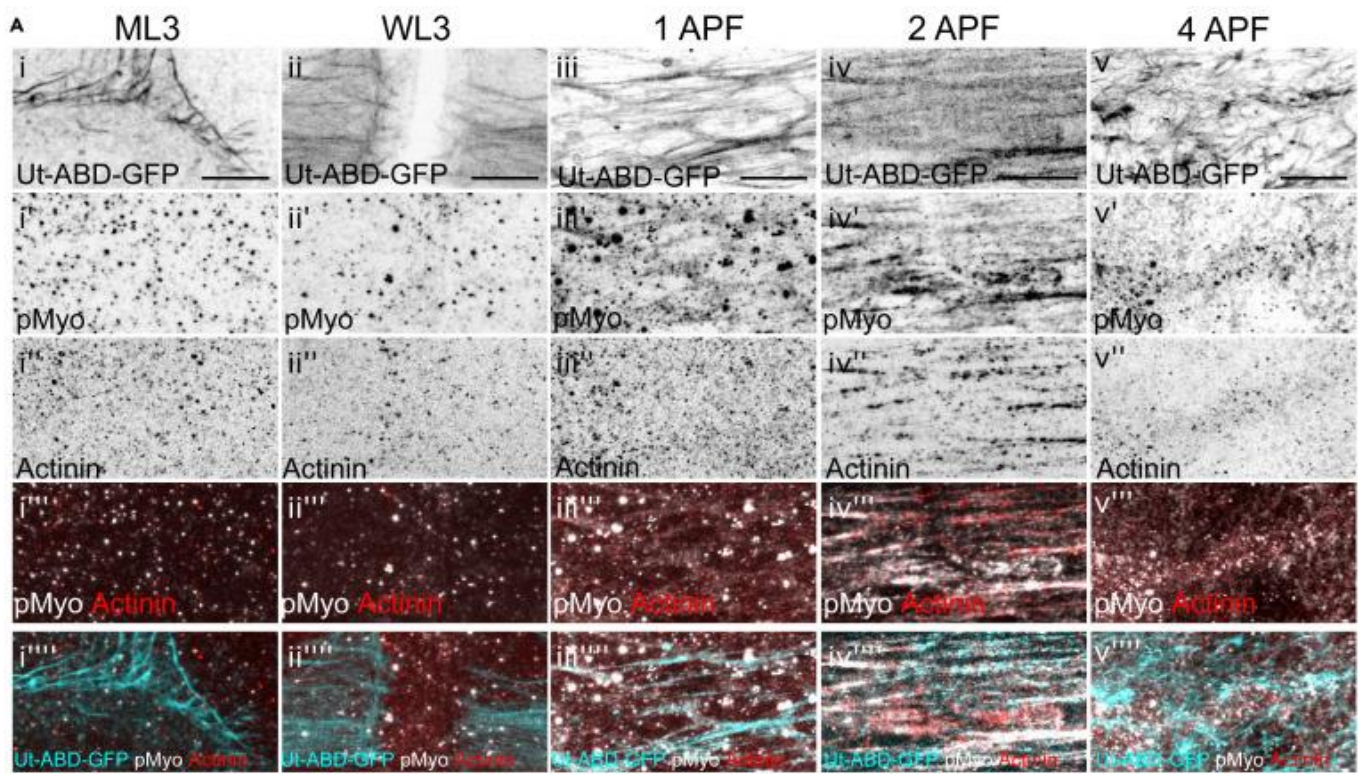


**Figure 3-9. The supracellular actomyosin has stress fibers and redundantly contributes to organ shortening**

(A) *btl* > *Ut-ABD-GFP* animals of various stages immune-stained for actinin and 98phosphor-myosin (pMyosin). Actin is visualized *Ut-ABD-GFP* in I to v, pMyosin in i' to v' and actinin in i'' to v''. i''' to v''' show merge of the pMyosin and actinin channels. i'''' to v'''' show the merge of all the three channels. Clear accumulation of pMyosin and actinin is seen at 2APF. Unless otherwise mentioned, all images are maximum intensity Z-projections of 15–30  $\mu\text{m}$  stacks, imaged at a Z-resolution of 0.3  $\mu\text{m}$ . Scale bars indicate 10  $\mu\text{m}$ .

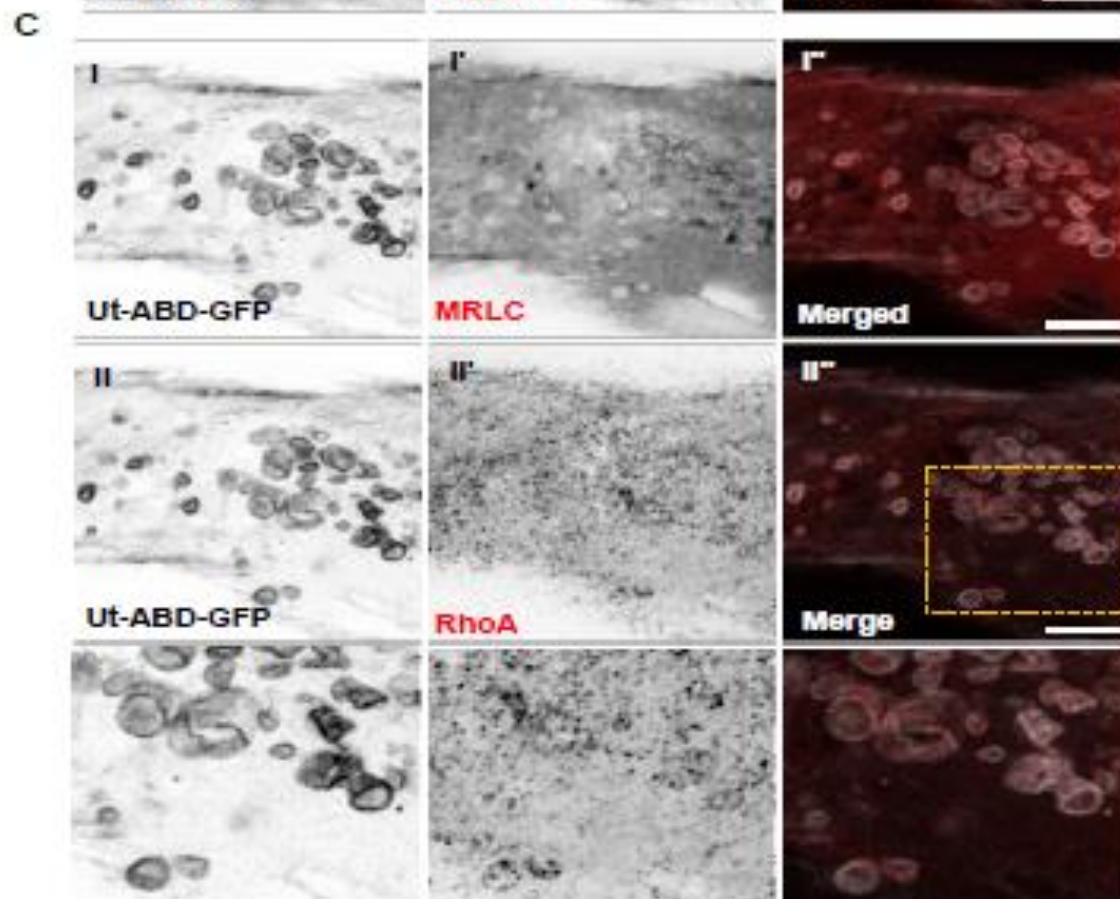
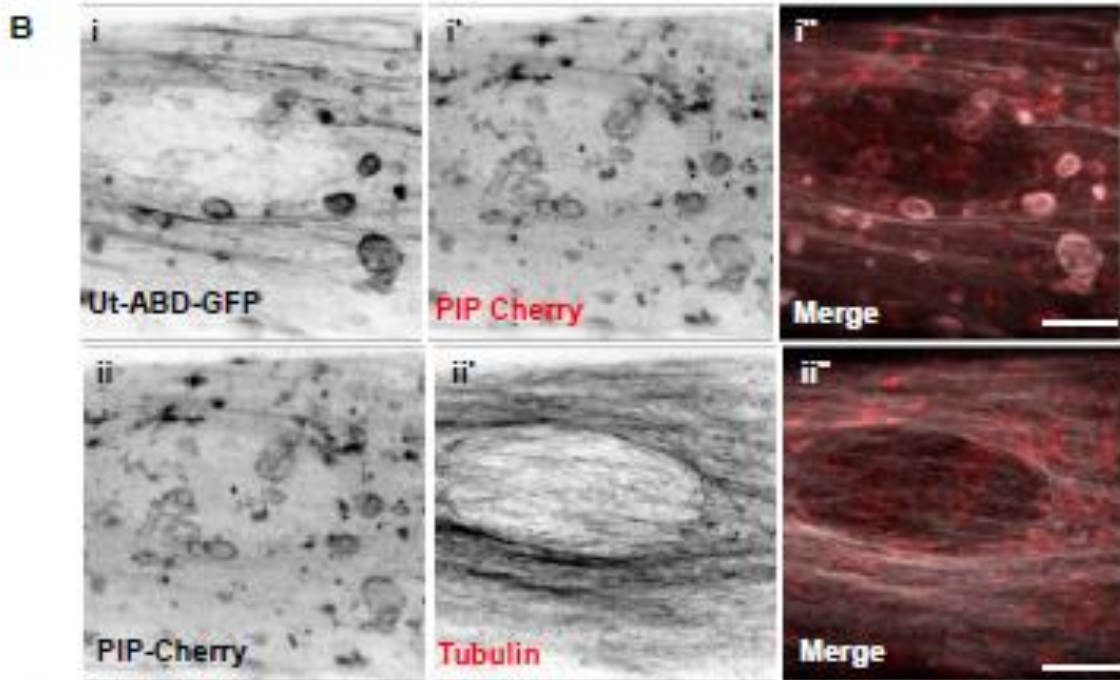
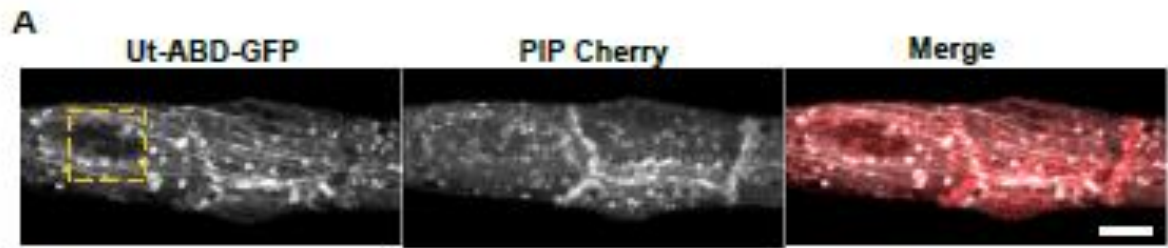
(B) The percentage of shortening of the DT region tr6-tr8 at 2APF and 6APF with respect to WL3 in control (*btl-gal4* > *Ut-ABD-GFP*; *UAS-Dicer*), *Rho1-KD* and *sqh-KD* (N = 8 to 15 animals; \*,  $p < 0.05$ ). The mean percentage shortening and SD are shown in the graph. Shortening defect is seen in the KDs at 2APF, which recovers to control values at 6APF.) Violin plots representing the average intertaenial distances of WL3, 2APF, and 6APF of control and *Rho1-KD* (N = 11 to 18 animals; \*,  $p, 0.05$ ; \*\*,  $p, 0.01$ ; \*\*\*\* $p, < 0.0001$ ). The solid lines represent the median value, and the dotted lines represent the quartiles. In *Rho1-KD* at 2APF, there is greater intertaenial spacing than the controls, and the spacing appears more variable. At 6APF, the KD and control look comparable. (Graph C was done by Shubham Kumar.

**3.2.11 Tracheal tube compression induces actin blebs in the posterior pupal DT**

We observed that stress fibers contribute to mechanical force generation during the acute phase of tube compression and redundantly support the aECM mediated posterior DT shortening. To support this hypothesis, we looked into other evidences and found that during early hours of pupation, in 2h pupal DT, the cell cortex takes part in dramatic cytoskeletal events. In 2h pupa,

we observed large vesicle like membrane structures (**Figure 3-10A**). while looking more in to these structures, we found that these structures were blebs.

The cell cortex is highly dynamic and it is made up of actin bundles, myosin filaments, actin binding proteins, microtubules etc (Chugh & Paluch, 2018; Svitkina, 2020). Due to the actomyosin activity below the plasma membrane, the cell cortex is always under mechanical stress. The forces generated at the cortex exert pressure in on the cytoplasm and can lead to membrane protrusions and bleb formation(Tinevez et al., 2009). Such spherical membrane protrusions arise frequently during the processes of cytokinesis, cell division, virus uptake, tumour cell migration, cell spreading and apoptosis-mediated cell death (Blaser et al., 2006; Mercer & Helenius, 2008; Mills, Stone, Erhardt, & Pittman, 1998; Tinevez et al., 2009). During mitotic cell rounding, due to extensive hydrostatic pressure membrane blebs form in the HeLa cells (Stewart et al., 2011). The blebs nucleate from the cellular cortex, detach from the cortex and actin nucleation starts around the bleb. The bleb formation is regulated by Rho GTPases through Rho-ROCK pathway and Myosin activity (Aoki et al., 2016; Ikenouchi & Aoki, 2017, 2022). ERM or Ezrin-Radixin-Moesin group of proteins also take part in bleb formation (Ikenouchi & Aoki, 2022).



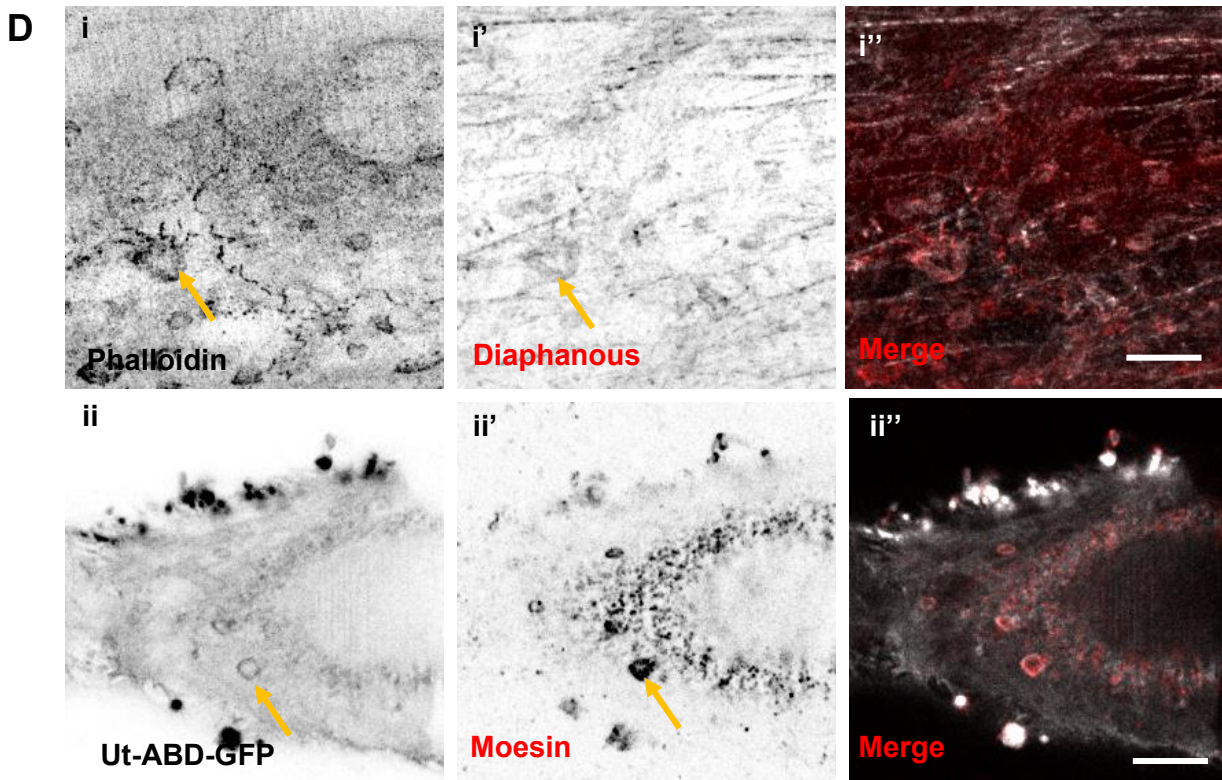


**Figure 3-10. Actin blebs form in the posterior DT cells during the acute tube compression phase**

(A) *btl* > *Ut-ABD-GFP*; *btl* > *PIP-Cherry* 2h pupa, tr-8 tracheal metamere showing giant large vesicle like structures). Actin is visualized by *Ut-ABD-GFP*, and membrane is visualized by *PIP-Cherry*. Maximum intensity projection images, Scale bars indicate 10  $\mu$ m.

(B) zoomed images of 2h posterior DT cells showing blebs both in actin and membrane channel, whereas these vesicle-like structures are not colocalized with tubulin.

(C) Actin organizers RhoA and Myosin localizes with these vesicles. (3-10Ci',3-10Cii'). The actin was visualized in the vesicles by using *sqh*. *sqh* AX3; *sqh*:*Utrophin*:*GFP*; *sqh*:*mCherry* larvae were immune-stained for RhoA. (3-10ci)

(D) Diaphanous and Moesin colocalizes with these vesicles (i', ii'), (arrowhead)

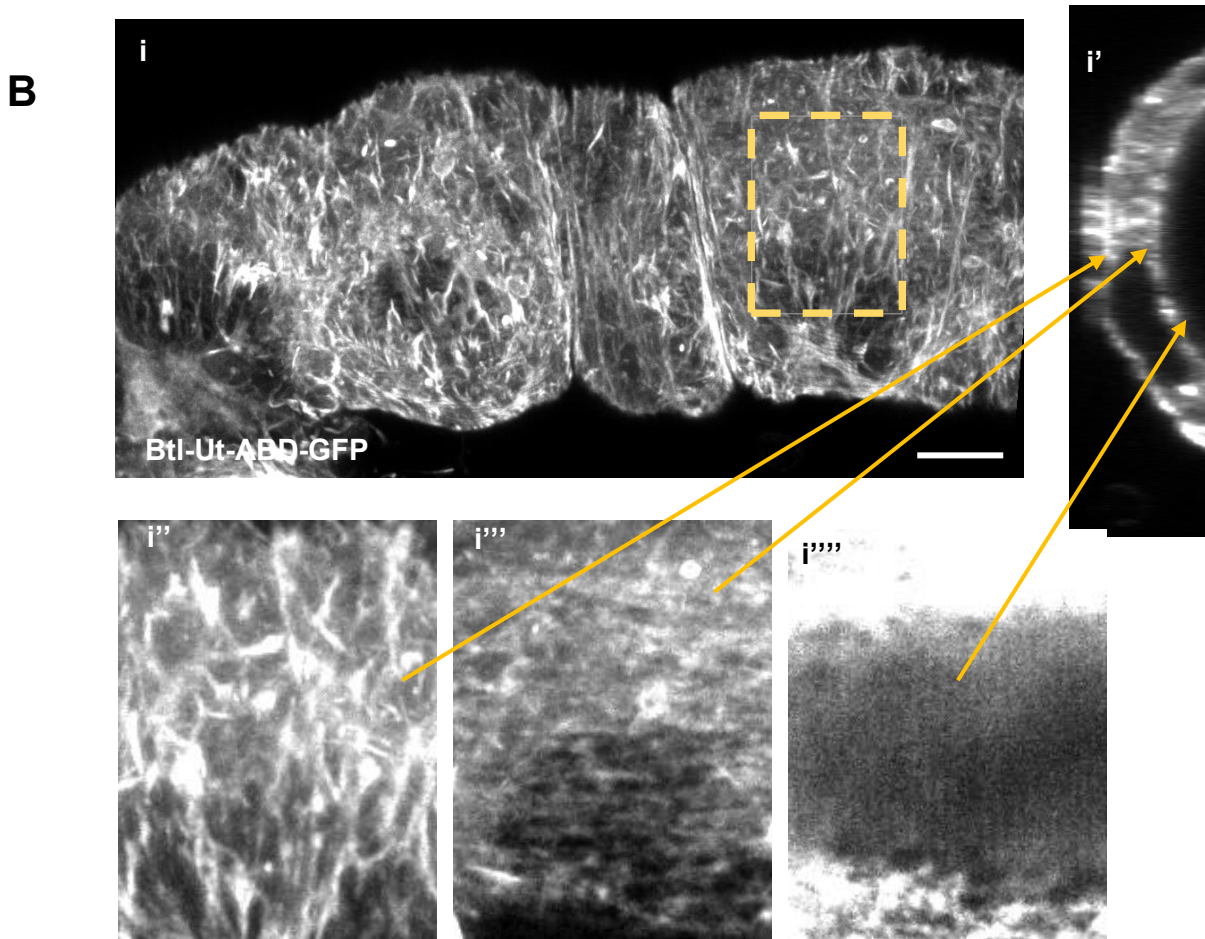
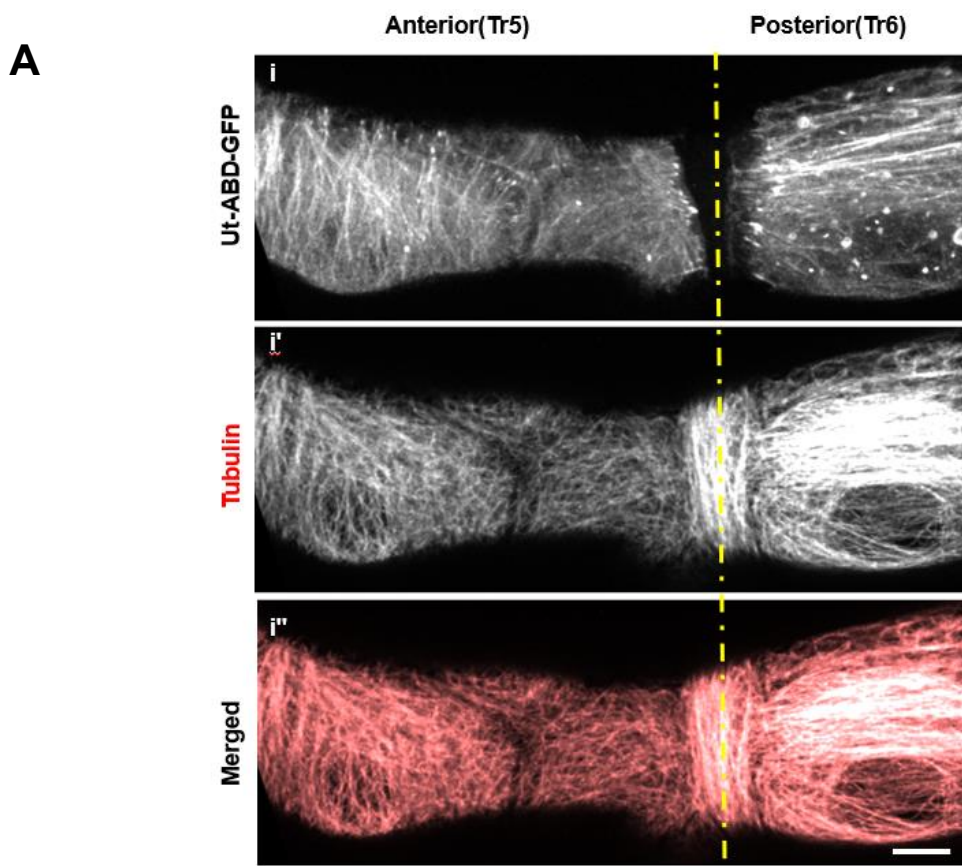
The bleb like structure that we observed in 2h posterior DT were membrane bound spherical structures present in the cytoplasm. These structures were visualised by UAS-PIP-Cherry (plasma membrane marker) driven by *btl*-GAL4 (**Figure 3-10Bi'**). These giant vesicles were membranous structures, few of them had actin cortex around the membrane (**Figure 3-10-Bi**). The actin cortex was visualised by UAS-Ut-ABD-GFP (Utrophin) driven by *btl*-GAL4. However, there was no tubulin localisation in these vesicles like structures. We looked at other markers of actin blebs i.e., Rho1 and Myosin. For myosin we used a reporter line *Sqh*AX3; *Sqh::Sqh*-mCherry, and immunostaining was used for Rho1. Both MRLC and Rho1 colocalized on the outer surface of the vesicles (**Figure 3-10Ci'-i''**). From these evidences we conclude that these vesicle-like giant structures were actin blebs and they probably formed during the acute tube shortening phase due to high mechanical pressure in the posterior DT cells. These actin blebs disappeared around 6h (**Fig11Dii**). Formin Diaphanous and ERM protein p-Moesin were colocalised with these blebs. For Diaphanous, we used a reporter line UAS-dia-GFP driven by *btl*-GAL4 (**Figure 3-10Di'**) and for Moesin we used an p-Moesin antibody (**Figure 3-10Dii'**).

Many instances, scientists used these blebs invitro to study membrane and actin cortex interaction and the cortex behaviour. These actin blebs can be isolated and used to study the de novo actin cortex formation in vitro. Studying these bleb formations and their cellular roles throughout the larval to pupal transition would be very intriguing. However, this is outside the purview of this study.

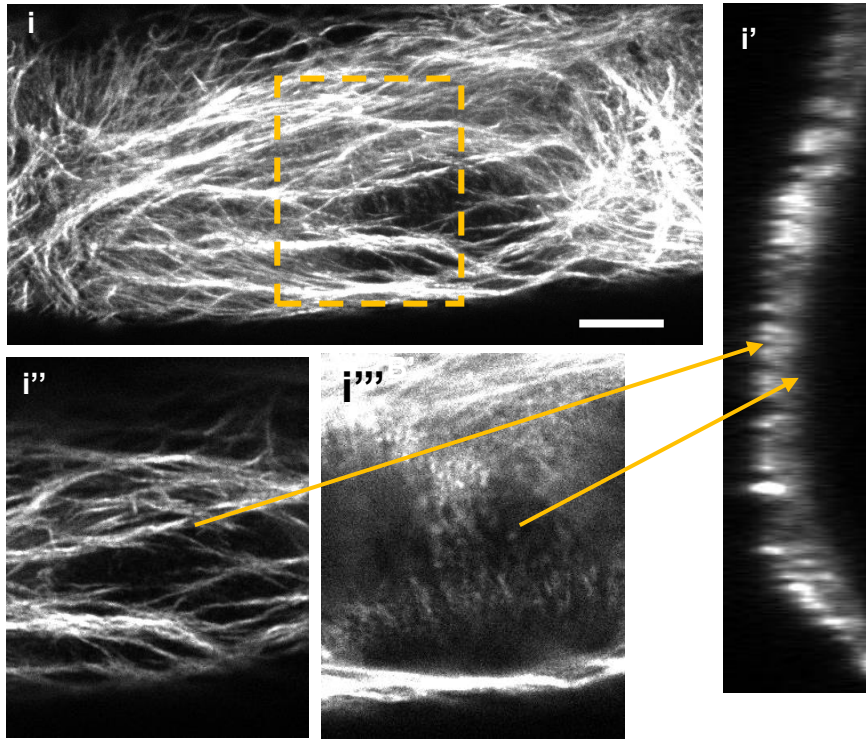
### **3.2.12 Differential cytoskeletal arrangement in *Drosophila* pupal tracheal epithelium.**

To understand more about the supracellular actin cables we extended our study to the anterior trachea. Surprisingly the actin arrangement in the anterior trachea was dramatically different from the posterior trachea. We investigated the anterior tracheal segments (tr4-tr5) in the early

pupa (0h and 2h). The anterior tracheal study was limited to tr4-tr5 because, since tr2 is covered with progenitor cells and tr3 is inaccessible during these stages due to the growing asps (air sac primordium) and covered with wing imaginal disc partially (Djabrayan, Cruz, de Miguel, Franch-Marro, & Casanova, 2014; Guha, Lin, & Kornberg, 2008; Rao et al., 2015; Weaver & Krasnow, 2008). Supracellular cables that formed in the anterior segments were perpendicular to the DT axis unlike the posterior segments, where the alignment was parallel to the DT axis. The differential actin cable arrangement can be seen at tr5-tr6 junctions very clearly (**Figure3-11Ai**). This differential anterior posterior actin arrangement can clearly be visualised in 0h pupa till 3h pupa. From 4h onwards these cables start disappearing. We further investigated the high order actin arrangement between anterior and posterior DT cells and found that in the anterior DT cells, actin arrangement differentiated along the basal to apical axis as well. In the anterior DT cells, there was three domains of actin bundle arrangement, basal supracellular actin bundles which were perpendicular to the tube axis, middle parallel supracellular actin bundles and apical taenidial F-actin rings. Whereas, as already described, the posterior DT cells shows two levels of DT arrangement, basal parallel supracellular actin cables and apical taenidial F-actin rings. Btl>Utrophin GFP 0h pupae were used for studying the actin arrangement in pupal trachea. Perpendicular actin bundles were formed in the anterior DT cells (tr5) of the 0h pupa (**Figure 3-11Bi**). The images were the maximum-intensity projection image of the z-stacks. The unique order of actin arrangement in anterior cells was clearly identified in the ortho view (**Figure 3-11Bi'**). On separately projecting the corresponding Z-planes, the basal perpendicular bundles, parallel bundles in the middle and apical teanidial rings were clearly distinguished (**Figure3-11Bi'', i''', i''''**). However, in them posterior two layer of actin arrangement was observed, basal parallel bundles and apical taenidial rings. (**Figure 3-11Ci'', i''''**). Surprisingly, after 6h, the anterior perpendicular supracellular actin arrangement



C



D

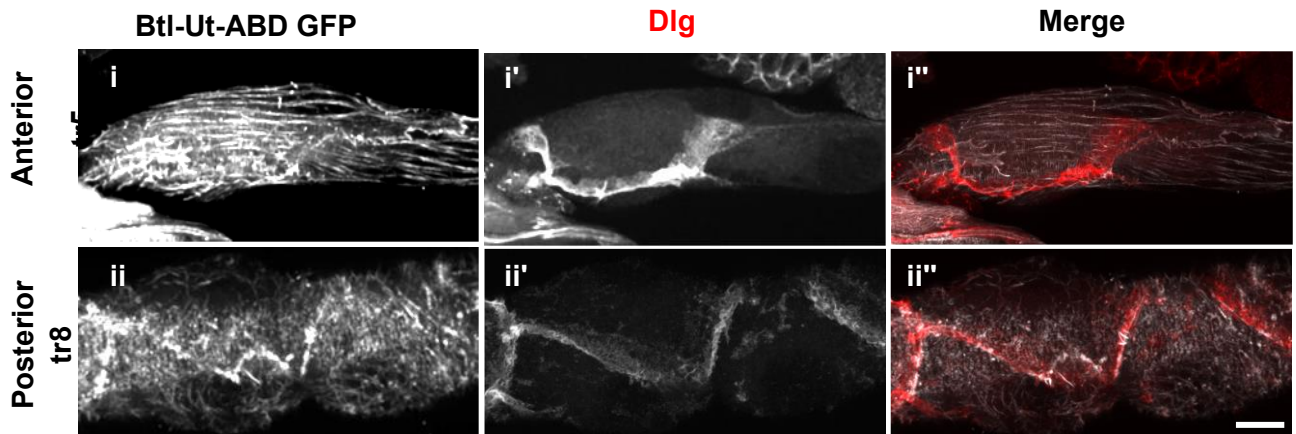


**Figure 3-11. Differential actin bundle arrangement in anterior and posterior pupal trachea in 0h APF**

(A) Tr-5 -tr-6 segmental junction showing differential actin and tubulin organisation between posterior trachea. *btl* > *Ut-ABD-GFP* 2h pupal DT stained for tubulin. Actin supracellular arrangement is visualized by *Ut-ABD-GFP* (3-11Ai). Actin show perpendicular arrangement to the DT axis in the anterior whereas parallel in the posterior. Tubulin shows similar arrangement like actin. (3-11Ai'). Maximum intensity projection images, Scale bars indicate 10  $\mu$ m.

(B) Three layer of actin arrangement in the anterior trachea (tr-5) of 0h pupa. *Ut-ABD-GFP* was used for labelling actin (3-11Bi), Ortho view of the anterior actin arrangement (3-11Bi'). The separated three layers of actin arrangement 3-11Bi''-i'''). The layers were extracted from a complete z-stack from the yellow box region. Bi'' is the basal actin layer, Bi''' is the middle layer and Bi'''' is the apical/ taenidial actin rings.

(C) 0h pupa of posterior DT showing two layers of actin arrangement. Actin was visualized by *Ut-ABD-GFP*. Parallel supracellular arrangement in posterior DT (tr-8) (Ci). (Ci') is the ortho view of actin arrangement, and (Ci'') and (Ci''') are basal and apical actin layers. The images were maximum-intensity projections of the extracted stacks from the yellow box region.

(D) DT of 6h pupa showing anterior (tr5) and posterior (tr8) segments. *Ut-ABD-GFP* pupa was dissected and immunostained for *Dlg* to demarcate the cell boundary. The anterior and posterior supracellular arrangement was altered. Parallel supracellular cables replaced the previous perpendicular structures (D'). In posterior segments, the parallel cable arrangement was completely lost, and disorientated cables were observed with a distinct junctional cortex.

Maximum intensity projection images, Scale bars indicate 10  $\mu$ m.

disappears and parallel supracellular cables form (**Figure3-11Di**).). In the posterior, the parallel actin cables were replaced by very thin disoriented actin fibers in 6h pupa and the junctional actin cortex was very prominent in the cells (**Figure3-11Dii**).

The anterior tracheal tissue is retained and modified to form segments of the pupal trachea in the late pupa (>12h), whereas the posterior DT (tr6-tr10) undergoes degeneration as it is functionally replaced by PAT(F. Chen & Krasnow, 2014; Fraire-Zamora et al., 2021). The differential cytoskeletal arrangement we have observed between the two halves of DT might be a mechanism to compartmentalize the anterior and posterior trachea and facilitate cellular processes leading to different fates. During tube compression, these differential actin organizations might protect the anterior DT cells, or these differential actin arrangements may indicate different forces at work in both the anterior and posterior tracheal DT. It would be interesting to investigate the key players involved in the actin arrangement and why DT cells exhibit such behavior.

### **3.3. Discussion**

This work shows clear evidence of distinct, well-defined LAJs in vivo. Although cadherin junctions have been observed on the lateral wall in several cases, these have almost always been identified in cultured cells and are usually visible as a region of the lateral membrane that is embellished with E-cad clusters. The LAJ that we saw in the tracheal DT epithelium has a belt-like arrangement and, albeit with a slightly altered outline, follows the ZA around the cellular boundary. This suggests that there may be mechanisms for regulating the positioning of the E-cad at LAJ clusters. Apicobasal polarity influences the position of E-cad at ZA. The distribution of proteins of the polarity complexes in the DT epithelium had no alteration with

respect to the classical picture in the epithelium. It would be interesting to know how the polarity pathway influences the position of two distinct cadherin belts in this tissue. Our research indicates that E-cad molecules at the ZA and LAJ develop various interactions with cytoskeletal regulators and have actin cortices of differing properties, but it is unclear how this is accomplished. All the catenins we looked at were associated with both ZA and LAJ. However, catenins and their associated proteins are stress sensors and can bind to different subsets of partners based on the tension experienced (Huveneers & de Rooij, 2013). More detailed analysis of the proteins binding at ZA and LAJ in the DT should shed light on these differences.

Formation of supracellular actomyosin bundles during development and morphogenesis is well studied in many systems (Röper, 2013). Coordination of such structures across cells almost always involves a junction associated signal (Sánchez-Corrales & Röper, 2018). Rho GTPases play a central role in actin cytoskeleton regulation (Etienne-Manneville & Hall, 2002). By virtue of regulating AJs on the one hand and being under the modulatory influence of Cadherin junctions on the other (Braga & Yap, 2005), these molecules are perfectly placed to mediate the influence of LAJ on LAJC and the actin cables. Both Cdc42 and Rho1 were found to be required for proper establishment of LAJC and subsequent actin cable formation. Cdc42 acts primarily through Arp2/3, WASP pathway whereas, Rho1 acts through formins and downstream myosin phosphorylation (Etienne-Manneville & Hall, 2002; Jaffe & Hall, 2005). Our KD experiments with GTPases and its downstream effectors indicate that both of these pathways contribute to bundle formation. In order to understand the differential functions of these pathways in relation to actin nucleation and bundle formation, further studies will be necessary. In *Drosophila* egg chambers, polarised filopodia emerge from the basal cortex to form the dorsoventrally oriented actomyosin supracellular cortex. Cdc42 controls the development of the actomyosin network and the formation of the filopodia

(Popkova et al., 2020). Rho1 was discovered to be irrelevant to the supracellular cortex's organization. High filopodial activity at the DT LAJC characterised the early stages preceding long actin cable production, which is analogous to the egg chamber scenario. Contrarily, the generation of cables and the activity of filopodia in the DT are both regulated by Cdc42 and Rho1.

Fraire-Zamora et al. clearly demonstrated that aECM remodeling was sufficient to complete the shortening of DT without any aid from the actomyosin cytoskeleton (Fraire-Zamora et al., 2021). Hence, it is not surprising that in our experiments the shortening of the tissue was completed even when the actomyosin supracellular structure was significantly abrogated in the KDs. The delay that accompanied shortening in such KDs shows that actomyosin might have an initial facilitatory role in the aECM driven shortening. The supracellular actin structure playing a passive role instead of actively contributing to tissue dynamics is not unknown. Indeed, in the classical model of *Drosophila* dorsal closure, it has been suggested that the supracellular actin cable formed is not required for the closure per se (Ducuing & Vincent, 2016). Instead, the cable integrates forces and retains tissue organization. Given that the inter taenidial spacing was changed at 2h APF in the KDS where cables are abrogated, it is tempting to speculate that the supracellular cortex, in this instance, serves a protective and coordinating role ensuring epithelial integrity while the aECM remodeling brings about the morphogenetic movements.

In early hours of the acute compression phase, actin blebs form in the posterior tracheal cells. These blebs are membrane vesicles, having an outer actomyosin cortex. Rho, formin diaphanous, ERM protein moesin colocalises with the outer cortex of these blebs. We have confirmed that these are not secretory vesicles or autophagosomes by analysing various secretory markers. Hence, we conclude that these blebs are most likely the by-products of the tube compression event. Perhaps these blebs form to equilibrate the membrane surface area

with the high pressure generated by virtue of compressive events. It would be really interesting to understand these bleb initiation, formation and maturation in real time. these can be a great tool to understand de novo cortex formation.

We further extended our study to the anterior segment and observed that actomyosin behave differently from the posterior segments. In the anterior actomyosin cables align perpendicular to the long axis of the DT. The actin arrangement is also different along the depth of the cell between the anterior and posterior DT. In the posterior DT cells, we observed two different domains of actin arrangement whereas in anterior DT cells we observed three domains of actin supracellular arrangement. It is worth noting that taken together this system offers a great opportunity to further analyse mechanisms at the level of actin nucleation and bundling that bring about diverse axes of actin polarisation in the tissue. Given that these events are concomitant with important developmental and morphogenetic windows, further correlation with pattern formation genes will help to explain the global regulatory paradigms that control such cell biology.

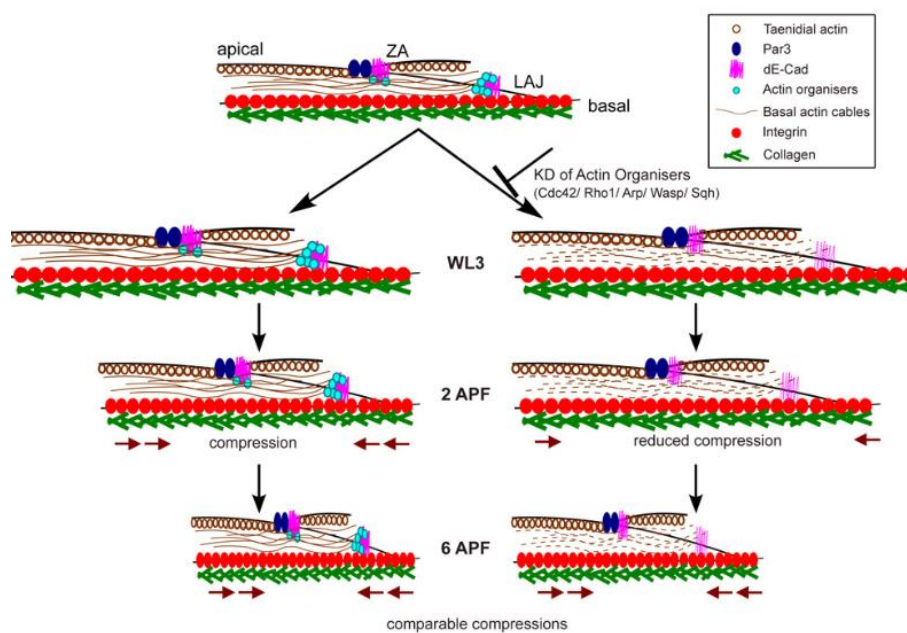


**Figure 3-12. Graphical representation of the supracellular actin cable-mediated tracheal tube compression (Image from (Pradhan, 2023, Lateral adherens junctions mediate a supracellular actomyosin cortex in drosophila trachea))**

**CHAPTER 4**

**SPECTRAPLAKIN SHORTSTOP MEDIATES  
SUPRACELLULAR ACTIN AND MT CROSS-TALK IN  
POSTERIOR PUPAL TRACHEA.**

## 4.1 Introduction

During morphogenesis, directed force generation and transmission are essential for maintaining tissue integrity through coordinated cell shape changes in a polarized epithelium. This coordinated behavior is mediated by cell adhesion complexes and their associated cytoskeletal machinery. As discussed in the introduction, cells are attached by junctional adhesion proteins apically. The junction-associated actomyosin cytoskeleton of adjacent cells further interacts via cadherin-catenin complexes. The actomyosin cytoskeleton has garnered much attention as the central player for directed force transmission and generation during development. However, the other two important cytoskeletal components, microtubules and intermediate filaments, have been relatively less well-studied (Vasileva & Citi, 2018). Microtubules (MT) are highly polarised hollow, cylindrical polymers made up of thirteen protofilaments of structurally asymmetric subunits of  $\alpha\beta$ -tubulin heterodimers. MT acts a dynamic intracellular roadways circumference and traversing throughout the cells (Sallee & Feldman, 2021). The polarization of microtubules is due to the presence of  $\alpha$ -tubulin at the minus end and  $\beta$ -tubulin at the plus end in a dynamic growing microtubule. This innate microtubule polarity is crucial for cell polarity because this programs associated motor proteins such as Kinesins and Dynein to directional cargo transport. During cargo transport, Dynein generally moves towards the minus end and the Kinesins towards the plus end (Mukherjee, Brooks, Bernard, Guichet, & Conduit, 2020). MT nucleation and stabilization at the minus end are regulated by the  $\gamma$ -tubulin ring complex, which serves as the major structural unit of the microtubule organizing center (MTOC) (Martin & Akhmanova, 2018). Tubulins undergo several post-translational modifications at their C-terminal end, including tyrosination, detyrosination, acetylation, formation of  $\Delta 2$ -tubulin, glycation etc., which affects the microtubule properties and function (Gadadhar, Bodakuntla, Natarajan, & Janke, 2017).

The primary roles of microtubules explored so far include polarized cargo and cell organelle transport, spindle formation during cell division, and support for various cellular processes, among others. These functions are commonly referred to as housekeeping functions and are crucial for all cellular processes including morphogenesis. However, a less explored role of microtubules is their active participation in force generation and transmission, alongside the actomyosin cytoskeleton (Röper, 2020).

Microtubules (MTs) play an essential role in the establishment and remodeling of adherens junctions (AJ), alongside the actomyosin cortex. In thyroid epithelial monolayer cells, it was reported that AJ establishment depends on MTs. Following colchicine treatment, there was a significant reduction in E-Cadherin accumulation at AJ (Yap, Stevenson, Abel, Cragoe, & Manley, 1995). Moreover, in lung epithelial cells, inhibiting MT plus-end expansion resulted in the disintegration of AJ, loss of F-actin, punctate catenin rearrangement, and ultimately the disappearance of junctions (Waterman-Storer, Salmon, & Salmon, 2000). These findings provide strong support for the claim that MT dynamics and organization influence actomyosin organization during AJ assembly. Microtubules play a crucial role in facilitating the transport of E-Cadherin and its recycling at the apical region of the terminal cells of *Drosophila* trachea. Interference with microtubules in *Drosophila* tracheal terminal cells has an impact on the levels of junctional E-Cadherin and Par-3, thereby influencing both cell rearrangement and branch elongation (Le Droguen, Claret, Guichet, & Brodu, 2015). The polarization of various epithelial tissues, such as the *Drosophila* pupal wing epithelium and the follicle cells of the *Drosophila* female gonad, relies on microtubules. Disruption of microtubules has a significant impact on the core planar cell polarity proteins (Matis et al., 2014; Shimada, Yonemura, Ohkura, Strutt, & Uemura, 2006; Viktorinová & Dahmann, 2013).

There are many evidences that showed that MTs potentially help the actomyosin complex in force generation during morphogenesis (Röper, 2020). In *Drosophila* embryos, the

actomyosin cytoskeleton and microtubules play a coordinated role in the development of salivary glands and placode formation (Alexander J. R. Booth, Guy B. Blanchard, Richard J. Adams, & K. Röper, 2014). The formation and maintenance of the apical-medial actomyosin cortex rely on non-centrosomal microtubules, which induce apical constriction of cells during this developmental process. These microtubules extend along the actomyosin cortex to carry out this function. Disruption of microtubules abolishes the dynamic pulsatility and inhibits the apical constriction (Alexander J. R. Booth et al., 2014). Formation of morphogenetic furrow in *Drosophila* larval eye disc depends on the enrichment of microtubules and F-actin-activated non muscle myosin II within the apical domain of the constricting cell (Corrigall, Walther, Rodriguez, Fichelson, & Pichaud, 2007). During the development of the amnio serosa in the *Drosophila* embryo, a transformation occurs where the cells change shape and elongate from columnar to squamous. In this process, dynamic microtubules play an active role in pushing the apical junctions to expand the apical surface, counteracting the restraining effect of the cortical actin band, which prevents precocious elongation of the cells (Pope & Harris, 2008). In the tracheal terminal cells (TCs) of *Drosophila*, during de novo lumen formation and branching, substantial remodelling of the MT and actin cytoskeleton happens, followed by vesicular and membrane transport (Gervais & Casanova, 2010; S. Sigurbjörnsdóttir, R. Mathew, & M. Leptin, 2014) (Best, 2019). TC morphogenesis is further governed by coordinated actin-MT interaction. During TC (terminal cell) morphogenesis, actin filaments located at the elongating tip cell, as well as the basolateral and luminal membranes, are regulated by actin regulators such as DSRF, Enabled, and Moesin. (Jayanandan et al 2014). The extension and stabilization of the lumen are on par with the growth of the cell body (Best, 2019; Gervais & Casanova, 2010; S. Sigurbjörnsdóttir et al., 2014). Additionally, a dynamic actin pool is responsible for forming filopodia, which align the subcellular lumen with the elongation axis at the basolateral side of the TC. Microtubules (MTs) are crucial in guiding and

directing tube growth by facilitating cargo transport (Gervais & Casanova, 2010; S. Sigurbjörnsdóttir et al., 2014). They also provide mechanical stability to the elongating TC. The interaction between MTs and the basolateral actin pool is imperative for the proper growth and development of the TC (Best, 2019).

Many studies have been done to understand the actin- MT cross talk which is mediated by a group of proteins called as spectraplakins. These are large, conserved cytoskeletal proteins with a specialized multidomain structure that can bind both actin and MTs. Spectraplakin has both a spectrin domain and a specialised plakin domain. N terminal domain of spectraplakin has two calponin homology (CH) domains, which help actin binding. The C-terminal has a microtubule-binding domain. Spectraplakins link the most catastrophe prone MT minus end to the actin filament (Alkemade et al., 2022), hence stabilising the MT bundles. Loss of spectraplakins has been demonstrated to have notable consequences on adhesion, morphology, polarity, and microtubule structural defect in vivo (Suozzi et al., 2012). Shortstop (Shot) is the single spectraplakin present in *Drosophila*. Shot binds to MTs and actin contributing to the cytoskeletal dynamics (Applewhite, Grode, Duncan, & Rogers, 2013; Applewhite et al., 2010; Röper et al., 2002). Shot mutants display a diverse range of pleiotropic phenotypes, encompassing various issues such as impaired establishment of perinuclear microtubules, loss of axon and dendrite growth, disrupted formation of muscle-tendon junctions, failures in tracheal TC fusion and dorsal closure during embryo development, as well as anomalies in oocyte selection and patterning (Gregory & Brown, 1998; Khanal, Elbediwy, Diaz de la Loza Mdel, Fletcher, & Thompson, 2016; Lee & Kolodziej, 2002; Subramanian et al., 2003). Shot has been reported to bind the minus-end-binding protein Patronin and the microtubule plus-end-binding protein EB1, both are necessary for the formation of acentrosomal MT networks (Khanal et al., 2016; Nashchekin, Busby, Jakobs, Squires, & St Johnston, 2021; Subramanian et al., 2003). (Ricolo & Araujo, 2020) in their recent study, showed that the spectraplakin Short-

stop (Shot) facilitates the MTs- actin interaction, which results in the directional elongation of the subcellular lumen within the TC cytoplasm.

The examples mentioned above highlight the crucial role of Spectraplakins in development and morphogenesis, and the significance of interactions between different components of the cytoskeleton such events. In our research, we made a novel discovery of lateral E-Cadherin junctions that facilitate the formation of a supracellular actomyosin cortex in early pupa. These specialized supracellular cables, aligned parallel to the tube axis, redundantly aid in the tube shortening process (Rojalin Pradhan, Kumar, & Mathew, 2023),Chapter 3). We were keen to investigate the behavior and function of MTs in this seemingly highly coordinated process. Furthermore, given the limited knowledge about MT dynamics during epithelial degeneration or tracheal tube shortening our findings in this regard will be of immense value. Therefore, our focus in this chapter centers on exploring the dynamics of microtubules in the already described tracheal epithelial degeneration and associated morphogenetic events.

## **4.2 Results**

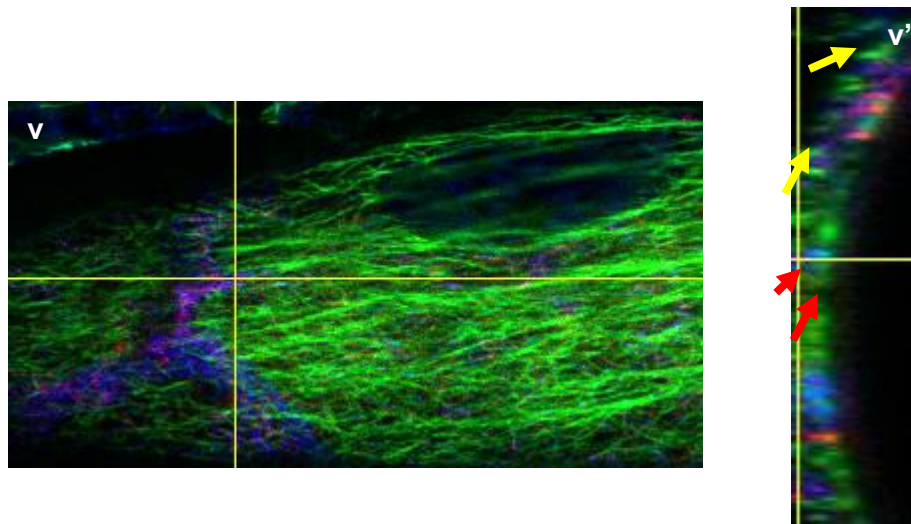
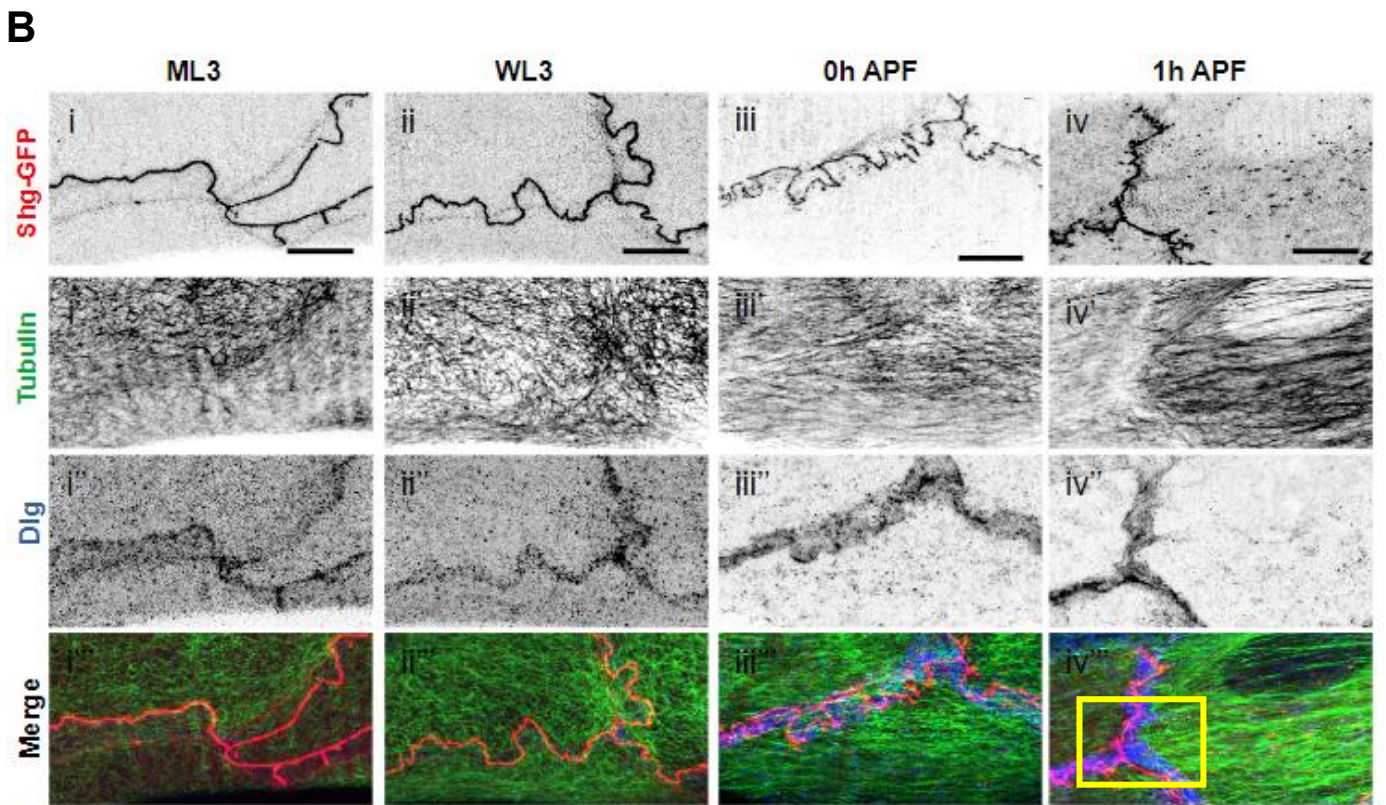
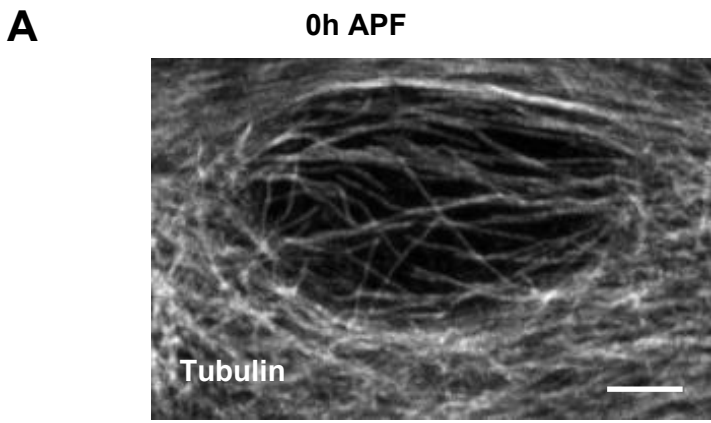
### **4.2.1 A basal mesh of microtubules form in posterior pupal trachea.**

To gain further insights into the cytoskeletal phenomena occurring in the posterior pupal trachea during the early pupal stage, we focused on studying microtubules (MTs). As mentioned in the introduction of this chapter, microtubules (MT) often collaborate with the actomyosin to carryout cellular and physiological processes. Building upon this knowledge, we expanded In this chapter we investigated the behavior of microtubules in the posterior pupal trachea and its relationship with supracellular actomyosin cables. During our investigation of the 0h pupal DT, we made an interesting discovery that microtubules form a parallel mesh in the posterior pupal trachea(**Figure 4-1A**). To understand the nature and

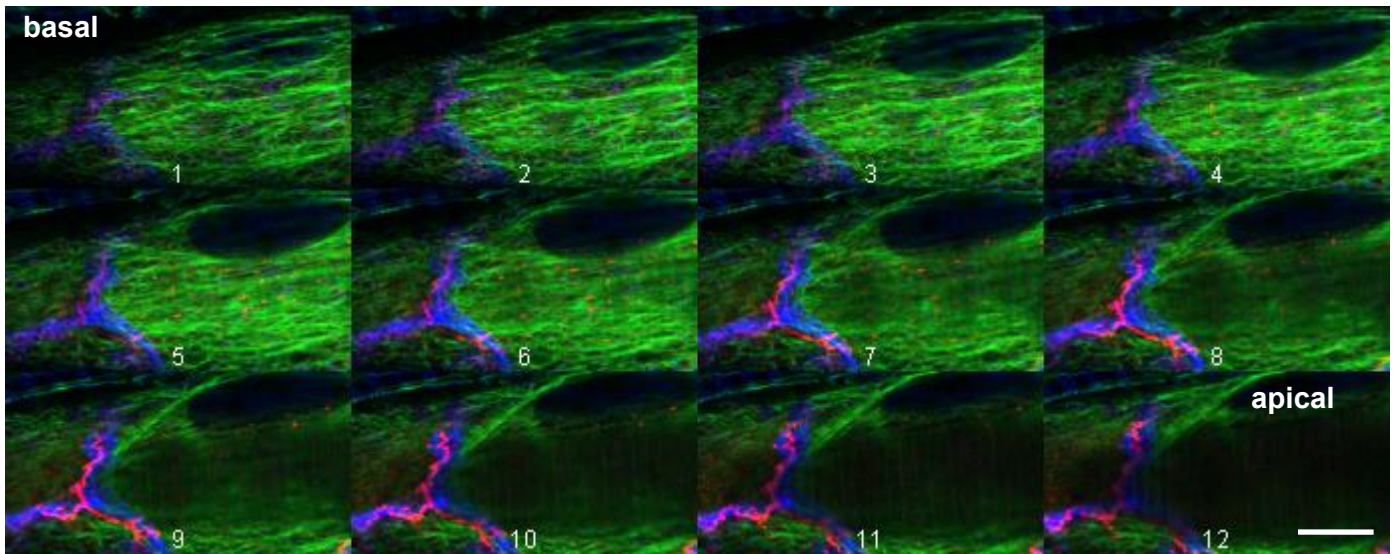
positioning of these microtubules, we delved into earlier larval stages, beginning from ML3. For characterization, we utilized Shg::GFP to mark adherens junctions (AJ) and Dlg as a basolateral domain marker. MTs were visualized using an alpha tubulin antibody. In the larval stages (ML3 and WL3), the microtubules appeared as a highly irregular mesh distributed throughout the cytoplasm (**Figure 4-1Bi', ii'**).

However, in the 0h and 1h pupal stages, we observed a rearrangement of this microtubule mesh into more regularly organized bundles aligned parallel with the DT tube axis (**Figure 4-1Biii', Aiv'**). Further investigation using the YZ orthogonal view revealed the presence of MTs in all three layers: apical, medial, and basal MT (**Figure 4-1Bv, v'**). The parallel MTs we observed were mainly basal in nature and closely localized to the basal edge of the Dlg spread. This close localization is indicated by the red arrow, and in some cases, basal MTs were clearly distinguishable due to clear separation (yellow arrows). To understand localization of MTs, we did a montage of all the z planes from basal to apical and found that parallel MTs were mostly basal (**Figure 4-1C**).

To validate our hypothesis, we conducted the experiment using the Par-3 protein trap line, a well-known apical marker. Both Par-3 and Dlg were used to understand the MT localization (**Figure 4-1Di-ii**). From the YZ orthogonal view of the region of interest (**Figure 4-1Dii'''**), we observed that the MT parallel bundles were situated close to the basal edge of the Dlg. The tracheal DT cells, as described earlier in Chapter-3, are thin and flattened with a tilted lateral membrane. The Par-3 localization at the lateral edge of the Dlg spread (red arrow) and the MTs' localization at the basal edge of Dlg (yellow arrow) were clearly visible in the orthogonal image. To gain more insight into the nature of this MT mesh, we considered acetylated tubulin and tyrosinated tubulin. By examining these two types of post-translational modifications in the tubulin mesh, we aimed to better understand the characteristics of these microtubules.



C



D

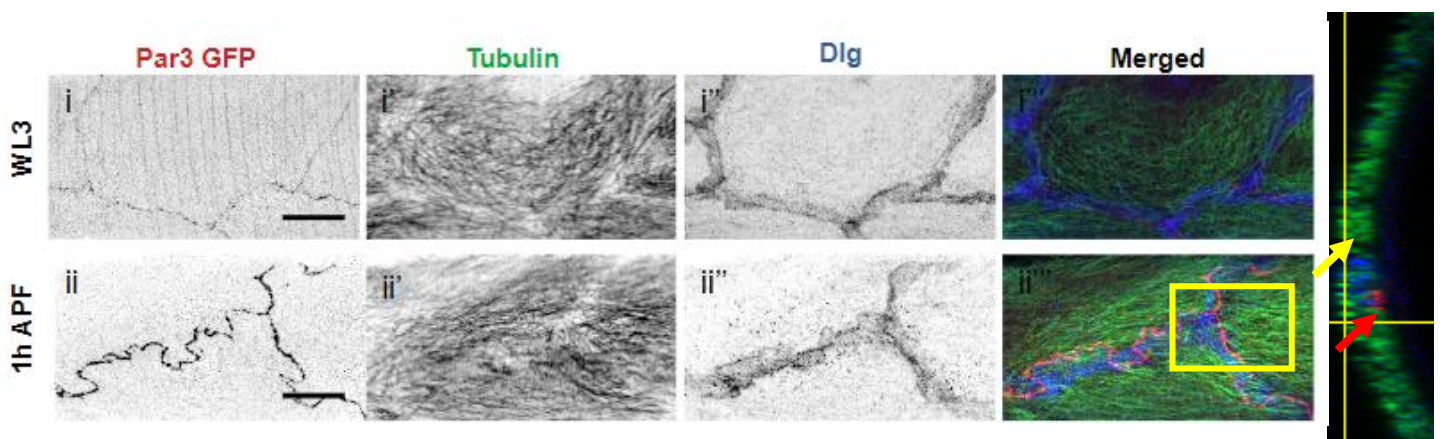


**Figure 4-1. Basal MT mesh forms in *Drosophila* posterior pupal trachea.**

(A) Maximum intensity projection image of 0h posterior pupal tracheal cell, immunostained for alpha-tubulin antibody.

(B) Images of posterior metameres, tr7/tr8 of the dissected DT of Shg::GFP larvae and pupa, immune-stained for tubulin and Dlg. Anterior is to the left, and posterior is to the right. The

images shown here are the maximum-intensity projection images of Z-stacks. Shg::GFP was used as AJ marker, and Dlg was used for demarcating the basolateral membrane. Microtubules were visualized by alpha-tubulin antibody staining of DT cells. Scale bars indicate 10  $\mu\text{m}$ . (i)-(iv) illustrates the two DE-Cad belts that run along the DT cells' periphery. The bright, sharp junction known as ZA and the additional punctate lateral accumulation of DE-Cad is LAJ. Junctions gradually became irregular in 1h and 2h pupa. (i')-(iv') shows the microtubule arrangement in posterior DT cells. Tubulin antibody was used to visualize microtubules. Microtubules showed very irregular and scattered patterns throughout the cytoplasm in ML3 and WL3 (i') and (ii'). Microtubule became parallel in 0h and 1h pupal DT cells (iii') and (iv'). The (v) shows the Y-Z orthogonal view from the ROI indicated by the box in (iv'''). Yellow arrows indicate the location of microtubules in 1h pupa; Microtubules are present both apical, medial, and basal from the Y-Z plane. But the parallel microtubules we look at are basally close to the Dlg spread. (Red arrow)

(C) The individual Z-planes were arranged from basal to apical sequentially as a montage. The Z-stack images were from posterior DT cells of 1h APF pupa. Each Z plane was marked with numbers sequentially from basal to apical manner. For AJ marker Shg::GFP was used, and Dlg was used as a basolateral marker. MTs were visualized by alpha-tubulin antibody. The montage showed that the parallel Mt alignment was mostly basal and

(D) Images of posterior DT cells of WL3 and 1h pupa, Par3 protein trap was used as an apical marker and Dlg for the basolateral marker to further explore more about the basal microtubule mesh. (ii') parallel microtubule mesh formed in 1h pupa. The Y-Z orthogonal view from the selected ROI from (ii''') showed that these microtubules were present at the basal surface. The red arrow indicated the apical par-3; below that Dlg lateral spread and the basal side, we can

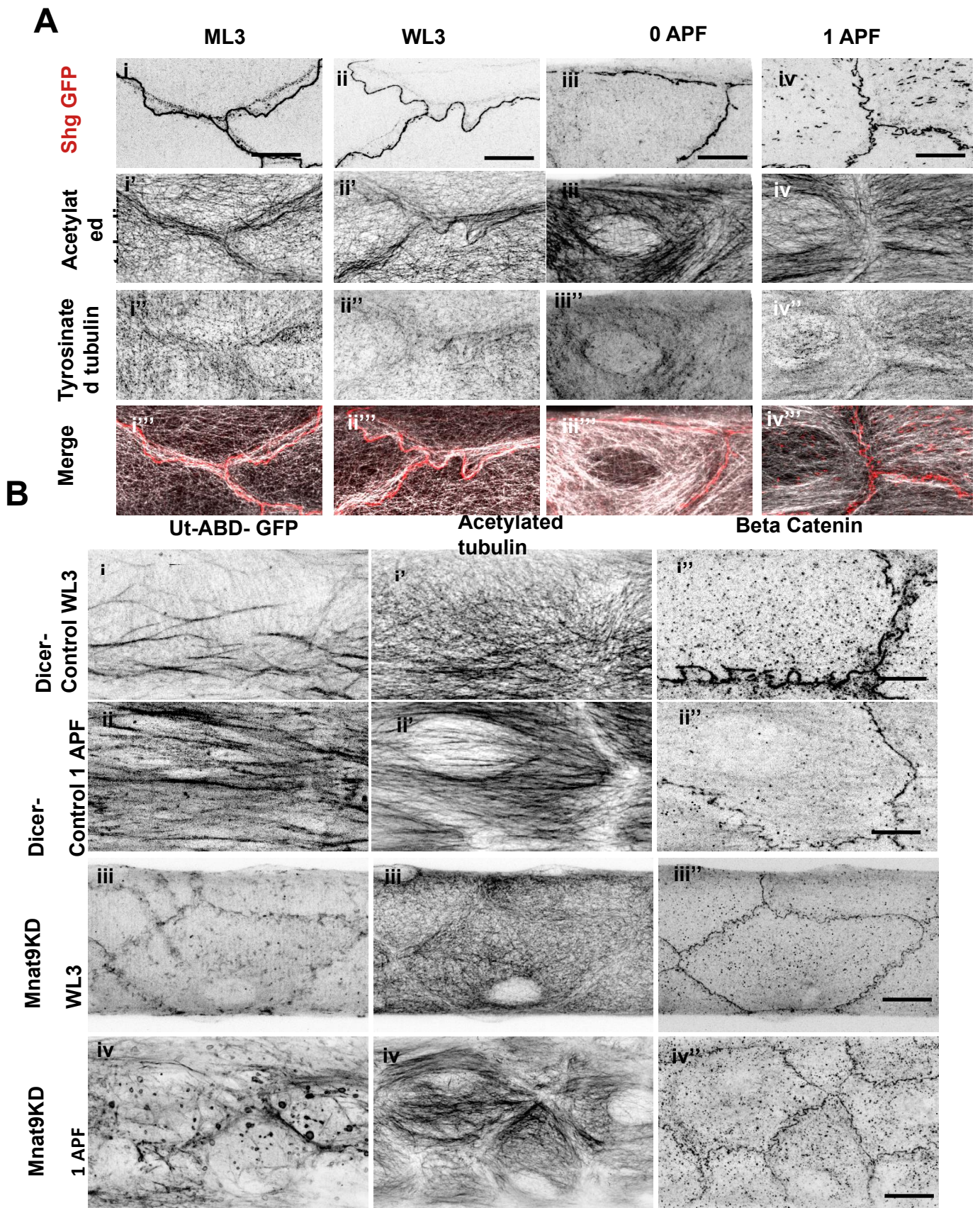
clearly visualize basal microtubule mesh. Indicated by a yellow arrow. Scale bars indicate 10  $\mu\text{m}$ .

#### **4.2.2 The basal MTs are stable and mostly acetylated.**

Post-translational modifications in microtubules (MT) play a crucial role in determining their properties and functions. These modifications can alter the mechanical characteristics of MTs. For instance, when the Lys40 (K40) residue of alpha tubulin is acetylated, it induces changes in the  $\alpha$ K40 loop architecture. As a result, the interaction between Lys60 and His283 in neighboring protofilaments is disrupted, leading to limited MT flexibility and increased resistance to breakage and disassembly (Gadadhar et al., 2017). The acetylation of MTs can serve as an indicator of stable MT bundles (Portran, Schaedel, Xu, Théry, & Nachury, 2017). On the other hand, tyrosination of microtubules indicates highly dynamic and newly formed growing MTs. In neuronal cells, a more dynamic population of tyrosinated tubulin is present in the growth cones, which plays a critical role in neuronal pathfinding (Gadadhar et al., 2017; Marcos et al., 2009). The presence of tyrosinated tubulin indicates the active and dynamic nature of these MTs in promoting cellular processes like growth and navigation. In *Drosophila* tracheal terminal cells tyrosinated tubulin, present in newly assembled MTs, exhibited a distinct concentration near the tip and in front of the lumen, indicating that these MTs are likely the most recently formed and incorporated, whereas the distribution of acetylated tubulin, which is commonly found in older and more stable microtubules (MTs), closely resembled that of the entire MT network (Gervais & Casanova, 2010). We investigated the acetylated and tyrosinated microtubule populations in the posterior tracheal cells from ML3 to 1h APF pupa. The microtubule mesh we observed was highly acetylated, indicating a high stability of these MT bundles. In ML3 and WL3 stages, these stable bundles appeared to be irregular (**Figure 4-2Ai'-ii'**), but by 1h APF, they were arranged into acetylated stable bundles, aligned parallel to

the DT axis (**Figure 4-2iii'-iv'**). Similarly, we examined the tyrosinated fraction of microtubules and observed that the dynamic MT population was limited in the DT cells. In ML3 and WL3 stages, the tyrosinated MTs appeared irregular and scattered (**Figure 4-2Ai''-ii''**), and by 0h and 1h APF pupal DT stages, these dynamic bundles were scarce but exhibited a parallel alignment, albeit much less prominently than in the acetylated tubulin channel (**Figure 4-2Aiii'-iv'**).

Mnat9a, also known as microtubule N-acetyl transferase 9a, is the sole MT N-acetyl transferase found in *Drosophila melanogaster*. This enzyme acetylates the N-terminal residues of alpha- and beta-tubulin, leading to the blocking of JNK signaling and enhancing cell survival during development. Additionally, Mnat9a is crucial for microtubule stability, as it inhibits Spastin-mediated depolymerization while promoting Ebl-mediated polymerization (Mok & Choi, 2021). To investigate the role of stable MTs in the posterior pupal trachea and its relationship with parallel supracellular actomyosin cables, we performed RNA interference (RNAi) targeting Mnat9a in the trachea using the *btl-gal4 > Ut-ABD-GFP; UAS-Dicer* driver line. Our results showed that destabilizing MTs through Mnat9a knockdown led to a partial impairment of both actin and MT parallel arrangement in posterior DT cells during the WL3 stage (**Figure 4-2B iii-iii'**). In pupae with Mnat9 KD DT cells, the parallel alignment of MTs was partially lost, and many MT bundles appeared irregular (**Figure 4-2B iv'**). The actin arrangement was also affected (**Figure 4-2B iv**) compared to the Dicer control at 1h APF (**Figure 4-2B ii-ii'**). To validate our observations, we conducted an orientation analysis using the Fiji plugin Orientation J and found that the angles of actin bundles relative to the DT axis were highly variable, indicating irregular orientation in Mnat9 KD at 1h APF compared to the Dicer control (**Figure 4-2C**). Thus, MT acetylation and the stably oriented MT assembly play a crucial role in stabilizing the supracellular actin cortex.



**C**

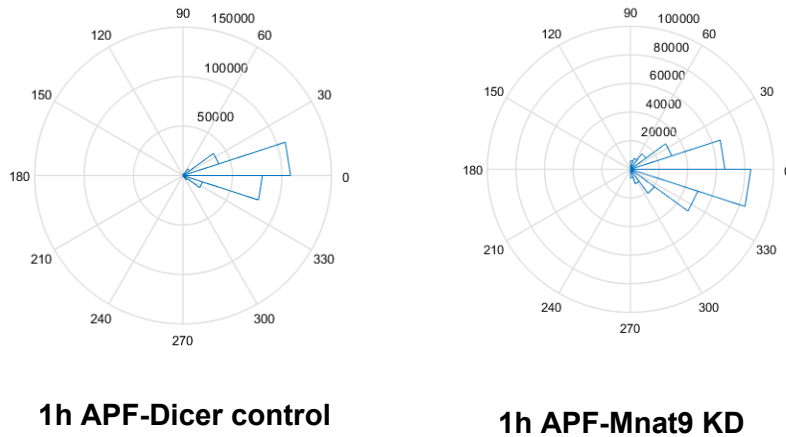


**Figure 4-2. The basal MTs are stable and mostly acetylated MTs.**

(A) Images of posterior metameres, tr7/tr8 of the dissected DT of Shg::GFP, immune-stained for tyrosinated alpha-tubulin and acetylated alpha-tubulin. Anterior is to the left, and posterior is to the right. Scale bars indicate 10  $\mu$ m.

(i)-(iv) The images show the ZA and LAJ in the posterior DT cells of ML3 to 1h APF.

(i')-(iv') The basal microtubule mesh is highly acetylated and stable. In 0h and 1h APF pupa, the acetylated MT follows the parallel pattern to the tube axis.

(i'')-(iv'') Very few tyrosinated microtubules were present in the cells, suggesting the basal microtubule mesh was highly stable.

(B) *btl-gal4 > Ut-ABD-GFP*; *UAS-Dicer* flies were crossed to *UAS-RNAi* lines of *Mnat9a*. All the images are from tr7/tr8 of the dissected trachea immunostained for acetylated tubulin and beta-catenin. Anterior is to the left, and posterior is to the right. Scale bars indicate 10  $\mu$ m.

(i)-(iv) shows actin as indicated by the *Ut-ABD-GFP* channel and (i')-(iv') shows the MT arrangement in both *Dicer* control and *Mnat9KD* (WL3, 1h APF) respectively. (i'')-(iv'') cell boundary is shown by beta catenin.

(C) The rose plots show the distribution of orientation of the actin cables in both Dicer control and Mnat9 KD and 1h pupa. The phenotypes observed in the Control, and KD were analyzed at the 1APF stage.

### **4.2.3 Actin supracellular cables and MT alignment in posterior pupal DT cells are distinct yet concurrent events.**

As discussed in Chapter-3, LAJs mediate the formation of a supracellular actin cortex in posterior pupal tracheal cells during early pupa. The process of bundle formation initiates from ML3 (**Figure 4-3i**), and the parallel alignment of these actin cables begins in WL3 (**Figure 4-3ii**). By 0h, clear parallel actin bundles become visible (**Figure 4-3iii**). These bundles continue to develop into stable, supracellular structures spanning the cells from 1h to 2h APF (**Figure 4-3iv-v**).

To understand the timing of these events, we examined microtubules alongside actin. We aimed to determine if these two processes occurred simultaneously. In ML3 and WL3, the microtubules were scattered throughout the cytoplasm in a mesh-like arrangement (**Figure 4-3i''-ii''**). However, in WL3 MTs were more structured than in the ML3 stage. At 0h APF, the microtubules started to bias towards a parallel arrangement with respect to the tube axis (**Figure 4-3iii''**). However, only after pupation, during 1h and 2h APF, we could clearly visualize the parallel MT bundles (**Figure 4-3iv''-v''**). At WL3, the microtubule (MT) mesh retains a relatively organized structure, indicating the existence of parallel bundles within it, supporting the initial arrangement of actin. This observation might not be immediately evident due to the high density of MTs within the cytoplasm. As the process progresses, MTs gradually reorganize into parallel cables, resembling the behavior of actin, although there appears to be a slight difference in the developmental timescale that is very difficult to resolve at this point. We conclude these two processes are concurrent and dependent on each other.

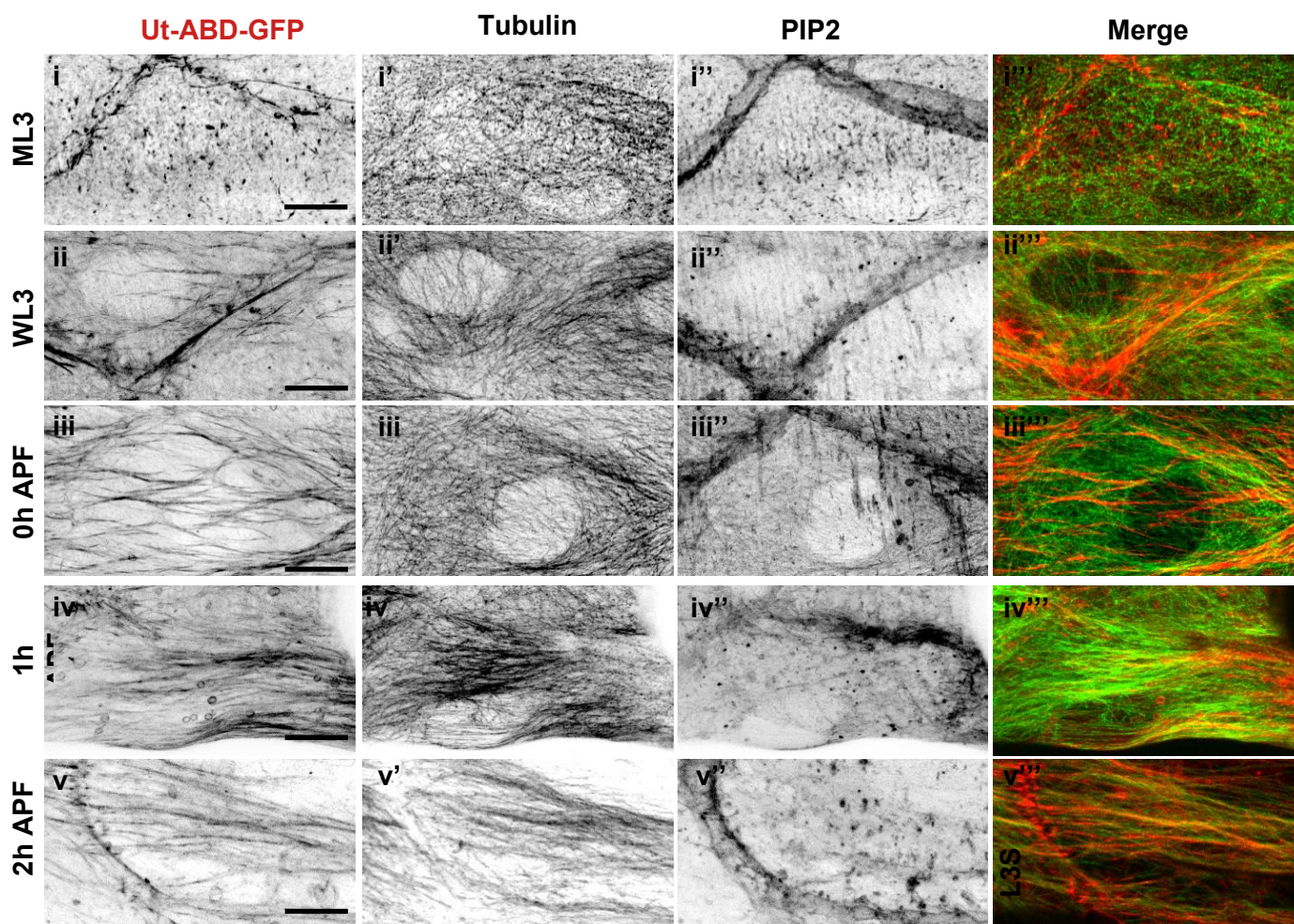


**Figure 4-3. The stable basal MTs follow parallel alignment like the supracellular actin cortex, indicating distinct yet concurrent events.**

Images of posterior metameres, tr7/tr8 of the dissected DT of *btl > Ut-ABD-GFP*; *btl > PLCδ-  
PH-Cherry (PIP2)*, immune-stained for alpha tubulin. Anterior is to the left, and posterior is to the right. All the images are maximum-intensity projection images. Scale bars indicate 10  $\mu$ m.

(i)-(v) shows the actin dynamics from ML3 to 2h APF pupa. The phenotypes are already described elaborately in Chapter-3. From WL3, the actin bundles start becoming parallel supracellular bundles. In 2h, the supracellular cables became stress fibers.

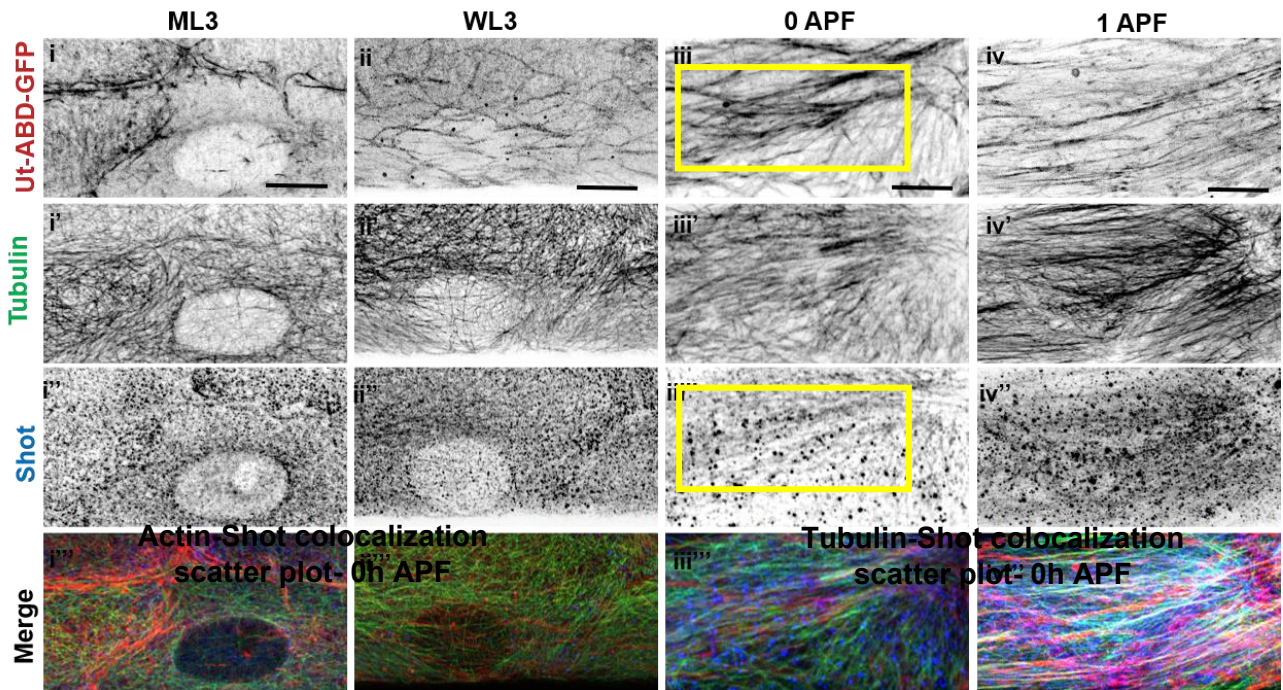
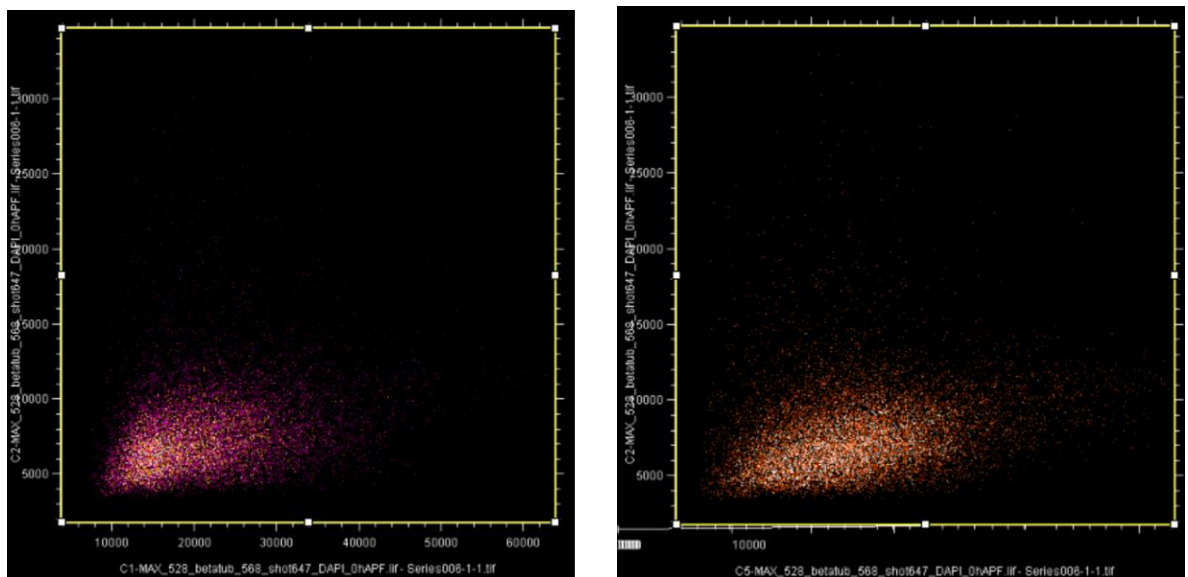
(i')-(ii') MT looks like a MT mesh scattered throughout the cytoplasm. In 0h APF, the MT starts orienting parallel to the tube axis, but the pattern is not that striking (iii').

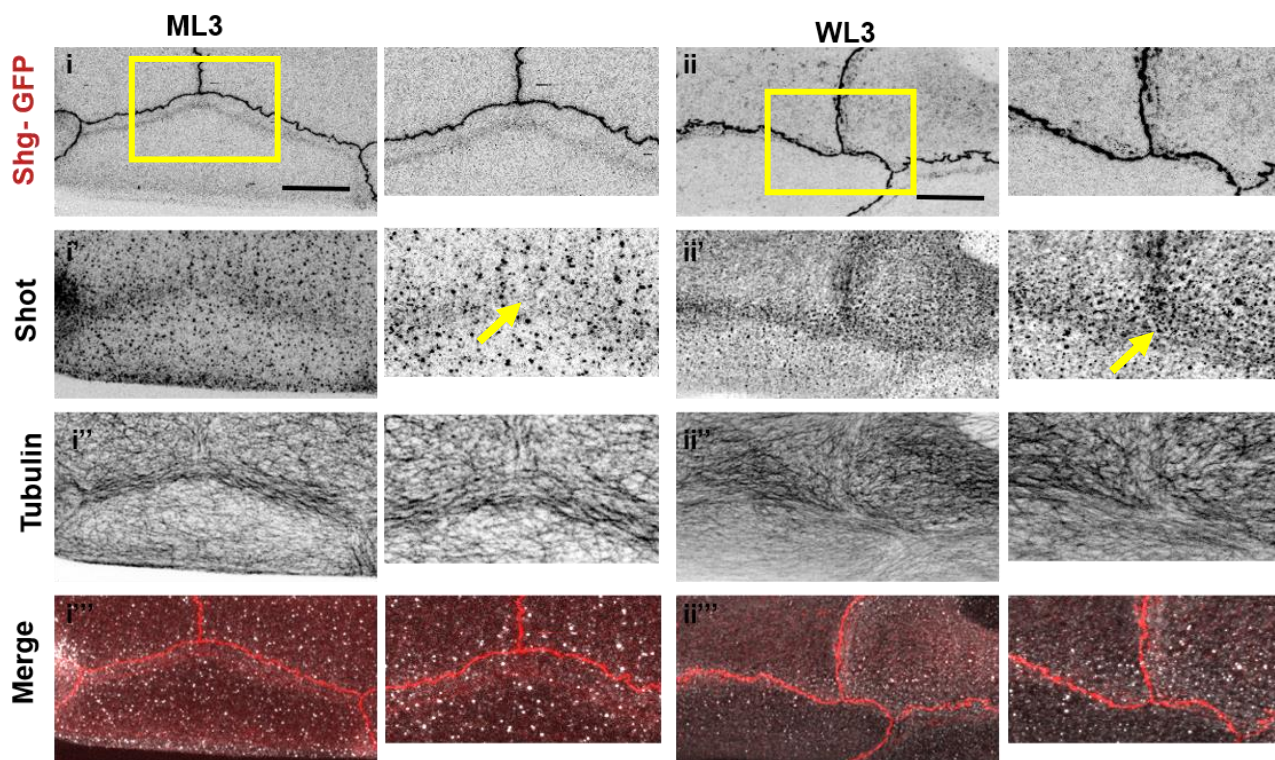
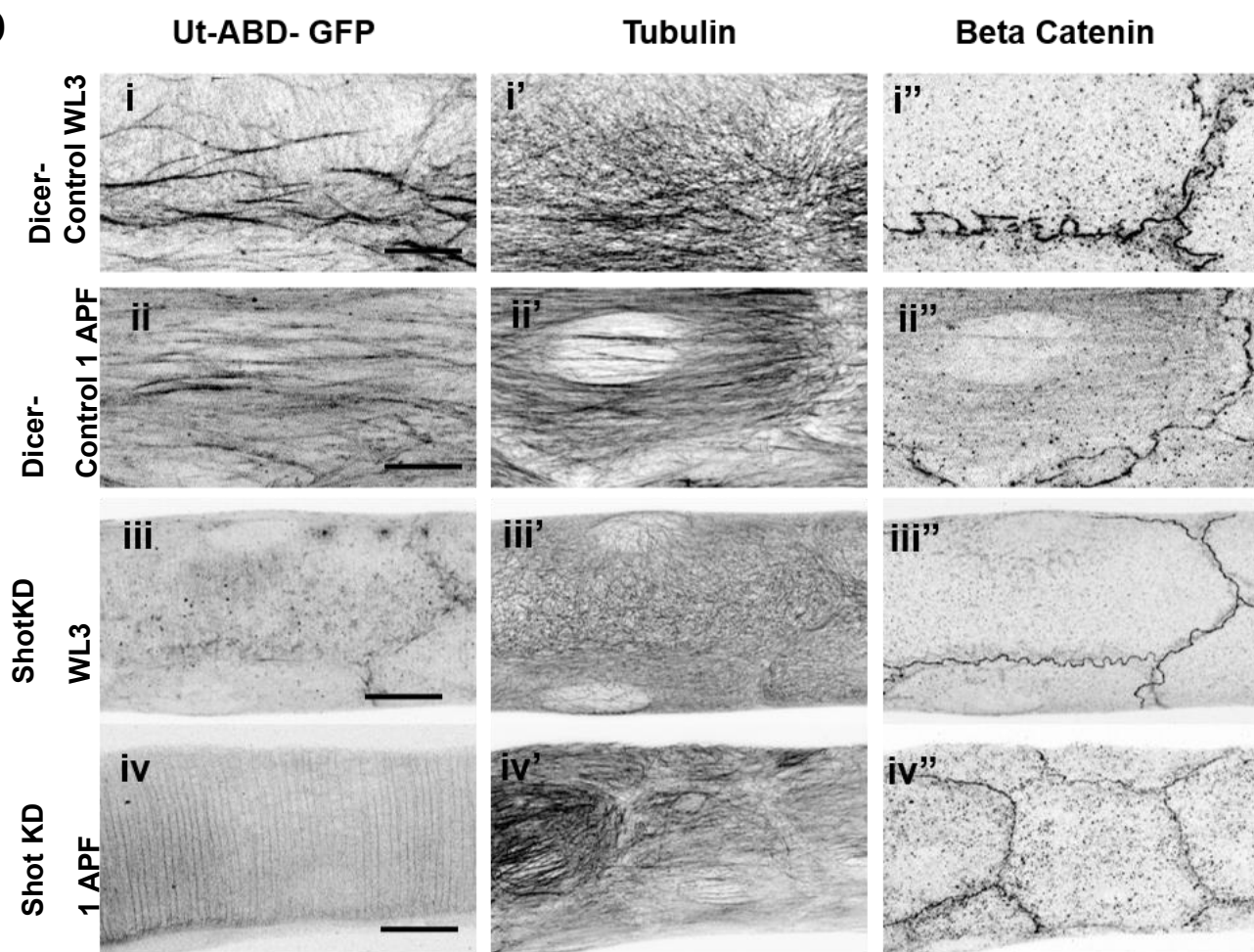
In 1h to 2h APF pupa, the MT mesh is arranged as a parallel MT mesh following actin pattern. (iv') and v'). The MTs and actin supracellular mesh formation are separate events yet share the same developmental time frame. It seems MTs also proceed through progressive organization into parallel cables, similar to actin.

#### **4.2.4 Spectraplakin Shortstop mediates actin-MT cross talk**

Spectraplakin Shortstop (Shot) mediates actin-MT crosstalk, acting as a crucial protein that crosslinks actin and microtubules. Our data revealed that actin bundling occurs before tubulin parallel arrangement, prompting us to investigate the role of *Drosophila*'s sole spectraplakin, Shortstop. We performed a time course analysis of Shot binding to MT and actin, ranging from ML3 to 1h pupal stages. In ML3 and WL3, Shot was uniformly present throughout the cytoplasm and around the LAJ (**Figure 4-4Ai''-ii''**) and (**zoomed image, yellow arrow indicating Shot localization at LAJ**). Meanwhile, MT appeared as a cytoplasmic mesh. By 0h APF, when tubulin parallel arrangement had started, actin had already formed parallel supracellular cables (**Figure 4-4Aiii'**). At this stage, Shot localized with both actin and tubulin bundles (**Figure 4-4iv''**), indicating a cross-linking event. This was further confirmed by the zoomed ROI from 0h APF, showing thick bundles where Shot colocalized with actin and MT (indicated by the yellow arrow). We conducted a colocalization analysis using the "Colocalization Finder" plugin in Fiji, examining Actin-Shot and Shot-Microtubules separately within the same region of interest (ROI). The resulting scatter plot data clearly indicated colocalization between Actin-Shot and Microtubules-Shot (**Figure 4-4B**). Even at 1h APF, Shot continued to localize with the actin-MT bundles, supporting its role in crosslinking actin and MT bundles and explaining the presence of parallel MTs in the posterior DT cells.

To explore the localization of Shot within the cell prior to the involvement of the supracellular cortex, we used Shg::GFP larvae. Subsequently, we performed dissection and conducted immunostaining for both tubulin and Shot. The results clearly displayed a distinct localization pattern near the LAJs in ML3 and WL3 (**Figure 4-4Ci'-ii'**). (This localization was also showed in the zoomed images from the ROIs taken from **Figure 4-4Ci'-ii'**, indicated by **yellow arrow**) This observation aligns with the discussions presented in Chapter 3, where the emergence of LAJC in ML3 and the pericellular belt-like arrangement of LAJC in WL3 were previously highlighted. It is plausible that Shot plays a role in stabilizing these LAJCs during the early establishment of the basal actin cortex in both ML3 and WL3 stages by actin-MT crosslinking. To gain further insights into Shot's role, we knocked down Shot in the trachea using the *btl-gal4 > Ut-ABD-GFP; UAS-Dicer* line. Shot knockdown in the trachea resulted in the loss of actin bundles during WL3. Comparing with the Dicer control at WL3, Shot KD showed only the presence of the junctional cortex, with the actin bundles completely lost (**Figure 4-4Diii**). At 1h APF of Shot RNAi pupa, actin supracellular bundles were absent (**Figure 4-4Div**), and prominent microtubule bundles were present. The presence of MT bundles was significant although the parallel arrangement might be slightly disrupted indicating the importance of MT and actin interaction for supracellular actin cortex stability. (**Figure 4-4Div'**). This highlights the significance of actin-MT crosslinking by Shot, which is critical for upholding the stability of the supracellular actomyosin cortex. MTs play a crucial role in initiating, organizing, and stabilizing the actomyosin cortex in the pupal trachea.

**A****B**

**C****D**

**Figure 4-4. Spectraplaklin Shortstop (shot) crosslinks actin and microtubule and is responsible for this parallel arrangement.**

(A) Images of posterior metameres, tr7/tr8 of the dissected DT of *btl > Ut-ABD-GFP*; immunostained for tubulin and shot. Anterior is to the left, and posterior is to the right. All the images are maximum-intensity projection images. Scale bars indicate 10  $\mu\text{m}$ .

(i)-(iv) shows actin and (ii')-(iv') shows microtubule in ML3 to 1h APF. (i'')-(ii'') In ML3 and WL3 shot was distributed uniformly throughout the cell cytoplasm with occasional perijunctional localization. As pupation commences, MT follows the actin supracellular bundle patterns. In 0h and 1h pupa shot was present on the actin and tubulin bundles, where both these bundles were together. (iii'')-(iv''). This localization can be seen in the zoomed images of the ROI from (iii''). The yellow arrows indicate the shot localization with actin and microtubule parallel bundles.

(B) Scattered plot showing the colocalization of Actin-Shot, and Shot-MT. The plots were generated using a Fiji plugin, "Colocalization Finder," using the 0h APF images of posterior DT cells of the genotype of flies described in (A).

(C) Dissected DT of *Shg::GFP* larvae, immunostained for tubulin and shot. Images of posterior metameres of tr7/tr8, anterior to the right and posterior to the left. Images are the maximum intensity projections of the z-stacks. Scale bars indicate 10  $\mu\text{m}$ . (i) and (ii) ZA and LAJ were shown by *Shg::GFP*. Shot was present near LAJs in ML3 and WL3 (i') and (ii'), and in the zoomed insets (yellow arrows).

(D) *btl-gal4 > Ut-ABD-GFP; UAS-Dicer* flies were crossed to UAS-RNAi lines of *Shot*. All the images are from *tr7/tr8* of the dissected trachea immunostained for tubulin and Beta-catenin. Anterior is to the left, and posterior is to the right. Scale bars indicate 10  $\mu$ m.

(i)-(iv) shows actin as indicated by the *Ut-ABD-GFP* channel, and (i')-(iv') shows the MT arrangement in both Dicer control and *Shot* KD (WL3, 1h APF), respectively. (i'')-(iv'') cell boundary is shown by beta catenin.

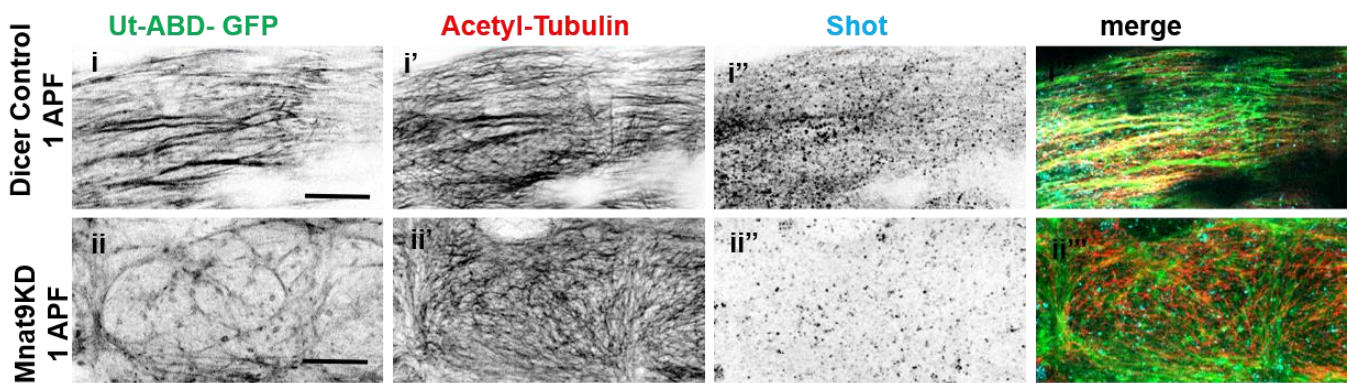


**Figure 4-5. Spectraplaklin Shortstop (*shot*) unable to crosslink actin and microtubule in *Mnat9* KD.**

(A) *btl-gal4 > Ut-ABD-GFP; UAS-Dicer* flies were crossed to UAS-RNAi lines of *Mnat9*. All the images are from *tr7/tr8* of the dissected trachea immunostained for acetylated tubulin and *shot*. Anterior is to the left, and posterior is to the right. For the control images, a single image from z-stacks was used. Scale bars indicate 10  $\mu$ m.

(i)-(ii) shows actin as indicated by the *Ut-ABD-GFP* channel, and (i') -(ii') shows the MT arrangement in both Dicer control and *Mnat9* KD (1h APF), respectively. (i'')-(ii'') shows the *shot* localization. *Shot* binds to stable MT and crosslinks it to actin. In *Mnat9*, KD MT was unstable and disorganized as acetylation properties were compromised (ii'). *Shot* could not

bind to MTs, or the presence of Shot was minimal on MTs in Mnat9KD compared to Dicer control (ii"). Hence crosslinking of actin and MT was diminished (ii'"), thus affecting the supracellular bundle organization, which is shown by the disrupted parallel arrangement of actin in the case of Mnat9KD (ii).

#### **4.2.5 Mnat9a is essential for Shot binding to Actin-Microtubules.**

MTs acquire stability through Mnat9a-mediated N-terminal acetylation. In a recent study by (Ricolo & Araujo, 2020) , it was shown that during tracheal terminal cell lumen formation, actin is present at the growing tip of the terminal cell. Furthermore, they demonstrated that during de novo lumen development, both acetylated tubulin and Shot are deposited before the subcellular lumen. This suggests that for the actin-MT interaction, Shot binds to acetylated MTs.

We examined Shot localization in Mnat9 KD DT cells. Surprisingly, we observed no specific Shot localization on the MT and Actin bundles in 1h APF. However, in the Dicer control 1h APF cells, we clearly observed the parallel bundling of actin and MTs (**Figure 4-5i-i'**) with Shot localized on the bundles (**Figure 4-5i-i''**). In contrast, in Mnat9KD cells, the parallel arrangement of MT and actin supracellular bundles were absent (**Figure 4-5ii-ii'**), and Shot was absent from the bundles (**Figure 4-5ii-ii''**).

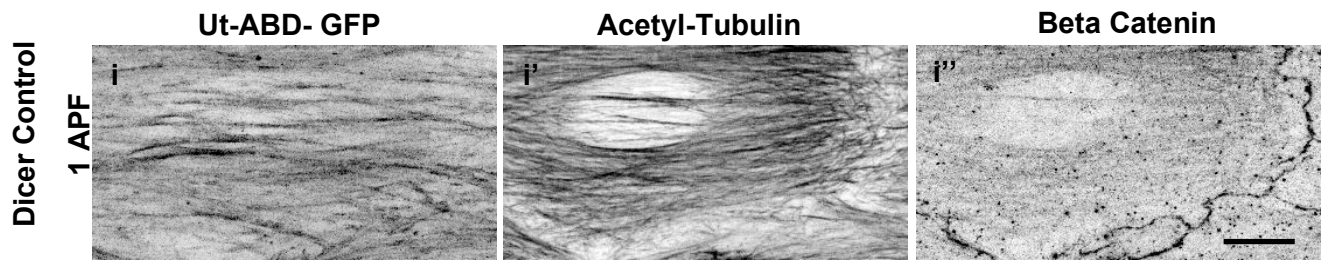
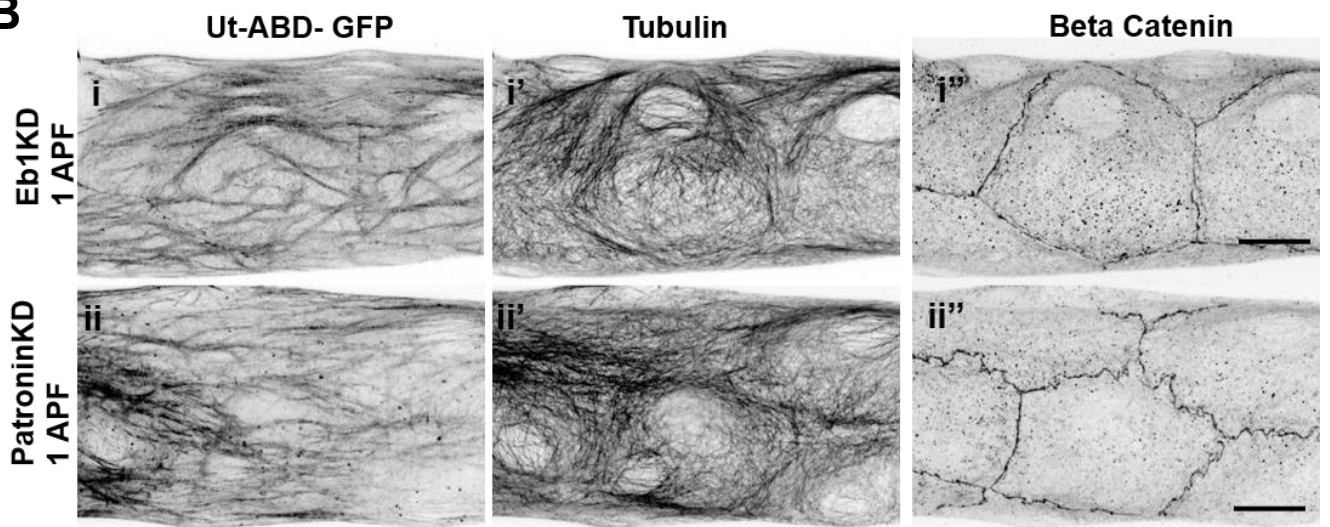
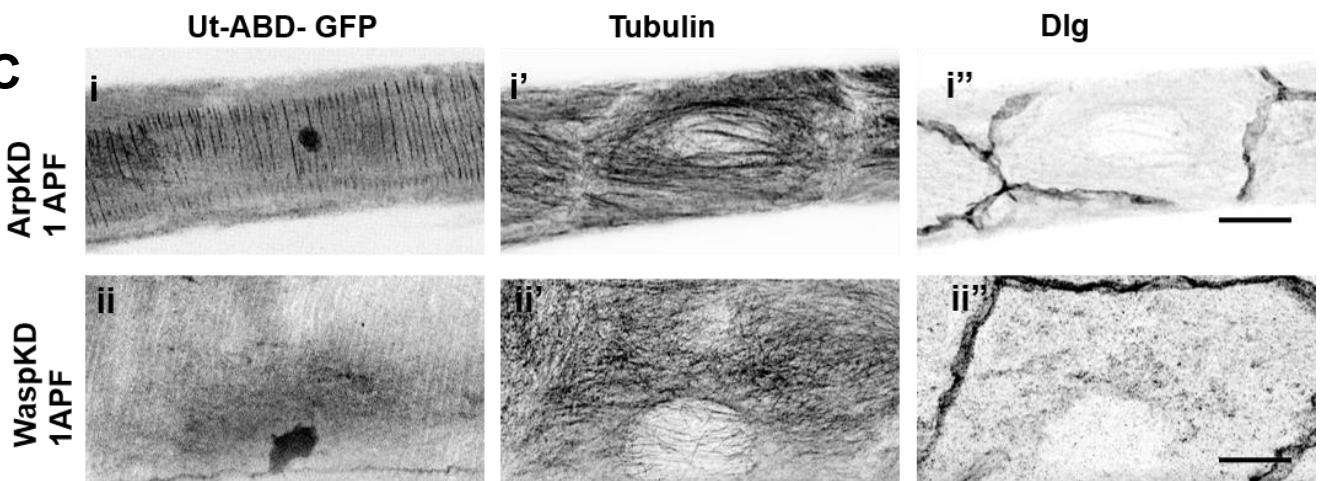
These findings describe the pivotal significance of Mnat9-mediated MT acetylation in upholding MT stability and promoting effective Shot binding. Further, it also reveals that MTs serve as precursors to actin organization, and in the absence of MT and actin intercommunication, the integrity of the supracellular actin cortex was significantly compromised or lost. Furthermore, our results suggest that Shot is crucial in facilitating MT-actin interactions, whereas Mnat9 indirectly regulates the intricate interplay between actin and microtubules.

#### 4.2.6 Microtubules stabilize actin supracellular cortex in *Drosophila* pupal DT.

We further explored the relationship between microtubules (MT) and the actin cortex in early pupal trachea, with a focus on the posterior DT cells. To gain a better understanding, we conducted knockdown experiments targeting microtubule end binding proteins, which play a crucial role in MT stability and function. Specifically, we knocked down Eb1, a plus end binding protein, and Patronin, a minus end binding protein, in *Drosophila* trachea.

Our observations revealed that the knockdown of Patronin and Eb1 resulted in irregular MT patterns in 1h APF DT cells (**Figure 4-6Bi'-ii'**). In this case both MTs and actin were affected compared to the control image (**Figure 4-6Ai-i'**). Notably, the organization and orientation of MTs were significantly impacted, which could be attributed to the direct effects of Patronin and EB1 on MT stabilization and organization. However, the actin cortex experienced notable changes, including alterations in bundle density, frequency, and possibly orientation, in cells where Eb1 and Patronin were knocked down. **Figure 4-6Bi-ii**. Additionally, to understand more about the MTs and supracellular actin cortex behaviour, we conducted knockdown experiments of actin organizers Wasp and Arp2/3 in tracheal cells. In this case, we observed a loss of the supracellular actin cortex in 1h pupa (**Figure 4-6Ci-ii**), while the microtubules showed an irregular to parallel arrangement (**Figure 4-6Ci'-ii'**). These observations further support the idea that MT mesh can form in the absence of actin bundles.

These findings suggest that the influence of actin bundles on MT organization is minimal. The data from Arp 2/3 and WASP KD experiments clearly demonstrate that MTs can still organize effectively even in the complete absence of the actin supracellular cortex. However, the slightly disrupted MT cortex in these cases implies that feedback input from the actin cortex, which might be necessary for maintaining the ongoing stability of the underlying MT structure.

**A****B****C**

### **Figure 4-6. MTs stabilize the actin supracellular cortex**

Btl-gal4 > Ut-ABD-GFP; UAS-Dicer flies were crossed to UAS-RNAi lines of Eb1, Patronin, Arp 2/3 and Wasp. All the images are from tr7/tr8 of the dissected trachea immunostained for tubulin and Dlg. Dlg was used to visualize the cell boundary. Anterior is to the left, and posterior is to the right. Scale bars indicate 10  $\mu$ m.

(A) Dicer control image of 1h pupal DT cells showing actin and MTs arrangement. Actin and MT both showed parallel alignment to the tube axis (i) and (i').

(B) KD of microtubule end binding proteins Eb1 and Patronin slightly affects the actin supracellular bundle thickness and orientation. (i) and (ii). MT arrangement in the posterior cells was affected (i') and (ii').

(C) In Arp2/3 and Wasp KD, actin supracellular bundles were absent (i) and (ii), but microtubules partially achieved parallel pattern, (i') and (ii'), compared to the control image

### **4.3 Discussion**

Our study revealed the formation of a basal mesh of microtubules in the posterior pupal trachea. These basal MT bundles were present at the basal edge of the Dlg domain. The behavior and positioning of these microtubules were further studied, and we found that they undergo a transition from an irregular mesh to parallel bundles aligned with the DT axis during the early pupal stage. In ML3 and WL3 the microtubules appeared as an irregular mesh distributed throughout the cytoplasm, while in 0h and 1h APF, they adopted a parallel arrangement. In WL3 we can see a more aligned and structured MT mesh compared to the ML3 and there could be underlying parallel bundles initiating and supporting the supracellular actomyosin cortex. This parallel alignment, observed in 0h and 1h APF, was mainly basal and closely associated with the basal edge of the Dlg spread. But medial and apical microtubules were also present,

but we looked in to mostly the basal MTs. These findings demonstrate that MTs also undergo a progressive organizational process, leading to the development of parallel cables akin to actin. However, a subtle temporal difference between these processes persists, posing a challenge for complete clarification at this stage. The alignment of MTs and organisation of parallel supracellular actin cortex are two separate, dependent yet concurrent events.

Mnat9a, the microtubule N-acetyl transferase, is crucial for microtubule stability through N-terminal acetylation (Mok & Choi, 2021). Our research showed that Mnat9a plays a significant role in stabilizing microtubules, leading to their acetylation and enhanced stability. Moreover, Mnat9a indirectly influences Shot binding to MTs. Shot, a spectraplakins protein, has been identified as a mediator of actin-MT crosstalk (Ricolo, Castro-Ribera, & Araújo, 2021). Our data indicated that Shot colocalized with both actin and tubulin bundles in the 0h APF stage, suggesting its role in crosslinking actin and MT bundles. Knockdown of Mnat9a resulted in the loss of Shot localization on the MT and actin bundles, emphasizing the importance of Mnat9a-mediated MT acetylation for Shot binding. These findings highlight the critical role of Mnat9a in MT stability and its indirect regulation of actin-microtubule interactions. This is the first study to report a novel role of Mnat9a in DT cells of *Drosophila* trachea.

The disruption of MTs has a more substantial impact on the organization of the supracellular actin than the converse. In Shot, Mnat, Wasp, and ARP KDs, it's evident that disturbing MTs significantly influences the arrangement of the supracellular actin, more so than the disruption of actin affects MT organization. In the case of Patronin and EB1 knockdowns, both MTs and actin display effects. When compared to the Dicer control, it's apparent that actin bundles exhibit a distinct phenotype in these KDs. While MTs are also more affected in these cases than in other knockdowns, this could be attributed to the direct effects of Patronin and EB1 on MTs and MT organization as they bind to MT ends. Overall, these

findings strongly indicate that MT organization takes precedence over actin organization. MTs influence the bundling, alignment, and orientation within the actin cortex. Quantifying the significance of each effect proves challenging. It's highly plausible that multiple cues from MTs to actin exist, and the various knockdowns differentially impact these cues, contributing to the pleiotropic phenotype observed. Importantly, these experiments do not solely establish MTs as the exclusive cues; multiple signals likely contribute to instructing the organization of the actin supracellular structure. However, the influence of actin bundles on MT organization is minimal. Data from Arp and WASP knockdowns demonstrate that MTs can effectively organize even in the total absence of the supracellular actin cortex. The slightly disrupted MT cortex in these cases suggests that feedback input from the actin cortex might be necessary to maintain the ongoing stability of the underlying MT structure.

In conclusion, this study sheds light on the microtubules and actin crosstalk in the posterior pupal trachea during early pupal development. The formation of a basal mesh of microtubules and their subsequent parallel alignment along with the establishment of actin supracellular cables were stabilized by crosslinking which was regulated by Shot. The crucial role of Mnat9a in MT stability and Shot binding to actin-MT bundles was also demonstrated. Furthermore, our knockdown experiments revealed that MT is more critical for actin organization. MT organization is upstream of actin organization. MTs appear to impact the bundling, alignment, and orientation within the actin cortex, confirming their role as one of several signals guiding actin organization. Moreover, it's possible that feedback from the actin cortex is required to maintain the ongoing stability of the underlying MT structure. This research contributes to our understanding of the complex cytoskeletal dynamics involved during the degeneration of the posterior pupal trachea in *Drosophila melanogaster*.

**CHAPTER 5**

**BASAL EXTRACELLULAR MATRIX REMODELS IN**

***DROSOPHILA* PUPAL TRACHEA**

## 5.1 Introduction

The extracellular matrix (ECM) is an integral part of the epithelium, essential in epithelial transition into functional shapes during development. In metazoans, the cells are arranged on top of the ECM and interact with each other to execute certain events. ECM accounts for a sizable portion of the metazoans' body mass. Proteoglycans, glycosaminoglycans, collagens, and non-collagenous glycoproteins are a few of the many families of molecules that make up the ECM. ECM molecules define tissue borders, modulate the accessibility of extracellular signals, support and anchor cells physically, and directly mediate intercellular communication (Broadie, Baumgartner, & Prokop, 2011). ECM provides the physical and biochemical scaffold to the cells in an epithelium. In holometabolous insects like *Drosophila melanogaster*, ECM is rather specialized (Isabella & Horne-Badovinac, 2015).

In *Drosophila*, two types of ECM can be found, specialized apical ECM (aECM) and basal ECM (bECM) or basement membrane. In *Drosophila*, aECMs perform critical functions in the physiology, development, and patterning of tissues and organs, shielding the organism from physical and chemical harm, infection, and dehydration. In *Drosophila*, the aECM is secreted by tracheal epithelium, hindgut and foregut epithelia. The epidermis also secretes a special aECM called cuticle. During embryonic and larval molting events and metamorphosis, this aECM is shed off and renewed to make space for growth and morphological changes to the body and organs. The insect epidermal cuticle comprises chitin, chitin-binding proteins, chitin-modifying enzymes, etc. The epidermal cuticle is composed of three layers: the outermost envelope, the innermost chitinous procuticle, and in the middle is, the epicuticle, which is rich in proteins (Locke, 2001; Moussian, 2010; Öztürk-Çolak, Moussian, & Araújo, 2016). Chitin-binding proteins have been hypothesized to be required for chitin organization and are encoded by various genes that vary across species. It has recently been found that the putative chitin-binding protein Obstructor-A (ObstA) drives the chitin

deacetylases Vermiform (Verm), Serpentine (Serp), and Knick kopf (Knk) to the extracellular space located adjacent to the apical plasma membrane for chitin organization (Hayashi & Kondo, 2018; Pesch, Riedel, & Behr, 2015; Öztürk-Çolak, Moussian, & Araújo, 2016). However, the cuticle architecture of the *Drosophila* trachea is very different from the cuticle of the rest of the organs. The tracheal cuticle spirals perpendicular to the tube axis,(G. & A, 1993; Hayashi & Kondo, 2018) and are known as taenidia. A very thin epicuticle can be found below the envelope. There is no discernible ordered texture on the chitinous procuticle. The cuticle ridges formed by intracellular actin rings formed by tracheal cells suggest cellular rather than mechanical patterning of taenidia. This finding suggests that tracheal cells actively contribute to the initiation, development, and overall organization of taenidia (Matusek et al., 2006; Öztürk-Çolak, Moussian, & Araújo, 2016; Öztürk-Çolak, Moussian, Araújo, et al., 2016).

In metazoans, the basal ECM is one of the most studied ECM (Davis, Horne-Badovinac, & Naba, 2019). The basal ECM or basement membrane (BM) is a specialized matrix that associates with the basal surfaces of epithelial tissues and endothelium, muscle, and other neural cells (Ozbek, Balasubramanian, Chiquet-Ehrismann, Tucker, & Adams, 2010). In an epithelia, the bECM is principally made up of two distinct web-like networks of Type IV Collagen (Collagen IV) and Laminin, which are strongly connected by proteins including Nidogen and the heparan sulfate proteoglycan (HSPG) Perlecan (Isabella & Horne-Badovinac, 2015). In insects, the bECM proteins are secreted by fat bodies and haemocytes and targeted to golgi for post-translational modification. After post-translational modification, these proteins are targeted to the bECM via secretory pathways (Isabella & Horne-Badovinac, 2015). ECM interacts with the intracellular environment via transmembrane proteins. Integrins are the primary transmembrane proteins of the basal membrane of an epithelium that interact with the RGD domain of collagen and laminin in a physical manner. Integrins, which form dimers of the subunits and communicate through intracellular effectors,

bind to BM proteins. It is evident that altering bECM structure or composition can significantly affect cell behavior by influencing the structure and function of integrins (Dai et al., 2018; Keeley et al., 2020). Integrins interact with the cellular microenvironment, especially the actin cytoskeleton, via its intracellular effector protein talin. Vinculin also plays an important role in talin binding to the F-actin bundles. The pseudokinase integrin-linked kinase (ILK), is an effector of integrins that helps it interacts with microtubules (Barrera-Velázquez & Ríos-Barrera, 2021).

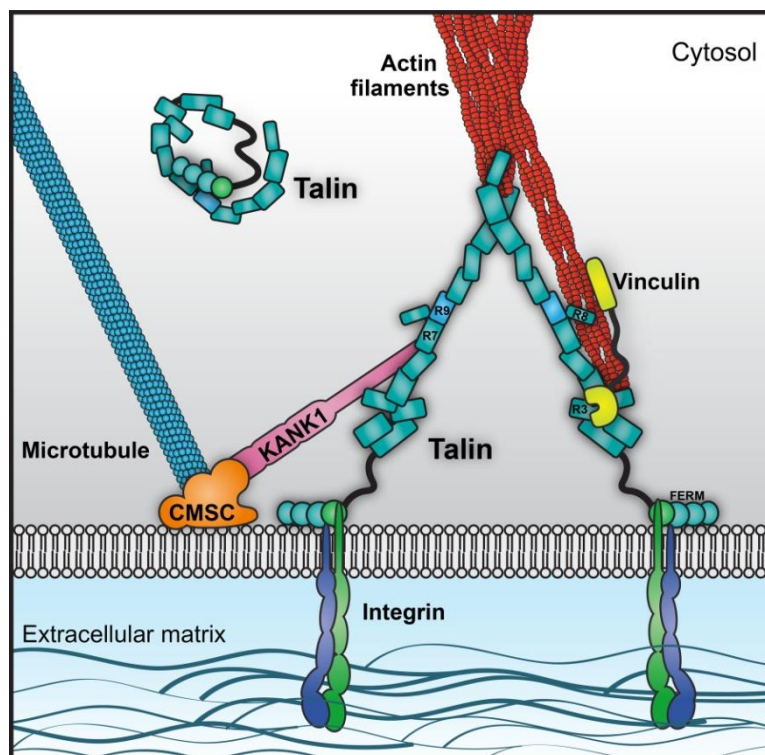


**Figure 5-1. Schematic showing the interaction of Integrin receptor complexes with ECM proteins** Model showing basal ECM interacts with the actin cytoskeleton via integrin and its cytosolic adapter protein talin. Image adapted from (Gough & Goult, 2018).

Apical and basal ECM crosstalk is very crucial for many developmental phenomena in *Drosophila melanogaster*. The bECM is important in maintaining the apical polarity and endocytic machinery. The apical ECM remodeling influences the bECM dynamics in many

developmental events. In the *Drosophila* trachea, de novo lumen formation depends on apical and basal membrane cross-talk. Coordination between the apical and basal membranes is crucial for establishing lumen in subcellular tubes. The absence of a proper apicobasal interaction enables the two membrane compartments to grow independently, which prevents the formation of a lumen in subcellular tubes or causes them to form improperly (JayaNandanan et al., 2014; Mathew et al., 2020). Actin and MTs must interact for synchronized growth of the apical and basal membranes. Actin is arranged into various networks throughout the cell and MTs link these actin networks to regulate this growth (Gervais & Casanova, 2010; JayaNandanan et al., 2014). Actin interacts with integrins and talin, probably bridging the gap between the basal plasma membrane and the cell cytoskeleton (Levi et al., 2006). In the wing disc epithelium of the *Drosophila* larva, acute cytoskeletal remodeling ensures the cell shape change from cuboidal to cylindrical. Whereas in pupa, wing disc eversion necessitates switching to cuboidal from columnar shape along with a convergent extension to facilitate wing elongation. This is accomplished through the coordinated secretion of Matrix Metalloprotease 2 (MMP2) which remodels bECM, and Stubble (Sb), a protease that remodels the aECM (Diaz-de-la-Loza et al., 2018; Robert P Ray et al., 2018; R. P. Ray et al., 2015). Similarly, in tracheal DT, aECM remodeling rearranges the actin cytoskeleton, which links apical extracellular matrix remodeling and cell shape changes (Dong, Hannezo, & Hayashi, 2014; Kato et al., 2016; Öztürk-Çolak, Moussian, Araújo, et al., 2016).

The Matrix Metalloprotease 1 (MMP1) is a key player in the remodeling of the extracellular matrix (ECM), which shortens the tracheal DT and changes the shape of pupal cells, according to recent findings by (Fraire-Zamora et al., 2021). This study also reported that no changes in the basement membrane happened from WL3 to 9 h APF as observed using a GFP-tagged form of the *Drosophila* collagen IV protein (Viking) (Viking::GFP). These findings suggested that collagen is not degraded during the initial shortening phase of the dorsal

trunks. This deduction was drawn from the results of a time-course experiment (depicted in the **Figure 5-2**), where they assessed the thickness of the basal extracellular matrix (bECM) using z stacks of the tracheal dorsal trunks. They concluded that bECM remains intact during the initial shortening phase of the dorsal trunks. Although these images offered a comprehensive view of the entire tracheal tube, they did not reveal subtle subcellular changes in the basal membrane, integrins, or basal extracellular matrix reporter proteins.

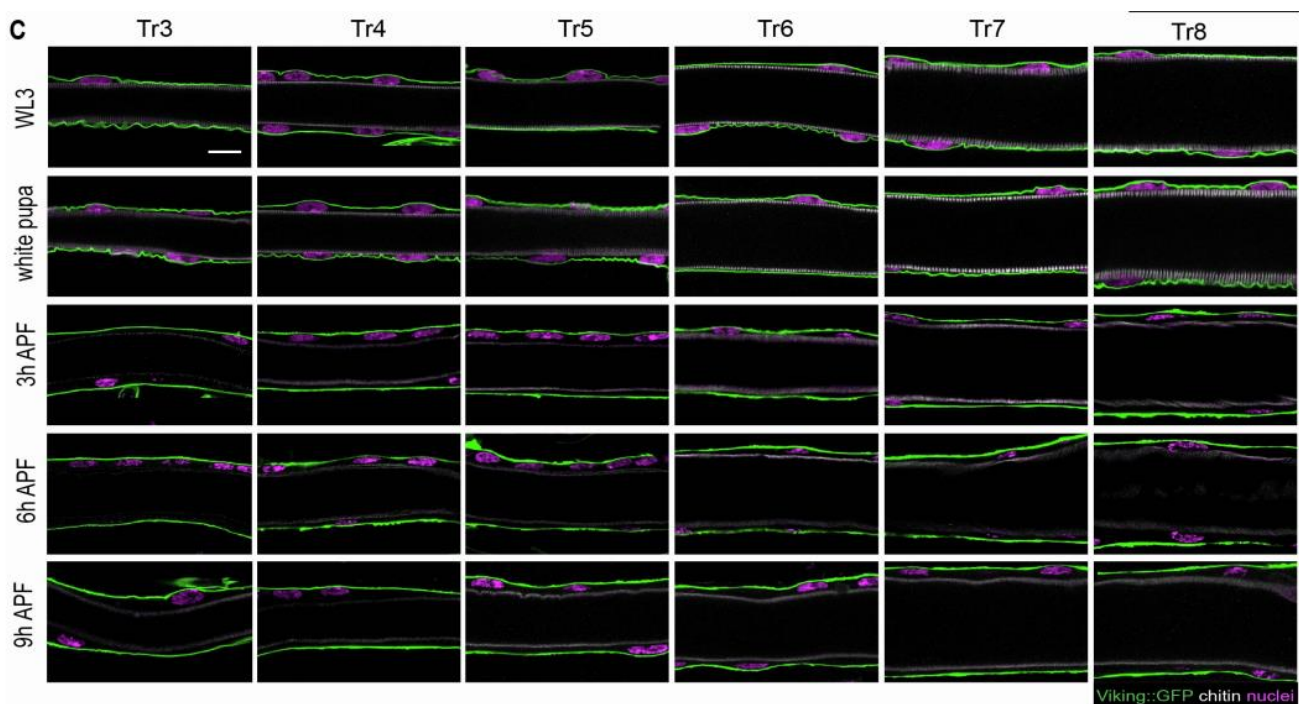


**Figure 5-2. Image showing the basal ECM and apical ECM during larval to pupal transition** Dorsal trunk images showing the tube cross-section pulled out from a z-stack. Viking GFP reporter was used to visualize the basal ECM. There is no change in the bECM thickness from WL3 to 9h APF pupa. Image adapted from (Fraire-Zamora et al., 2021).

Crosstalk between the apical and basal ECM is paramount for developmental events. Nevertheless, the mechanisms through which morphogenetic forces are transferred between the two cellular domains and how apical remodeling is mechanically connected to the basal ECM remain unclear. Initial investigations have underscored the significance of apicobasal crosstalk and coordination during morphogenesis, but the subcellular effectors and the underlying mechanisms governing this cross-talk may vary across different systems. No information is available at the subcellular scale regarding these mechanisms during the tracheal tube shortening process. Our research has demonstrated that LAJ-associated basal F-actin bundles play a role in the tracheal tube shortening process. The bundles contribute to the slope of the shortening kinetics although their contribution is redundant compared to the ECM-mediated compression mechanism with respect to the final magnitude of shortening (Rojalin Pradhan et al., 2023), as explained in Chapter 3 of this thesis. We hypothesized that the dynamic aECM changes and cytoskeletal remodeling during tracheal tube degeneration would have concomitant alternations in the bECM, and this chapter elaborates our investigations in that direction.

## **5.2 Results**

### **5.2.1 Basal ECM remodeling in *Drosophila* posterior pupal DT**

We investigated the larval and pupal basal ECM during tracheal tube degeneration using Viking::*GFP* protein trap, which is a widely used reporter line (Haigo & Bilder, 2011; Pastor-Pareja & Xu, 2011). While examining the mid-L3 (ML3) stage larvae, we found that bECM had a relatively homogeneous and velvety appearance in the posterior DT (**Figure 5-3i**). UAS-Lifeact-Ruby reporter line driven by *btl-Gal4* was used for visualization of actin. Larvae and pupae expressing Vkg::*GFP* and trachea specific lifeact ruby were dissected and stained for Dlg. To ensure a standardized data set consistent with the cytoskeletal events described in the

previous chapters, we employed the lifeact ruby reporter line as a representative of developmental events. This approach allowed us to compare ECM dynamics with other cytoskeletal phenomena effectively at corresponding developmental phases. In WL3, the basal ECM exhibits a rougher appearance, and by the 1hour pupal stage, it acquires a sheared appearance (**Figure 5-3ii-iii**). The basal ECM in the 1-hour pupa exhibited a highly irregular, disoriented, and sheared phenotype, suggesting an ongoing remodeling process. According to the data from (Fraire-Zamora et al., 2021) the thickness of the basal ECM remains constant during pupation until 9 hours after puparium formation (APF), ruling out the possibility of delamination. It is likely that the basal actin cables are exerting some force, leading to the shearing remodeling observed in the basal ECM.

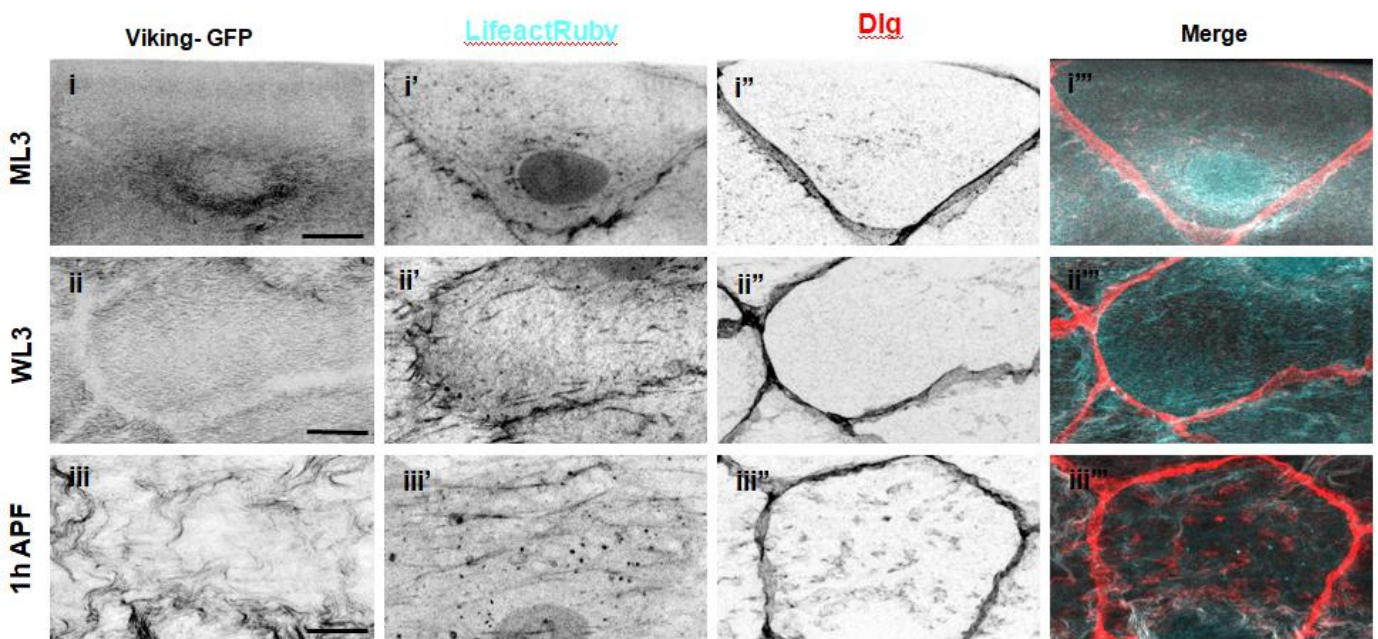


**Figure 5-3. Basal ECM remodels in the posterior pupal dorsal trunk**

Images from the posterior metameres, tr7/tr8 of the DT of *btl > Lifeact-Ruby; Vkg::GFP* larvae immune-stained for Dlg. The Anterior is to the left, and the posterior is to the right. Scale bar is 10  $\mu$ m. *Vkg::GFP* was used to visualize basal ECM and Lifeact ruby for F-actin.

The bECM appeared velvety in mid-L3 larva (i) and junctional actin was prominent (i'). Around nucleus bECM was more irregular. Lifeact Ruby and Dlg was used for visualization of actin and cell boundary. In WL3, bECM became rougher than ML3 (ii) and actin fibers started emanating from LAJ (ii'). In 1h pupa, the bECM was more irregular and disintegrated (iii) and at the same time supracellular bundles appeared (iii').

## 5.2.2 Remodeling of basal Extracellular Matrix starts around the cell boundary in ML3

During our investigation of the ML3 larval stages, we observed the initiation of bECM remodeling events from ML3 onwards. As we delved deeper into the role of LAJ in these remodeling events, we made an intriguing discovery: the bECM degenerative phenotype originated from the cell boundary, near the LAJ, in ML3 (**Figure 5-4i**). Subsequently, bECM degeneration spread throughout the cells after the ML3 stage (**Figure 5-4ii**). This finding led us to consider the possibility that LAJ and associated actin cortex might play a role in mediating bECM remodeling during ML3. Given that LAJ-associated LAJC supports the formation of basal supracellular actin cables, we suspected a potential relationship between these two events. Consequently, we decided to explore the connection between LAJ associated basal actin cortex, and bECM remodeling aiming to unravel the relationship between these processes.

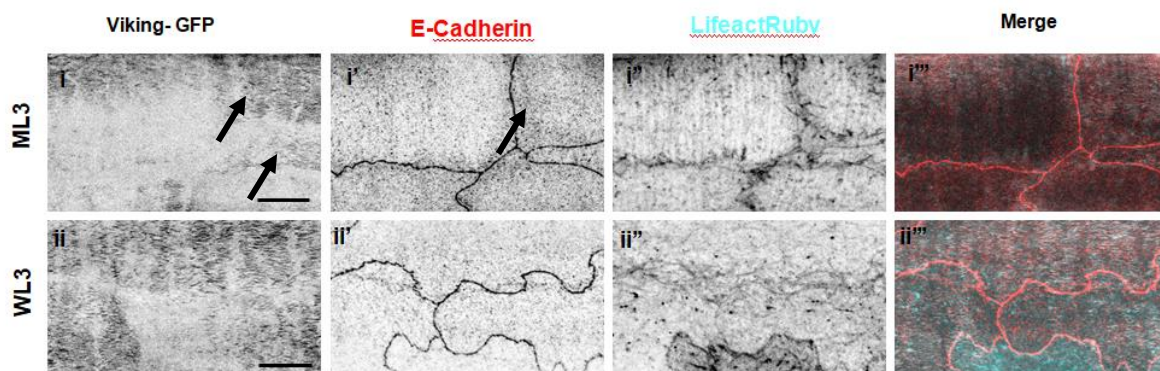


### **Figure 5-4. Basal ECM remodeling starts around LAJ in ML3**

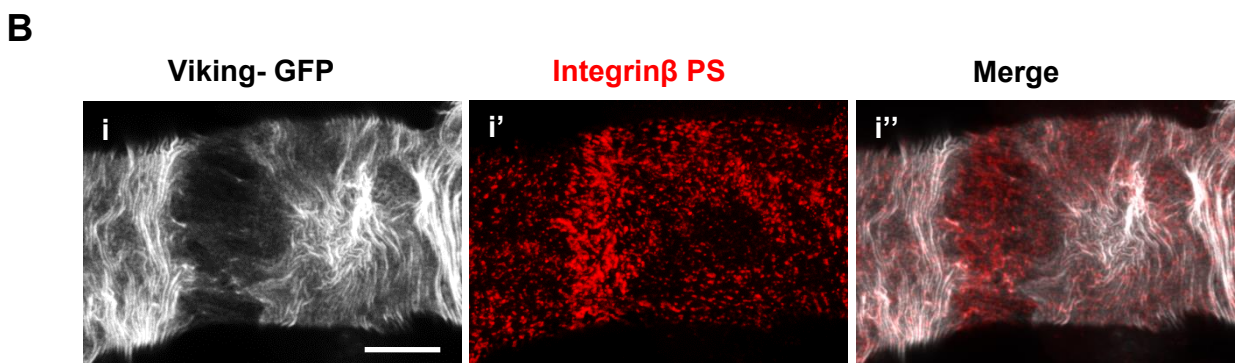
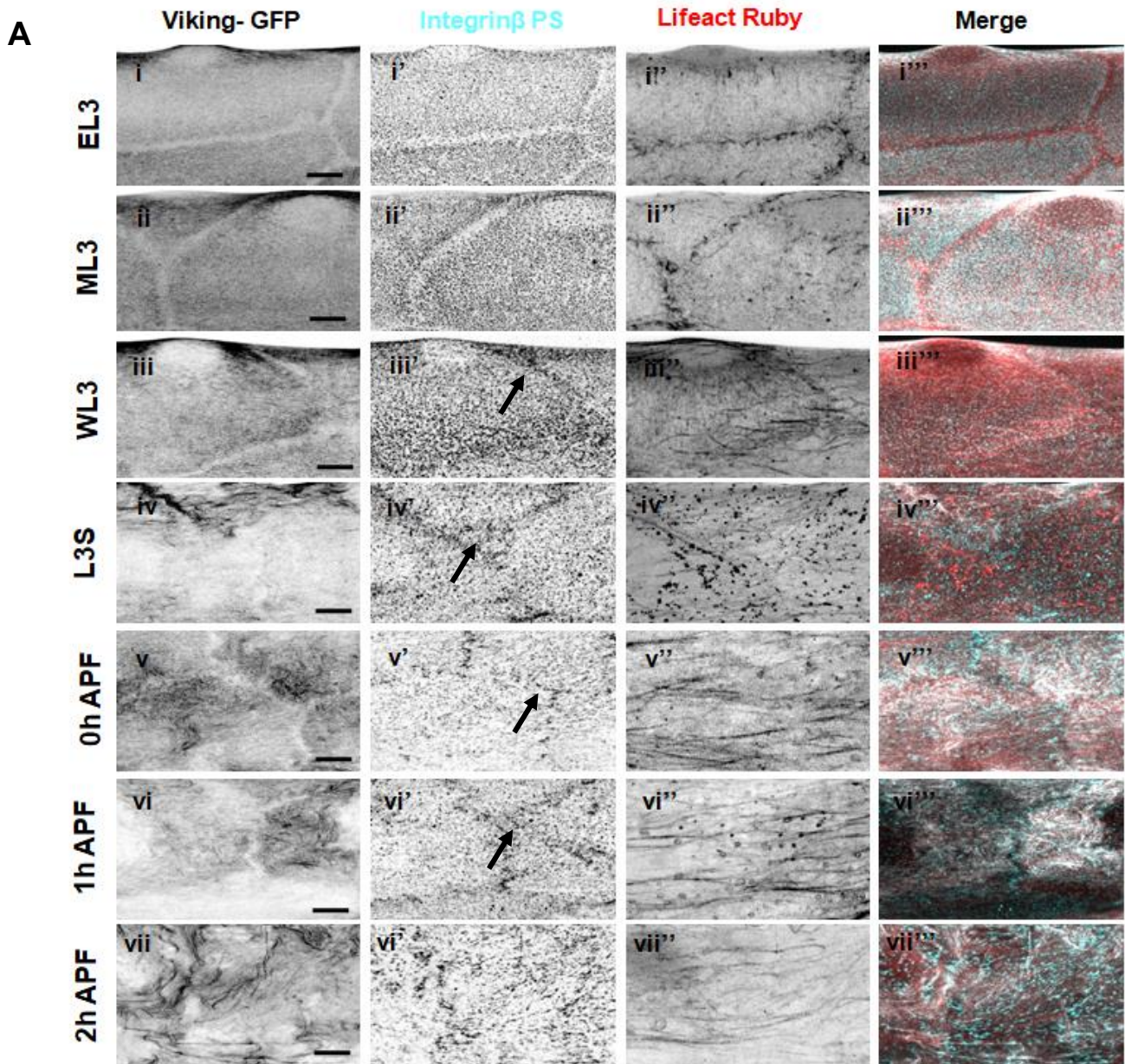
Images from the posterior metameres, tr7/tr8 of the DT of *Vkg::GFP; btl> Lifeact-Ruby* immunostained for E-Cadherin. The Anterior is to the left, and the posterior is to the right. Scale bar is 10  $\mu\text{m}$ .

(i) In ML3 the bECM remodelling starts from the cell periphery near LAJC(i'), indicated by black arrow head. In WL3, bECM become more irregular throughout the basal surface (ii).

### **5.2.3 Basal ECM remodeling and supracellular actin bundle formation follow the same developmental window**

To establish a correlation between the basal supracellular actin bundling and the basal ECM remodeling, we decided to expand our study. Conducting a time-course experiment, we examined bECM phenotypes from EL3 to 2h APF in early pupa. As mentioned in the introduction, integrins are crucial receptors in the basal membrane, playing a significant role in cell and bECM interaction. Previous reports have highlighted that changes in the basement membrane can impact integrin function, leading to severe cellular defects. Consequently, we utilized integrins as an additional marker to identify degenerative changes in the bECM. Our hypothesis was that alterations in the bECM must influence the patterns of integrins (Crest, Diz-Munoz, Chen, Fletcher, & Bilder, 2017; Dai et al., 2018; Hollfelder). We decided to look at myospheroid (integrin  $\beta\text{PS}$ ) the expression of which has been previously characterized in trachea. It was already showed by (Levi et al., 2006) that talin and integrin mutants show tracheal terminal branching defects. We commenced our investigation from EL3 to gain a deeper understanding of the bECM phenotype. In EL3, the bECM exhibited a smooth and uniform appearance (**Figure 5-5Ai**), while actin appeared junctional, consistent with the EL3 actin phenotype described in Chapter-3 (**Figure 5-5Ai''**). Integrins displayed a regular and

uniform distribution throughout the basal membrane, except at the cell periphery (**Figure 5-5Ai'**). In ML3, the bECM transitioned to a velvety appearance as actin emanated from the LAJ (**Figure 5-5Aii**). However, the integrin phenotype remained unchanged. Degenerative bECM phenotypes were initiated from the ML3 stage. In WL3 and L3S, the bECM became increasingly irregular as basal actin bundling commenced, as shown in (**Figure 5-5Aiii-iv**) and (**Figure 5-5Aiii''-iv''**). Integrins began adopting a punctate pattern and appeared at the cell periphery (**Figure 5-5Aiii'-iv'**, **arrowhead**). As pupation commenced, from 0h to 2h pupa, the bECM exhibited a more degenerated and sheared appearance (**Figure 5-5Av-vii**), while Integrins displayed an increasingly punctate and irregular distribution (**Figure 5-5Av'-vii'**). During the transition from 0h pupa to 2h pupa, supracellular actin cables started forming (**Figure 5-5Av''-vii''**), eventually maturing into mechanically active stress fibers by the 2h pupal stage. The bECM showed greater disorientation in the 2h pupa, suggesting significant forces exerted on the basal membrane, which likely accounted for their impact on both Integrins and the basal ECM. As we already shown that these stressfibres were basal in nature and were present closer to the basal membrane (**see Chapter-3, Figure 3-1L, 3-2C**). After 3h APF bECM was highly degenerated and integrin showed irregular patterns in posterior DT (**Figure 5-5Bi-ii**). We used shg-GFP to visualize LAJ in ML3 to 1h pupa and found that integrin accumulated near the pericellular space at LAJ from WL3 on wards till 1h APF (**Figure 5-5Cii-iii arrow head**), whereas absent in ML3 (**Figure 5-5Ci**). It would be intriguing to investigate and unravel the underlying mechanism behind the observed behavior of integrins in response to basal ECM remodeling.



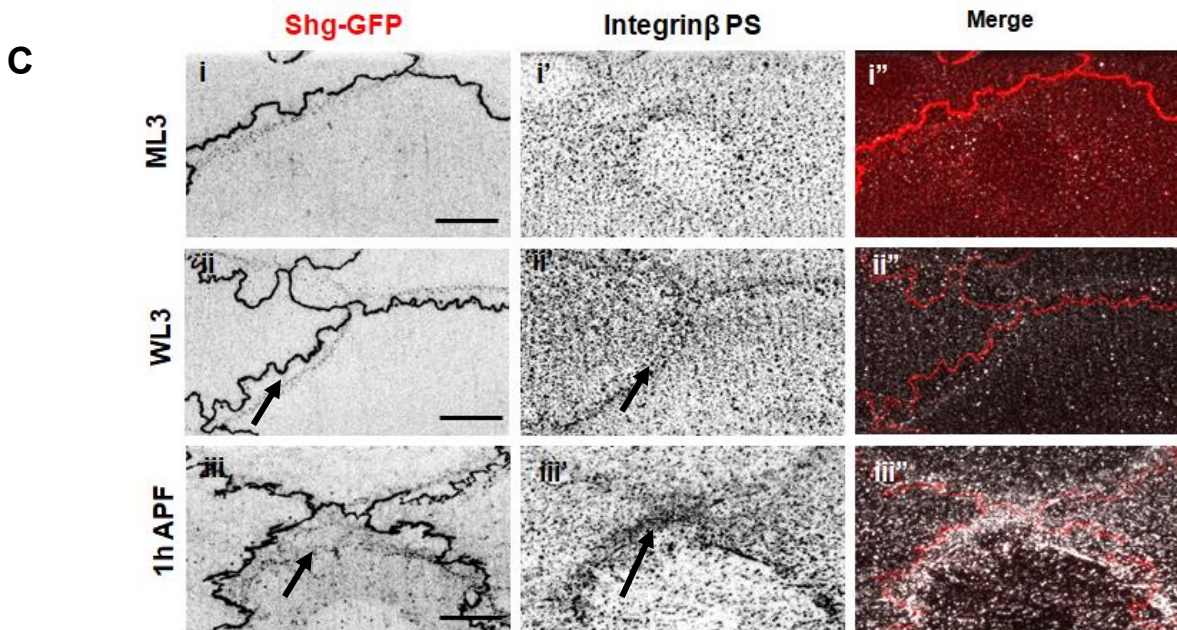


**Figure 5-5. Basal ECM remodeling coincides with the actin dynamics in the early pupal trachea.**

Images from the posterior metameres, tr7/tr8 of the DT of Vkg::GFP; btl> Lifect-Ruby immunostained for integrin. The Anterior is to the left, and the posterior is to the right. Scale bar is 10  $\mu$ m. bECM was visualized by Vkg::GFP, and actin by Lifesct-Ruby.

(A) (i)-(vii) bECM phenotype from EL3 to 2h APF respectively. EL3 bECM was smooth which gradually become irregular and highly sheared in 2h pupa.

(i') Integrin showed uniform spread and absent from cell boundary in EL3 and ML3. In WL3, L3S, 0h and 1h APF integrin became punctate and accumulated near the cell boundary (iii'-vi'). Junctional localization was shown by black arrow heads.

(B) bECM was highly degenerated in 3h pupa (i) and integrin showed abnormal highly irregular patterns (i').

(C) (i)-(iii) ML3, WL3 and 1h APF posterior tracheal DT cells showing LAJ. Shg::GFP was used for visualization of LAJs. (i') Integrin was absent near LAJs in ML3 but in WL3 and 1h APF integrin accumulation was observed at LAJs (ii'-iii'). Integrin also became more irregular and punctate.

### 5.3 Discussion

This study provides the first evidence of severe bECM remodeling during the acute tube compression phase in the *Drosophila* pupal trachea. While bECM remodeling is known to be integral to various developmental events, such as dorsal closure and pupal wing disc eversion (Barrera-Velázquez & Ríos-Barrera, 2021; Diaz-de-la-Loza et al., 2018), the unique nature of the observed bECM remodeling in this study sets it apart. Notably, the bECM thickness remains unchanged during this phase (Fraire-Zamora et al., 2021), ruling out the possibility of delamination, and the remodeling occurs specifically on the basal surface. The study also reveals a striking correlation between the actin bundling events at the lateral adherens junctions (LAJ) and the bECM remodeling. Both these events are occurring within the same time frame. This suggests a potential contribution of these processes to the tube compression phenomenon. Previous studies by (Fraire-Zamora et al., 2021) have demonstrated the involvement of MMP1-mediated apical ECM (aECM) remodeling in driving dorsal trunk (DT) compression and (Rojalin Pradhan et al., 2023) demonstrated that the supracellular cables redundantly contributing to these events. It is well-reviewed by (Barrera-Velázquez & Ríos-Barrera, 2021) that the apical and basal ECM are connected via microtubules and actin cytoskeleton through talin-integrin complexes, emphasizing the importance of apical and basal cross-talk during development and morphogenesis. The relationship between aECM and bECM remodeling has been shown previously in wing morphogenesis during pupal stages, but the exact order of these remodeling events was not clearly elucidated (Diaz-de-la-Loza et al., 2018). The data from this

study demonstrate that bECM remodeling initiates in ML3, concurrent with the establishment of LAJ cortex, while aECM remodeling occurs during early pupal stages. Investigating the regulation and timing of these events could provide valuable insights into the underlying mechanisms governing these processes and the reasons for their temporal differences. The role of integrins in this context remains mysterious, and studying the pericellular localization of integrins and their relationship with LAJ could prove to be a captivating subject for further research. It is worth mentioning that the study focused solely on the posterior segments, and exploring the anterior segments could provide a comprehensive understanding of this phenomenon. In conclusion, this study sheds light on the dynamic behavior of the basal ECM and integrins during tracheal tube degeneration, offering valuable insights into tissue development and homeostasis. The intriguing correlation between basal ECM remodeling and integrin behavior calls for further investigation to unravel the mechanisms driving these processes and their functional implications in tracheal development. Analyzing this phenomenon in greater detail, along with actin dynamics, could potentially unveil variations in basal ECM and integrin behavior, ultimately contributing to a deeper understanding of the epithelial degenerative event.

**CHAPTER 6**

**CONCLUSION**

The current understanding of epithelial degeneration mechanisms in *Drosophila melanogaster*, including the tracheal system, is largely limited to apoptosis-mediated organ degeneration. In the last decade, the late larval and pupal trachea of *Drosophila* has been interrogated for cellular processes occurring concomitant with the stages of organ degradation in the system. These studies have provided significant insights into various events that accompany organ degradation, including primordial cell migration, posterior tracheal cell replacement, pupal abdominal trachea (PAT) formation, air sac development, apoptosis-mediated larval cell death, anterior tracheal retention, and hormone-driven tracheal tube shortening through aECM remodeling (F. Chen & Krasnow, 2014; Fraire-Zamora et al., 2021; Weaver & Krasnow, 2008). Despite these valuable contributions, the sub-cellular processes that take place during these stages and prepare the system for the degeneration and transition remained relatively unexplored. The highly consistent behavior of cells within the anterior and posterior regions of the larval trachea, despite striking differences between the two regions, suggests a high degree of coordination between cellular processes at tissue scale. None of the previous studies have focused on such degenerative changes at the cell and tissue scale, leaving the events preceding cell death largely unexplored.

In this study, we aimed to bridge this knowledge gap and provide crucial data that will contribute to filling the missing pieces of the puzzle. The thesis presents a comprehensive investigation into the degeneration and reorganization of the epithelial tissue during metamorphosis, with a specific focus on the *Drosophila* tracheal system as our model. Our research delved into the degenerative trachea during the larval-to-pupal transition, seeking to identify degenerative phenotypes and focusing on all layers of the tissue, including the epithelium and associated ECM layers. Our studies paid particular attention to the adherens

junctions, cytoskeleton, and extracellular matrix. Detailed findings from this investigation are presented in Chapters 3 to 5 of this thesis.

Chapter 3 describes the identification of a novel non-canonical belt of lateral punctate E-cadherin molecules, referred to as lateral adherens junctions (LAJs), in addition to the classical zonula adherens in the *Drosophila* tracheal epithelium. While LAJ has been identified in in vitro systems and suspected to be present in vivo, this is the first study to conclusively demonstrate the existence of LAJ in vivo. These LAJs encircle the cells in the lateral membrane basal to the zonula adherens and are functionally active with various adherens junction components. LAJs are present below the Dlg domain close to the basal membrane and mediates a basal actin cortex (LAJC). The LAJC further develops into a supracellular actomyosin mesh during the larval-to-pupal transition. Actin organizers, Rho1 and CDC42, regulate the initiation of the basal actin cortex, with the Rho1-ROK-MRLC and CDC42-ARP-WASP pathways playing independent roles in the basal actin cortex formation. This supracellular network is composed of alternating bands of  $\alpha$ -actinin and phospho-myosin, which contributes to force generation and transmission at 2h APF. Stress fibers along the anterior-posterior axis of the dorsal trunk facilitate tissue compression redundantly via aECM remodeling in the early pupal trachea. Chapter 4 describes that microtubules also exhibit a similar pattern of supracellular arrangement, and the spectraplakins protein, Shortstop (Shot), mediates actin-microtubule crosstalk in early pupa. Shot tends to bind to stable acetylated microtubules, and Microtubule-associated N-acetyl transferase 9 (Mnat9) plays a crucial role in microtubule stability, thus affecting shot activity and actomyosin cortex organization. The actin microtubule crosstalk is crucial for stabilizing the supracellular actin cortex. Additionally, the study explored the behavior of the basal extracellular matrix (bECM) component collagen (Viking) and its relationship with the actomyosin cortex. The degeneration of the basal ECM

during pupation coincides with actin-bundling events, suggesting a supportive role of the bECM in this process. These findings are described in Chapter-5.

In conclusion, our study provides insight to a deeper understanding of the dynamic processes involved in tissue degeneration and reorganization during metamorphosis, particularly in the context of the *Drosophila* tracheal system. The findings shed light on the intricate interplay between cellular components, cytoskeletal rearrangements, and extracellular matrix behavior, providing valuable insights into the development and remodeling of epithelial tissues during the metamorphic process. We hope to contribute valuable insights into the intricate mechanisms underlying tissue remodeling during metamorphosis by examining the degeneration process in a comprehensive manner. Our work addresses the subcellular and cellular levels of degenerative changes, shedding light on events that occur before cell death. Moreover, this thesis provides novel insights into the existence and functionality of LAJs in the *Drosophila* tracheal epithelium during larval and pupal stages.

However, further extensive studies are required to fully understand the dependency and interdependency of the actomyosin cortex and microtubule and the physiological importance of actin-MTs cross-talk during DT tube compression. The dynamicity of the actin-MT interaction can be done by live imaging though these experiments will be ex vivo. That can give us further insight into this cross-talk. The ultrastructure of actomyosin cortex and MT and the cross-linkers can be unraveled by super-resolution microscopy. Finally, the ECM degeneration events and their relation with the actomyosin cortex can be solved in the future by functional analysis by RNAi of actin and MT organizers in *Drosophila* trachea.

## **REFERENCES**

- Abe, K., & Takeichi, M. (2008). EPLIN mediates linkage of the cadherin catenin complex to F-actin and stabilizes the circumferential actin belt. *Proc Natl Acad Sci U S A*, *105*(1), 13-19. doi:10.1073/pnas.0710504105
- Affolter, M., & Caussinus, E. (2008). Tracheal branching morphogenesis in *Drosophila*: new insights into cell behaviour and organ architecture. *Development*, *135*(12), 2055-2064. doi:10.1242/dev.014498
- Affolter, M., Montagne, J., Walldorf, U., Groppe, J., Kloter, U., LaRosa, M., & Gehring, W. J. (1994). The *Drosophila* SRF homolog is expressed in a subset of tracheal cells and maps within a genomic region required for tracheal development. *Development*, *120*(4), 743-753. doi:10.1242/dev.120.4.743
- Alberts, B. ((2015)). *Molecular Biology of the Cell (6th ed.)*: W.W. Norton & Company.
- Alberts, B., Johnson, A., Lewis, J., Raff, M., Roberts, K., & Walter, P. (2008). *Molecular biology of the cell*, 5th edn. Garland Science. *New York*.
- Alkemade, C., Wierenga, H., Volkov, V. A., Preciado López, M., Akhmanova, A., ten Wolde, P. R., . . . Koenderink, G. H. (2022). Cross-linkers at growing microtubule ends generate forces that drive actin transport. *Proceedings of the National Academy of Sciences*, *119*(11), e2112799119. doi:doi:10.1073/pnas.2112799119
- Aoki, K., Maeda, F., Nagasako, T., Mochizuki, Y., Uchida, S., & Ikenouchi, J. (2016). A RhoA and Rnd3 cycle regulates actin reassembly during membrane blebbing. *Proceedings of the National Academy of Sciences*, *113*(13), E1863-E1871. doi:doi:10.1073/pnas.1600968113
- Apple juice-agar plates. (2009). *Cold Spring Harbor Protocols*, *2009*(7), pdb.rec11871. doi:10.1101/pdb.rec11871

- Applewhite, D. A., Grode, K. D., Duncan, M. C., & Rogers, S. L. (2013). The actin-microtubule cross-linking activity of *Drosophila* Short stop is regulated by intramolecular inhibition. *Mol Biol Cell*, *24*(18), 2885-2893. doi:10.1091/mbc.E12-11-0798
- Applewhite, D. A., Grode, K. D., Keller, D., Zadeh, A. D., Slep, K. C., & Rogers, S. L. (2010). The spectraplakins Short stop is an actin-microtubule cross-linker that contributes to organization of the microtubule network. *Mol Biol Cell*, *21*(10), 1714-1724. doi:10.1091/mbc.e10-01-0011
- Ashburner, M., Golic, K. G., & Hawley, R. S. *Drosophila: a laboratory handbook*. Second edition.
- Assémat, E., Bazellières, E., Pallesi-Pocachard, E., Le Bivic, A., & Massey-Harroche, D. (2008). Polarity complex proteins. *Biochim Biophys Acta*, *1778*(3), 614-630. doi:10.1016/j.bbamem.2007.08.029
- Bainbridge, S. P., & Bownes, M. (1981). Staging the metamorphosis of *Drosophila melanogaster*. *J Embryol Exp Morphol*, *66*, 57-80.
- Barrera-Velázquez, M., & Ríos-Barrera, L. D. (2021). Crosstalk between basal extracellular matrix adhesion and building of apical architecture during morphogenesis. *Biol Open*, *10*(11). doi:10.1242/bio.058760
- Bate, M., & Arias, A. M. (1993). *The development of Drosophila melanogaster* (Vol. 2): Cold Spring Harbor Laboratory Press New York.
- Baum, B., & Georgiou, M. (2011). Dynamics of adherens junctions in epithelial establishment, maintenance, and remodeling. *J Cell Biol*, *192*(6), 907-917. doi:10.1083/jcb.201009141
- Behr, M., Wingen, C., Wolf, C., Schuh, R., & Hoch, M. (2007). Wurst is essential for airway clearance and respiratory-tube size control. *Nat Cell Biol*, *9*(7), 847-853. doi:10.1038/ncb1611

- Beitel, G. J., & Krasnow, M. A. (2000). Genetic control of epithelial tube size in the *Drosophila* tracheal system. *Development*, *127*(15), 3271-3282. doi:10.1242/dev.127.15.3271
- Bershadsky, A. (2004). Magic touch: how does cell–cell adhesion trigger actin assembly? *Trends in Cell Biology*, *14*(11), 589-593. doi:<https://doi.org/10.1016/j.tcb.2004.09.009>
- Best, B. T. (2019). Single-cell branching morphogenesis in the *Drosophila* trachea. *Developmental Biology*, *451*(1), 5-15. doi:<https://doi.org/10.1016/j.ydbio.2018.12.001>
- Betschinger, J., Mechtler, K., & Knoblich, J. A. (2003). The Par complex directs asymmetric cell division by phosphorylating the cytoskeletal protein Lgl. *Nature*, *422*(6929), 326-330. doi:10.1038/nature01486
- Beutel, O., Maraschini, R., Pombo-García, K., Martin-Lemaitre, C., & Honigsmann, A. (2019). Phase Separation of Zonula Occludens Proteins Drives Formation of Tight Junctions. *Cell*, *179*(4), 923-936.e911. doi:10.1016/j.cell.2019.10.011
- Bilder, D., Schober, M., & Perrimon, N. (2003). Integrated activity of PDZ protein complexes regulates epithelial polarity. *Nat Cell Biol*, *5*(1), 53-58. doi:10.1038/ncb897
- Blaser, H., Reichman-Fried, M., Castanon, I., Dumstrei, K., Marlow, F. L., Kawakami, K., . . . Raz, E. (2006). Migration of zebrafish primordial germ cells: a role for myosin contraction and cytoplasmic flow. *Dev Cell*, *11*(5), 613-627. doi:10.1016/j.devcel.2006.09.023
- Bonello, T. T., & Peifer, M. (2019a). Scribble and Discs-large direct adherens junction positioning and supermolecular assembly to establish apical-basal polarity. *bioRxiv*, 654509.
- Bonello, T. T., & Peifer, M. (2019b). Scribble: A master scaffold in polarity, adhesion, synaptogenesis, and proliferation. *Journal of Cell Biology*, *218*(3), 742-756.

- Booth, A. J. R., Blanchard, G. B., Adams, R. J., & Röper, K. (2014). A dynamic microtubule cytoskeleton directs medial actomyosin function during tube formation. *Dev Cell*, 29(5), 562-576. doi:10.1016/j.devcel.2014.03.023
- Booth, Alexander J. R., Blanchard, Guy B., Adams, Richard J., & Röper, K. (2014). A Dynamic Microtubule Cytoskeleton Directs Medial Actomyosin Function during Tube Formation. *Developmental Cell*, 29(5), 562-576. doi:<https://doi.org/10.1016/j.devcel.2014.03.023>
- Braga, V. M. M., & Yap, A. S. (2005). The challenges of abundance: epithelial junctions and small GTPase signalling. *Current Opinion in Cell Biology*, 17(5), 466-474. doi:<https://doi.org/10.1016/j.ceb.2005.08.012>
- Brand, A. H., & Perrimon, N. (1993). Targeted gene expression as a means of altering cell fates and generating dominant phenotypes. *Development*, 118(2), 401-415. doi:10.1242/dev.118.2.401
- Broadie, K., Baumgartner, S., & Prokop, A. (2011). Extracellular matrix and its receptors in *Drosophila* neural development. *Dev Neurobiol*, 71(11), 1102-1130. doi:10.1002/dneu.20935
- Brodu, V., & Casanova, J. (2006). The RhoGAP crossveinless-c links tracheless and EGFR signaling to cell shape remodeling in *Drosophila* tracheal invagination. *Genes Dev*, 20(13), 1817-1828. doi:10.1101/gad.375706
- Bryant, D. M., & Mostov, K. E. (2008). From cells to organs: building polarized tissue. *Nat Rev Mol Cell Biol*, 9(11), 887-901. doi:10.1038/nrm2523
- Buckley, C. D., Tan, J., Anderson, K. L., Hanein, D., Volkmann, N., Weis, W. I., . . . Dunn, A. R. (2014). The minimal cadherin-catenin complex binds to actin filaments under force. *Science*, 346(6209), 1254211. doi:doi:10.1126/science.1254211

- Buckley, C. E., & St Johnston, D. (2022). Apical-basal polarity and the control of epithelial form and function. *Nat Rev Mol Cell Biol.* doi:10.1038/s41580-022-00465-y
- Bulgakova, N. A., & Brown, N. H. (2016). *Drosophila* p120-catenin is crucial for endocytosis of the dynamic E-cadherin-Bazooka complex. *J Cell Sci*, 129(3), 477-482. doi:10.1242/jcs.177527
- Bulgakova, N. A., & Knust, E. (2009). The Crumbs complex: from epithelial-cell polarity to retinal degeneration. *J Cell Sci*, 122(Pt 15), 2587-2596. doi:10.1242/jcs.023648
- Buszczak, M., Paterno, S., Lighthouse, D., Bachman, J., Planck, J., Owen, S., . . . Spradling, A. C. (2007). The carnegie protein trap library: a versatile tool for *Drosophila* developmental studies. *Genetics*, 175(3), 1505-1531. doi:10.1534/genetics.106.065961
- Campbell, K., Knust, E., & Skaer, H. (2009). Crumbs stabilises epithelial polarity during tissue remodelling. *J Cell Sci*, 122(Pt 15), 2604-2612. doi:10.1242/jcs.047183
- Campos-Ortega José A., H. V. (1997). *The Embryonic Development of Drosophila melanogaster* (1 ed. Vol. 1). Heidelberg: Springer Berlin, Heidelberg.
- Cavey, M., Rauzi, M., Lenne, P.-F., & Lecuit, T. (2008). A two-tiered mechanism for stabilization and immobilization of E-cadherin. *Nature*, 453(7196), 751-756. doi:10.1038/nature06953
- Caviglia, S., & Luschnig, S. (2013). The ETS domain transcriptional repressor Anterior open inhibits MAP kinase and Wingless signaling to couple tracheal cell fate with branch identity. *Development*, 140(6), 1240-1249. doi:10.1242/dev.087874
- Caygill, E. E., & Brand, A. H. (2016). The GAL4 System: A Versatile System for the Manipulation and Analysis of Gene Expression. *Methods Mol Biol*, 1478, 33-52. doi:10.1007/978-1-4939-6371-3\_2

- Centanin, L., Dekanty, A., Romero, N., Irisarri, M., Gorr, T. A., & Wappner, P. (2008). Cell autonomy of HIF effects in *Drosophila*: tracheal cells sense hypoxia and induce terminal branch sprouting. *Dev Cell*, *14*(4), 547-558. doi:10.1016/j.devcel.2008.01.020
- Chandrasekaran, A., Upadhyaya, A., & Papoian, G. A. (2019). Remarkable structural transformations of actin bundles are driven by their initial polarity, motor activity, crosslinking, and filament treadmilling. *PLoS Comput Biol*, *15*(7), e1007156. doi:10.1371/journal.pcbi.1007156
- Chen, F. Preparation and Immunofluorescence Staining of the Trachea in *Drosophila* Larvae and Pupae.
- Chen, F., & Krasnow, M. A. (2014). Progenitor outgrowth from the niche in *Drosophila* trachea is guided by FGF from decaying branches. *Science*, *343*(6167), 186-189. doi:10.1126/science.1241442
- Chen, X., Kojima, S., Borisy, G. G., & Green, K. J. (2003). p120 catenin associates with kinesin and facilitates the transport of cadherin-catenin complexes to intercellular junctions. *J Cell Biol*, *163*(3), 547-557. doi:10.1083/jcb.200305137
- Cheshire, A. M., Kerman, B. E., Zipfel, W. R., Spector, A. A., & Andrew, D. J. (2008). Kinetic and mechanical analysis of live tube morphogenesis. *Developmental Dynamics*, *237*(10), 2874-2888. doi:<https://doi.org/10.1002/dvdy.21709>
- Chihara, T., & Hayashi, S. (2000). Control of tracheal tubulogenesis by Wingless signaling. *Development*, *127*(20), 4433-4442. doi:10.1242/dev.127.20.4433
- Choi, J., Troyanovsky, R. B., Indra, I., Mitchell, B. J., & Troyanovsky, S. M. (2019). Scribble, Erbin, and Lano redundantly regulate epithelial polarity and apical adhesion complex. *Journal of Cell Biology*, *218*(7), 2277-2293.
- Chugh, P., & Paluch, E. K. (2018). The actin cortex at a glance. *Journal of Cell Science*, *131*(14). doi:10.1242/jcs.186254

- Chung, S., Chavez, C., & Andrew, D. J. (2011). Trachealess (Trh) regulates all tracheal genes during *Drosophila* embryogenesis. *Developmental Biology*, 360(1), 160-172. doi:<https://doi.org/10.1016/j.ydbio.2011.09.014>
- Citi, S., Guerrero, D., Spadaro, D., & Shah, J. (2014). Epithelial junctions and Rho family GTPases: the zonular signalosome. *Small GTPases*, 5(4), 1-15. doi:10.4161/21541248.2014.973760
- Citi, S., Spadaro, D., Schneider, Y., Stutz, J., & Pulimeno, P. (2011). Regulation of small GTPases at epithelial cell-cell junctions. *Mol Membr Biol*, 28(7-8), 427-444. doi:10.3109/09687688.2011.603101
- Coopman, P., & Djiane, A. (2016). Adherens Junction and E-Cadherin complex regulation by epithelial polarity. *Cell Mol Life Sci*, 73(18), 3535-3553. doi:10.1007/s00018-016-2260-8
- Corrigall, D., Walther, R. F., Rodriguez, L., Fichelson, P., & Pichaud, F. (2007). Hedgehog Signaling Is a Principal Inducer of Myosin-II-Driven Cell Ingression in *Drosophila* Epithelia. *Developmental Cell*, 13(5), 730-742. doi:<https://doi.org/10.1016/j.devcel.2007.09.015>
- Crest, J., Diz-Munoz, A., Chen, D.-Y., Fletcher, D. A., & Bilder, D. (2017). Organ sculpting by patterned extracellular matrix stiffness. *Elife*, 6, e24958.
- Dai, J., Estrada, B., Jacobs, S., Sánchez-Sánchez, B. J., Tang, J., Ma, M., . . . Martín-Bermudo, M. D. (2018). Dissection of Nidogen function in *Drosophila* reveals tissue-specific mechanisms of basement membrane assembly. *PLoS Genet*, 14(9), e1007483. doi:10.1371/journal.pgen.1007483
- Davis, M. N., Horne-Badovinac, S., & Naba, A. (2019). In-silico definition of the *Drosophila melanogaster* matrisome. *Matrix Biol Plus*, 4, 100015. doi:10.1016/j.mbplus.2019.100015

- de Vreede, G., Schoenfeld, J. D., Windler, S. L., Morrison, H., Lu, H., & Bilder, D. (2014). The Scribble module regulates retromer-dependent endocytic trafficking during epithelial polarization. *Development*, *141*(14), 2796-2802.
- Desai, R., Sarpal, R., Ishiyama, N., Pellikka, M., Ikura, M., & Tepass, U. (2013). Monomeric  $\alpha$ -catenin links cadherin to the actin cytoskeleton. *Nature Cell Biology*, *15*(3), 261-273.  
doi:10.1038/ncb2685
- Diaz-de-la-Loza, M.-d.-C., Ray, R. P., Ganguly, P. S., Alt, S., Davis, J. R., Hoppe, A., . . . Thompson, B. J. (2018). Apical and Basal Matrix Remodeling Control Epithelial Morphogenesis. *Developmental Cell*, *46*(1), 23-39.e25.  
doi:<https://doi.org/10.1016/j.devcel.2018.06.006>
- Djabrayan, Nareg J. V., Cruz, J., de Miguel, C., Franch-Marro, X., & Casanova, J. (2014). Specification of Differentiated Adult Progenitors via Inhibition of Endocycle Entry in the *Drosophila* Trachea. *Cell Reports*, *9*(3), 859-865.  
doi:<https://doi.org/10.1016/j.celrep.2014.09.043>
- Dong, B., Hannezo, E., & Hayashi, S. (2014). Balance between apical membrane growth and luminal matrix resistance determines epithelial tubule shape. *Cell reports*, *7*(4), 941-950.
- Dow, J. A., & Romero, M. F. (2010). *Drosophila* provides rapid modeling of renal development, function, and disease. *Am J Physiol Renal Physiol*, *299*(6), F1237-1244.  
doi:10.1152/ajprenal.00521.2010
- Du, L., Zhou, A., Patel, A., Rao, M., Anderson, K., & Roy, S. (2017). Unique patterns of organization and migration of FGF-expressing cells during *Drosophila* morphogenesis. *Developmental Biology*, *427*(1), 35-48.  
doi:<https://doi.org/10.1016/j.ydbio.2017.05.009>

- Ducuing, A., & Vincent, S. (2016). The actin cable is dispensable in directing dorsal closure dynamics but neutralizes mechanical stress to prevent scarring in the *Drosophila* embryo. *Nature Cell Biology*, *18*(11), 1149-1160. doi:10.1038/ncb3421
- Duffy, J. B. (2002). GAL4 system in *Drosophila*: A fly geneticist's swiss army knife. *genesis*, *34*(1-2), 1-15. doi:<https://doi.org/10.1002/gene.10150>
- Ebnet, K., Aurrand-Lions, M., Kuhn, A., Kiefer, F., Butz, S., Zander, K., . . . Vestweber, D. (2003). The junctional adhesion molecule (JAM) family members JAM-2 and JAM-3 associate with the cell polarity protein PAR-3: a possible role for JAMs in endothelial cell polarity. *J Cell Sci*, *116*(Pt 19), 3879-3891. doi:10.1242/jcs.00704
- Etienne-Manneville, S., & Hall, A. (2002). Rho GTPases in cell biology. *Nature*, *420*(6916), 629-635. doi:10.1038/nature01148
- Faix, J., & Rottner, K. (2006). The making of filopodia. *Curr Opin Cell Biol*, *18*(1), 18-25. doi:10.1016/j.ceb.2005.11.002
- Fanning, A. S., Little, B. P., Rahner, C., Utepbergenov, D., Walther, Z., & Anderson, J. M. (2007). The unique-5 and -6 motifs of ZO-1 regulate tight junction strand localization and scaffolding properties. *Mol Biol Cell*, *18*(3), 721-731. doi:10.1091/mbc.e06-08-0764
- Farquhar, M. G., & Palade, G. E. (1963). Junctional complexes in various epithelia. *J Cell Biol*, *17*(2), 375-412. doi:10.1083/jcb.17.2.375
- Fraire-Zamora, J. J., Tosi, S., Solon, J., & Casanova, J. (2021). Control of hormone-driven organ disassembly by ECM remodeling and Yorkie-dependent apoptosis. *Curr Biol*, *31*(23), 5261-5273.e5264. doi:10.1016/j.cub.2021.09.057
- Förster, D., & Luschnig, S. (2012). Src42A-dependent polarized cell shape changes mediate epithelial tube elongation in *Drosophila*. *Nature Cell Biology*, *14*(5), 526-534. doi:10.1038/ncb2456

- G., M., & A, K. M. (1993). *Development of the Drosophila tracheal system in The Development of Drosophila melanogaster*. Cold Spring Harbor, NY: Cold Spring Harbor Laboratory Press.
- Gadadhar, S., Bodakuntla, S., Natarajan, K., & Janke, C. (2017). The tubulin code at a glance. *J Cell Sci*, 130(8), 1347-1353. doi:10.1242/jcs.199471
- Gallop, J. L. (2020). Filopodia and their links with membrane traffic and cell adhesion. *Seminars in Cell & Developmental Biology*, 102, 81-89. doi:<https://doi.org/10.1016/j.semcdb.2019.11.017>
- Gervais, L., & Casanova, J. (2010). In vivo coupling of cell elongation and lumen formation in a single cell. *Curr Biol*, 20(4), 359-366. doi:10.1016/j.cub.2009.12.043
- Gervais, L., Lebreton, G., & Casanova, J. (2012). The making of a fusion branch in the *Drosophila* trachea. *Dev Biol*, 362(2), 187-193. doi:10.1016/j.ydbio.2011.11.018
- Glasheen, B. M., Robbins, R. M., Piette, C., Beitel, G. J., & Page-McCaw, A. (2010). A matrix metalloproteinase mediates airway remodeling in *Drosophila*. *Dev Biol*, 344(2), 772-783. doi:10.1016/j.ydbio.2010.05.504
- Glazer, L., & Shilo, B. Z. (1991). The *Drosophila* FGF-R homolog is expressed in the embryonic tracheal system and appears to be required for directed tracheal cell extension. *Genes Dev*, 5(4), 697-705. doi:10.1101/gad.5.4.697
- Goode, B. L., & Eck, M. J. (2007). Mechanism and function of formins in the control of actin assembly. *Annu Rev Biochem*, 76, 593-627. doi:10.1146/annurev.biochem.75.103004.142647
- Gough, R. E., & Goult, B. T. (2018). The tale of two talins – two isoforms to fine-tune integrin signalling. *FEBS Letters*, 592(12), 2108-2125. doi:<https://doi.org/10.1002/1873-3468.13081>

- Gregory, S. L., & Brown, N. H. (1998). kakapo, a gene required for adhesion between and within cell layers in *Drosophila*, encodes a large cytoskeletal linker protein related to plectin and dystrophin. *J Cell Biol*, *143*(5), 1271-1282. doi:10.1083/jcb.143.5.1271
- Guha, A., Lin, L., & Kornberg, T. B. (2008). Organ renewal and cell divisions by differentiated cells in *Drosophila*. *Proceedings of the National Academy of Sciences*, *105*(31), 10832-10836. doi:10.1073/pnas.0805111105
- Guha, A., Lin, L., & Kornberg, T. B. (2009). Regulation of *Drosophila* matrix metalloprotease Mmp2 is essential for wing imaginal disc:trachea association and air sac tubulogenesis. *Developmental Biology*, *335*(2), 317-326. doi:<https://doi.org/10.1016/j.ydbio.2009.09.005>
- Guillemin, K., Groppe, J., Ducker, K., Treisman, R., Hafen, E., Affolter, M., & Krasnow, M. A. (1996). The pruned gene encodes the *Drosophila* serum response factor and regulates cytoplasmic outgrowth during terminal branching of the tracheal system. *Development*, *122*(5), 1353-1362. doi:10.1242/dev.122.5.1353
- Gumbiner, B. M. (2005). Regulation of cadherin-mediated adhesion in morphogenesis. *Nat Rev Mol Cell Biol*, *6*(8), 622-634. doi:10.1038/nrm1699
- Haigo, S. L., & Bilder, D. (2011). Global tissue revolutions in a morphogenetic movement controlling elongation. *Science*, *331*(6020), 1071-1074.
- Han, S. P., & Yap, A. S. (2012). The cytoskeleton and classical cadherin adhesions. *Subcell Biochem*, *60*, 111-135. doi:10.1007/978-94-007-4186-7\_6
- Hannema, S. E., & Hughes, I. A. (2007). Regulation of Wolffian duct development. *Horm Res*, *67*(3), 142-151. doi:10.1159/000096644
- Harris, T. J. (2012). Adherens junction assembly and function in the *Drosophila* embryo. *Int Rev Cell Mol Biol*, *293*, 45-83. doi:10.1016/b978-0-12-394304-0.00007-5

- Harris, T. J., & Tepass, U. (2010). Adherens junctions: from molecules to morphogenesis. *Nat Rev Mol Cell Biol*, *11*(7), 502-514. doi:10.1038/nrm2927
- Hayashi, S., & Kondo, T. (2018). Development and Function of the *Drosophila* Tracheal System. *Genetics*, *209*(2), 367-380. doi:10.1534/genetics.117.300167
- Hirokawa, N., & Heuser, J. E. (1981). Quick-freeze, deep-etch visualization of the cytoskeleton beneath surface differentiations of intestinal epithelial cells. *J Cell Biol*, *91*(2 Pt 1), 399-409. doi:10.1083/jcb.91.2.399
- Hollfelder, D. F. M. and Reim, I.(2014). Distinct functions of the laminin  $\beta$  LN domain and collagen IV during cardiac extracellular matrix formation and stabilization of alary muscle attachments revealed by EMS mutagenesis in *Drosophila*. *BMC Dev. Biol*, *14*, 26.
- Homem, C. C., & Peifer, M. (2008). Diaphanous regulates myosin and adherens junctions to control cell contractility and protrusive behavior during morphogenesis. *Development*, *135*(6), 1005-1018. doi:10.1242/dev.016337
- Hong, S., Troyanovsky, R. B., & Troyanovsky, S. M. (2010). Spontaneous assembly and active disassembly balance adherens junction homeostasis. *Proc Natl Acad Sci U S A*, *107*(8), 3528-3533. doi:10.1073/pnas.0911027107
- Hong, S., Troyanovsky, R. B., & Troyanovsky, S. M. (2013). Binding to F-actin guides cadherin cluster assembly, stability, and movement. *Journal of Cell Biology*, *201*(1), 131-143. doi:10.1083/jcb.201211054
- Hosono, C., Matsuda, R., Adryan, B., & Samakovlis, C. (2015). Transient junction anisotropies orient annular cell polarization in the *Drosophila* airway tubes. *Nat Cell Biol*, *17*(12), 1569-1576. doi:10.1038/ncb3267
- Huang, J., Zhou, W., Dong, W., Watson, A. M., & Hong, Y. (2009). From the Cover: Directed, efficient, and versatile modifications of the *Drosophila* genome by genomic

- engineering. *Proc Natl Acad Sci U S A*, 106(20), 8284-8289.  
doi:10.1073/pnas.0900641106
- Huveneers, S., & de Rooij, J. (2013). Mechanosensitive systems at the cadherin–F-actin interface. *Journal of Cell Science*, 126(2), 403-413. doi:10.1242/jcs.109447
- Ikenouchi, J., & Aoki, K. (2017). Membrane bleb: A seesaw game of two small GTPases. *Small GTPases*, 8(2), 85-89. doi:10.1080/21541248.2016.1199266
- Ikenouchi, J., & Aoki, K. (2022). A Clockwork Bleb: cytoskeleton, calcium, and cytoplasmic fluidity. *The FEBS Journal*, 289(24), 7907-7917.  
doi:<https://doi.org/10.1111/febs.16220>
- Imam, F., Sutherland, D., Huang, W., & Krasnow, M. A. (1999). stumps, a *Drosophila* gene required for fibroblast growth factor (FGF)-directed migrations of tracheal and mesodermal cells. *Genetics*, 152(1), 307-318. doi:10.1093/genetics/152.1.307
- Indra, I., Choi, J., Chen, C. S., Troyanovsky, R. B., Shapiro, L., Honig, B., & Troyanovsky, S. M. (2018). Spatial and temporal organization of cadherin in punctate adherens junctions. *Proc Natl Acad Sci U S A*, 115(19), E4406-e4415.  
doi:10.1073/pnas.1720826115
- Indra, I., Troyanovsky, R. B., Shapiro, L., Honig, B., & Troyanovsky, S. M. (2020). Sensing Actin Dynamics through Adherens Junctions. *Cell Reports*, 30(8), 2820-2833.e2823.  
doi:<https://doi.org/10.1016/j.celrep.2020.01.106>
- Isabella, A. J., & Horne-Badovinac, S. (2015). Building from the Ground up: Basement Membranes in *Drosophila* Development. *Curr Top Membr*, 76, 305-336.  
doi:10.1016/bs.ctm.2015.07.001
- Ishiuchi, T., & Takeichi, M. (2011). Willin and Par3 cooperatively regulate epithelial apical constriction through aPKC-mediated ROCK phosphorylation. *Nat Cell Biol*, 13(7), 860-866. doi:10.1038/ncb2274

- Ishiyama, N., & Ikura, M. (2012). The three-dimensional structure of the cadherin-catenin complex. *Subcell Biochem*, 60, 39-62. doi:10.1007/978-94-007-4186-7\_3
- Ivanov, A. I., Bachar, M., Babbitt, B. A., Adelstein, R. S., Nusrat, A., & Parkos, C. A. (2007). A unique role for nonmuscle myosin heavy chain IIA in regulation of epithelial apical junctions. *PLoS One*, 2(7), e658. doi:10.1371/journal.pone.0000658
- Jaffe, A. B., & Hall, A. (2005). RHO GTPASES: Biochemistry and Biology. *Annual Review of Cell and Developmental Biology*, 21(1), 247-269. doi:10.1146/annurev.cellbio.21.020604.150721
- Jaspers, M. H., Pflanz, R., Riedel, D., Kawelke, S., Feussner, I., & Schuh, R. (2014). The fatty acyl-CoA reductase Waterproof mediates airway clearance in *Drosophila*. *Dev Biol*, 385(1), 23-31. doi:10.1016/j.ydbio.2013.10.022
- JayaNandanan, N., Mathew, R., & Leptin, M. (2014). Guidance of subcellular tubulogenesis by actin under the control of a synaptotagmin-like protein and Moesin. *Nat Commun*, 5, 3036. doi:10.1038/ncomms4036
- Kametani, Y., & Takeichi, M. (2007). Basal-to-apical cadherin flow at cell junctions. *Nat Cell Biol*, 9(1), 92-98. doi:10.1038/ncb1520
- Kametani, Y., & Takeichi, M. (2007). Basal-to-apical cadherin flow at cell junctions. *Nature Cell Biology*, 9(1), 92-98. doi:10.1038/ncb1520
- Kato, K., Dong, B., Wada, H., Tanaka-Matakatsu, M., Yagi, Y., & Hayashi, S. (2016). Microtubule-dependent balanced cell contraction and luminal-matrix modification accelerate epithelial tube fusion. *Nat Commun*, 7, 11141. doi:10.1038/ncomms11141
- Keeley, D. P., Hastie, E., Jayadev, R., Kelley, L. C., Chi, Q., Payne, S. G., . . . Sherwood, D. R. (2020). Comprehensive Endogenous Tagging of Basement Membrane Components Reveals Dynamic Movement within the Matrix Scaffolding. *Dev Cell*, 54(1), 60-74.e67. doi:10.1016/j.devcel.2020.05.022

- Kerman, B. E., Cheshire, A. M., Myat, M. M., & Andrew, D. J. (2008). Ribbon modulates apical membrane during tube elongation through Crumbs and Moesin. *Developmental Biology*, 320(1), 278-288. doi:<https://doi.org/10.1016/j.ydbio.2008.05.541>
- Khanal, I., Elbediwy, A., Diaz de la Loza Mdel, C., Fletcher, G. C., & Thompson, B. J. (2016). Shot and Patronin polarise microtubules to direct membrane traffic and biogenesis of microvilli in epithelia. *J Cell Sci*, 129(13), 2651-2659. doi:10.1242/jcs.189076
- Klämbt, C., Glazer, L., & Shilo, B. Z. (1992). breathless, a *Drosophila* FGF receptor homolog, is essential for migration of tracheal and specific midline glial cells. *Genes Dev*, 6(9), 1668-1678. doi:10.1101/gad.6.9.1668
- Kobielak, A., Pasolli, H. A., & Fuchs, E. (2004). Mammalian formin-1 participates in adherens junctions and polymerization of linear actin cables. *Nat Cell Biol*, 6(1), 21-30. doi:10.1038/ncb1075
- Kovacs, E. M., Verma, S., Ali, R. G., Ratheesh, A., Hamilton, N. A., Akhmanova, A., & Yap, A. S. (2011). N-WASP regulates the epithelial junctional actin cytoskeleton through a non-canonical post-nucleation pathway. *Nat Cell Biol*, 13(8), 934-943. doi:10.1038/ncb2290
- Laprise, P., Lau, K. M., Harris, K. P., Silva-Gagliardi, N. F., Paul, S. M., Beronja, S., . . . Tepass, U. (2009). Yurt, Coracle, Neurexin IV and the Na<sup>+</sup>, K<sup>+</sup>-ATPase form a novel group of epithelial polarity proteins. *Nature*, 459(7250), 1141-1145.
- Larsson, L.-I. (2006). Distribution of E-cadherin and  $\beta$ -catenin in relation to cell maturation and cell extrusion in rat and mouse small intestines. *Histochemistry and Cell Biology*, 126(5), 575-582. doi:10.1007/s00418-006-0193-2
- Le Droguen, P.-M., Claret, S., Guichet, A., & Brodu, V. (2015). Microtubule-dependent apical restriction of recycling endosomes sustains adherens junctions during morphogenesis

- of the *Drosophila* tracheal system. *Development*, 142(2), 363-374.  
doi:10.1242/dev.113472
- Lecuit, T. (2005). Adhesion remodeling underlying tissue morphogenesis. *Trends in Cell Biology*, 15(1), 34-42. doi:<https://doi.org/10.1016/j.tcb.2004.11.007>
- Lecuit, T., & Le Goff, L. (2007). Orchestrating size and shape during morphogenesis. *Nature*, 450(7167), 189-192. doi:10.1038/nature06304
- Lee, S., & Kolodziej, P. A. (2002). Short Stop provides an essential link between F-actin and microtubules during axon extension. *Development*, 129(5), 1195-1204.  
doi:10.1242/dev.129.5.1195
- Levayer, R., & Lecuit, T. (2012). Biomechanical regulation of contractility: spatial control and dynamics. *Trends Cell Biol*, 22(2), 61-81. doi:10.1016/j.tcb.2011.10.001
- Levayer, R., & Lecuit, T. (2013). Oscillation and polarity of E-cadherin asymmetries control actomyosin flow patterns during morphogenesis. *Dev Cell*, 26(2), 162-175.  
doi:10.1016/j.devcel.2013.06.020
- Levi, B. P., Ghabrial, A. S., & Krasnow, M. A. (2006). *Drosophila* talin and integrin genes are required for maintenance of tracheal terminal branches and luminal organization. *Development*, 133(12), 2383-2393. doi:10.1242/dev.02404
- Liu, R., Billington, N., Yang, Y., Bond, C., Hong, A., Siththanandan, V., . . . Sellers, J. R. (2021). A binding protein regulates myosin-7a dimerization and actin bundle assembly. *Nature Communications*, 12(1), 563. doi:10.1038/s41467-020-20864-z
- Llimargas, M. (1999). The Notch pathway helps to pattern the tips of the *Drosophila* tracheal branches by selecting cell fates. *Development*, 126(11), 2355-2364.  
doi:10.1242/dev.126.11.2355

- Llimargas, M. (2000). Wingless and its signalling pathway have common and separable functions during tracheal development. *Development*, 127(20), 4407-4417. doi:10.1242/dev.127.20.4407
- Locke, M. (2001). The Wigglesworth Lecture: Insects for studying fundamental problems in biology. *J Insect Physiol*, 47(4-5), 495-507. doi:10.1016/s0022-1910(00)00123-2
- Loganathan, R., Cheng, Y. L., & Andrew, D. J. Organogenesis of the *Drosophila* Respiratory System.
- Loganathan, R., Cheng, Y. L., & Andrew, D. J. (2016). Organogenesis of the *Drosophila* Respiratory System. In J. Castelli-Gair Hombria & P. Bovolenta (Eds.), *Organogenetic Gene Networks: Genetic Control of Organ Formation* (pp. 151-211). Cham: Springer International Publishing.
- Lubarsky, B., & Krasnow, M. A. (2003). Tube morphogenesis: making and shaping biological tubes. *Cell*, 112(1), 19-28. doi:10.1016/s0092-8674(02)01283-7
- M, W. J. (1980). *The tracheal system*. London: Academic Press.
- Marcos, S., Moreau, J., Backer, S., Job, D., Andrieux, A., & Bloch-Gallego, E. (2009). Tubulin tyrosination is required for the proper organization and pathfinding of the growth cone. *PLoS One*, 4(4), e5405. doi:10.1371/journal.pone.0005405
- Martin, M., & Akhmanova, A. (2018). Coming into Focus: Mechanisms of Microtubule Minus-End Organization. *Trends Cell Biol*, 28(7), 574-588. doi:10.1016/j.tcb.2018.02.011
- Martín-Blanco, E., & Knust, E. (2001). Epithelial morphogenesis: filopodia at work. *Curr Biol*, 11(1), R28-31. doi:10.1016/s0960-9822(00)00039-7
- Mason, F. M., Tworoger, M., & Martin, A. C. (2013). Apical domain polarization localizes actin-myosin activity to drive ratchet-like apical constriction. *Nat Cell Biol*, 15(8), 926-936. doi:10.1038/ncb2796

- Mathew, R., Rios-Barrera, L. D., Machado, P., Schwab, Y., & Leptin, M. (2020). Transcytosis via the late endocytic pathway as a cell morphogenetic mechanism. *Embo j*, *39*(16), e105332. doi:10.15252/emj.2020105332
- Matis, M., Russler-Germain, D. A., Hu, Q., Tomlin, C. J., & Axelrod, J. D. (2014). Microtubules provide directional information for core PCP function. *eLife*, *3*, e02893. doi:10.7554/eLife.02893
- Matsuda, R., Hosono, C., Saigo, K., & Samakovlis, C. (2015). The intersection of the extrinsic hedgehog and WNT/wingless signals with the intrinsic Hox code underpins branching pattern and tube shape diversity in the *Drosophila* airways. *PLoS Genet*, *11*(1), e1004929. doi:10.1371/journal.pgen.1004929
- Matsuzawa, K., Ohga, H., Shigetomi, K., Shiiya, T., Hirashima, M., & Ikenouchi, J. (2021). MAGIs regulate aPKC to enable balanced distribution of intercellular tension for epithelial sheet homeostasis. *Commun Biol*, *4*(1), 337. doi:10.1038/s42003-021-01874-z
- Mattila, P. K., & Lappalainen, P. (2008). Filopodia: molecular architecture and cellular functions. *Nature Reviews Molecular Cell Biology*, *9*(6), 446-454. doi:10.1038/nrm2406
- Matusek, T., Djiane, A., Jankovics, F., Brunner, D., Mlodzik, M., & Mihály, J. (2006). The *Drosophila* formin DAAM regulates the tracheal cuticle pattern through organizing the actin cytoskeleton. *Development*, *133*(5), 957-966. doi:10.1242/dev.02266
- Medeiros, N. A., Burnette, D. T., & Forscher, P. (2006). Myosin II functions in actin-bundle turnover in neuronal growth cones. *Nature Cell Biology*, *8*(3), 216-226. doi:10.1038/ncb1367

- Meng, W., Mushika, Y., Ichii, T., & Takeichi, M. (2008). Anchorage of microtubule minus ends to adherens junctions regulates epithelial cell-cell contacts. *Cell*, *135*(5), 948-959. doi:10.1016/j.cell.2008.09.040
- Meng, W., & Takeichi, M. (2009). Adherens junction: molecular architecture and regulation. *Cold Spring Harb Perspect Biol*, *1*(6), a002899. doi:10.1101/cshperspect.a002899
- Mercer, J., & Helenius, A. (2008). Vaccinia virus uses macropinocytosis and apoptotic mimicry to enter host cells. *Science*, *320*(5875), 531-535. doi:10.1126/science.1155164
- Michelson, A. M., Gisselbrecht, S., Buff, E., & Skeath, J. B. (1998). Heartbroken is a specific downstream mediator of FGF receptor signalling in *Drosophila*. *Development*, *125*(22), 4379-4389. doi:10.1242/dev.125.22.4379
- Milligan, C. E., Prevette, D., Yaginuma, H., Homma, S., Cardwell, C., Fritz, L. C., . . . Schwartz, L. M. (1995). Peptide inhibitors of the ice protease family arrest programmed cell death of motoneurons in vivo and in vitro. *Neuron*, *15*(2), 385-393. doi:[https://doi.org/10.1016/0896-6273\(95\)90042-X](https://doi.org/10.1016/0896-6273(95)90042-X)
- Mills, J. C., Stone, N. L., Erhardt, J., & Pittman, R. N. (1998). Apoptotic membrane blebbing is regulated by myosin light chain phosphorylation. *J Cell Biol*, *140*(3), 627-636. doi:10.1083/jcb.140.3.627
- Miyaguchi, K. (2000). Ultrastructure of the zonula adherens revealed by rapid-freeze deep-etching. *J Struct Biol*, *132*(3), 169-178. doi:10.1006/jsbi.2000.4244
- Mok, J. W., & Choi, K. W. (2021). Novel function of N-acetyltransferase for microtubule stability and JNK signaling in *Drosophila* organ development. *Proc Natl Acad Sci U S A*, *118*(4). doi:10.1073/pnas.2010140118
- Morais-de-Sá, E., Mirouse, V., & St Johnston, D. (2010). aPKC phosphorylation of Bazooka defines the apical/lateral border in *Drosophila* epithelial cells. *Cell*, *141*(3), 509-523. doi:10.1016/j.cell.2010.02.040

- Moussian, B. (2010). Recent advances in understanding mechanisms of insect cuticle differentiation. *Insect Biochem Mol Biol*, 40(5), 363-375. doi:10.1016/j.ibmb.2010.03.003
- Mukherjee, A., Brooks, P. S., Bernard, F., Guichet, A., & Conduit, P. T. (2020). Microtubules originate asymmetrically at the somatic golgi and are guided via Kinesin2 to maintain polarity within neurons. *Elife*, 9. doi:10.7554/eLife.58943
- Mullen, R. D., & Behringer, R. R. (2014). Molecular Genetics of Müllerian Duct Formation, Regression and Differentiation. *Sexual Development*, 8(5), 281-296. doi:10.1159/000364935
- Myster, S. H., Cavallo, R., Anderson, C. T., Fox, D. T., & Peifer, M. (2003). *Drosophila* p120catenin plays a supporting role in cell adhesion but is not an essential adherens junction component. *J Cell Biol*, 160(3), 433-449. doi:10.1083/jcb.200211083
- Nashchekin, D., Busby, L., Jakobs, M., Squires, I., & St Johnston, D. (2021). Symmetry breaking in the female germline cyst. *Science*, 374(6569), 874-879. doi:10.1126/science.abj3125
- Niessen, C. M., Leckband, D., & Yap, A. S. (2011). Tissue organization by cadherin adhesion molecules: dynamic molecular and cellular mechanisms of morphogenetic regulation. *Physiol Rev*, 91(2), 691-731. doi:10.1152/physrev.00004.2010
- Noren, N. K., Liu, B. P., Burrridge, K., & Kreft, B. (2000). p120 catenin regulates the actin cytoskeleton via Rho family GTPases. *J Cell Biol*, 150(3), 567-580. doi:10.1083/jcb.150.3.567
- Norum, M., Tång, E., Chavoshi, T., Schwarz, H., Linke, D., Uv, A., & Moussian, B. (2010). Trafficking through COPII stabilises cell polarity and drives secretion during *Drosophila* epidermal differentiation. *PLoS One*, 5(5), e10802. doi:10.1371/journal.pone.0010802

- Ohshiro, T., Emori, Y., & Saigo, K. (2002). Ligand-dependent activation of breathless FGF receptor gene in *Drosophila* developing trachea. *Mechanisms of Development*, *114*(1), 3-11. doi:[https://doi.org/10.1016/S0925-4773\(02\)00042-4](https://doi.org/10.1016/S0925-4773(02)00042-4)
- Ohshiro, T., & Saigo, K. (1997). Transcriptional regulation of breathless FGF receptor gene by binding of TRACHEALESS/dARNT heterodimers to three central midline elements in *Drosophila* developing trachea. *Development*, *124*(20), 3975-3986. doi:10.1242/dev.124.20.3975
- Ooshio, T., Fujita, N., Yamada, A., Sato, T., Kitagawa, Y., Okamoto, R., . . . Takai, Y. (2007). Cooperative roles of Par-3 and afadin in the formation of adherens and tight junctions. *J Cell Sci*, *120*(Pt 14), 2352-2365. doi:10.1242/jcs.03470
- Oshima, K., & Fehon, R. G. (2011). Analysis of protein dynamics within the septate junction reveals a highly stable core protein complex that does not include the basolateral polarity protein Discs large. *J Cell Sci*, *124*(Pt 16), 2861-2871. doi:10.1242/jcs.087700
- Oshima, K., Takeda, M., Kuranaga, E., Ueda, R., Aigaki, T., Miura, M., & Hayashi, S. (2006). IKK epsilon regulates F actin assembly and interacts with *Drosophila* IAP1 in cellular morphogenesis. *Curr Biol*, *16*(15), 1531-1537. doi:10.1016/j.cub.2006.06.032
- Otani, T., Ichii, T., Aono, S., & Takeichi, M. (2006). Cdc42 GEF Tuba regulates the junctional configuration of simple epithelial cells. *Journal of Cell Biology*, *175*(1), 135-146. doi:10.1083/jcb.200605012
- Ozbek, S., Balasubramanian, P. G., Chiquet-Ehrismann, R., Tucker, R. P., & Adams, J. C. (2010). The evolution of extracellular matrix. *Mol Biol Cell*, *21*(24), 4300-4305. doi:10.1091/mbc.E10-03-0251
- Pastor-Pareja, J. C., & Xu, T. (2011). Shaping cells and organs in *Drosophila* by opposing roles of fat body-secreted Collagen IV and perlecan. *Dev Cell*, *21*(2), 245-256. doi:10.1016/j.devcel.2011.06.026

- Pesch, Y. Y., Riedel, D., & Behr, M. (2015). Obstructor A organizes matrix assembly at the apical cell surface to promote enzymatic cuticle maturation in *Drosophila*. *J Biol Chem*, 290(16), 10071-10082. doi:10.1074/jbc.M114.614933
- Pitsouli, C., & Perrimon, N. (2010). Embryonic multipotent progenitors remodel the *Drosophila* airways during metamorphosis. *Development*, 137(21), 3615-3624. doi:10.1242/dev.056408
- Pitsouli, C., & Perrimon, N. (2013). The Homeobox Transcription Factor Cut Coordinates Patterning and Growth During *Drosophila* Airway Remodeling. *Science Signaling*, 6(263), ra12-ra12. doi:doi:10.1126/scisignal.2003424
- Plant, P. J., Fawcett, J. P., Lin, D. C., Holdorf, A. D., Binns, K., Kulkarni, S., & Pawson, T. (2003). A polarity complex of mPar-6 and atypical PKC binds, phosphorylates and regulates mammalian Lgl. *Nat Cell Biol*, 5(4), 301-308. doi:10.1038/ncb948
- Pope, K. L., & Harris, T. J. C. (2008). Control of cell flattening and junctional remodeling during squamous epithelial morphogenesis in *Drosophila*. *Development*, 135(13), 2227-2238. doi:10.1242/dev.019802
- Popkova, A., Stone, O. J., Chen, L., Qin, X., Liu, C., Liu, J., . . . Wang, X. (2020). A Cdc42-mediated supracellular network drives polarized forces and *Drosophila* egg chamber extension. *Nature Communications*, 11(1), 1921. doi:10.1038/s41467-020-15593-2
- Portran, D., Schaedel, L., Xu, Z., Théry, M., & Nachury, M. V. (2017). Tubulin acetylation protects long-lived microtubules against mechanical ageing. *Nat Cell Biol*, 19(4), 391-398. doi:10.1038/ncb3481
- Pradhan, R., Kumar, S., & Mathew, R. (2023). Lateral adherens junctions mediate a supracellular actomyosin cortex in *Drosophila* trachea. *iScience*, 26(4), 106380. doi:<https://doi.org/10.1016/j.isci.2023.106380>

- Pradhan, R., Urbietta-Ortiz, V. A., Kumar, S., Mathew, R., & Ríos-Barrera, L. D. (2022). Shaping subcellular tubes through vesicle trafficking: Common and distinct pathways. *Semin Cell Dev Biol*. doi:10.1016/j.semcdb.2022.03.024
- Priya, R., & Yap, A. S. (2015). Active tension: the role of cadherin adhesion and signaling in generating junctional contractility. *Curr Top Dev Biol*, 112, 65-102. doi:10.1016/bs.ctdb.2014.11.016
- Rao, P. R., Lin, L., Huang, H., Guha, A., Roy, S., & Kornberg, T. B. (2015). Developmental compartments in the larval trachea of *Drosophila*. *Elife*, 4. doi:10.7554/eLife.08666
- Ratheesh, A., & Yap, A. S. (2012). A bigger picture: classical cadherins and the dynamic actin cytoskeleton. In *Nat Rev Mol Cell Biol* (Vol. 13, pp. 673-679). England.
- Ray, R. P., Ganguly, P. S., Alt, S., Davis, J. R., Hoppe, A., Tapon, N., . . . Thompson, B. J. (2018). Apical and basal matrix remodeling control epithelial morphogenesis. *Developmental cell*, 46(1), 23-39. e25.
- Ray, R. P., Matamoro-Vidal, A., Ribeiro, P. S., Tapon, N., Houle, D., Salazar-Ciudad, I., & Thompson, B. J. (2015). Patterned Anchorage to the Apical Extracellular Matrix Defines Tissue Shape in the Developing Appendages of *Drosophila*. *Dev Cell*, 34(3), 310-322. doi:10.1016/j.devcel.2015.06.019
- Rezakhaniha, R., Agianniotis, A., Schrauwen, J. T., Griffa, A., Sage, D., Bouten, C. V., . . . Stergiopoulos, N. (2012). Experimental investigation of collagen waviness and orientation in the arterial adventitia using confocal laser scanning microscopy. *Biomech Model Mechanobiol*, 11(3-4), 461-473. doi:10.1007/s10237-011-0325-z
- Ribeiro, C., Neumann, M., & Affolter, M. (2004). Genetic control of cell intercalation during tracheal morphogenesis in *Drosophila*. *Curr Biol*, 14(24), 2197-2207. doi:10.1016/j.cub.2004.11.056

- Ricolo, D., & Araujo, S. J. (2020). Coordinated crosstalk between microtubules and actin by a spectraplakins regulates lumen formation and branching. *Elife*, 9. doi:10.7554/eLife.61111
- Ricolo, D., Castro-Ribera, J., & Araújo, S. J. (2021). Cytoskeletal players in single-cell branching morphogenesis. *Dev Biol*, 477, 22-34. doi:10.1016/j.ydbio.2021.05.001
- Riento, K., & Ridley, A. J. (2003). Rocks: multifunctional kinases in cell behaviour. *Nature reviews Molecular cell biology*, 4(6), 446-456.
- Riga, A., Castiglioni, V. G., & Boxem, M. (2020). New insights into apical-basal polarization in epithelia. *Current Opinion in Cell Biology*, 62, 1-8. doi:<https://doi.org/10.1016/j.ceb.2019.07.017>
- Robertson, C. W. (1936). The metamorphosis of *Drosophila melanogaster*, including an accurately timed account of the principal morphological changes. *Journal of Morphology*, 59(2), 351-399. doi:<https://doi.org/10.1002/jmor.1050590207>
- Rusu, A. D., & Georgiou, M. (2020). The multifarious regulation of the apical junctional complex. *Open Biology*, 10(2), 190278. doi:10.1098/rsob.190278
- Röper, K. (2013). Supracellular actomyosin assemblies during development. *Bioarchitecture*, 3(2), 45-49. doi:10.4161/bioa.25339
- Röper, K. (2015). Chapter Four - Integration of Cell–Cell Adhesion and Contractile Actomyosin Activity During Morphogenesis. In A. S. Yap (Ed.), *Current Topics in Developmental Biology* (Vol. 112, pp. 103-127): Academic Press.
- Röper, K. (2015). Integration of cell-cell adhesion and contractile actomyosin activity during morphogenesis. *Curr Top Dev Biol*, 112, 103-127. doi:10.1016/bs.ctdb.2014.11.017
- Röper, K. (2020). Microtubules enter centre stage for morphogenesis. *Philos Trans R Soc Lond B Biol Sci*, 375(1809), 20190557. doi:10.1098/rstb.2019.0557

- Röper, K., Gregory, S. L., & Brown, N. H. (2002). The 'spectraplakins': cytoskeletal giants with characteristics of both spectrin and plakin families. *J Cell Sci*, *115*(Pt 22), 4215-4225. doi:10.1242/jcs.00157
- Saczko-Brack, D., Warchol, E., Rogez, B., Kröss, M., Heissler, S. M., Sellers, J. R., . . . Veigel, C. (2016). Self-organization of actin networks by a monomeric myosin. *Proceedings of the National Academy of Sciences*, *113*(52), E8387-E8395. doi:doi:10.1073/pnas.1612719113
- Sahai, E., & Marshall, C. J. (2002). ROCK and Dia have opposing effects on adherens junctions downstream of Rho. *Nat Cell Biol*, *4*(6), 408-415. doi:10.1038/ncb796
- Sallee, M. D., & Feldman, J. L. (2021). Microtubule organization across cell types and states. *Current Biology*, *31*(10), R506-R511. doi:<https://doi.org/10.1016/j.cub.2021.01.042>
- Samakovlis, C., Hacohen, N., Manning, G., Sutherland, D. C., Guillemin, K., & Krasnow, M. A. (1996). Development of the *Drosophila* tracheal system occurs by a series of morphologically distinct but genetically coupled branching events. *Development*, *122*(5), 1395-1407. doi:10.1242/dev.122.5.1395
- Samakovlis, C., Manning, G., Steneberg, P., Hacohen, N., Cantera, R., & Krasnow, M. A. (1996). Genetic control of epithelial tube fusion during *Drosophila* tracheal development. *Development*, *122*(11), 3531-3536. doi:10.1242/dev.122.11.3531
- Sato, M., Kitada, Y., & Tabata, T. (2008). Larval cells become imaginal cells under the control of homothorax prior to metamorphosis in the *Drosophila* tracheal system. *Developmental Biology*, *318*(2), 247-257. doi:<https://doi.org/10.1016/j.ydbio.2008.03.025>
- Sato, M., & Kornberg, T. B. (2002). FGF Is an Essential Mitogen and Chemoattractant for the Air Sacs of the *Drosophila* Tracheal System. *Developmental Cell*, *3*(2), 195-207. doi:[https://doi.org/10.1016/S1534-5807\(02\)00202-2](https://doi.org/10.1016/S1534-5807(02)00202-2)

- Scholl, A., Ndoja, I., & Jiang, L. (2021). *Drosophila* Trachea as a Novel Model of COPD. *Int J Mol Sci*, 22(23). doi:10.3390/ijms222312730
- Schottenfeld-Roames, J., Rosa, J. B., & Ghabrial, A. S. (2014). Seamless tube shape is constrained by endocytosis-dependent regulation of active Moesin. *Curr Biol*, 24(15), 1756-1764. doi:10.1016/j.cub.2014.06.029
- Shahbazi, M. N., Megias, D., Epifano, C., Akhmanova, A., Gundersen, G. G., Fuchs, E., & Perez-Moreno, M. (2013). CLASP2 interacts with p120-catenin and governs microtubule dynamics at adherens junctions. *J Cell Biol*, 203(6), 1043-1061. doi:10.1083/jcb.201306019
- Shaye, D. D., Casanova, J., & Llimargas, M. (2008). Modulation of intracellular trafficking regulates cell intercalation in the *Drosophila* trachea. *Nature Cell Biology*, 10(8), 964-970. doi:10.1038/ncb1756
- Shimada, Y., Yonemura, S., Ohkura, H., Strutt, D., & Uemura, T. (2006). Polarized Transport of Frizzled along the Planar Microtubule Arrays in *Drosophila* Wing Epithelium. *Developmental Cell*, 10(2), 209-222. doi:<https://doi.org/10.1016/j.devcel.2005.11.016>
- Shindo, M., Wada, H., Kaido, M., Tateno, M., Aigaki, T., Tsuda, L., & Hayashi, S. (2008). Dual function of Src in the maintenance of adherens junctions during tracheal epithelial morphogenesis. *Development*, 135(7), 1355-1364. doi:10.1242/dev.015982
- Shishido, E., Higashijima, S., Emori, Y., & Saigo, K. (1993). Two FGF-receptor homologues of *Drosophila*: one is expressed in mesodermal primordium in early embryos. *Development*, 117(2), 751-761. doi:10.1242/dev.117.2.751
- Sigurbjörnsdóttir, S., Mathew, R., & Leptin, M. (2014). Molecular mechanisms of de novo lumen formation. *Nature Reviews Molecular Cell Biology*, 15(10), 665-676. doi:doi:10.1038/nrm3871

- Sigurbjörnsdóttir, S., Mathew, R., & Leptin, M. (2014). Molecular mechanisms of de novo lumen formation. *Nat Rev Mol Cell Biol*, *15*(10), 665-676. doi:10.1038/nrm3871
- Smith, A. L., Dohn, M. R., Brown, M. V., & Reynolds, A. B. (2012). Association of Rho-associated protein kinase 1 with E-cadherin complexes is mediated by p120-catenin. *Mol Biol Cell*, *23*(1), 99-110. doi:10.1091/mbc.E11-06-0497
- Stephens, R., Lim, K., Portela, M., Kvensakul, M., Humbert, P. O., & Richardson, H. E. (2018). The scribble cell polarity module in the regulation of cell signaling in tissue development and tumorigenesis. *Journal of molecular biology*, *430*(19), 3585-3612.
- Stewart, M. P., Helenius, J., Toyoda, Y., Ramanathan, S. P., Muller, D. J., & Hyman, A. A. (2011). Hydrostatic pressure and the actomyosin cortex drive mitotic cell rounding. *Nature*, *469*(7329), 226-230. doi:10.1038/nature09642
- Subramanian, A., Prokop, A., Yamamoto, M., Sugimura, K., Uemura, T., Betschinger, J., . . . Volk, T. (2003). Shortstop recruits EB1/APC1 and promotes microtubule assembly at the muscle-tendon junction. *Curr Biol*, *13*(13), 1086-1095. doi:10.1016/s0960-9822(03)00416-0
- Suoizzi, K. C., Wu, X., & Fuchs, E. (2012). Spectraplakins: master orchestrators of cytoskeletal dynamics. *J Cell Biol*, *197*(4), 465-475. doi:10.1083/jcb.201112034
- Sutherland, D., Samakovlis, C., & Krasnow, M. A. (1996). branchless encodes a *Drosophila* FGF homolog that controls tracheal cell migration and the pattern of branching. *Cell*, *87*(6), 1091-1101. doi:10.1016/s0092-8674(00)81803-6
- Svitkina, T. M. (2020). Actin Cell Cortex: Structure and Molecular Organization. *Trends in Cell Biology*, *30*(7), 556-565. doi:<https://doi.org/10.1016/j.tcb.2020.03.005>
- Sánchez-Corrales, Y. E., & Röper, K. (2018). Alignment of cytoskeletal structures across cell boundaries generates tissue cohesion during organ formation. *Current Opinion in Cell Biology*, *55*, 104-110. doi:<https://doi.org/10.1016/j.ceb.2018.07.001>

- Taguchi, K., Ishiuchi, T., & Takeichi, M. (2011). Mechanosensitive EPLIN-dependent remodeling of adherens junctions regulates epithelial reshaping. *J Cell Biol*, *194*(4), 643-656. doi:10.1083/jcb.201104124
- Takeichi, M. (2014). Dynamic contacts: rearranging adherens junctions to drive epithelial remodelling. *Nature Reviews Molecular Cell Biology*, *15*(6), 397-410. doi:10.1038/nrm3802
- Takeichi, M. (2014). Dynamic contacts: rearranging adherens junctions to drive epithelial remodelling. *Nat Rev Mol Cell Biol*, *15*(6), 397-410. doi:10.1038/nrm3802
- Takekuni, K., Ikeda, W., Fujito, T., Morimoto, K., Takeuchi, M., Monden, M., & Takai, Y. (2003). Direct binding of cell polarity protein PAR-3 to cell-cell adhesion molecule nectin at neuroepithelial cells of developing mouse. *J Biol Chem*, *278*(8), 5497-5500. doi:10.1074/jbc.C200707200
- Tanaka-Matakatsu, M., Uemura, T., Oda, H., Takeichi, M., & Hayashi, S. (1996). Cadherin-mediated cell adhesion and cell motility in *Drosophila* trachea regulated by the transcription factor Escargot. *Development*, *122*(12), 3697-3705. doi:10.1242/dev.122.12.3697
- Tanentzapf, G., & Tepass, U. (2003). Interactions between the crumbs, lethal giant larvae and bazooka pathways in epithelial polarization. *Nat Cell Biol*, *5*(1), 46-52. doi:10.1038/ncb896
- Tang, V. W., & Briehner, W. M. (2012).  $\alpha$ -Actinin-4/FSGS1 is required for Arp2/3-dependent actin assembly at the adherens junction. *J Cell Biol*, *196*(1), 115-130. doi:10.1083/jcb.201103116
- Tepass, U. (1996). Crumbs, a component of the apical membrane, is required for zonula adherens formation in primary epithelia of *Drosophila*. *Dev Biol*, *177*(1), 217-225. doi:10.1006/dbio.1996.0157

- Tepass, U. (2012). The apical polarity protein network in *Drosophila* epithelial cells: regulation of polarity, junctions, morphogenesis, cell growth, and survival. *Annu Rev Cell Dev Biol*, 28, 655-685. doi:10.1146/annurev-cellbio-092910-154033
- Tepass, U., & Hartenstein, V. (1994). The development of cellular junctions in the *Drosophila* embryo. *Dev Biol*, 161(2), 563-596. doi:10.1006/dbio.1994.1054
- Tepass, U., Theres, C., & Knust, E. (1990). crumbs encodes an EGF-like protein expressed on apical membranes of *Drosophila* epithelial cells and required for organization of epithelia. *Cell*, 61(5), 787-799. doi:10.1016/0092-8674(90)90189-1
- Tinevez, J.-Y., Schulze, U., Salbreux, G., Roensch, J., Joanny, J.-F., & Paluch, E. (2009). Role of cortical tension in bleb growth. *Proceedings of the National Academy of Sciences*, 106(44), 18581-18586. doi:doi:10.1073/pnas.0903353106
- Tsarouhas, V., Senti, K. A., Jayaram, S. A., Tiklová, K., Hemphälä, J., Adler, J., & Samakovlis, C. (2007). Sequential pulses of apical epithelial secretion and endocytosis drive airway maturation in *Drosophila*. *Dev Cell*, 13(2), 214-225. doi:10.1016/j.devcel.2007.06.008
- Umeda, K., Ikenouchi, J., Katahira-Tayama, S., Furuse, K., Sasaki, H., Nakayama, M., . . . Furuse, M. (2006). ZO-1 and ZO-2 independently determine where claudins are polymerized in tight-junction strand formation. *Cell*, 126(4), 741-754. doi:10.1016/j.cell.2006.06.043
- Vaezi, A., Bauer, C., Vasioukhin, V., & Fuchs, E. (2002). Actin cable dynamics and Rho/Rock orchestrate a polarized cytoskeletal architecture in the early steps of assembling a stratified epithelium. *Dev Cell*, 3(3), 367-381. doi:10.1016/s1534-5807(02)00259-9
- Vasileva, E., & Citi, S. (2018). The role of microtubules in the regulation of epithelial junctions. *Tissue Barriers*, 6(3), 1539596. doi:10.1080/21688370.2018.1539596
- Verma, S., Han, S. P., Michael, M., Gomez, G. A., Yang, Z., Teasdale, R. D., . . . Yap, A. S. (2012). A WAVE2-Arp2/3 actin nucleator apparatus supports junctional tension at the

- epithelial zonula adherens. *Mol Biol Cell*, 23(23), 4601-4610. doi:10.1091/mbc.E12-08-0574
- Viktorinová, I., & Dahmann, C. (2013). Microtubule Polarity Predicts Direction of Egg Chamber Rotation in *Drosophila*. *Current Biology*, 23(15), 1472-1477. doi:<https://doi.org/10.1016/j.cub.2013.06.014>
- Vincent, S., Wilson, R., Coelho, C., Affolter, M., & Leptin, M. (1998). The *Drosophila* protein Dof is specifically required for FGF signaling. *Mol Cell*, 2(4), 515-525. doi:10.1016/s1097-2765(00)80151-3
- Waijers, S., Ramalho, J. J., Koorman, T., Kruse, E., & Boxem, M. (2015). The *C. elegans* Crumbs family contains a CRB3 homolog and is not essential for viability. *Biol Open*, 4(3), 276-284. doi:10.1242/bio.201410744
- Warner, S. J., & Longmore, G. D. (2009). Distinct functions for Rho1 in maintaining adherens junctions and apical tension in remodeling epithelia. *J Cell Biol*, 185(6), 1111-1125. doi:10.1083/jcb.200901029
- Waterman-Storer, C. M., Salmon, W. C., & Salmon, E. D. (2000). Feedback interactions between cell-cell adherens junctions and cytoskeletal dynamics in newt lung epithelial cells. *Mol Biol Cell*, 11(7), 2471-2483. doi:10.1091/mbc.11.7.2471
- Watson, C., & Kreuzaler, P. (2011). Remodeling mechanisms of the mammary gland during involution. *The International Journal of Developmental Biology*, 55(7-8-9), 757-762. doi:10.1387/ijdb.113414cw
- Weaver, M., & Krasnow, M. A. (2008). Dual origin of tissue-specific progenitor cells in *Drosophila* tracheal remodeling. *Science*, 321(5895), 1496-1499. doi:10.1126/science.1158712

- WHITTEN, J. M. (1957). The Post-embryonic Development of the Tracheal System in *Drosophila melanogaster*. *Journal of Cell Science*, s3-98(41), 123-150. doi:10.1242/jcs.s3-98.41.123
- Wigglesworth, V. B. Respiration.
- WIGGLESWORTH, V. B. (1953). Surface Forces in the Tracheal System of Insects. *Journal of Cell Science*, s3-94(28), 507-522. doi:10.1242/jcs.s3-94.28.507
- Wildenberg, G. A., Dohn, M. R., Carnahan, R. H., Davis, M. A., Lobdell, N. A., Settleman, J., & Reynolds, A. B. (2006). p120-catenin and p190RhoGAP regulate cell-cell adhesion by coordinating antagonism between Rac and Rho. *Cell*, 127(5), 1027-1039. doi:10.1016/j.cell.2006.09.046
- Wodarz, A., Hinz, U., Engelbert, M., & Knust, E. (1995). Expression of crumbs confers apical character on plasma membrane domains of ectodermal epithelia of *Drosophila*. *Cell*, 82(1), 67-76. doi:10.1016/0092-8674(95)90053-5
- Wollrab, V., Belmonte, J. M., Baldauf, L., Leptin, M., Nédeléc, F., & Koenderink, G. H. (2018). Polarity sorting drives remodeling of actin-myosin networks. *Journal of Cell Science*, 132(4). doi:10.1242/jcs.219717
- Woods, D. F., & Bryant, P. J. (1991). The discs-large tumor suppressor gene of *Drosophila* encodes a guanylate kinase homolog localized at septate junctions. *Cell*, 66(3), 451-464. doi:[https://doi.org/10.1016/0092-8674\(81\)90009-X](https://doi.org/10.1016/0092-8674(81)90009-X)
- Wu, S. K., Budnar, S., Yap, A. S., & Gomez, G. A. (2014). Pulsatile contractility of actomyosin networks organizes the cellular cortex at lateral cadherin junctions. *European Journal of Cell Biology*, 93(10), 396-404. doi:<https://doi.org/10.1016/j.ejcb.2014.09.001>
- Wu, S. K., Gomez, G. A., Michael, M., Verma, S., Cox, H. L., Lefevre, J. G., . . . Yap, A. S. (2014). Cortical F-actin stabilization generates apical–lateral patterns of junctional

- contractility that integrate cells into epithelia. *Nature Cell Biology*, 16(2), 167-178.  
doi:10.1038/ncb2900
- Wu, S. K., & Yap, A. S. (2013). Patterns in space: coordinating adhesion and actomyosin contractility at E-cadherin junctions. *Cell Commun Adhes*, 20(6), 201-212.  
doi:10.3109/15419061.2013.856889
- Yalonetskaya, A., Mondragon, A. A., Elguero, J., & McCall, K. (2018). I Spy in the Developing Fly a Multitude of Ways to Die. *J Dev Biol*, 6(4). doi:10.3390/jdb6040026
- Yamada, S., & Nelson, W. J. (2007). Localized zones of Rho and Rac activities drive initiation and expansion of epithelial cell-cell adhesion. *J Cell Biol*, 178(3), 517-527.  
doi:10.1083/jcb.200701058
- Yamanaka, T., Horikoshi, Y., Sugiyama, Y., Ishiyama, C., Suzuki, A., Hirose, T., . . . Ohno, S. (2003). Mammalian Lgl forms a protein complex with PAR-6 and aPKC independently of PAR-3 to regulate epithelial cell polarity. *Curr Biol*, 13(9), 734-743.  
doi:10.1016/s0960-9822(03)00244-6
- Yamanaka, T., & Ohno, S. (2008). Role of Lgl/Dlg/Scribble in the regulation of epithelial junction, polarity and growth. *Frontiers in Bioscience-Landmark*, 13(17), 6693-6707.
- Yap, A. S., Stevenson, B. R., Abel, K. C., Cragoe, E. J., Jr., & Manley, S. W. (1995). Microtubule integrity is necessary for the epithelial barrier function of cultured thyroid cell monolayers. *Exp Cell Res*, 218(2), 540-550. doi:10.1006/excr.1995.1189
- Yonemura, S. (2011). Cadherin-actin interactions at adherens junctions. *Curr Opin Cell Biol*, 23(5), 515-522. doi:10.1016/j.ceb.2011.07.001
- Zhang, J., Betson, M., Erasmus, J., Zeikos, K., Bailly, M., Cramer, L. P., & Braga, V. M. (2005). Actin at cell-cell junctions is composed of two dynamic and functional populations. *J Cell Sci*, 118(Pt 23), 5549-5562. doi:10.1242/jcs.02639

Öztürk-Çolak, A., Moussian, B., & Araújo, S. J. (2016). *Drosophila* chitinous aECM and its cellular interactions during tracheal development. *Dev Dyn*, 245(3), 259-267. doi:10.1002/dvdy.24356

Öztürk-Çolak, A., Moussian, B., Araújo, S. J., & Casanova, J. (2016). A feedback mechanism converts individual cell features into a supracellular ECM structure in *Drosophila* trachea. *Elife*, 5. doi:10.7554/eLife.09373